Université de Toulouse

THÈSE

En vue de l'obtention du

DOCTORAT DE L'UNIVERSITÉ DE TOULOUSE

Délivré par :
Institut National Polytechnique de Toulouse (INP Toulouse)

Discipline ou spécialité :

Hydrologie, Hydrochimie, Sol, Environnement (H2SE)

Présentée et soutenue par :
Andrea BACHRATA

le : jeudi 11 octobre 2012

Titre :

Modélisation du renoyage d'un coeur du réacteur nucléaire fortement dégradé

Ecole doctorale :
Sciences de l'Univers, de l'Environnement et de l'Espace (SDU2E)

Unité de recherche :
SKP 33.0GKDR

Directeur(s) de Thèse :
M. Quintard
F. Fichot

Rapporteurs :

J. C. Batsale
F. Topin

Membre(s) du jury :

D. Stemmelen
B. Goyeau
W. Ma
M. Prat

Together we all are Engaging the public, one-on-one, with a message that connects and communicates, $E=mc^2$.

5th WiN Global President

Acknowledgement

The three years of my Doctoral studies were performed at “Institut de Radioprotection et de sûreté nucléaire”. Firstly, I would like to thank to Jean-Claude Micaelli, François Barré, Jean Michel Bonnet and Joelle Fleurot who welcome me in their divisions and well coordinated my work. I am very thankful for a valuable combination of doctoral studies and practical research at IRSN.

I am especially grateful to Prof. Michel Quintard, director of research at “Institut de Mécanique de Fluides de Toulouse” for providing guidance of this thesis. The work of Prof. Quintard in the area of two-phase flow in porous medium represents an important contribution to the international research. His work is groundwork in this area and the results of his research were very useful for this thesis.

Secondly, I would like to thank my supervisor at IRSN, Florian Fichot, for providing an excellent guidance and practical support. Thanks to his confidence in my competences, I was able to perform my thesis in France, at IRSN, that I had never visited before. During my thesis, he was always ready to help and answer my questions concerning severe accidents, thermohydraulics or code simulations. I am very thankful for his availability, motivation and friendship. The work with him was a very valuable step in the formation of my professional career.

I would like to thank also Georges Repetto, head of project PEARL, as well as all the experimental team. The cooperation between the experimental team and code developers is very important and not always possible. Thus, I am very happy that the experiments made at IRSN were not delayed and the results were available.

Finally, I would like to thank all the people who contributed to my professional development, supported me and were interested in my work and future. I am very thankful to Nadia Langomazino, head of “Women in Nuclear” in Provence region who invited me to be a member of her team. Many people that I met at WiN Global, WiN Europe and WiN France organization motivated me. I would like to thank also many sponsors, WiN Europe, Slovak nuclear society, ASME, Anna Kollarova from WiN Slovakia as well as „l’Oréal-Unesco-Académie des sciences”. Thanks to these sponsors, I was able to participate at many conferences, to meet interesting people and to present my work.

I thank also my husband and my parents, for their love and encouragements.

Context

Nomenclature

Latin letters

$A_{\beta e}$	interface at the enter and exit of medium for phase β (β=s, l, g), m2
$A_{\beta\sigma}$	interface between the phases β and σ (β,σ =s, l, g), in elementary volume, m^2
$b_{\beta\sigma}$	closure vector related to $\widetilde{T}_\beta$ at $\nabla\langle T_\sigma\rangle^\sigma$ (β,σ =s, l, g), m
Cp	calorific capacity, $J.kg^{-1}.K^{-1}$
Ca	capillary number
D_h	hydraulic diameter, m
g	gravity acceleration, $m.s^{-2}$
h	specific enthalpy, $J.kg^{-1}$
H	characteristic length of unit cell
h_β^{sat}	specific enthalpy of the phase (β =g, l) at saturation temperature, $J.kg^{-1}$
$h_{\beta i}^{\sigma\gamma}$	effective coefficient of thermal transfer characterizing the exchange $\left(\langle T_\beta\rangle^\beta - T_{sat}\right)$for the phase σ on interface $A_{\sigma\gamma}$ (β,σ,γ =s, l, g), $W.m^{-3}.K^{-1}$
k	thermal conductivity $W.m^{-1}.K^{-1}$
$k_{r\beta}$	relative permeability for the phase (β =g, l)
K	absolute permeability, m2
$K_{\beta\beta}$	principal tensor of thermal effective conductivity for the phase β (β =s, l, g), $W.m^{-1}.K^{-1}$
$K_{\beta\sigma}$	coupled tensor of thermal effective conductivity for the phase β (β,σ =s, l, g), $W.m^{-1}.K^{-1}$
l_i	periodicity vector used to describe the Unite Cell, m
l_β	characteristic length at microscopic scale associated to phase β (β =s, l, g), m
L	characteristic length at macroscopic scale, m
$\dot{m}$	mass flow rate of evaporation, $kg.m^{-3}.s^{-1}$
n	unity normal vector
$n_{\beta\sigma}$	unity normal vector at interface $A_{\beta\sigma}$, directed from phase β to phase σ.
Nu	Nusselt number
P	pressure, Pa
Pc	capillary pressure, Pa
Pr	Prandtl number
q	heat flux, W.m-2
Re	Reynolds number
$s_{\sigma i}^\beta$	closure variable related to $\widetilde{T}_\beta$ at $\left(\langle T_\omega\rangle^\sigma - T_{sat}\right)$ (β,σ=s, l, g)

S_l $\varepsilon_l/\varepsilon$, saturation
t time, s
T temperature, K
T_{sat} saturation temperature, K
v velocity, $m.s^{-1}$
V elementary representative volume, m^3
V_β volume of phase β (β=s,l, g) in V, m^3
w velocity of interface liquid-gas, m.s-1

Greek letters

α void fraction (fraction of the gas phase in volume)
Δh $= h_g^{sat} - h_l^{sat}$, latent heat of evaporation, $J.kg^{-1}$
ρ density, $kg.m^{-3}$
φ convective heat flux $W.m^{-2}$
μ kinematic viscosity m^2/s
σ surface tension, $N.m^{-1}$
ε_β V_β/V, volumetric fraction of β phase (β=s, l, g)
ε $=1-\varepsilon_s$, porosity
ζ exponent in temperature function in a transition boiling regime
θ temperature function in a transition boiling regime
ω_s volumetric power generated in phase s, $W.m^{-3}$

Indices
s solid phase
l liquid phase
g gas phase
nb nucleate boiling
fb film boiling
CHF critical heat flux

List of figures

List of tables

1. INTRODUCTION

On s'intéresse dans cette thèse à des situations accidentelles sur des réacteurs nucléaires au cours desquelles le cœur composé des crayons fissiles ne peut être refroidi sur une durée prolongée. Ces accidents, qualifiés de « graves », conduisent à une fusion partielle ou totale du cœur si on ne parvient pas à ré-injecter de l'eau. Bien que ce type d'accident ait longtemps été considéré comme hautement improbable, il était déjà survenu aux Etats-Unis en 1979. De plus, les événements récents au Japon sur les centrales nucléaires de Fukushima ont montré que ce type d'accident peut survenir plus fréquemment qu'on ne le supposait et que son impact sur l'environnement et la vie publique est considérable. Même si les accidents graves sont peu probables, leur étude et la mitigation de leur conséquences est un objective primordial des études de sûreté. Le principe appliqué dans la sûreté nucléaire est la défense en profondeur qui s'appuie sur plusieurs niveaux successifs de protection. Dans ce contexte, la stratégie de la défense en profondeur est :

- Prévention des accidents ;
- Limitation des conséquences
- Prévention de leur développement.

La défense en profondeur est structurée en cinq niveaux de protection [INSAG99]. La mitigation des accidents graves discutée dans cette thèse est incluse dans la quatrième niveau de protection. Dans ce niveau, le gestion des accidents graves est incluse et a pour objectif de maintenir l'intégrité du confinement. Le niveau cinq de la défense approfondie est le plus grave et concerne les post-mesures des accidents graves (non discuté dans cette thèse).

Un accident grave survient généralement suite à un défaut de refroidissement du cœur i.e. « Blackout » perte totale des alimentations électriques ou « APRP »- perte du refroidissement primaire sans disponibilité du système d'injection de secours. L'objectif des procédures de gestion des accidents graves est la prévention et la mitigation de ce type d'accident. C'est aussi exigé par les autorités de sûreté nucléaire dans le monde où la prévention et la mitigation des accidents graves devrait être incluse dans le concept des réacteurs futurs. Il existe plusieurs stratégies pour stabiliser et contrôler le cœur dégradé i.e. la rétention des matériaux radioactifs dans la cuve par le noyage de la cuve et du puits de cuve ou la récupération et le refroidissement de ces matériaux hors de la cuve (principe de l'EPR). Ces systèmes sont basés sur des dispositifs passifs et peuvent arrêter la progression d'un accident grave comme par exemple l'injection de secours passive, ou le refroidissement passif de l'enceinte de confinement.

Par contre, l'implémentation de ces systèmes passifs dans le concept des réacteurs actuels (Gen II) est difficile. Dans ce cas, l'arrêt de la progression de l'accident et la sauvegarde de la cuve peuvent être envisagés grâce à un renvoi d'eau sur le cœur par récupération des systèmes d'injection et/ou lignage de différents circuits au primaire. Toutefois, l'envoi d'eau sur le

cœur n'est pas une action anodine; d'une part, l'efficacité du renoyage comme moyen de récupération de la situation n'est pas toujours démontrée ; d'autre part, le renoyage peut engendrer des risques supplémentaires de perte du confinement en raison de la forte production d'hydrogène qui peut accompagner le renoyage et de l'éventuel pressurisation de la cuve .

1.1 ACCIDENTS AVEC LA DEGRADATION DU CŒUR

Un accident grave, comme on l'a déjà précisé, a généralement pour origine une indisponibilité durable des moyens de refroidissement du cœur dont la puissance résiduelle ne peut plus être évacuée. En une à quelques heures, suite à des défaillances multiples, humaines et/ou matérielles, incluant l'échec des procédures de sauvegarde, les éléments combustibles se dégradent. Une suite de phénomènes nombreux et complexes se déroule alors, selon divers scénarios dépendant des conditions initiales de l'accident et des actions des opérateurs; ces scénarios sont susceptibles, à terme, de conduire à la perte de l'intégrité du confinement et à des risques de relâchements importants de produits radioactifs à l'extérieur de l'enceinte de confinement.

Dans le domaine des accidents graves, les phénomènes physiques mis en jeu sont extrêmement complexes et sortent généralement du cadre des connaissances acquises hors du domaine nucléaire principalement à cause des très hautes températures et de la spécificité des matéraiux. Les objectifs de la recherche sont donc de parvenir à comprendre au mieux ces phénomènes physiques et de réduire les incertitudes quant à leur quantification. Les scenarios des accidents comme TMI-2 ou Fukushima Daiichi peuvent aider à comprendre les différente étapes d'un accident. Par contre, il est impossible d'effectuer, dans ce domaine, des essais à taille réelle et de reproduire toutes les situations envisageables. C'est pourquoi il est nécessaire de réaliser des essais élémentaires, permettant d'étudier séparément chaque phénomène physique, puis de confirmer sur des essais globaux les interactions entre ces phénomènes physiques.

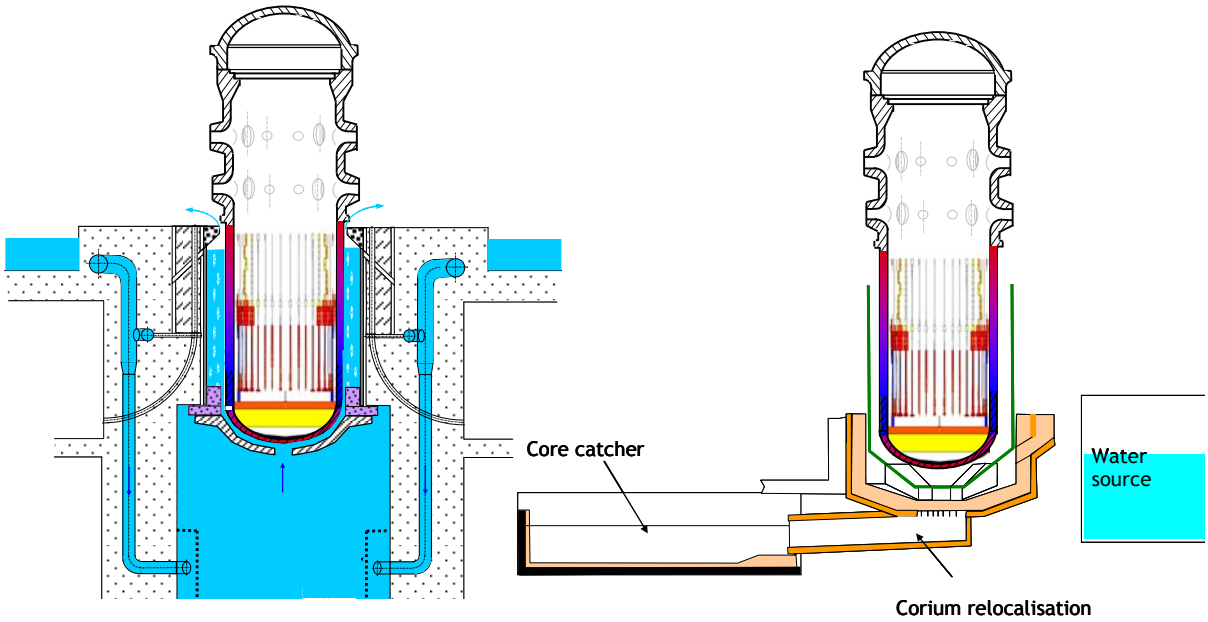

Figure 1.1: Rétention en cuve par noyage de puits de cuve (gauche), récupérateur du corium (droite)

Lors du dénoyage prolongé du cœur du réacteur, le combustible s'échauffe progressivement sous l'effet de la puissance résiduelle, qui n'est plus évacuée. Une réaction exothermique d'oxydation des gaines de combustible en Zircaloy par la vapeur d'eau se produit, menant à une production importante d'hydrogène et de puissance thermique. Par ailleurs, des réactions métallurgiques entre le combustible et la gaine produisent des eutectiques à bas point de fusion, entraînant des relocalisations de matériaux dans le cœur. Sous l'effet de l'échauffement, les produits de fission les plus volatils, puis les produits de fission semi-volatils sont relâchés par le combustible.

Progressivement, il se forme, dans le cœur, un bain de matériaux fondus, appelé corium qui va ensuite s'écouler au fond de la cuve. Au contact de l'eau restant au fond de la cuve, une interaction entre le corium et l'eau se produit, se traduisant par une fragmentation grossière du corium, pouvant être suivie d'un phénomène plus violent, appelé explosion de vapeur.

1.2 RENOYAGE COMME UN SCENARIO DE MITIGATION

Au cours de la dégradation du coeur, il est possible de mettre en œuvre des moyens ultimes d'appoint en eau au niveau du circuit primaire ou du circuit secondaire, par l'intermédiaire de « lignages » de différents circuits. Le renoyage d'un coeur dégradé, qui est un phénomène complexe, pourrait permettre, dans certaines conditions, d'arrêter la progression de l'accident. Par contre, il y a différents risques liés à la sûreté lors d'un renoyage :

- Production massive de vapeur associée à une production d'hydrogène et provoquant une pressurisation rapide ;
- Possible risque d'explosion de vapeur en cas de retour d'eau sur des matériaux fondus;

- Oxydation des métaux par la vapeur produite, se traduisant par une production d'hydrogène importante et rendant plus explosive l'atmosphère dans l'enceinte;
- Relâchement accru des produits de fission.

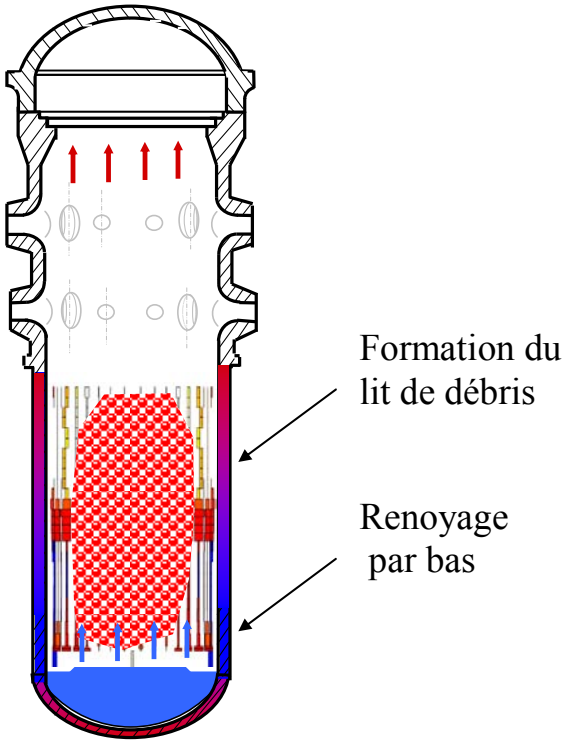

Figure 1.2: Renoyage (injection d'eau) dans un coeur fortement dégradé- formation du lit de débris

De façon plus concrète, le renoyage peut intervenir dans toutes les configurations possibles de l'état du cœur :

- Crayons intactes ou peu dégradés (température inférieure à 1500°C) ;
- Lit de débris ;
- Bain de corium liquide.(température supérieure à 2200°C)

Le sujet de cette thèse concerne le renoyage d'un cœur de réacteur fortement endommagé et se présentant sous forme d'un « lit de débris » ou amas de particules résultant de l'effondrement des crayons très fragilisés par l'oxydation et les températures élevées. Dès lors que les crayons se sont effondrés, la configuration du cœur est beaucoup plus tortueuse qu'en géométrie intacte ou faiblement dégradée. En effet, il se forme un milieu poreux, ce qui augmente sensiblement les pertes de charge et rend beaucoup plus difficile l'accès de l'eau dans ces zones effondrées. Lorsque l'eau ne peut atteindre certaines parties du lit de débris, on suppose en général que ces parties continuent à chauffer jusqu'à leur température de fusion, ce qui donne naissance au bain fondu. On peut noter qu'un lit de débris peut aussi se former en fond de cuve, lors de la coulée du corium dans l'eau.

1.3 CONTEXTE ET ENJEUX DE L'ETUDE

Dans ce contexte, les objectifs de la recherche sont de parvenir à comprendre au mieux les phénomènes physiques intervenant lors du renvoi d'eau dans un lit de débris à haute température. On cherche ainsi à réduire les incertitudes quant à leur quantification, afin d'être capable de développer des modèles applicables aux réacteurs. Ces modèles, regroupés au sein de codes de calcul informatiques, doivent permettre de prévoir le déroulement de renoyage d'un cœur dégradé en cas d'accident grave.

Un programme de R&D a été lancé à l'IRSN, avec l'objectif de réduire au mieux les incertitudes relatives a l'évaluation des conséquences d'un renoyage sur un cœur quelque soit son état de dégradation et de disposer de modèles détaillés, validés, permettant de faire des évaluations réalistes (sans conservatisme excessif) des phénomènes associés au renoyage. Ce programme est basé sur des expériences et de la modélisation avec un fort lien entre les deux types d'actions. L'objectif est de développer le modèle détaillé dans le logiciel de calcul ICARE-CATHARE, permettant en particulier de bénéficier du module 3D pour l'aspect écoulements multidimensionnels dans le cas de milieu poreux de type lit de débris. Actuellement, le logiciel ICARE-CATHARE V2 résulte d'un couplage entre le logiciel mécaniste de dégradation du cœur ICARE2, développé par l'IRSN, et le logiciel de thermohydraulique CATHARE2, développé par le CEA en collaboration avec EDF, AREVA et l'IRSN. Il constitue un outil de synthèse de l'ensemble des connaissances phénoménologiques sur la dégradation du cœur. En particulier, le couplage du logiciel ICARE avec le logiciel CATHARE2 permet, grâce a l'utilisation du module thermohydraulique 3D de CATHARE2, une modélisation 2D des écoulements et du comportement du combustible dans la cuve.

De plus, avant cette thèse, des modèles spécifiques avaient été développés afin de simuler plus particulièrement les écoulements dans des milieux poreux, représentatifs des géométries dégradées du cœur. Toutefois, les modèles dans ICARE-CATHARE présentaient un certains nombre de limites:

- Ils ne traitaient pas le renoyage pour toutes les configurations susceptibles d'être rencontrées lors d'un transitoire de dégradation ;
- Ils ne disposaient que d'une validation très limitée, en particulier pour ce qui concerne le renoyage.

Dans ce contexte précis, ce travail de thèse s'intéresse plus particulièrement au modèle de renoyage d'un lit de débris en vue de son amélioration. Ainsi, le plan de ce document s'inscrit dans la logique de l'étude réalisée. En effet, dans un premier temps, un étude bibliographique des programmes expérimentaux déjà réalisés a été faite afin de rassembler les données susceptibles d'être utiles à la compréhension du renoyage ou à la validation des modèles. Les études portent sur l'analyse de deux types d'expériences : expériences d'assèchement ou renoyage d'un lit de débris. Parmi tous ces essais, on présentera plus précisément l'ensemble

des essais réalisé en France sur les dispositifs PETIT (1998) et PRELUDE (2009-2012) qui ont servi à la validation.

L'objectif du deuxième chapitre est de présenter le modèle macroscopique, pour un écoulement diphasique dans un milieu poreux, initialement développé dans la thèse du Duval (2002). Il est caractérisé par un traitement du déséquilibre thermique entre les phases solide, liquide et gazeuse. Il inclut aussi deux équations de quantité de mouvement (une pour chacune des phases fluides). D'autres modèles sont également mentionnés lorsqu'ils apportent des éléments intéressants que nous avons souhaité reprendre. Dans cette thèse, des améliorations significatives sont apportés sur les lois de transfert de chaleur dans différentes régimes d'ébullition. Les critères caractérisant la transition entre différents régimes d'écoulements ont été complétés. Le modèle présenté dans cette thèse a été directement implémenté dans le code de calculs ICARE-CATHARE. Finalement, la validation quantitative sur les données expérimentales est présentée. On montre que le modèle fournit des résultats satisfaisants. Le modèle est capable de prédire la progression du renoyage dans le cœur, la production du vapeur et le pic de pression pour différents diamètres de particules et différents débits d'injection testés.

Chapter 1

INTRODUCTION

1. INTRODUCTION

Many industrial systems involve the flow of water within a hot porous medium inducing boiling. Such systems are usually designed to remove heat for the solid matrix (heat exchangers made of foam or rod/tube bundles or micro-channels). Among those systems, most of the existing nuclear reactors are designed to be cooled by water. The geometry of the porous medium, in that case, consists of assemblies of vertical rods (fuel elements where heat is produced). In case of a failure resulting in a loss of water for an extended period of time, the fuel assemblies cannot be cooled and may collapse and be fragmented into particles, forming a porous "debris bed" which is much more difficult to cool down than the initial assemblies because of a much lower permeability. The main topic of this thesis is the study of the injection of water into such a debris bed, mostly from the points of view of heat transfers and two-phase flow modeling.

In this first Chapter, we start by explaining the context of this work from the points of view of nuclear safety as well as thermalhydraulics.

Industrial context

The TMI-2 accident and recently Fukushima accident demonstrated that nuclear safety strategy has to cover accident sequences involving massive core melt progression in order to develop reliable mitigation strategies for both, existing and advanced reactors. Although severe accidents should be (by design) of a very low likelihood and might be caused only by multiple failures, accident management is implemented for managing their course and mitigating their consequences. The fundamental safety principle applied in nuclear branch is *defence in depth*. The basic philosophy of this concept is an idea of multiple levels of protection.

The strategy for defence in depth is twofold:

- First to prevent accidents;
- Second, to limit potential consequences and to prevent their development to more serious conditions.

Defence in depth is generally structured in five levels of protection [INSAG99]. The severe accident management strategy discussed in this work is included in the fourth level. This level namely includes accident and severe accident management, directed to maintain the integrity of the confinement. The fifth level is the most serious and represents post-severe accident measures (not discussed in this work).

The accidents leading to core degradation are e.g. "Blackout"- total loss of alternative current electrical power or Loss Of Coolant Accident (LOCA) without availability of high and low-

pressure injection (low-pressure core melting scenario). The aim of the severe accident management is to prevent the development of the accident scenario to more serious conditions. The combination of engineering judgment and probabilistic methods is used to determine the preventive and mitigative measures. The mitigation of severe accidents with core melting is required by safety authorities and thus is implemented into the design of Gen III of pressurized water reactors. Some examples of mitigation strategies for new concepts of reactors may be found for in-vessel [Bachrata10] or ex-vessel retention [Fischer04]. These strategies lead to long-term stabilization and coolability of the corium melt during severe accident that is one of the goals of the near-future new light water reactor plants.

The main idea of in-vessel retention consists in flooding the reactor cavity to submerge the vessel completely or at least submerge the lower head (see Figure 1.1). The pressurized water reactor (PWR) lower head containing the melt pool is cooled from outside, which keeps the outer surface of the vessel wall cool enough to prevent vessel failure. The decay heat is transferred through the reactor pressure vessel wall (RPV) to the surrounding water and then to the atmosphere of the containment of the nuclear power plant (NPP). The aim of this strategy is to localise and to stabilise the corium inside RPV.
The applicability of the in-vessel retention concept is only for low power density, medium size reactors, such as Loviisa and the AP1000 design. For very large, high power density reactors (e.g. EPR), ex-vessel strategy for corium localisation and stabilisation should be used (see Figure 1.1). The ex-vessel corium retention is an alternative approach to localise and stabilize the corium. This approach is based either on corium retention in core catcher located in reactor cavity below RPV (e.g. VVER-1000 design under construction in China) or corium spreading and retention in special spreading compartment (e.g. EPR). However, preventing the spreading/dispersion of such large amounts of radioactive materials appears to be more attractive in order to avoid very long and very expensive post-accident tasks.

The in-vessel or ex-vessel retention strategies will terminate a further progress of severe accident, *passively*, with the core in a stable, coolable configuration, thus avoiding the largely uncertain accident evolution with the molten debris on the containment floor. Most of the severe accident mitigation scenarios are thus based on passive safety technology. The safety systems include passive safety injection, passive residual heat removal, and passive containment cooling. These systems provide long-term core cooling and decay heat removal without the need for operator actions and without reliance on active safety-related systems.

However, the implementation of one of those passive technologies within the design of an operating nuclear power plants (Gen II) is difficult from the financial or technical points of view. The reflooding (injection of water) that will be discussed in this thesis is possible if one or several water sources (*active systems*) become available during the accident (see Figure 1.2). The injection of water into the core (even if degraded) could, in certain conditions, stop the progression of severe accident. This may significantly contribute to the extension of safety margin of pressurized water reactors. On the other hand, it must also be recognized that at

elevated core temperatures, the rate of oxidation of metals may be very high if steam is available. Therefore, reflood is likely to lead to an enhanced hydrogen formation and the risk of containment damage (if hydrogen/air deflagration occurs). However, from a safety point of view, it is important to evaluate chances of coolability of the reactor core during a severe accident. This is in line with the safety philosophy of defence in depth which requires to foresee and to analyse all options to stop an accident at any stage.

1.1 ACCIDENTS WITH CORE DEGRADATION

The loss of coolant accidents leading to core degradation already happened, in 1979 at TMI-2 and in 2011 at Fukushima Daiichi power plants. The TMI-2 event was attributed to operator action that led to securing emergency core cooling pumps because pressurizer level instruments indicated the primary system was filling with water. At Fukushima Daiichi loss of power (offsite, onsite emergency diesel, and then station battery) led to a loss of core and spent fuel pool cooling function. The Fukushima Daiichi involved three reactors (BWR) and four spent fuel pools while TMI-2 involved a single reactor (PWR).

The TMI-2 accident developed a large core melt pool of primarily oxidic mixture (UO_2-ZrO_2), which was surrounded by water. It formed a thick crust all around and was not coolable and one part of the melt pool relocated down to the lower plenum. Large fractions of the reactor core were severely damaged and redistributed in the RPV. Some parts of the core (either intact fuel rods of severely damaged assemblies forming debris beds) could be cooled down before reaching their melting point. For the relocated molten materials at the bottom, although the melt was above 2500^{o}C, no thermal attack on the vessel wall was found except from the hot spot. At the hot spot the vessel wall was heated up to 1100^{o}C for 30 min and than cooled down rapidly. The fuel damage sequence at Fukushima Daiichi was probably similar (based on calculation and first interpretation of plant data). Compared to TMI-2, the initial estimates suggest that primary containment vessels were damaged and fuel was relocated out of the Fukushima Daiichi vessels. The findings from these accidents provide the guideline for developing scenarios for the evolution of a severe accident in the lower head. The investigations of these accidents enhance the experimental knowledge available in the prototypic scale. All other approaches to the problem are based on a combination of expert judgment, small-scale experiments and extrapolation to reactor conditions. Since experiments with radioactive corium are not feasible this is the only way to investigate the problem.

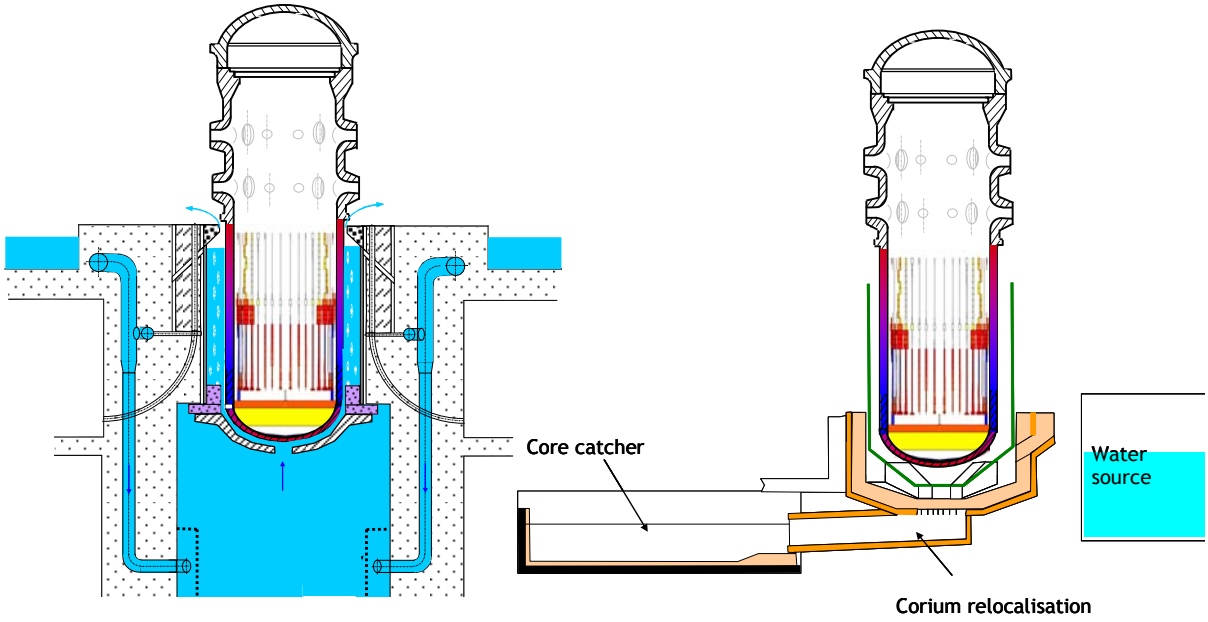

Figure 1.1: In-vessel retention concept (left), ex-vessel retention concept (right)

The phenomenology of severe accidents includes two phases: early phase and late phase of the accident. The *early phase* of the severe accident is characterized by the continued undercooling of the core and can result in loss of integrity of the fuel rods and of the structural materials in the core. The core degradation and melting follow. During core degradation, several processes, such as Zircaloy-steam reaction (oxidation) and melting and freezing of the materials, take place. Any attempt to inject water during core degradation can lead to quenching (fast cooling) but also to further fragmentation of core materials. The fragmentation of fuel rods and melting of reactor core materials can result in the formation of a "debris bed". In a *late phase* of accident, if the core cannot be cooled down, core melt-down occurs and the melt relocates through the downcomer or through the core bottom plate down to the lower plenum. Fragmentation and re-solidification of molten core debris will occur if water is present in the lower plenum when the debris relocates. The residual water will evaporate and the dryout of the partially quenched debris can lead to thermal attack and failure of the vessel lower head and, in turn, release of core material into the cavity.

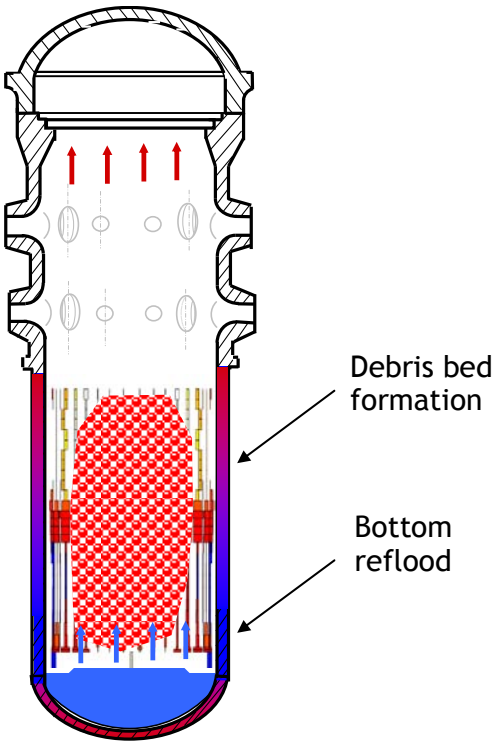

Figure 1.2: Reflood (injection of water) into degraded reactor core- debris bed formation

1.2 REFLOODING AS A SEVERE ACCIDENT SCENARIO

The reflooding (injection of water), in certain conditions, may stop the progression of severe accident or at least, limit the extent of degradation. But, first, the efficiency of reflooding should be estimated, especially for debris beds where the low permeability might considerably slow down the progression of water. Secondly, the associated phenomena leading to containment failure should be investigated. There is a risk of hydrogen formation and strong

steam production that could result in the pressurization and heat-up of the containment. That is the reason why the reflood scenario is considered with care in Severe Accident Management Guidelines (SAMG). For instance, there exist restrictions concerning the water injection e.g. it is recommended that the operator cannot inject low liquid flow during 1h30 after the criteria summarized in SAMG [IRSN06].
These restrictions find their origin in the existing knowledge concerning the effects of water injection on a degraded core. But this knowledge is quite poor today, due to the complexity of the physical phenomena involved and to the lack of experimental data and adequate models. The safety requirements concerning core reflooding call for a reduction of the various uncertainties about the following issues:

- *Hydrogen production kinetics*, with respect to design of recombiners and to significant local concentrations in the containment that could cause dynamic phenomena (ignition, flame acceleration and deflagration–detonation transition).
- *Pressurization of the primary circuit*, with respect to vessel lower head failure or induced break in the loops of the reactor cooling system.
- *In-vessel steam explosion*, with respect to risks of vessel failure and "missile" generation (corium and structures).
- *Re-emission of fission products*, with respect to source term, particularly for containment bypass sequences.

The objectives of current R&D programs are to reduce the uncertainties related to the evaluation of consequences of core reflooding at any stage of its degradation. One of the objectives is to develop detailed models, validated and applicable to the reactor scale in order to evaluate the realistic consequences of reflood at any stage of core geometry. Generally, the reflood scenarios concern different types of core geometries:

- *Intact or partially degraded fuel rods*, where the temperature is below 1500°C. Here, if the liquid flow is sufficient, the stop of progression of core degradation is possible. The associated phenomena are the high steam and hydrogen production.
- *Debris bed*, where the water access can be more questionable. The porous medium geometry result in higher pressure losses and thus the water access is more difficult.
- *Molten pool*, where the temperatures are above 2200°C. This geometry can appear locally or in the whole lower plenum after the corium relocalisation. The coolability is very limited.

The reflooding of debris bed is a current objective of severe accident studies. Particulate debris beds may form during different stages of a severe core melt accidents, e.g. in the degrading hot core, due to thermal stresses during reflooding, in the lower plenum, by melt flow from the core into water in the lower head etc. The debris may include solid fragments of fuel pellets and/or fragments or frozen masses of metallic claddings. Actually, a debris bed will consist in a heterogeneous distribution of solid debris, frozen melts and remnants of fuel

rods (and particularly around the in-core corium molten pool with the presence of a crust). Three main phenomena lead to fuel fragmentation [Dorsselaere06]:

- Pellet fragmentation during the reactor normal operation, which only depends on the fuel burn-up. A model approach leads to fragment sizes from 1 to 5 mm.
- Spallation caused by growth of fission product bubbles in the fuel. This leads to a range of sizes from grain size (some tens of micrometers) to the natural size (a few millimeters).
- Penetration of liquid zirconium into the fragmented pellet. This could dissolve partly the UO_2 pellets and thus reduce the particle size.

This thesis will mainly deal with those debris beds formed after the collapse of fuel assemblies. Their porosity is in the range 0.3-0.5 but it may be lower if molten materials have migrated in and filled up the porosities.
Injection of water will occur mainly from the bottom, because of reactor design. However, in some situations, injection may occur from the top (this aspect will not be treated in this thesis).

1.3 MODELING OF REFLOOD OF DEBRIS BED

There is a strong interest to understand and predict the conditions for which it is possible to cool a severely damaged reactor core. Thus, the heat transfer and fluid flow with liquid-vapor phase change in porous media has been studied experimentally and theoretically.

The available knowledge about debris bed cooling consists in many international experimental programs that were performed in the past 30 years, in models that were developed and in quantitative evaluations of reactor scenarios that could be done using these models or dedicated severe accident codes. The first experimental studies about the reflooding of a debris bed focused on top water injection [Ginsberg86]. A one-dimensional top flooding analysis concluded that even if there is still a significant amount of water (~20%) anywhere in the bed, the access of water into the bed might become very limited because of the counter-current steam flow. Dry channels or dry pockets of particles appear, as observed by [Ginsberg86]. The POMECO experiments [Kazachkov02] also showed a limitation of bed cooling under top flooding conditions. Beds of low porosity (<0.4) and small particles (<2 mm) are not easily coolable, except when water is injected from the bottom. If coolant is supplied from the bottom, the limitation of coolability will occur at much higher heating rates. The maximum power (per unit of surface) that can be extracted from the bed by evaporation is usually referred to as the “dryout heat flux” (DHF). The value of DHF depends on several factors, including the porosity, the height of the bed and the volumetric power dissipated in the particles. In his experiments, Tutu [Tutu84] observed that the measured heat fluxes were an order of magnitude larger than those observed under top-flooding conditions. The effect can be understood because of the water supply via regions of low void fraction (in contrast to

top flooding) and the co-current flow mode. Moreover, in the situation of bottom reflooding studies, it was observed that both the average heat flux and the maximum heat flux increase with increasing water injection rate. Secondly it was observed that the pressure difference across the particulate layer can enhance multi-dimensional effects and lead to an increase of the time needed to completely quench the particle bed [Wang88]. The multi-dimensional process were observed also in DEBRIS experiments with liquid entering the bed from inner channels [Schafer06], [Rashid11]. However, the bottom-quenching experiments showed that the quench front propagated in a one dimensional manner, at least for the experiments performed with a rather low initial bed temperature (below 450°C). In realistic bed configurations with non-uniform height, and possible bed heterogeneities, multi-dimensional effects are to be expected because of easier water inflow, mostly from the sides. In this case, the conditions of local equilibrium which have been assumed in many models may no longer be valid. In addition, when there is a significant heat generation and rapid evaporation-condensation, the system may become rapidly far from local thermal equilibrium. That issue will be considered in the present work.

The current theoretical attempts are to obtain *macro-scale models*, in particular through the use of a volume averaging theory [Quintard00], [Quintard94]. The method to obtain the energy balance equations is the same as in [Whitaker77] and the hereafter proposed models differ mainly by additional hypotheses and new closure relation sets. These families of models could be roughly distinguished according to the treatment of the energy equation:

- Local thermal equilibrium (one temperature model), i.e. phase averaged temperatures are nearly equal.
- Local thermal non-equilibrium (two, three temperatures model), i.e. phase averaged temperatures may no be equal.

The one-equation models are generally based on the assumption of local thermal equilibrium [Moyne00]. Here, local thermal equilibrium means that the macroscopic temperatures of the three phases are close enough so that a single temperature is enough to describe the heat transport process. Theoretical attempts were made to obtain local-non equilibrium macro-scale models [Quintard97]. The reason is that, in situations of water flooding of an overheated porous bed, a one-temperature description is inadequate to describe correctly the transients associated with the quench front. When the assumption of local thermal equilibrium fails to be valid, one possible solution is to develop separate transport equations for each phase. This leads to macroscopic models which are referred to as non-equilibrium models. The problem of a two-phase flow in a porous medium with local thermal non-equilibrium has received less attention from a theoretical point of view. A three-equation model has been developed by Petit et al. [Petit98] using the method of volume averaging. However this model does not take into account the phase change process. On the other hand, three-equation models have been proposed heuristically but as was emphasized by [Quintard97], this leads to intuitive macroscopic models and to erroneous interpretation since these models are not derived from pore-scale transport equations through some scaling-up theory.

A generalized three-equation model for the macroscopic description of the two-phase flow heat and mass transfer in porous medium was developed by [Duval02], [Duval04]. The model is obtained based on a pore-scale quasi-static assumption for the momentum equation closure [Auriault87] [Lasseux96] i.e., the interfaces do not change rapidly in comparison with viscous dissipation. It is important to notice that this assumption may break down in the case of intense boiling. The heat transfer closure raises the traditional problem of representing complex non-local effects in space and time, which often are best represented by full convolution products. The outcome of Duval (2002) studies are the effective transport coefficients determined on the basis of a comprehensive analysis of the relationship between the pore-scale physics and the macroscopic description. The pore-scale closure problems allowed to determine all the effective transport coefficients for unit cells representative for the porous medium. In particular, attention was paid to simple one-dimensional unit cells for which analytical solutions could be obtained. In this thesis, we will start from that last model to analyse its deficiencies and propose improvements, keeping, as much as possible, the benefits from the previous theoretical developments.

1.4 OBJECTIVES OF THIS THESIS

In this context, the objectives of the present research work are to understand the physical phenomena that occur in the case of reflooding of debris bed initially at high temperature. Here, we want to reduce the uncertainties in order to be capable to develop models applicable to reactor situations. These models, implemented into computer codes should be able to predict the scenario of reflood of degraded core in a case of severe accident.

A large R&D program is made at IRSN, which includes experimental facilities as well as model development. The present work was aimed at interpreting the experimental results obtained in those new facilities and to develop a detailed heat transfer and two-phase flow model into the computer code ICARE-CATHARE .

Before this thesis, specific models were developed to simulate the flow in porous medium, that is a representative geometry of degraded core [Bechaud01]. However, the models showed some limitations:

- The evaluation of the characteristic geometries and reflood conditions were not completed;
- The validation of models was very limited.

In this context, this thesis constitutes the first comprehensive set of modeling and validation covering a large range of reflooding conditions. The plan of this document corresponds to the methodology that was followed. Firstly, the studies of worldwide experimental programs concerning the dry-out and reflood of debris bed were made. Two sources of information were used for more detailed analyses: PETIT dry-out experiment (1998) and PRELUDE

experimental program (2009-2012). The interpretation of those experiments provides useful information about the characteristic features of water progression, steam production and pressure gradient. The objective of the second Chapter is to present the macroscopic model of two-phase flow in porous medium initially developed in the thesis of Duval [Duval02]. It is characterized by treatment of non-equilibrium between three phases (solid, liquid and gas). It includes also two momentum balance equations. Other models are also briefly discussed. In the next Chapter, significant improvements of the model were proposed and concern mainly the heat transfer modeling for different flow boiling zones. The criteria characterizing the transition between different flow regimes were also completed. In the next Chapter, the proposed model of reflood of debris bed is implemented into ICARE-CATHARE code and the quantitative validation of model results with PETIT dry-out and PRELUDE reflood experimental results is presented. The reflood calculations concern the experiments with different initial temperatures, injection velocities and particle diameters. Finally, the issue of validity and applicability of the model at the large scale corresponding to the reactor is discussed. Some applications are shown in the last chapters in order to show the phenomena playing an important role at a large scale. Those preliminary reactor application also demonstrate the interest of the developed model for optimizing accident management procedures involving water injection.

Chapter 2

EXPERIMENTAL STUDIES

2. EXPERIMENTAL STUDIES

The available knowledge about debris bed cooling consists in many international experimental programs that were performed in the past 30 years, in models proposed to interpret the experiments or to simulate the behavior of larger debris bed, allowing quantitative evaluations of reactor scenarios. The experimental knowledge is summarized in the present Chapter. It will be divided into two different types of experiments: dry-out and reflood experiments. Since the present work deals mainly with heat transfer modeling, more emphasis will be put on reflood experiments.

This bibliographic study of international experimental programs includes dry-out tests (SILFIDE, STYX, POMECO, DEBRIS and PETIT), top reflood tests (Ginsberg, Dhir, DEBRIS) and bottom reflood tests (Tutu, DEBRIS and PRELUDE). The dry-out experimental studies have focused on the determination of the "critical" or "dry-out" heat flux DHF which is the maximum volumetric power that can be removed by unit surface of a debris bed by evaporating water. It gives the limiting volumetric power for which it is possible to ensure that a steady state at saturation temperature can be maintained. As it will be explained later, dry-out occurs when water penetration from the top of the bed is stopped (at least at one location of the bed) by the counter current of steam generated in the bed. The first experiments considered in this Chapter were performed in the 80's and from that time, the experimental techniques improved in order to get more accurate and representative results. In spite of the progress made, the experimental conditions may still influence the dry-out heat flux and are still a matter of discussion. Some conclusions will be summarized here.

Two sources of information were used for more detailed analyses: PETIT dry-out experiment and PRELUDE experimental program. The reason for that comes from the direct access to experimental data instead of using published data which are often incomplete. Those experimental results will be used later for the validation of the two-phase flow model (see Chapter 5). Therefore, in this Chapter, a thorough discussion and interpretation of the results are given, in order to draw conclusions about the physical phenomena that should be taken into account in the modeling.

- **Heating mode**

The first Tutu [Tutu84] and Ginsberg [Ginsberg86] reflood experiments were performed by *preheating the particles with a circulation of hot air*. As an alternative, the POMECO debris bed [Kazachkov02] was heated using *internal heaters*. A discussion about the heating method was provided by Ma and Dinh [Ma10] who concluded that the heaters should be small and evenly distributed. However, the *induction heating* was selected by many experimental programs as the most relevant method to simulate decay heat generated by reactor core. This heating technique was used at UCLA by Wang and Dhir [Wang88] and more recently in

SILFIDE [Atkhen06], DEBRIS [Rashid11] or PRELUDE facilities [Repetto12]. Compared to electrical heating, which creates local hot spots, the uniform induction heating is considered to produce different phase distributions and hydrodynamic patterns within the porous media in the boiling regimes. Inductively heated beds, like in the SILFIDE experiment, lead to a preferential vaporization in contact with the debris. This may have consequences for the capabilities of penetrating liquid coolant to replace the vaporized one, or in overheating phenomena, as observed in SILFIDE [Atkhen06]. Moreover, the objective of current experimental programs as PRELUDE [Repetto12] is to maintain the power during reflooding in order to simulate the reactor representative situation. Compared with previous experiments, the PRELUDE results showed that the power maintained during reflood extends the duration of steam production while its impact on local cooling during quenching was observed to be negligible [Repetto12].

- **Debris bed configuration**

A bed-averaged porosity (normally around 40% for beds of single size spheres) is usually measured and difficult to calculate. However, realistic particle beds could also vary laterally in height and they might contain regions with different composition and porosity. Locally, mixtures of particles of different sizes, i.e. multigrain compositions, and with irregular shapes are to be expected. Spatial variations of such local configurations are to be expected rather than uniform conditions [Burger04]. The experiments dealing with homogeneous beds gave an idea of the boiling, dry-out or post-dry-out phenomena (Ginsberg, Tutu or Dhir experiments). However, recent objectives are to evaluate the influence of multidimensional effects. Heterogeneities lead to preferential flow paths, and are known to have a strong impact on hydrodynamic instability patterns, such as natural convection. For instance, **heterogeneous configurations** of a particle bed such as mound-like accumulations or gap structures could favor lateral water access to bottom regions. These configurations were studied at DEBRIS [Rashid11] or STYX experiments [Lindholm06] and have actually led to a higher dry-out heat flux (DHF).

- **Particle diameter and debris bed height**

In addition to the bed porosity, the mean particle size is an important parameter (notably through its impact on permeability and exchange coefficients) which has not be clearly defined up to now. The objective of different studies [Lindholm06], [Li11] was to investigate two-phase flow regimes and frictional resistance characteristics in porous media packed with multidiameter spheres. The effective particle diameter was found to be comparable to the area mean diameter of the particles [Li11]. In all studies of dry-out heat [Dhir97], [Burger06] it was concluded that the **particle diameter** represents the most important length scale and it is one the most sensitive parameters of models [Yakush11]. For large particles spatial variations in the porous medium properties and their effect on the constitutive relations, and coupling (i.e. boundary conditions) between the overlying liquid layer and the porous medium are

considered to be important parameters. The DEBRIS experiments observed that the DHF decreases with particle diameter [Schafer06].
Dhir (1997) also distinguished two types of debris bed according to their **height: deep or shallow**. Their experimental observations identified different mechanisms for the dry-out in these beds. It was concluded that the deep bed dries out primarily in the lower regions of the bed where water flowing down by gravity is not sufficient to compensate for the evaporation rate. However, the particles are not constrained and can rearrange themselves depending on the nature of the forces that act on them. Thus, the channels can be formed that tend to grow in diameter in the direction of vapor flow. The effect of the presence of the channels might reduce the effective height of the volumetrically heated porous layer and thereby lead to a higher dry-out heat flux [Dhir97].

- **System pressure**

It was observed by several authors [Rashid01], [Lindholm06] that with increasing **system pressure**, the pressure drop across the porous bed does not change significantly, but there is a strong increase in dry-out heat flux, which results in enhanced coolability of the bed. This can be attributed to the fact that the vapor density increases strongly so the mass flow rate at dry-out conditions is larger. The decrease of latent heat of vaporization (with increasing pressure) has a less significant effect in the maximum heat flux.

2.1 DRY-OUT OF DEBRIS BED

Most of the research on natural convection in volumetrically heated pools and on dry-out heat flux in particulate layers was dedicated to resolution of issues related to post-accident heat removal. Some studies were also motivated by their application to heat removal in nuclear waste disposal or single and two-phase convection in geological systems [Dhir97], [Jamialahmadi05], [Fitzgerald98], [Fourar00].
Removal of decay heat from a debris bed by transferring heat to water is an interesting issue either for in-vessel or ex-vessel situations of PWR severe accidents. Knowledge of maximum possible heat removal rate from a particulate bed without dry-out is essential for assessment of the risks associated to core damage accidents and for development of strategies to mitigate their consequences. A debris bed formed in the residual water located in the lower plenum may help to delay the time of the vessel failure. If the heat flux due to decay heat is below the maximum possible heat removal rate without dry-out, the debris bed will be in a coolable state. When the critical heat flux is reached, a flooding phenomenon occurs, i.e. the counter-current of steam induces friction forces which are sufficient to limit the downward progression of water. Therefore, there is not enough water entering the bed to compensate evaporation. This leads to a (partial) dry-out at a particular location in the bed. Then, due to the poorer heat transfer in the dry regions, they will heat up and possibly reach their melting temperature. If the molten region expands, it may reach the vessel and threaten its integrity.

2.1.1 Theoretical studies on dry-out heat flux

In a pure 1D configuration with a water reservoir on top of the porous bed, the up-flowing steam and the down-flowing water are in counter-current flow configuration. A limit of coolability, corresponding to the dry-out heat flux, can be determined by the counter-current flooding limit. Thus, the friction laws for the flow in the porous particle bed determine the dry-out heat flux. The motion of the fluids is hindered by the friction along the particles as well as by the existence of the other phase [Schmidt06]. The two-phase frictional pressure drop is usually based on some modified form of the single-phase Ergun equation:

$$-\left.\frac{\mathrm{dP}}{\mathrm{dz}}\right|_{\text{friction}} = \frac{\mu\ \mathrm{j}}{\mathrm{K}} + \frac{\rho\,\mathrm{j}^2}{\eta} \tag{2.1}$$

For uniform spherical particles, the intrinsic permeability and passability are correlated with the average particle diameter d_p and the porosity ε by the Carman-Kozeny relation [Carman37] and Ergun law [Ergun52]:

$$\mathrm{K} = \frac{\mathrm{d_p^2}\varepsilon^3}{\mathrm{A}(1-\varepsilon)^2} \tag{2.2}$$

$$\eta = \frac{\mathrm{d_p}\varepsilon^3}{\mathrm{B}(1-\varepsilon)} \tag{2.3}$$

where the Ergun constants A and B are estimated experimentally and usually $A=180$ and $B=1.75$ are used.

Most models for multiphase flows in a porous medium are based on an extension of the equation (2.1), in which each fluid phase is driven by its own pressure gradient. A modified form of this equation is used for each of the two phases. Firstly, it was shown that for a two-phase flow through the porous medium of low specific permeability ($<10^{-10}$ m^2), at a low Reynolds number (Darcy flow regime), the frictional pressure drop encountered by each phase can be described by the Darcy law provided the permeability is modified [Muskat49]. Thus the second term on the right-hand side of equation (2.1) is neglected and K is replaced by $K.K_{rL}$ in the equation for the liquid phase, and by $K.K_{rG}$ in the equation for the gas phase, where K_{rL} and K_{rG} are called the relative permeabilities. In most studies, the relative permeabilities have been expressed as a function of phase saturation volume fractions only but they are likely to depend also on other parameters [Kaviany91], [Scheidegger60].

Firstly, there was a lack of experimental data concerning the porous beds of large specific permeability ($>10^{-8}$ m^2) and at large Reynolds numbers where the inertia term (the second term on the right-hand side of equation (2.1)) cannot be neglected. In the absence of such data, Lipinski (1982), following the approaches commonly accepted [Kaviany91] simply extended the foregoing result to large permeability beds replacing η in equation (2.1) by $\eta.\eta_{rG}$ for the gas phase (with $\eta_{rG}= K_{rG}$), and by $\eta.\eta_{rL}$ for the liquid phase (with $\eta_{rL}= K_{rL}$). Later, several variants for the relative permeability and passability were proposed to better

reproduce the results obtained in dryout heat flux experiments, but the general form of friction terms was unchanged. Lipinski (1981) used $K_r=\beta^3$ (β=phase volume fraction in the pores) and assumed the same exponent for the relative passability $\eta_r=\beta^3$. Based on his own dry-out experiments that yielded a smaller dry-out heat flux, Reed (1982) proposed an exponent *m=5* for the relative passabilities. This exponent was also used by Lipinski in later publications (1984). The dry-out heat flux calculated with this approach fits well with the experimental values for top fed particulate bed configurations. Additionally, Hu and Theofanous (1991) pointed out that in most of the experiments the ratio of the test section diameter to the particle size was too small, yielding increased water flow along the walls. They proposed an exponent *m=6* yielding a smaller dry-out heat flux. The summary of the classical models is given Table 2.1.

Table 2.1: Relative permeability and passability in the classical formulations

	Relative permeability		Relative passability	
	K_{rG}	K_{rL}	η_{rG}	η_{rL}
Lipinski (1981) Brooks and Corey (1966)	α^3	$(1-\alpha)^3$	α^3	$(1-\alpha)^3$
Reed (1982)	α^3	$(1-\alpha)^3$	α^5	$(1-\alpha)^5$
Hu and Theofanous (1991)	α^3	$(1-\alpha)^3$	α^6	$(1-\alpha)^6$

*Note: Later in this thesis, Lipinski model will be related to exponent 3 in the relative passability term and Reed model to exponent 5.

However, there is still a lack of information on interfacial drag forces. Except the work of Schulenberg and Muller [Schulenberg87], there are no experimental data which were directly used to estimate the interfacial gas-liquid drag and this force is sometimes neglected in analysis of two-phase flows through porous beds. Tutu and Ginsberg (1984) concluded, from air-water experiments, for the case of zero liquid flux, that for beds of large particle size (>6 mm), the interfacial gas-liquid drag term is important, in particular at low superficial velocities. Afterwards, the interfacial drag force decreases with decreasing particle size. Schulenberg and Muller (1987) proposed a correlation for interfacial drag as follows:

$$F_i = 350(1-\alpha)^7 \alpha \frac{\rho_l K}{\eta\sigma}(\rho_l - \rho_g)g\left(\frac{j_g}{\alpha} - \frac{j_l}{(1-\alpha)}\right)^2 \tag{2.4}$$

This term was introduced in previous 1D reflooding calculations to check the sensitivity [Fichot06]. However, its impact could not be estimated properly because of the strong dependence of the results with other terms, including heat exchange terms. Even now, it seems that there is no other satisfactory correlation available in the literature. The momentum balance equations including the interfacial friction are as follows:

$$-\nabla p_l = -\rho_l g + \frac{\mu_l}{K K_{rl}(\alpha)} j_l + \frac{\rho_l}{\eta \eta_{rl}(\alpha)} |j_l| j_l - \frac{F_i}{1-\alpha} \tag{2.5}$$

$$-\nabla p_g = -\rho_g g + \frac{\mu_g}{KK_{rg}(\alpha)} j_g + \frac{\rho_g}{\eta\eta_{rg}(\alpha)} |j_g| j_g + \frac{F_i}{\alpha} \tag{2.6}$$

where F_i is the interfacial drag force and other variables can be found in Nomenclature.

Recently, a very interesting work [Yakush11] has shown that it is possible to optimize the model parameters in order to get the best fit of existing data on either the DHF value or the pressure gradient across the bed. It appears that the interfacial drag term has a negligible impact on DHF and that the best value of the exponent in the relative permeability and passability is close to 4. However, interfacial friction is more important to be able to predict the pressure gradient.

The average velocity of each phase is calculated from the pressure gradient of the phase. The introduction of the two pressure fields leaves the equation system unclosed. To close the equation system, a relation must be introduced. Leverett generalized the concept of capillary pressure and assumed that the pressure difference between the two phases was proportional to the average pressure jump in the pores. It is generally modeled as a function of the saturation:

$$p_c = \langle p_g \rangle^g - \langle p_l \rangle^l = \sigma \cos\theta \left(\varepsilon(K)^{-1} \right)^{1/2} J(S) \tag{2.7}$$

where J is the Leverett function expressed according to [Leverett41]:

$$J(S) = \begin{cases} 1.5 - 9.2S + \frac{88}{3}S^2 - \frac{880}{27}S^3 & \text{for } 0 < S < 0.3 \\ 0.62 - 0.4S & \text{for } 0.3 \le S < 0.8 \\ 14.7 - 53.2S + 66S^2 - \frac{55}{2}S^3 & \text{for } 0.8 \le S < 1 \end{cases} \tag{2.8}$$

Lipinski 0D criterion

Among all the existing models, the Lipinski model is still a reference because it estimates the order of magnitude of the dry-out heat flux, in a large range of particle diameters. This quasi-steady model is based on the momentum balance equations presented above. The model includes the capillary effects. This model provides the maximum heat flux that may be extracted by steam at the top of the debris bed [Decossin00]. For particle diameters greater than 1mm, the dry-out heat flux is as follows:

$$\phi_{dry} = \frac{h_{lv}\sqrt{\rho_v(\rho_l-\rho_v)g\eta\left(1+\frac{\lambda_c}{H}\right)}}{\left(1+\left(\frac{\rho_v}{\rho_l}\right)^{1/4}\right)^2}$$
$$\lambda_c = \frac{\sigma\sqrt{\frac{\varepsilon}{K}}}{\sqrt{5}(\rho_l-\rho_v)g} \qquad (2.9)$$

The quantity λ_c represents the depth of the bed drained by liquid due to capillary forces, K and η are the permeability and passability terms detailed in (2.2) and (2.3) and other variables can be found in Nomenclature. If the capillary effects tend to zero, the only force that remains in the square root is the gravity.

Lipinski 1D criterion

The Lipinski 0D model gives no information about the internal phenomena in a debris bed (like the profile of void fraction and position of local dry-out) and their impact on the robustness of the predicted value of dry-out heat flux. From this point of view, the extension 1D represents a significant progress. This allows determining the dry-out heat flux and the saturation profiles at the top of the bed. The determination of dry-out heat flux in the general case requires a numerical resolution that reduces to an algebraic relation if the capillary forces are neglected. The saturation profile can be calculated for different internal distributions of volumetric power and 1D distributions of particle diameters (stratified beds). The advantage of the 1D model is the prediction of the position of dry-out zone. Lipinski defines also the height of the bed for which the formulation is valid [Decossin00]. The following formulation is valid for debris bed height higher than 80mm if the bed is composed by steel particles submerged into water:

$$\phi_{dry} = \sqrt{\frac{q_t^4}{4q_l^2}+q_t^2}-\frac{q_t^2}{2q_l}$$
$$q_t = h_{lv}\frac{\sqrt{\rho_v(\rho_l-\rho_v)g\eta\left(1+\frac{\lambda_c}{H}\right)}}{\left(1+\left(\frac{\rho_v}{\rho_l}\right)^{1/6}\right)^3} \quad q_l = h_{lv}\frac{(\rho_l-\rho_v)gK\left(1+\frac{\lambda_c}{H}\right)}{\left(\mu_v^{1/4}+\mu_l^{1/4}\right)^4} \qquad (2.10)$$

where μ_v and μ_l are the viscosities of steam and liquid and other variables can be found in Nomenclature.

2.1.2 Database of dry-out experimental results

In the experimental procedures, the bed is heated up to the saturation temperature at a constant pressure until steady-state boiling condition is reached. Then, the heating power is increased in small steps until the dry-out is reached. A significant and fast increase in bed temperature above the saturation temperature is associated to the occurrence of dry-out [Rashid11]. Hu and Theofanous (1991) criticized this measurement method and explained that the resulting dry-out heat flux values would be too high because the power was increased further before the dry-out was detected.

The most recent dry-out experiments were made in the last ten years in Europe in the SILFIDE, STYX, POMECO and DEBRIS facilities. In those experiments, the **top flooding** is **driven by gravity** from the water pool above the bed. The debris bed is filled with water before the heating starts. The facilities are shown in Figure 2.1 and test conditions are summarized in Table 2.1.

The SILFIDE experiments [Decossin00] were made at EDF in order to enhance R&D on debris bed coolability for in-vessel or ex-vessel scenarios in French PWRs. The STYX experiments [Lindholm06] were made at VTT in Finland to simulate an ex-vessel particle bed in the conditions of Olkiluoto power plant. The main objective of SILFIDE was to simulate the multidimensional convection within a volumetrically heated debris bed (i.e. truly generated within the simulated debris) whereas the STYX experiment simulated irregularly shaped multi-grain configurations heated electrically.

- The difference in the formation of **dry zone** in homogeneous beds was observed between SILFIDE and STYX experiments. In STYX experiments under top flooding, the dry zone formed near the bottom of the bed. In SILFIDE experiments, the dry-out areas located in the upper part of the bed were observed due to 2D situation. In conclusion, in the 2D situation, the lateral water flows prevents dry-out near the bottom and produces different results compared to STYX 1D situation.
- Moreover, the STYX experiments concluded that the bed **heterogeneities** and **pressure** influence the critical heat flux. The critical heat flux in heterogeneous beds was observed to be only 20-26% higher than in homogeneous beds. The pressure effect on critical heat flux was more obvious; it increased up to 50% at 0.7MPa compared to that observed at atmospheric pressure [Lindholm06].
- The analytical studies of dry-out heat flux correlations were performed both by STYX and SILFIDE experimental groups. In conclusion, the existing calculation models e.g. Lipinski 1D underestimates the critical heat flux compared to that observed in SILFIDE

2D facility and overestimates the critical heat flux compared to that observed in STYX heterogeneous particle bed facility.

The POMECO experiments [Kazachkov02] were made at KTH in Sweden in order to study the ex-vessel debris bed coolability that can occur in a Swedish BWR after melt-water interaction scenario in the containment cavity. The DEBRIS experiments [Rashid11] were made at IKE in Germany. In both experiments, a special geometry, with a downcomer was constructed. The downcomer offers a low resistance flow path for water and as in realistic multidimensional configurations; the lateral water access and water inflow via bottom regions are favored. When the downcomer is closed at the top, the **boiling tests** are realized under **top flooding** (gravity driven flow). When the downcomer is open both at top and bottom, **bottom flooding** occurs due to natural circulation.

- The DEBRIS experiments were performed for polydispersed beds (mixture of steel balls of 2, 3 and 6mm diameter) at different system pressure (0.1, 0.3 and 0.5 MPa). It was concluded that with increasing system pressure and change from top to bottom flooding flow condition, a strong increase of dry-out heat fluxes can be observed which improves the bed coolability.
- The POMECO experiment focused on low porosity, small particle size (<1mm), heated electrically. Those experiments confirmed that the downcomers enhance the magnitude of dry-out heat flux. The experimental analysis concentrated on identification of the effective diameter in the bed packed with nonspherical particles. For the effective diameter (calculated with Sauter average), the dry-out heat flux was well predicted by Reed's model for top-flooding. Reed's model is too low (more conservative) with increasing flow rate of the bottom injection [Repetto12]. It was shown that the beds with porosity ~40% and particle size ~2 mm were coolable with top flooding. Lower porosity and smaller particle beds are not easily coolable, except when water is injected from the bottom [Sehgal11].

These experiments allowed concluding that the dry-out heat flux of bottom-flooding with open downcomer could be nearly two times higher than that of top-flooding with closed downcomer).

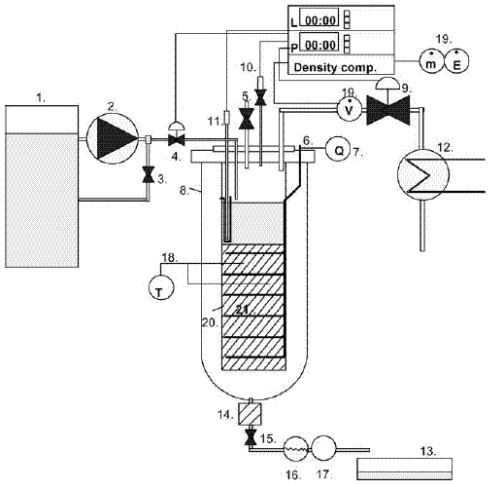

STYX facility

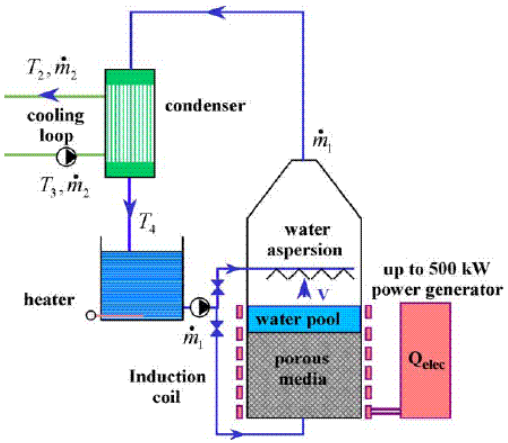

SILFIDE facility

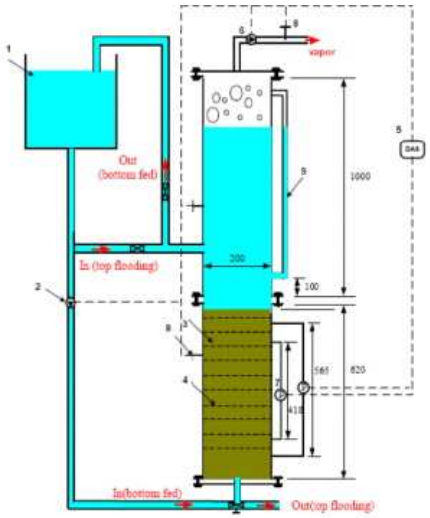

POMECO facility

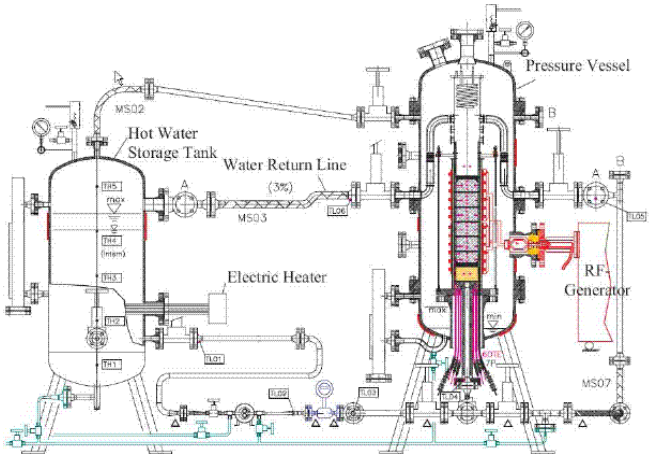

DEBRIS facility

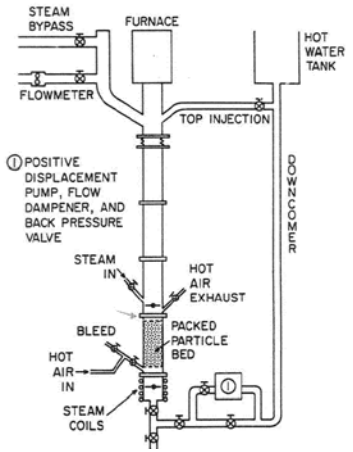

Ginsberg, Tutu facility

Figure 2.1: Dry-out and reflood of debris bed experimental facilities

Table 2.2: Test conditions at different dry-out and reflood facilities

DRY-OUT EXPERIMENTS				
	STYX (VTT Finland)	**SILFIDE** (EDF France)	**POMECO** (KTH Sweden)	**DEBRIS** (IKE Germany)
Particle diameter	0.25-10mm (mass-averaged size 3.4mm)	2; 3.17 and 7.18mm	0.2-1mm	3-6mm
Dimensions	300mm x 600mm	500mm x600mm x100mm	H=450mm (bed diameter 350mm)	H=640mm (125mm bed diameter)
Particle material	Al_2O_3	Steel	Stainless steel	Pre-oxidized stainless steel
Pressure	Atmospheric – 0.7 MPa	Atmospheric	Atmospheric	Atmospheric -0.5 MPa

REFLOOD EXPERIMENTS					
	Ginsberg (USA)	**Tutu** (USA)	**Dhir** (USA)	**DEBRIS** (IKE Germany)	
Particle diameter	0.89mm, 3.18mm, 6.35mm, 12.7mm	3.175mm	4.8mm	3 and 6mm	
Dimensions	H=300mm - 400mm (bed diameter 108mm)	H=422mm (bed diameter 108mm)	H=550mm (bed diameter 186.2mm)	640mm (125mm bed diameter)	
Particle material	Stainless steel	Stainless steel 302	Stainless steel	Pre-oxidized stainless steel	
Water subcooling	0	0	0-75	80	
Initial temperature	Top flooding 260 °C – 704 °C	Bottom flooding 238 °C, 321 °C, 502 °C	Top flooding, Bottom flooding 889-979 °C	Top flooding 200-900°C	Bottom flooding 430°C
Liquid flow	Driven by the gravity head	1.01, 1.98, 4.42, 7.4mm/s	Driven by the gravity head	Driven by the gravity head	

2.2 PETIT DRY-OUT EXPERIMENT

A series of boiling experiments in porous medium were performed during F. Petit's doctoral thesis in 1998 [Petit98] at ENSAM in Bordeaux, France. The objective of those experiments was to observe different flow regimes occurring during boiling in a porous medium with internal source i.e. liquid single-phase flow, two-phase flow and gas-single phase flow. The experimental results will be summarized here. The experimental results will be later compared with two-phase flow model results (see Chapter 5 dedicated to validation of modeling).

2.2.1 Description of PETIT's facility

The experimental facility is a rectangular tube made of glass with dimensions 25x25x250mm (see Figure 2.2). The tube is filled with steel particles up to ¾ of its height. The tests were performed with 6mm diameter particles with porosity 0.45 [Petit98]. The particle bed was heated uniformly by induction from its elevation 40mm up to 140mm. The maximum heating power of the inductor was 3000W. A variable range of heating power was tested (10-60%). From the beginning of experiment, there was a water source injection at the bottom of the rectangular tube. The effect of different liquid flow rates on the appearance of boiling regimes was tested (for the following values 9.9, 15, 20.1, 27.9 ml/min).

The positions of thermocouples are shown on Figure 2.2. The thermocouples were installed as follows:

- TC2: Thermocouple installed above the porous medium, in a free space at the top of the tube.
- TC3: Thermocouple installed at the highest elevation of the porous medium, in a pore.
- TC4: Thermocouple installed about 1.5cm below TC3, close to a particle.
- TC5: Thermocouple installed about 1.5cm below TC4, in a pore.
- TC6: Thermocouple measuring the temperature of a particle. It is located at the interface between the zone that is not heated (at bottom) and the zone that is heated.
- TC7: Thermocouple installed in a pore, at the same position as TC6.
- TC8: Thermocouple installed in a free space under the porous medium.

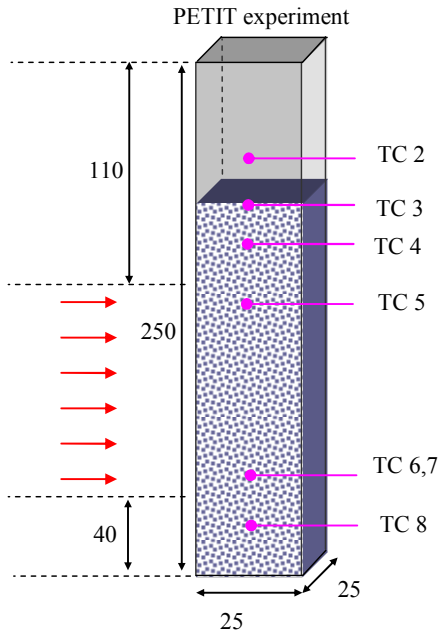

Figure 2.2: Petit experimental facility (dimensions in mm)

The evolution of the system during the tests was observed as follows (see Figure 2.3):

- Increase of temperature up to saturation temperature.
- Stabilization of system at saturation temperature. The duration of steady state depends on the injected power.
- For a sufficiently high power (i.e. 38% for a flow 15 ml/min) the dry-out appears.
- In dry-out zone, there is a strong increase of temperatures.
- Thermal equilibrium resulting in a stabilization of temperature appears (see Figure 2.3), it depends on injected power, liquid flow and losses in the system.

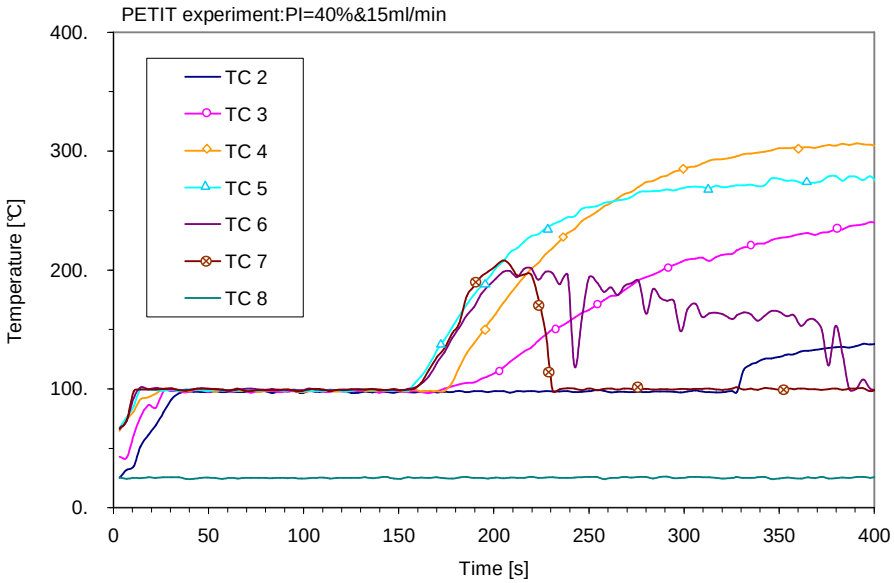

Figure 2.3: Evolution of system during heating. Petit experiment with heating power of 1200 W and liquid flow 15 ml/min

2.2.2 Experimental results

The first experiments measured the increase of temperature in porous medium up to the saturation temperature. At the initial state, the tube was filled with water with temperature 11°C (temperature indicated by thermocouples in [Petit98]). The water was injected at the bottom and the heating power corresponded to 15% of maximum heating power of the inductor i.e. 450W.

The temperature evolution measured at TC3 for different liquid flows is shown in Figure 2.4 (left). Compared to temperature evolution at TC4, the increase of temperature starts later. The reason is that TC3 is situated about 1.5cm above TC4 and there is no direct influence of the inductor, therefore it is heated by convection only, which is a slower process. The high increase of the temperature between 80 and 100 s is due to the effect of boiling in the upstream area. This seems to demonstrate that steam and water are not at thermal equilibrium, which has to be taken into account in the modeling.
The temperature profile at TC2 is shown in Figure 2.15 (right). The later increase of temperature at this position is more visible. From the time 80 s, some "instabilities" appear in the flow. This is clearly visible as oscillations of the thermocouple temperature because it is situated at the top of the tube, above the porous medium. On the other hand, after 80s, the experimental fluctuations are not predicted by calculations, probably because they are produced by intermittent dry-out and rewetting of the thermocouple, which cannot be modeled with a purely macroscopic approach.
At this point, we must also mention a limit of the comparison between experimental and theoretical results. The temperature as measured by the thermocouples is likely to represent a value closer to a point pore-scale value, given the characteristics of the device, while it is not clear what is the size of the control volume, nor which weighting function is associated with the measurement. The true measure is probably some time and space average, with a characteristic time roughly less than 1s and a characteristic control volume length smaller than the pore radius. On the opposite, theoretical results are obviously volume averaged values, and, in addition, they are time-averaged in the semi-heuristic model proposed to take care of the various pore-scale boiling regimes. Therefore, a direct comparison is not entirely relevant.

Finally, if the injected power is sufficiently high, the zone with *gas single phase* will appear at a certain elevation in the porous medium. The dependence of this elevation on the injected power and liquid flow rate was studied experimentally. In the Petit experiment, the elevation where the dry zone appeared was identified. According to Petit [Petit98], this elevation was identified from visual observations as well as temperature measurements for the cases where a steady state was reached. When a first dry-out occurred in the porous medium, the injected power was decreased in order to avoid fast temperature escalation. The Figure 2.5 shows that the position of dry-out zone depends on power to liquid flow ratio.

Those results will be used to validate the convective heat transfer correlations, as well as the boiling heat transfer correlation in the nucleate boiling regime (for particle temperature close to saturation)

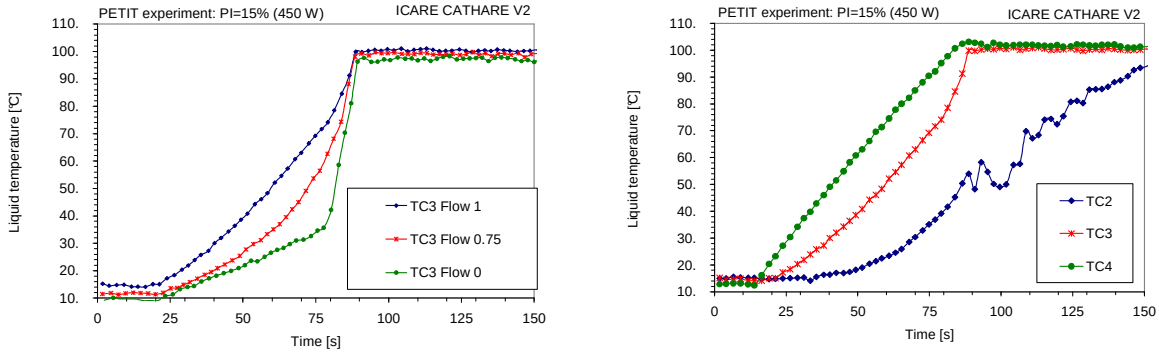

Figure 2.4: Temperature evolution at TC 3. 1: 15 ml/min, Flow 0.75: 2.175 ml/min, Flow 0: natural circulation (left); Temperature evolutions for a test with liquid flow 15 ml/min (right)

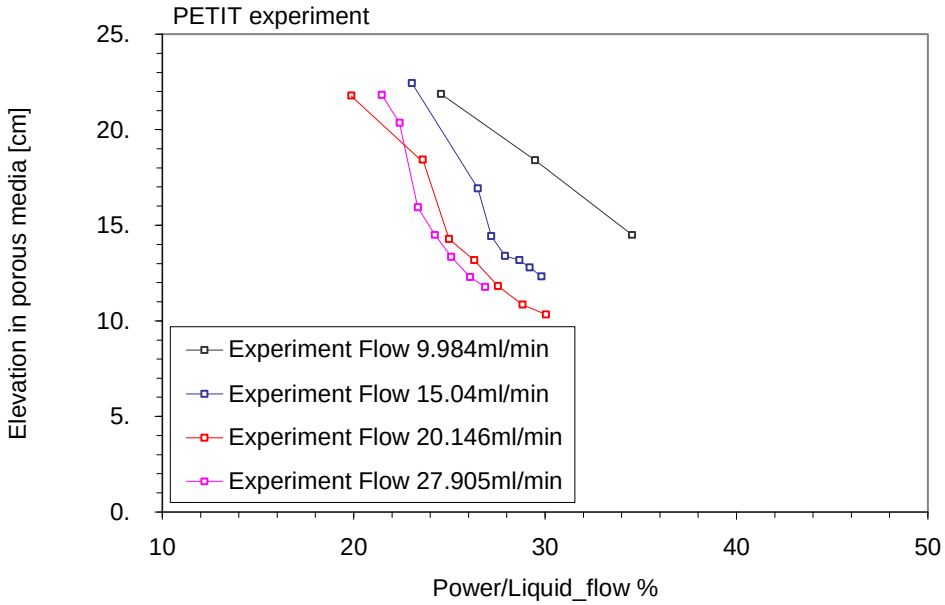

Figure 2.5: Position of dry-out as a function of power divided by liquid injection flow rate

2.3 REFLOOD OF DEBRIS BED

Reflooding of a debris bed is a crucial issue for reactor safety, as it was explained in the introduction. Different in-vessel reflooding situations may exist in PWRs, depending on time since the beginning of the accident and on core configurations at time of reflooding. Firstly, the water is injected into the cold legs of the primary circuit which results in a core **bottom reflooding**. Afterwards, water is simultaneously injected into the cold and hot legs. Hot leg injection corresponds to a core **top reflooding**. The phenomenology is different for each situation. Bottom flooding induces co-current flows of water and steam whereas top flooding

induces strong counter-current flows, similar to the dry-out process. After the first corium relocation into the vessel lower plenum, those procedures could be equivalent, since water can only enter from the top [Dorsselaere06].

2.3.1 Top and bottom reflooding

Limitation of coolability occurs at much higher heating rates (or dry-out heat fluxes), if there is coolant. It was already shown by the experiments of [Hofmann84] that water supply from the **bottom** could yield more than twice the values of maximum heat flux (or DHF) removed from the bed. This was measured for a case with 3 mm spheres and water supply from a lateral water column of the same height as the bed, i.e. driven by hydrostatic pressure. The experiments with downcomer at DEBRIS [Rashid11] and POMECO [Kazachkov01] facilities also had a low resistance flow path for water. As it was explained before, in top-flooding experiments with opened downcomer, the water flowing through the downcomer establishes an upwards flow from the bed's bottom (bottom-flooding) which enhances the coolability of the heated bed and increased the dry-out heat flux.

The effect can be understood from the water supply via regions of low void (in contrast to top flooding) and the co-current flow mode. In counter-current flow mode under top flooding conditions), there is an instability (Rayleigh-Taylor type) of relative flow of liquid and vapor destroying the flow pattern and yielding transition to patterns where phases are well mixed and the "counter-current flow limitation (CCFL)" occurs. An alternative understanding is to assume a drastic increase of friction between liquid and debris occurring with significantly reduced volume for the liquid, thus yielding the failure of steady state and resulting in transient boil-off. The "counter-current flow limitation" as a limitation of downflow of water against upflow of steam, due to interfacial instabilities, is usually taken as the basic physical explanation [Burger06]. For the bottom flooding the water flow has the same direction as the vapor flow, therefore, there is no possibility of water flow limitation. Indeed, it will be shown from experimental results that the steam flow produced is proportional to the injected water flow. The dry-out is therefore controlled by water inflow from the bottom as well as from the top. This is why the dry-out heat flux rises with increasing flow rate of bottom injection [Repetto12].

In realistic bed configurations with non-uniform height, non uniform porosity or non uniform permeability, the local flows of water and steam may be either co-current or counter-current, depending on the location. Lateral flow is driven by the lateral pressure gradient establishing due to void fraction increase and high steam velocity in the bed, compared to the hydrostatic head of the liquid water. We see here that the pressure gradient generated by the very intense steam generation during reflooding plays a critical role in the distribution of phase when the bed presents some non-uniformity. This important issue will be discussed further with the interpretation of PRELUDE tests.

2.3.2 Database of reflood experimental results

The reflood experimental procedure differs from dry-out experiments. Here, the debris bed is heated and there is no presence of water. The bed is heated up to the desired temperature and, quenched with water. The water can be injected from the top or from the bottom. The facilities are shown in Figure 2.1 and test conditions are summarized in Table 2.1.

A first series of quenching experiments were performed in Brookhaven National Labs (United States) by Ginsberg [Ginsberg86], Tutu [Tutu84] and Dhir [Wang88]. Later, the bottom and top reflooding experiments were studied in Europe in IKE (Stuttgart) DEBRIS facility [Schäfer06]. All those experimental programs brought interesting data for reflood analysis of debris bed initially at high temperature and will be summarized in this section. However, the current experimental issues are to ensure a more representative geometry and volumetric heating of particles, compared to previous experiments. Recently, IRSN has started the experimental program PEARL (and its preliminary experiment PRELUDE) to study the debris bed reflooding [Repetto11]. The studied geometry and current measuring techniques significantly enhance the database of experimental results. This experimental program will be discussed separately, in Section 2.5.

In Ginsberg experiments, the debris bed was heated up to 700°C and quenched from top. The Tutu experimental program studied the bottom reflood of debris bed initially heated to 500°C. The DEBRIS experiments concentrated both on top and bottom flooding with maximum initial debris bed temperatures of 900°C and 430°C respectively. The main observations are recalled below.

- In Ginsberg top flooding experiments the formation of dry channels was observed. Those channels remained unquenched during the initial downward water progression period, and were quenched only during the final upward refill period. In these experiments, the quenching process was characterized by two steps: partial quench front propagating downwards followed by another front traveling upwards after water had reached the bottom of the bed [Ginsberg86]. The same phenomena were observed in DEBRIS top reflood experiments, where the water penetrated into the bed preferably near wall regions. It was explained as an effect of lower temperature and higher porosity (wall effect). Once the water reached the bottom of the bed, the quench front started to move upwards and the temperature measurements indicated a more or less one-dimensional progression of the quench front.
- The DEBRIS [Schäfer06] and Tutu experiments [Tutu84] studied bottom-flooding phenomena. The Tutu bottom reflooding experiments with imposed liquid flow showed that the average heat flux and the maximum heat flux were observed to increase with increasing water injection rate. For particular cases, the measured heat fluxes were an order of magnitude larger than those observed in top-flooding conditions. The bottom-flooding quenching experiments in DEBRIS facility were mainly one-dimensional

compared to the top-flooding case but not enough tests have been made up to now to draw general conclusions. In particular, there is a potential for an onset of natural convection that may affect the flow configuration.

- The Wang and Dhir experiments [Wang88] were different from the others because the inflow of water was driven by a pressure gradient (water height in an external tank). They concluded that an increased pressure difference across the particulate layer enhances the multi-dimensional effects, i.e. both upwards and lateral progression of water. Another interesting aspect of those experiments was the study of the impact of Zircaloy. The Zircaloy-Steam exothermal reaction increased the local temperature as well as the non condensable (Hydrogen) partial pressure and slowed down the quench front. How ever, this effect of chemical reaction within the debris bed and presence of non condensable gas is outside of the scope of this thesis.

2.4 PEARL EXPERIMENTAL PROGRAM

The objective of the PEARL experimental program [Stenne09] (**P**rogramme **E**xpérimental **A**nalytique sur le **R**enoyage de **L**its de débris) is to extend the validation of debris reflooding models in 2D and 3D situations. It is conducted by IRSN in the frame of the SARNET2 network of excellence on Severe Accident within the 7th European Frame Work Program [Stenne09], and also supported by EDF, The aim is to predict the consequences of the water reflooding of a severely damaged reactor core where a large part of the core has collapsed and formed a debris bed. This means the prediction of debris coolability, front propagation and steam production during the water injection.

The sketch of PEARL facility is shown in Figure 2.6. The debris bed (porous medium: Ø540mm, h=500mm made of 500kg of stainless steel spherical particles) is heated by means of an induction system. It is also possible to have a non heated part at the periphery of the heated bed, in order to simulate a situation where the debris bed does not cover all the reactor core section, which is quite likely. In PEARL experiments, the effect of different pressures, up to 10bar, will be studied. A volumetric power in the particles will be maintained during reflood to simulate the residual power. Concerning the particle diameter in the debris bed, a parallel study is made in order to better estimate the specific exchange surface resulting from the fragmentation of fuel pellets and degradation of claddings [Coindreau09]. Reference particle diameters of 1, 2 and 5 mm were chosen and their effect on reflood process will be tested. Finally, the different reflood scenarios will be performed by changing the inlet water flow 2-20m3/h/m2 (0.555-5.55 mm/s) and subcooling (0, 20 and 50°C). The series of PEARL experiments **will be performed in 2013**. PEARL experiments are foreseen to be performed in configuration never done before, regarding the scaling (*multi-dimensional effects*) and the thermal hydraulics conditions (*high temperature, high pressure and high power deposition during the reflooding* to be representative of the residual power).

To reach these objectives, a step-wise experimental approach has been adopted consisting in launching in 2009 a preliminary program, named PRELUDE, discussed in the following section. The objective of PRELUDE were to test the performance of the induction heating system and to optimize the instrumentation in a two-phase flow (temperature, pressure, water and steam mass flow rates), for a better design of the PEARL facility. However, numerous and significant results could be already obtained in PRELUDE, providing a completely new database for validation of models.

Table 2.3: PEARL test matrix

PEARL test matrix (reference case are in bold)	
Inlet water flow rate (m3/h/m2)	2, 5, **10** and 20
Sub-cooling (K)	0, 20 and **50**
Power (W/kg)	100, **200** and 300
Average particle size (mm)	<1, **2** and 5
Initial pressure (bar)	1, **3** and 5
Initial temperature (K)	**~1300**
Porosity	**0.3 to 0.4**
Smaller particle diameters (~ 0.5mm) to obtain a non-coolable case	

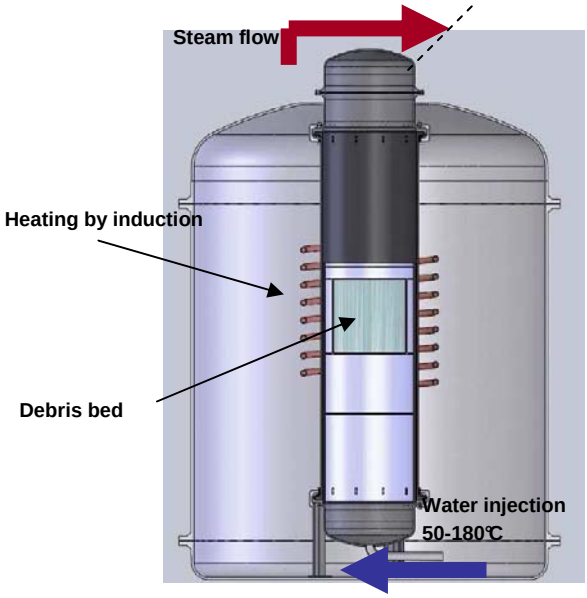

Figure 2.6: PEARL experimental facility

2.5 PRELUDE REFLOOD EXPERIMENTS

The PRELUDE tests were performed at IRSN in Cadarache in 2009-2012. The author of this thesis did not participate to the construction of the facility neither to the test performances. On the other hand, during the thesis, all the experimental data were analyzed and the results were used for validation of the two-phase flow model that will be presented in Chapter 3. In this

Section, the important characteristics of the facility will be summarized. The more detailed information about the design and instrumentation of the facility can be found in [Repetto11]. PRELUDE experiment was designed to optimize the instrumentation and the design of PEARL. The PRELUDE has smaller dimensions and runs only at atmospheric pressure. However, a series of experiments that were performed in 2010-2012 in the PRELUDE facility have provided yet a large amount of new data that significantly enhance the database of experimental results. This includes the prediction of debris cooling rate, front propagation, steam production and pressure difference across the bed during the quenching following water injection. They provide relevant data to understand the progression of the quench front and the intensity of heat transfer. On the basis of those experimental results, thermal hydraulic features at the quench front have been analyzed.

2.5.1 Description of PRELUDE facility

PRELUDE facility (Figure 2.7 A) includes several components:

- A water tank for reflooding with water flow measurement,
- A test section varying from Ø110 mm to Ø290 mm containing an instrumented debris bed with thermocouples and pressure sensors,
- An induction furnace (coil around the test device - Figure 2.7 B),
- A downstream heated vertical tube to remove steam from test section, including temperature and steam mass flow rate measurements.

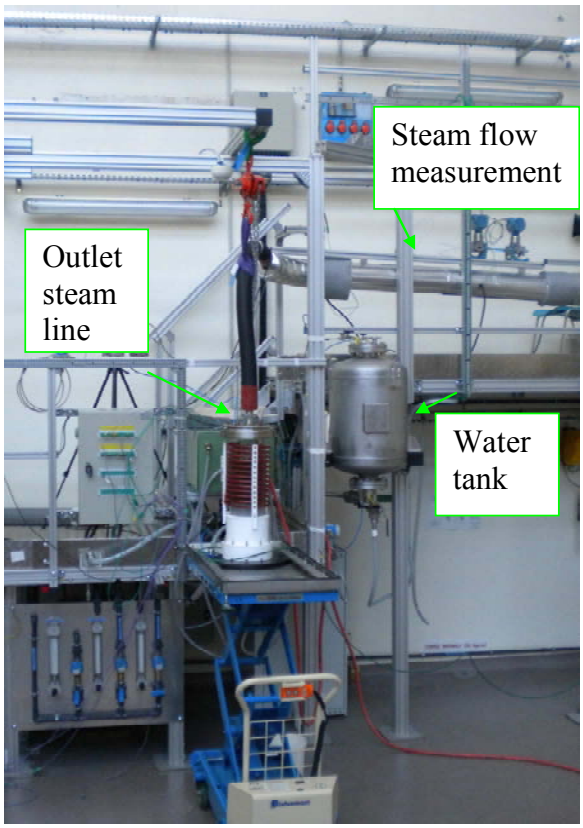

A)

B)

C)

Figure 2.7: PRELUDE facility and test section with inductive heating

The experiment started using a High Frequency generator (25kW/9-50kHz). In order to increase the power deposition inside the porous medium, in particular for small particles size, a Very High frequency generator (6kW/400kHz) was adopted with slight modification of the inductive coil (circular copper plates illustrated on Figure 2.7 C).
The debris bed is inserted inside a quartz tube with different possible configurations as can be seen in Figure 2.8:

- debris bed (p = 0,400 ± 0,003) with stainless steel balls (dp = Ø 1, 2, 4, or 8 mm),
- mixed particles (2/4 mm, 4/8mm,..) to decrease the porosity (p = 0.376 ± 0.006),
- uniform or non uniform shape of the debris.

The stainless steel particles were placed above a bed made of quartz particles with diameter Ø 4 mm (see Figure 2.9 A) in order to avoid placing a metallic grid which would heat-up and possibly melt because of the induction process.

Figure 2.8: Debris bed configuration

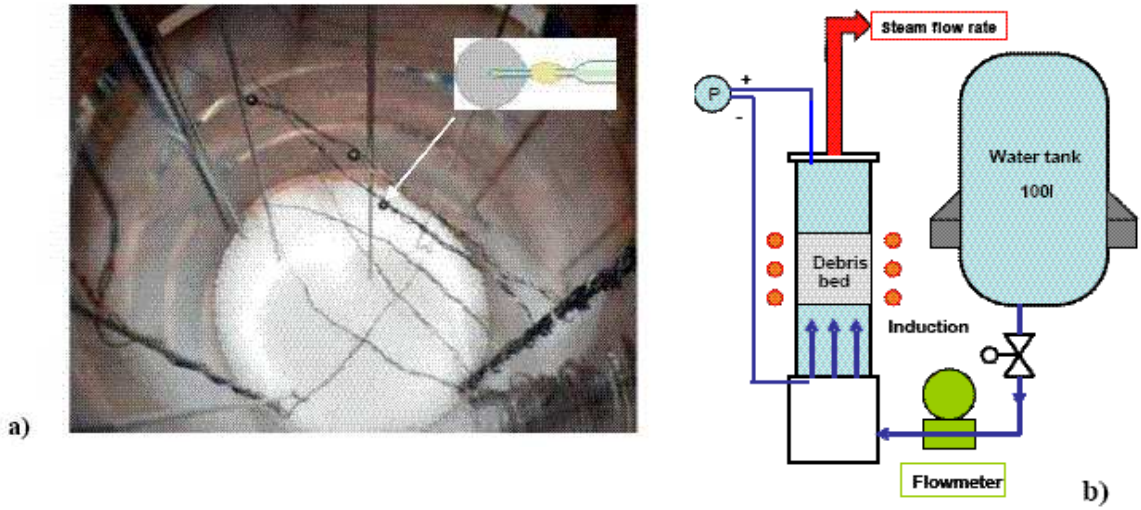

Figure 2.9: Instrumentation for temperature measurement and thermalhydraulics

The measured physical variables are as follows:

- Water and steam mass flow rate generated during reflooding,

- Temperature of the steam at different points outside the debris bed (type K thermocouples),
- Temperature of steam inside the bed (thermocouples at different elevations: 10, 50, 100, 150 and 190 mm and radial positions : center, mid radius and periphery – Figure 2.9 A),
- Temperature of particles inside the bed (thermocouples inserted and welded into particles),
- Distribution of the heating power (calculation by local temperatures increases of thermocouples),
- Pressure at different points at the boundaries of the debris bed,
- Pressure at several points inside the debris bed (this is a recent instrumentation which was not available for all experiments).

Specific effort has been done on the measurement of the pressure drop across the porous medium during the reflooding that is shown in Figure 2.9 B.
The power deposition, by means of electromagnetic induction technology, is evaluated by calculation using the temperature evolution in the different radial and axial location of the thermocouples, during the heat up phase and the heat capacity of the stainless steel (taken around 500 $kJ.K^{-1}.kg^{-1}$) with the simple relation given below:

$$P(W/kg) = \frac{\partial T}{dt} * Cp \qquad (2.11)$$

For all the tests, the power distribution in the debris was quite homogeneous. There is no "skin effect" as it would occur for a massive metallic element. This was obtained by a pre-oxidation of the particles which prevents the *electrical* contact between particles. Only the *induced* current is transmitted from each particle to its neighbors.

2.5.2 PRELUDE test matrix

The PRELUDE experiments were made between 2009-2012 with different test conditions. In this paragraph, the experimental conditions will be summarized (see Table 2.4).

- **Campaign with vessel diameter 110mm**

Preliminary reflooding tests (6 in total) were carried out in 2009 involving a debris bed of Ø4 mm particles inside a 110mm external diameter, and 100mm height test section (5 kg of steel particles), at atmospheric pressure. Inlet water superficial velocity was 4 to 30 $m^3/h/m^2$ that is in the range comparable to that foreseen in the PEARL test matrix (2 to 50 $m^3/h/m^2$). Power deposition was 300W/kg maintained or not during the reflooding phase. Initial debris bed temperature before the reflooding was 150, 230, 310°C and 700°C.
This campaign demonstrated the feasibility of reflooding experiments up to 700°C (1000K), with variation of mass flow rate due to forced flow injection. Jointly, additional heating

PRELUDE tests (without reflooding) were performed to evaluate the power distribution using stainless steel particles, with Ø2, Ø4 and Ø8 mm and mixed particles (Ø2/Ø4 or Ø4/Ø8mm).

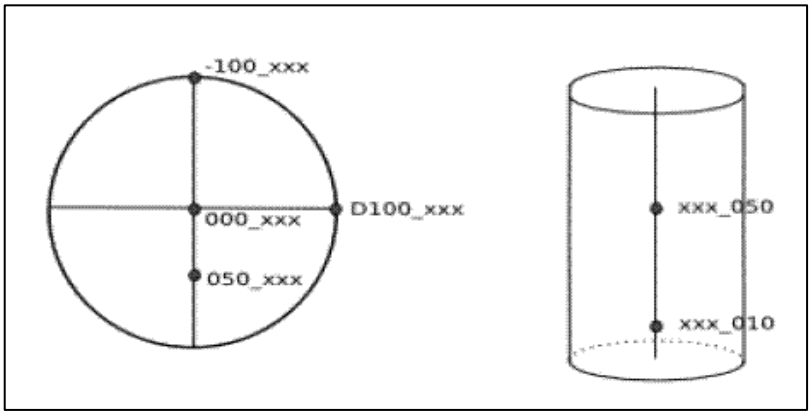

Figure 2.10: Thermocouple position at PRELUDE test with vessel diameter 110mm

- **Campaign with vessel diameter 180mm**

The bigger test section contains 24 kg of slightly oxidized Stainless steel and needs a high frequency generator (up to 400 kHz) for the inductive furnace to reach the nominal power deposition at about 200W/kg. The first campaign (10 tests) of reflooding experiments, using the Ø180mm test section was performed by the end of 2009 with the Ø4mm diameter particles. The most significant experiments allowed to test instrumentation during reflooding in the PRELUDE facility by progressive increase of the initial temperature of the debris (200 to 930°C) and the power deposition in the debris bed (40 to 140W/kg under the nominal value).

The next campaign (15 tests) was performed in 2010 for the same debris bed for two temperature levels (400 and 700°C) up to the nominal power deposit: 200W/kg and particle diameter **4 mm**. The thermalhydraulics conditions mainly were focused on the variation of the inlet flow velocity (values foreseen for the large scale PEARL experiments : 2, 5 10 and 20 m3/h/m2). Under the same test conditions, 10 tests with particle diameter **2mm** were made. The last 8 tests were performed with particle diameter **1mm**. In these tests, temperatures as well as the injected water flow were limited due to instability of the porous medium induced by fluidization phenomenon. In these experiments, the power deposition was also limited to 70 W/kg due the lower efficiency of the inductive process with the smallest particles size.

- **Campaign PRELUDE HT with vessel diameter 180mm**

The campaign (18 tests) was performed in 2011 for the debris bed at temperatures 400-950°C. The nominal power deposit was 200W/kg but two tests were realized with the power deposit 300W/kg. The test section was Ø180mm but the tube was changed for a new one with height

900mm. The debris bed height remained 200mm. The thermohydraulics conditions mainly were focused on the variation of the inlet flow velocity between 5-50 m3/h/m2.

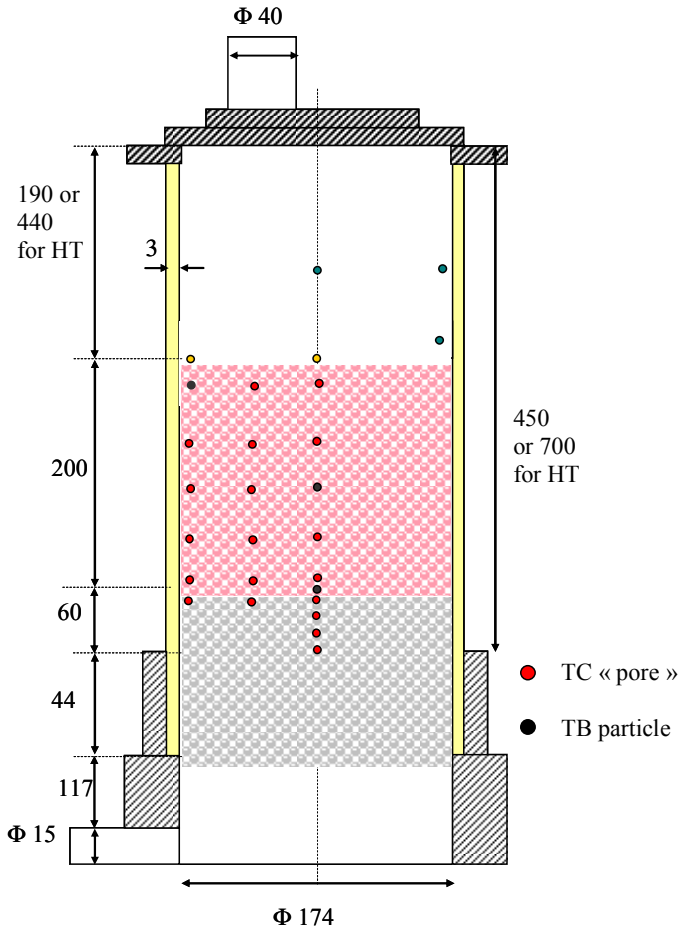

Figure 2.11:PRELUDE experimental facility (dimensions in mm)

- **Campaign PRELUDE 2D with vessel diameter 290mm**

The PRELUDE biggest test section contains 55 kg of slightly oxidized Stainless steel particles. The first campaign (12 tests) of reflooding experiments, using the Ø290mm test section was performed in 2012 with the Ø4mm diameter particles. To enhance the 2D effects during reflooding, a “bypass” zone with thickness 2.5cm filled with 8mm quartz particles was places at the periphery (see Figure 2.12). The thermohydraulics conditions were focused on the variation of the inlet flow velocity between 2-20 m3/h/m2, distributed power 0, 150, 300W/kg and initial debris bed temperature between 200-900°C.

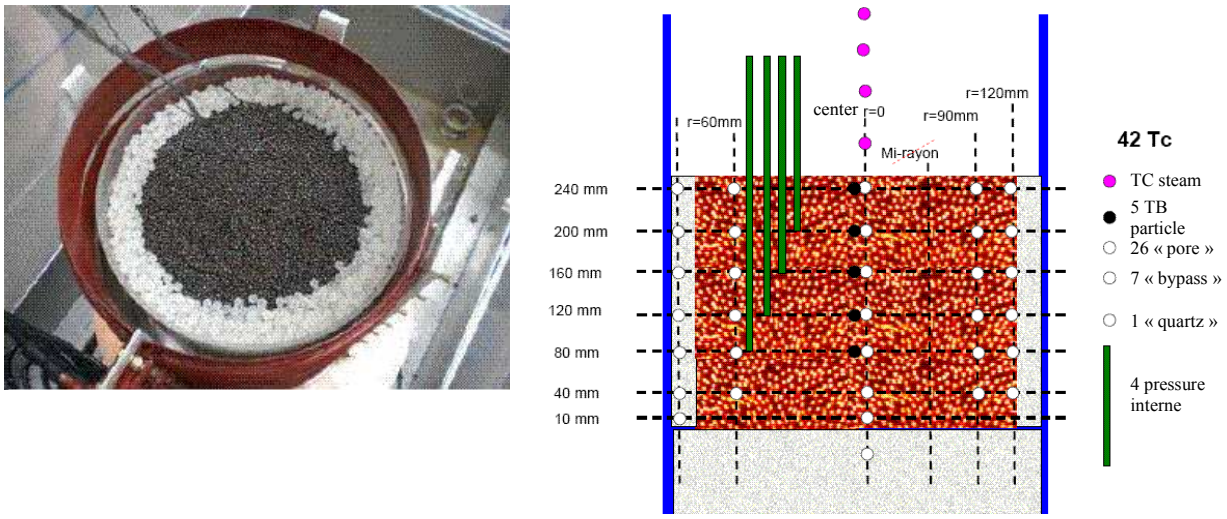

Figure 2.12: PRELUDE 2D facility with quartz "bypass" (left)

Table 2.4: PRELUDE campaigns 2009-2012

Campaign	Test section	Particle diameter	Bed temperature	Power	N° of tests	Water flow
C1 2009	110x100mm (5 kg debris bed)	4mm	150-700°C	300W/kg	6	2-50m3/h/m2 at the bottom; it is equal to 0.555-13.88mm/s; to be divided by porosity in pores
C2 End 2009	180x200mm (24 kg debris bed)	4mm	200-930°C	40-140W/kg	10	
C3 2010	180x200mm (24 kg debris bed)	4mm	400-700°C	200W/kg	15	
C4 2010	180x200mm (24 kg debris bed)	2mm	400-700°C	160-200W/kg	10	
C5 End 2010	180x200mm (24 kg debris bed)	1mm	220-700°C	70W/kg	8	
C6 2011 HT	180x200mm (24 kg debris bed)	4mm	400-950°C	200 or 300W/kg	18	
C7 2012 2D	290x250mm (55 kg debris bed)	4mm Bypass 8mm	200-900°C	0, 150 or 300W/kg	12	

2.5.3 Analysis of experimental results

The series of experiments that were performed provide relevant data to understand the progression of the quench front and the intensity of heat transfer. On the basis of those experimental results, thermal hydraulic features at the quench front have been analyzed. In addition, reproducibility tests have been performed and have shown that some outstanding disturbances which were observed in some measurements are not produced randomly but are

reproduced for every test. Therefore, such disturbances result only from local non-homogeneities of the debris bed and are not stochastic. This increases the confidence on the experimental measurements.
On Figure 2.13 we can see the cumulated mass of injected water, the cumulated mass of produced steam and the deduced water mass that should remain in the test section. A quite good agreement in the balance has been verified by measuring the weight of the water mass in the test section. This demonstrates that the measurement of outlet steam flow rate is accurate.

The analysis concentrated on tests with initial temperature 400 and 700°C. For the analysis of experimental results, about 40 tests were selected from the campaigns **C3, C4, C5 and C6** (see Table 2.4). Reproducibility tests were also analyzed in order to confirm the results. The conclusions drawn in this section represent an important step in understanding the reflooding of a debris bed, which is a necessary step to provide guidance for model development (that will be presented in detail in Chapter 4).

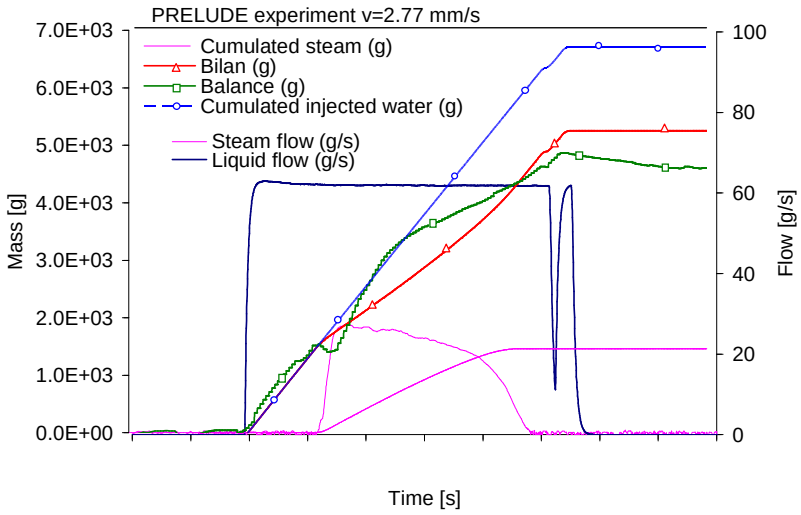

Figure 2.13: The cumulated injected water and steam production. The difference is consistent with the total water amount remaining in the test section
(calculated- bilan, measured-balance)

2.5.3.1 Progression of quench front

The basic phenomenology comes from the observations that were made in most of the PRELUDE tests. First, water enters the porous medium that is initially at high temperature (e.g. 300-600°C above the quenching temperature). The initial heat transfer and evaporation rate are low because the heat transfer coefficient is low i. e. there is no contact between liquid and solid because temperature is above Leidenfrost value (in average) [Leidenfrost56]. As water continues to progress the first quenching of particles occurs at the bottom and thus, high evaporation rate occurs. From there, the quenching front starts to progress, initially with a

velocity that is close to water injection velocity and, later, at a lower constant velocity (for most of the tests) (see Figure 2.14).

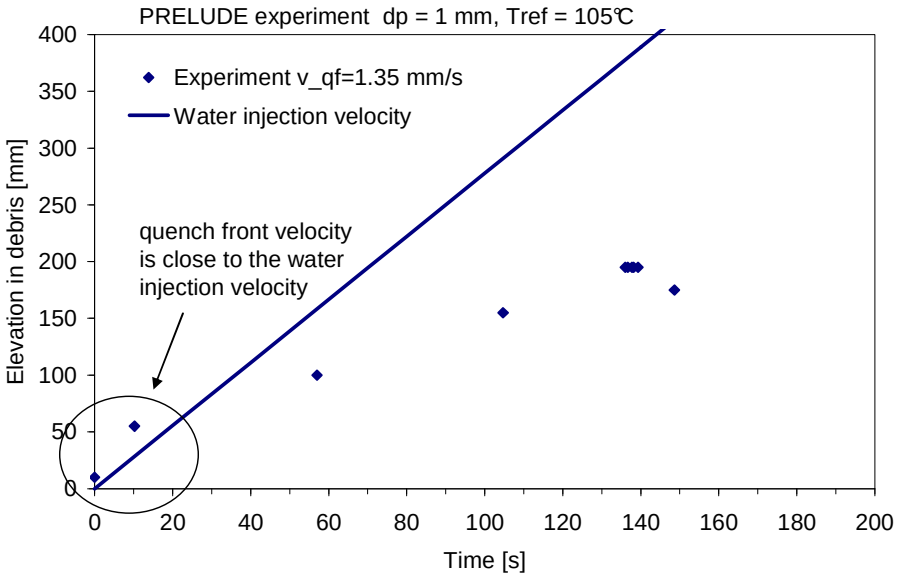

Figure 2.14: Example of quench front progression

When the progression becomes stable, the position of the quench front corresponds roughly to a balance between the cumulated evaporation rate downstream of the quench front position and the local water flow rate. The velocity of the quench front is one of the key parameters to be validated in reflood analysis. The quench front velocity is identified from the determination of the highest elevation where temperature is at the saturation temperature. In PRELUDE tests, it may be evaluated within the column from measurements at three different radii and five different elevations (see Figure 2.15). It should be noted that the accuracy on the instant of quenching depends on the reference temperature that is taken for comparison. On Figure 2.15 we can see that the saturation temperature is not a good reference because it is measured with some error (few degrees) due to temperature instability. In order to be more accurate, it is better to choose T_{sat}+5 or T_{sat}-5 as a reference temperature but they do not provide the same information. In Figure 2.16 we can see the quench front velocity calculated for two different tests. We can see that the reference temperature that was taken in the analysis has an impact on the interpretation of experimental results. Here, the interpretation of temperature measurements can lead to an uncertainty as high as 50% on the quench front velocity. Moreover, the short height of debris bed (200 mm) and limited number of thermocouples impact the accuracy e.g. especially when the transient effects following the entrance of water into the bed persist up to a significant part of the bed height.

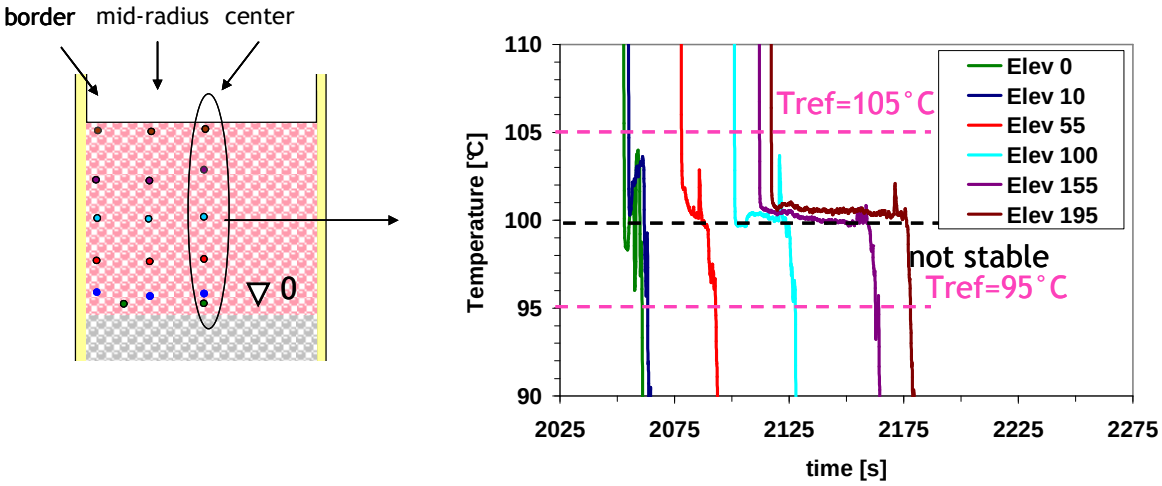

Figure 2.15: Identification of quench front velocity from experimental measurements

First, the conditions of existence of a steady-state progression of quench front are analyzed. It is interesting to study if a steady-state progression occurs because this will significantly help in future analysis of large scale beds and allow some model simplifications. Moreover, when the steady-state progression exists, its velocity may be used to correlate some relevant parameters characterizing the particle bed or the water injection, as it will be explained later. Analyzing the PRELUDE experimental results we can conclude that there exists a *steady-state propagation* of the quench front for all the cases considered here. It indicates that the dynamic processes occurring in the bed are "fast" with respect to the injection velocity (no significant delay of quenching) but "stable" (no acceleration or dramatic increase of steam production). The quench front velocity is the same for the central and mid-radius positions. It is faster near the wall, probably because the initial temperature is lower and the porosity slightly higher.

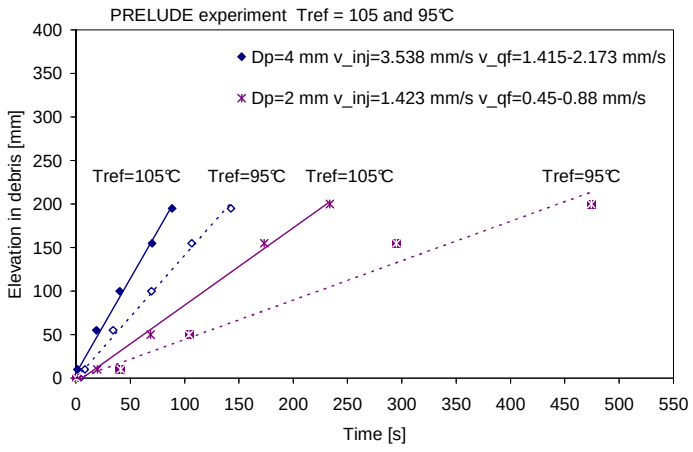

Figure 2.16: Reference temperature and its impact on interpretation of experimental results. The quench front velocities may differ up to 50%

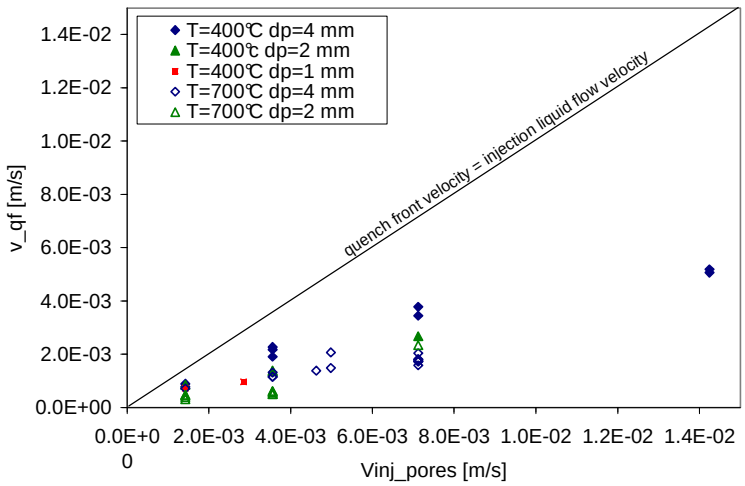

Figure 2.17: Quench front velocities for different tests

Finally, we show that the steady state propagation of the quench front allows a simpler analysis of experimental measurements. On Figure 2.17 we compare the quench front velocity with injection velocity. The quench front velocity is always lower than the water injection velocity. Moreover we can see that the quench front velocity is approximately proportional to the injection liquid flow velocity. As it is expected, the quench front velocity depends also on the initial temperature of debris bed and particle diameter. Decreasing the initial temperature, the quench front velocity increases. The analysis shows visible impact of particle diameter on quench front velocity between 4 and 2 mm particles, i.e., quench front velocity is lower for lower particle diameter due to the friction terms that are higher for 2mm particles. However, that conclusion could not be verified for 1 mm particles because of the limited number of experimental data for this small diameter.

2.5.3.2 Conversion factor between produced steam and injected water

If there is a steady state propagation of the quench front, some balance equations may be simplified and some variables can be expressed as a function of the propagation velocity. The conversion factor between the produced steam flow and the injection liquid flow (Q_g/Ql) is of particular interest.

A peak of steam production may occur Figure 2.18 (B), resulting from the fast initial quench front velocity and from the initial accumulation of subcooled water in the porous column. It is followed by a steady state production of steam that is consistent with the steady state progression of the quench front. There are also tests where the water reaches the top of the debris bed before the steady state is established Figure 2.18 (C). In that case, the steam flow measured at the outlet is lower than the flow actually generated within the bed. It is a drawback of that measurement technique. A similar behavior in steam flow production was already observed in previous studies [Tutu84] but the measurements were incomplete. Adapting the formulations of Tutu [Tutu84] and Tung and Dhir [Tung83], the energy balance (see Figure 2.19) is written as:

$$\frac{Q_g}{Q_l} = \frac{v_{QF}(1-\varepsilon)\rho_s Cp_s(T_s - T_{sat}) + v_l(1-\varepsilon)\rho_s Cp_s(T_{sat} - T_l) - v_l\rho_l\varepsilon Cp_l(T_{sat} - T_l)}{\left[\Delta h^{vap} + Cp_g(T_s - T_{sat})\right]v_l\rho_l\varepsilon} \quad (2.12)$$

where v_{QF} is the velocity of progression of quench front T_s is the initial temperature of solid.

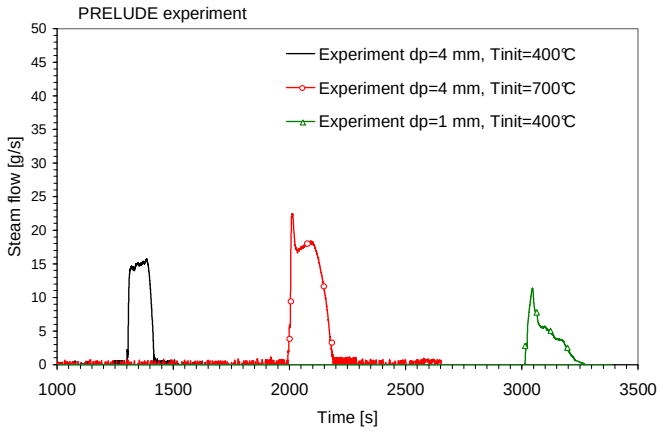

Figure 2.18: Examples of steam flow production during reflood at different PRELUDE tests

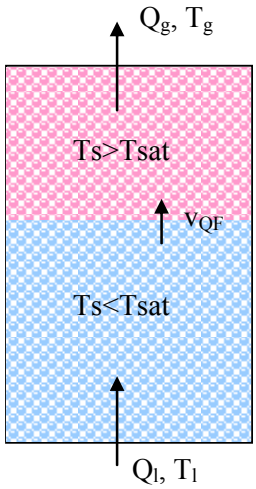

Figure 2.19: Schema of energy balance

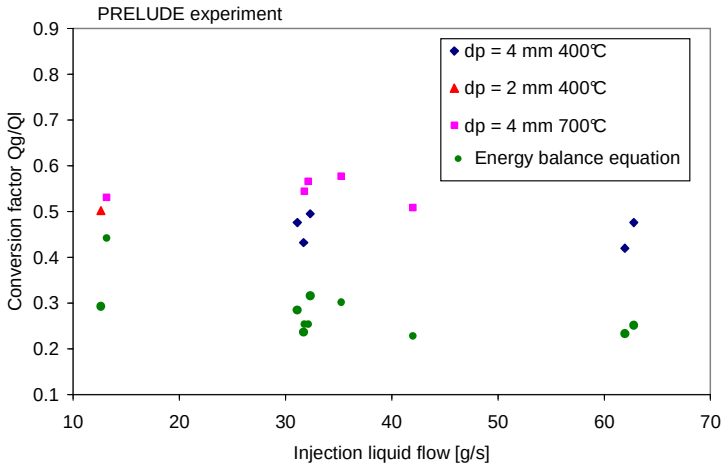

Figure 2.20: Calculated and experimentally observed conversion factor for different tests

From Eq. (2.12) we can see that there exists a simple relation between the quench front velocity and the conversion factor. On Figure 2.17 it is clear that the measured quench front velocity is always lower than the liquid injection velocity. On Figure 2.20 we compare the experimental and calculated (Eq. (2.12)) conversion factors. The experimental conversion factors are presented only for test cases where a steady-state steam production was identified (Figure 2.18 A, B). On Figure 2.20 we can see that the experimental conversion factors are higher than calculated. This may be due to the fact that the quench front velocity used for the calculation was measured in the centre but for most of the cases the quench front velocity at the border was higher so the conversion factor is expected to be higher. Another explanation is that the liquid velocity at the quench front location may be slightly higher than the injection velocity. This will be illustrated by calculations in Chapter 5.

2.5.3.3 Particle to fluid heat transfer

The experimental results were analyzed to obtain the heat flux profile as a function of particle temperature. Assuming a uniform temperature and heat source in the particle where the thermocouple is located, one can make a simple heat balance between accumulation, heat source and outward exchanged flux, Q , to obtain the heat flux density from the temperature signal using the formula:

$$Q = \frac{mC_p}{S}\frac{dT}{dt} - \frac{Q_s}{S} \tag{2.13}$$

where m is the mass of the particle where the thermocouple is located, S is its surface, and Q_s is the maintained volumetric power during reflood. The analysis of experimental results allows us to estimate the profile and intensity of heat transfer and thus to reconstruct the transition heat flux profile and maximum heat flux that was removed from particles. If the *time needed to quench the particle* is significantly *higher than the time needed to for heat conduction inside the particle*, this method can be used to identify the heat flux density removed from particle.

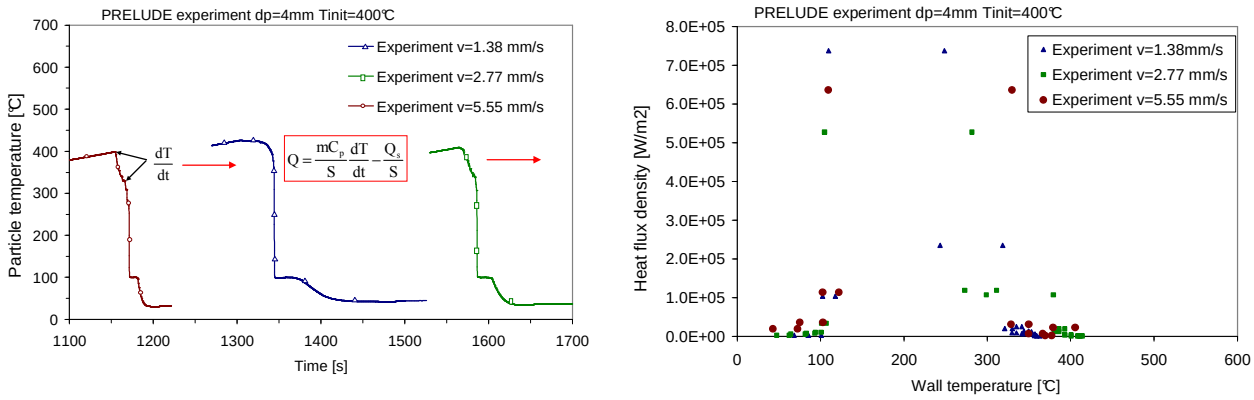

Figure 2.21: Technique used to identify heat flux density (left); identified heat flux density during quenching for different tests (right)

The technique used to analyze the data presented in Eq. (2.13) identifies only an interval of particle temperature where the maximum heat flux density was registered (see Figure 2.21). This analysis gives us an idea about the maximum transferred heat flux density during the quenching that was of the order of $10^5 W/m^2$. The further analysis is twofold (i) the time needed to quench the particle can be calculated (ii) the measured heat flux density can be later compared to that obtained from model predictions.

The minimum time needed to quench the particle to saturation temperature can be calculated as follows, assuming the heat flux density is at the value calculated above:

$$\frac{dT}{dt} = \frac{Q_V}{mCp} = \frac{QS}{\rho CpV} = \frac{10^5 * 3}{7900 * 500 * 0.002} = 38 \Rightarrow t = \frac{\Delta T}{38} = \frac{(400-100)}{38} = 7.9\,s \qquad (2.14)$$

with the density and thermal capacity of steel, particle diameter 4mm with initial temperature 400°C. The low Biot number can confirm the hypothesis, that the temperature gradient in the particle is negligible:

$$Bi = \frac{\alpha r}{\lambda} = \frac{(Q/\Delta T)r}{\lambda} = \frac{(10^5/300) * 0.002}{43} = 0.015 < 0.1 \Rightarrow \theta_{x=0}/\theta_{x=1} \to 1 \qquad (2.15)$$

where α is the convective heat transfer coefficient, *r* is the characteristic length and λ is the solid thermal conductivity. The mathematical proof of criterion that for *Bi<0.1* the temperature ratio $\theta_{x=0}/\theta_{x=1}$ is negligible can be found in [Hejzlar04]. The calculations in Eq. (2.13) are for a steel particle with diameter 4mm and initial temperature 400°C as in PRELUDE test. In severe accidents applications, the debris bed is formed mainly with uranium dioxide particles. The thermal conductivity of uranium dioxide at high temperature is only about 5W/mK which would increase by a factor 8 the Biot number in Eq. (2.13). On the other hand, the initial temperature of debris bed in a reactor would be higher and that would decrease the Biot number. For UO_2, the criterion in Eq. (2.13) is also fulfilled. An alternative approach [Hewitt84] to calculate the time needed to uniformise the temperature in a spherical particle can be calculated according to formula (see also Figure 2.22):

$$t = \frac{0.4\rho Cp\ r^2}{\lambda} = 0.15\,s \qquad (2.16)$$

and this confirms that the time needed to quench the particle is significantly higher than the time needed to uniform its temperature, i.e., *7.9 s* compared to *0.15 s* (61s compared to 1.4s for UO_2).

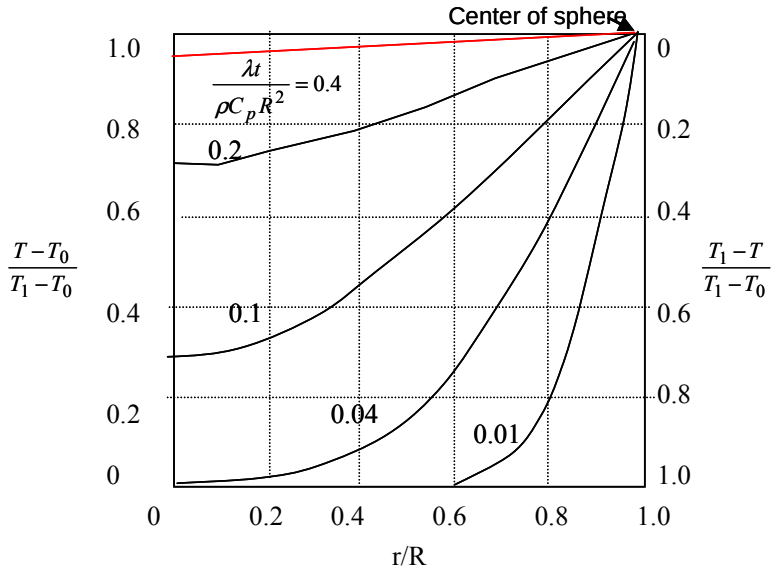

Figure 2.22: Particle temperature distribution for various values of the Fourier number

2.5.3.4 Analysis of pressure measurements

In PRELUDE experiments, the pressure difference over the height of porous medium was recorded. We assume a division of the flow into three zones (see Figure 2.23) where we can identify three different contributions:

- Quenched zone: it is the zone from z_0 to z_1. Its contribution to the pressure difference follows Darcy's law for the single-phase liquid flow Eq. (2.1). As the liquid velocities are small (few mm/s), the largest contribution to the pressure difference in that zone is the hydrostatic pressure.
- Two-phase flow zone: it is the zone from z_1 to z_2, where both liquid and steam are present. In this zone, the pressure difference follows the generalized Darcy's laws for two-phase flows through porous media (Eq. (2.5) and Eq. (2.6)).
- Gas single-phase zone: it is the zone from z_2 to H, where only steam is present. However, some liquid could be present as droplets if sufficient entrainment occurs. But droplets have not been observed in the camera recording of the experiments. In some tests, the presence of liquid at the top of the porous medium was observed (and calculated) before the porous medium was completely quenched but this was due to the faster progression of water along the walls. In case of gas single-phase flow, the pressure difference follows the Darcy/Ergun law (because of much higher Reynolds numbers than for the liquid flow). The gas flow velocity can be directly calculated from the steam flow measured at the top of the experimental facility.

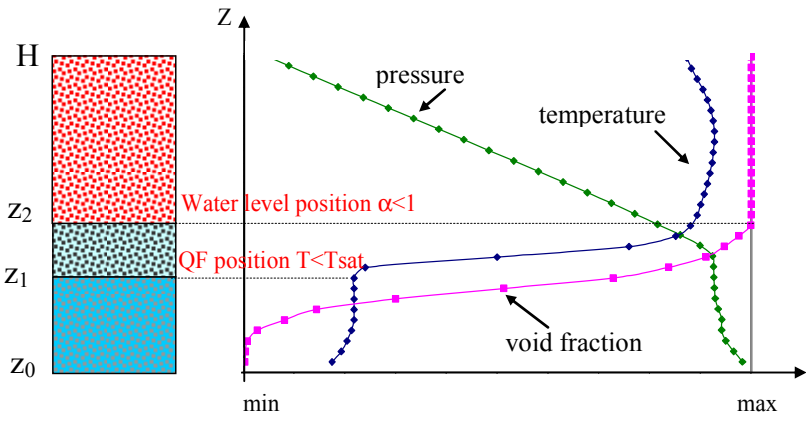

Figure 2.23: Different zones during reflood

In PRELUDE experiments, pressure difference between z_0 and H is recorded. Assuming that the liquid progresses with the quench front velocity (identified from temperature measurements), we can eliminate the contribution of hydrostatic pressure. From that simple analysis, we observe that the pressure may be fitted by a linear function (see Figure 2.24 left), thus we can write:

$$\frac{dP}{dt} = v_{QF}\frac{dP}{dz} = a \tag{2.17}$$

where v_{QF} is the quench front velocity, P is the pressure and a is a fit from linear regression of pressure curve. Applying Eq. (2.17), we can identify the pressure difference for each test and to show its dependence for instance on the gas flow velocity (Figure 2.24 right). From Figure 2.24 (left) we can conclude that the pressure drop is proportional to the height of the still unquenched bed and thus, the pressure difference decreases linearly with time, as the quench front progresses. Moreover it confirms the steady-stead progression of quench front. The results show the very good consistency between all measurements: steam flow rate, pressure difference and quench front velocity. Further analysis of pressure losses are a matter of current investigation. But in order to really identify pressure losses coefficients, more temperature measurements and local pressure measurements are needed.

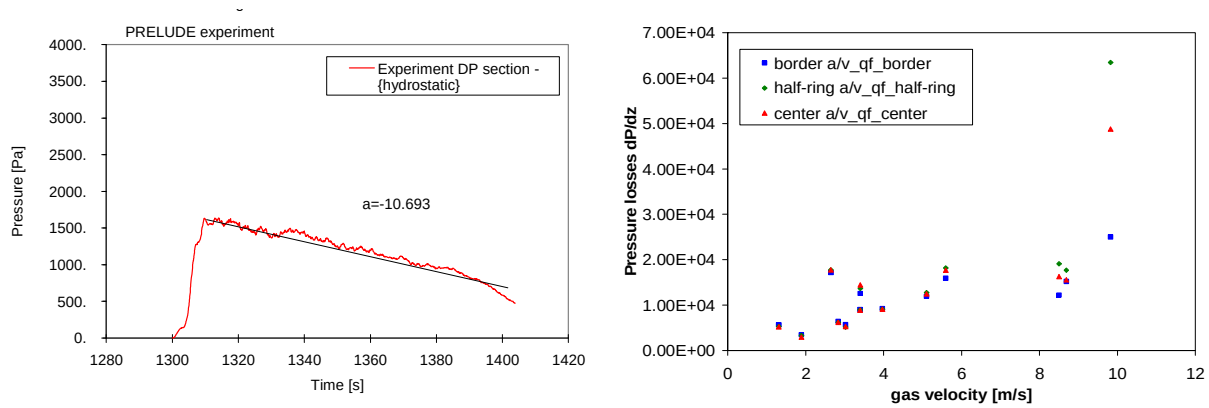

Figure 2.24: Pressure difference for different tests (less hydrostatic contribution)

2.5.3.5 Instability in progression of quench front

It was previously observed experimentally by Wand and Dhir [Wang88] that the pressure differences across the debris bed could enhance multi-dimensional effects and lead to reduction in the time necessary to completely quench the particulate bed. In our analysis, we assume that the liquid flow rate can be increased in the upward direction if the pressure gradient generated by vapor phase is sufficiently high, i.e., at least higher than the hydrostatic pressure gradient.

From the PRELUDE experimental results, we try to confirm this assumption and to find a criterion for the multi-dimensional progression of the quench front. In the previous section we concluded that in PRELUDE experiments, there was a quasi-steady progression of quench front. The quench front velocity was identified to be the same for the central and mid-radius positions. However, there are tests where the quench front velocity is significantly faster near the wall. First, we calculate the ratio between the minimum and maximum quench front velocity for each PRELUDE test. This ratio identifies the multi-dimensional effects i.e. it is considered one-dimensional as long as this ratio is close to 1. Secondly, we try to correlate this parameter to the pressure gradient generated by the steam flow. This pressure gradient is calculated from the generalized Darcy equation for the vapor phase:

$$\frac{\mathrm{dP}}{\mathrm{dz}} = -\frac{\mu_{\mathrm{g}}}{\mathrm{K}\alpha^{\mathrm{n}}}\,\mathrm{j_g} - \frac{\rho_{\mathrm{g}}}{\eta\alpha^{\mathrm{n}}}\,\mathrm{j_g^2} \tag{2.18}$$

where K and η are the permeability and passability respectively, j_g is the gas flow velocity, α is the void fraction and n is the relative permeability and passability exponent (see Table 2.1). For this equation, the steam velocity in the pores was calculated from the steam flow measurements at the outlet of test section, i.e. during steady-state (see Figure 2.18 case B):

$$\mathrm{j_g} = \frac{\mathrm{Q_g}}{\rho_{\mathrm{g}}\mathrm{S}} = \frac{\mathrm{Q_g}}{\rho_{\mathrm{g}}\left(\frac{\pi\phi^2}{4}\right)\varepsilon} \tag{2.19}$$

Where Φ is the diameter of the test section (e.g. 180mm) and ε is the porosity (e.g. 0.4). If the steady-state interval is not clearly identified i.e case C in Figure 2.18, the value of the peak as well as the mean value were considered, which results in interval of uncertainty for *dp/dz*.

On Figure 2.25 we can see how the multi-dimensional effects are actually enhanced as the pressure gradient generated by the steam flow increases. Here, the criterion for multi-dimensional effects seems to appear when the pressure gradient is above $2.8\rho_{\mathrm{l}}\mathrm{g}$. Also Fitzgerald and Woods [Fitzgerald98] have shown that the front may become unstable if a sufficient fraction of liquid vaporizes so that the pressure gradient in the advancing vapor exceeds that in liquid.

It is important to note, that this criterion was obtained analyzing the PRELUDE experimental results, where the facility is in its conception 1D (no designed by-pass). In a realistic bed

configuration, additional factors would also induce multi-dimensional effects, such as non-uniform porosity and permeability, variable height or non uniform temperature.

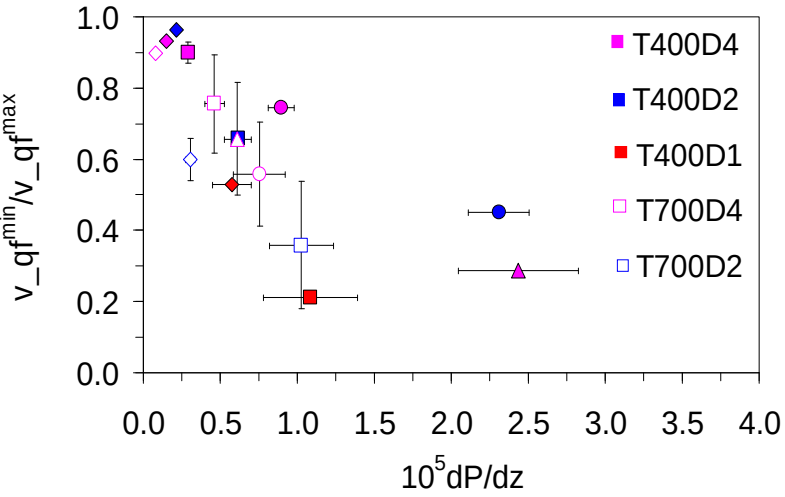

Figure 2.25: Multi-dimensional effects and their dependence on pressure increase. T- Initial bed temperature, D- particle diameter

2.5.3.6 Temperature profile and thickness of heat transfer layer

Following the division of the homogeneous porous medium into different zones (see Figure 2.26), we can "theoretically" identify different flow regimes during reflood:

- Subcooled convection: in the zone from z_0 to z_1. The quench front position is at z_1. In this region the particle temperature is under the saturation temperature.
- Nucleate boiling: in the zone from z_1 to z_2. Upstream the quench front, the particles are permanently wetted and the temperature is close to the saturation temperature and below the maximum heat flux temperature (also called "burn-out" temperature).
- Transition boiling region: in the zone from z_2 to z_3. Above the quench front, when temperature exceeds the maximum heat flux temperature, non-stable two-phase flow establishes at the particle surface, with intermittent wetting of the particles.
- Steam convection or film boiling: in the zone from z_3. The gas phase is predominant (intermediate or high quality). If the liquid is present we assume that there is no direct contact of liquid with particles - film boiling.

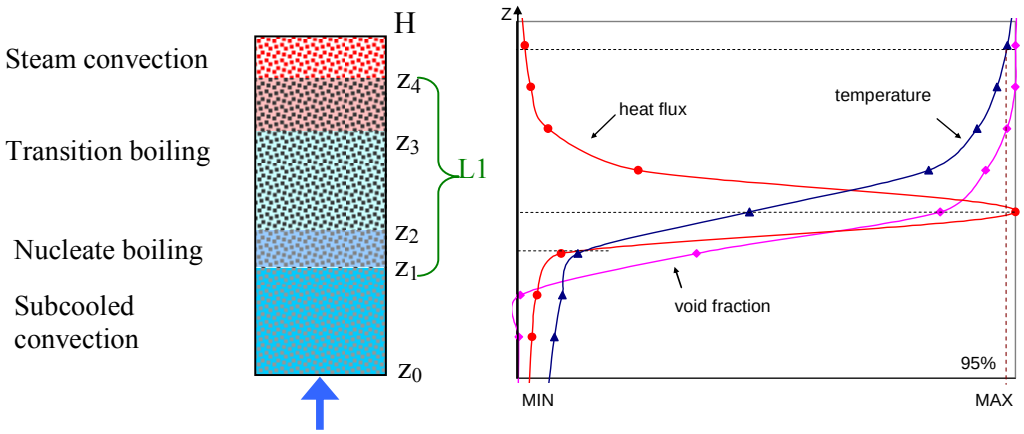

Figure 2.26: Heat transfer layer length according to different boiling regimes

In the literature, the Leidenfrost temperature [Leidenfrost56] identifies the transition criterion between the film boiling regime and transition boiling. At the atmospheric pressure, this temperature should be about 300°C. However, from the temperature profile in Figure 2.27 we can see that the quenching at PRELUDE experiments starts before. This motivates us to study the heat transfer layer length L1 that is different indicator for quenching (see Figure 2.26).

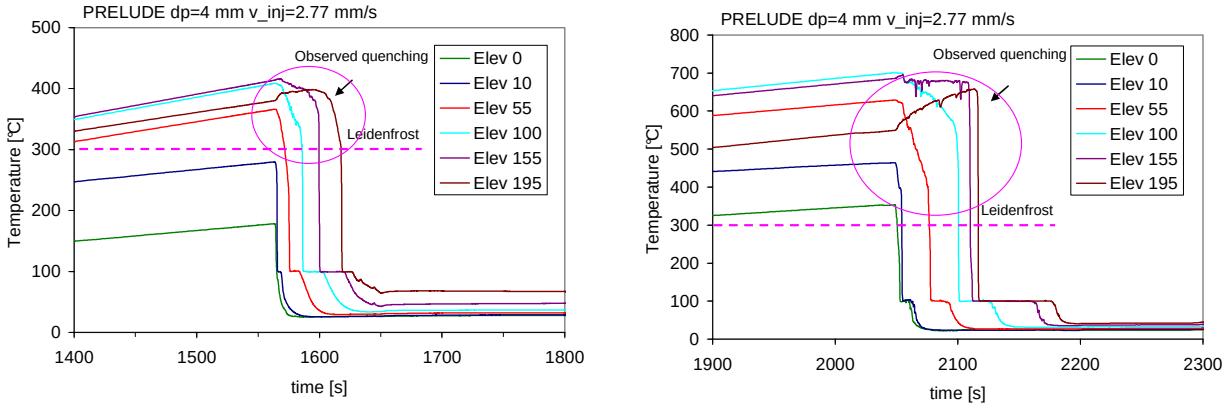

Figure 2.27: Temperature profile at different PRELUDE tests. Test with initial temperature 400°C (left) and 700°C (right)

In this paragraph we will describe the technique applied to identify a "heat transfer layer length". We define the heat transfer layer length as a thickness of two-phase flow region that can be seen in Figure 2.26. We assume that:

- The heat transfer layer length is constant during reflood and moves along with the quench front progression. This is valid if there is a homogeneous debris bed (in geometry and temperature) and if a quasi-steady progression of quench front is identified.
- The heat transfer layer length can be identified from axial temperature profile at any instant during reflood. It is the difference between the position of quench front and elevation where the temperature is close to its initial temperature before reflood but starts to be influenced by quenching, for instance *T/Tinit=0.95*.

From the temperature measurements e.g. thermocouples at center radius, we can identify the axial temperature profiles. On Figure 2.28 (left) we can see an example of maximum temperatures reached in one PRELUDE test. On Figure 2.28 (right) we can see an axial temperature profile for this test at instant *t* during quenching.

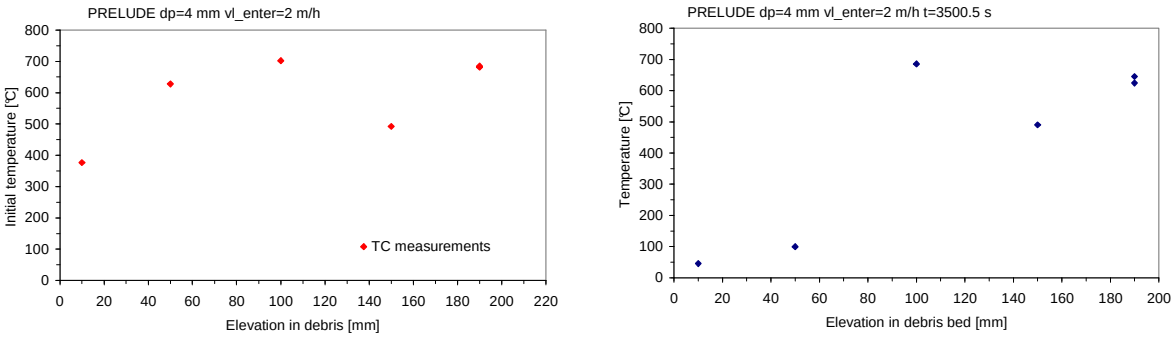

Figure 2.28: Initial axial temperature profile (left) and profile during quenching (right)

We can also relate the temperatures during quenching to their initial temperature before reflood. The results for one PRELUDE test at instant *t* are summarized in Table 2.5. From the experimental measurements at instant *t* (see Figure 2.28 right) we can see that about 50mm of debris bed height is quenched. Also we can see that the temperature of the debris bed at about 100mm is not influenced by the front progression, so the temperature is not changed and only steam is present in this region. The first conclusion, but leading probably to a not very accurate definition, is to assume that the thickness of the two-phase flow zone is about 50mm (simple difference between upper steam region limit 100mm and the quench front position that is 50mm).

Table 2.5: Axial temperatures at instant *t* during quenching at one PRELUDE test

TC elevation [mm]	Temperature T [°C]	Initial temperature Tinit [°C]	T/Tinit
10	45.5	376.65	0.12
50	99.8	627.71	0.16
100	685.16	702.18	0.98
150	490.01	492.14	0.995
190	624.13	681.7	0.92
190	645	684.7	0.94

Secondly, we try to identify the thickness of the heat transfer layer length more precisely. Here, it is necessary to have an idea about the whole axial temperature profile. On Figure 2.28 (right) we can see that we do not have initially a precise information about the elevation where the temperature is equal to a given value at instant *t*. In order to get this information, we study closely the temperature measurements. In Section 2.5.3.1 we concluded, that there is a quasi-steady state progression of the quench front. We identified the elevation and instant,

when the temperatures passed across the reference quenching temperature, i.e., saturation temperature. Moreover, the experimental results were fitted by linear regression. From the linear equation, we can predict the elevation, where the temperature passes across the saturation temperature at any instant during quenching. In this paragraph, we apply the same technique for different temperatures, [650, 600, 550,…150 °C]. We try to identify, if the experimental points can be also fitted by linear regression. From the linear equation we can thus calculate the elevation where the temperature passed across the points [650, 600, 550,…150°C] at instant *t*. On Figure 2.29 we can see an example of temporal evolution of TC measurements at temperature 450°C. We can see that the experimental points can be fitted by linear regression. In order to obtain an interval of uncertainty, we can also study only two TC measurements, for instance at elevation 50 and 100mm that surround the instant of quenching *t* that we selected. From the linear equation we can thus calculate the elevation, where the temperature 450°C is reached at instant *t*. We can repeat this procedure for any selected temperature e.g. 650, 600, 550, …150°C. On Figure 2.30 we can finally see a reconstruction of the axial temperature profile at instant *t* for one PRELUDE test.

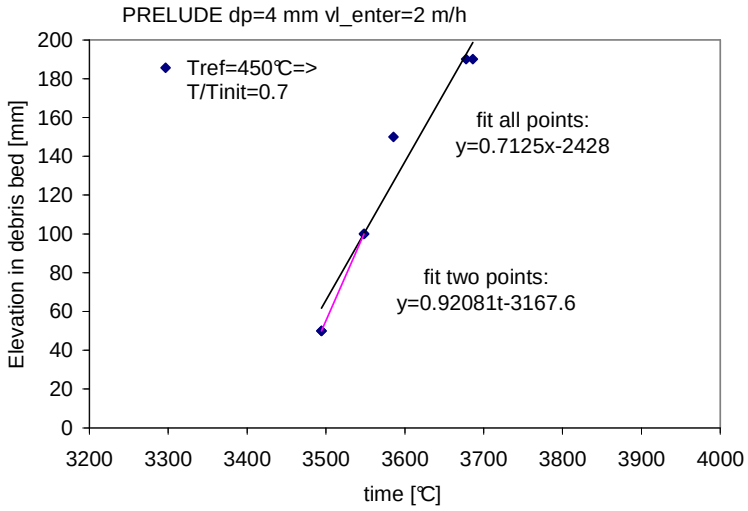

Figure 2.29: Elevation and instant when the measured TC temperatures pass across the temperature 450°C for one PRELUDE test

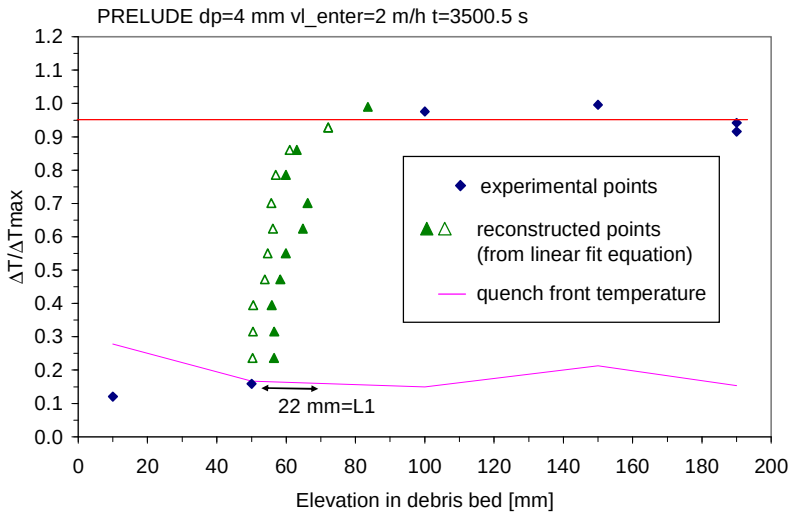

Figure 2.30: Identification of heat transfer layer length from the axial temperature profile

This method of identification of the heat transfer layer length was used to analyze the PRELUDE experimental data with initial temperature 700°C, particle diameter 2 and 4 mm and water injection flow 0.555-2.77 mm/s. On Figure 2.31 we can see the dependence of the heat transfer layer length on the Weber number:

$$\begin{aligned} \mathrm{L1} &= 0.45\,\mathrm{We}^{0.32} = \mathrm{f}\left(\mathrm{v}_{\mathrm{pore}}{}^{0.65}\right) \\ \mathrm{We} &= \frac{\rho_{\mathrm{l}}\,\mathrm{v}_{\mathrm{pore}}^{2}\left(\dfrac{\mathrm{d_p}\,\varepsilon}{1-\varepsilon}\right)}{\sigma} \end{aligned} \tag{2.20}$$

Where L1 is the heat transfer layer length in [m] and other variables can be found in the Nomenclature.

Tutu et al. [Tutu84] also concluded that the heat transfer layer L1 depends on water injection velocity, and is higher for higher velocities, but they did not estimate the dependency. The same conclusion was demonstrated by Ishii and Obot from visual experiments [Obot88] who observed different flow regimes in the post-CHF region in tube bundles. They qualified the regime length introducing its dependence on the Capillary number [Obot88]:

$$\begin{aligned} \mathrm{L1} &= \mathrm{Ca}^{0.5} \\ \mathrm{Ca} &= \frac{\mu\,\mathrm{v}}{\sigma} \end{aligned} \tag{2.21}$$

where v is the liquid velocity, μ viscosity and σ surface tension.

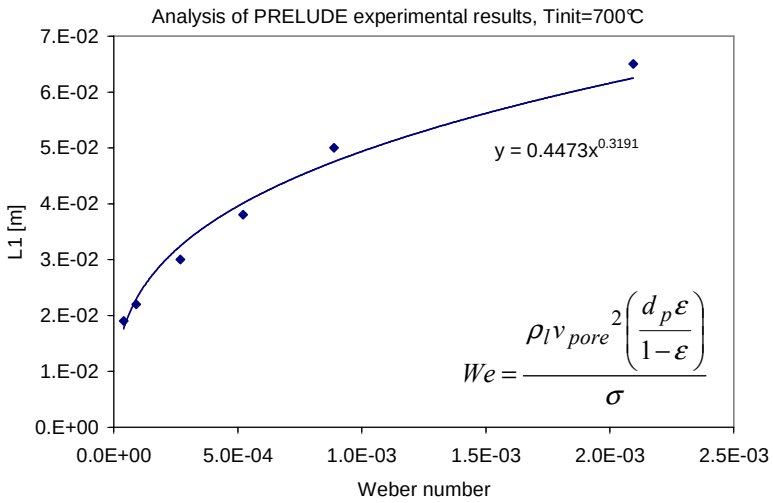

Figure 2.31: Heat transfer layer length and its dependence on Weber number

2.5.3.7 Discussion on uncertainties in experimental measurements

The PRELUDE experimental results were analyzed in the paragraphs above. The conclusions were drawn from the analysis:

- Temperature measurements in pores/particles,
- Outlet steam flow measurements,
- Generated pressure.

As it was already mentioned, the author of this thesis did not perform the PRELUDE tests and did not participate directly in the measurements. That is the reason why we will not detail here the techniques of experimental measurements. Only a few points will be discussed here, for which uncertainties were identified when analyzing the experimental results.

Firstly, it was concluded that there may be an uncertainty on the porosity or measured height of the debris bed. For PRELUDE tests with internal test diameter 174mm, the debris bed height was indicated to be 200mm. From the values of the particle diameter 4mm, porosity 0.4, steel density 7900kg/m^3 and mass of steel particles 24kg, a simple calculation verifies the debris bed height:

$$H = \frac{\left(\frac{m}{\rho}\right)\left(\frac{1}{1-\varepsilon}\right)}{\frac{\pi S^2}{4}} = \frac{\frac{24}{7900}\frac{1}{0.6}}{\frac{\pi 0.174^2}{4}} = 210\text{mm} \qquad (2.22)$$

which is not in full agreement with the indicated debris bed height 200mm. However, after this analysis, the debris bed height 210mm for some tests was later confirmed by the experimental team. Moreover, the debris bed porosity composed of smaller particles, e.g., 2 or 1mm was later specified to be slightly less than 0.4.

Secondly, it was shown that a limited debris bed height (only 210mm) and limited number of thermocouples impact the experimental uncertainty. On Figure 2.32 we can see that for certain tests there are some entrance effects generated when water enters the debris bed. Here, the entrance effects e.g. due to the temperature or geometry difference between quartz bed/steel bed, may persist up to 25% of the debris bed height. The generated instabilities influence thus the quench front progression and temperature measurements. Later on, the quench front is stabilized and quasi-steady state progression is observed but the debris bed height, which is only 200mm may be insufficient to observe a full stabilization of the front.

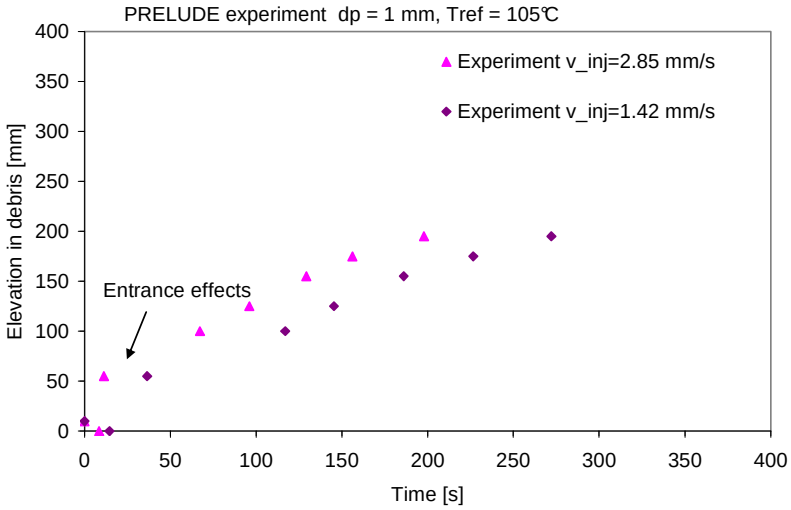

Figure 2.32: Quench front progression for two tests where dp=1mm. Quench front is destabilized at the bottom of the debris bed.

Concerning the temperature measurements, the experimental results seem to be very reliable. The experimental team stated that the uncertainty on position of thermocouples is maximum ±3mm. Some tests with identical test conditions i.e. geometry, heating, reflood parameters were made, in order to confirm the experimental measurements. Those tests were analyzed and the initial conditions were verified. Small differences in initial conditions e.g. temperature, water injection, resulted in a small difference in the quench front progression as can be seen on Figure 2.33. It is important to note that the linear regression of experimental points that was used for many of the previous analysis also involve a systematic error. On Figure 2.34 we can see an example of the standard deviation between the experimental points and linear regression. In the later analysis it is recommended to compare experimental and calculated points and not only the quench front velocities resulting from the linear fit. Thus, we can see if the experimental points are spread around the calculation points.

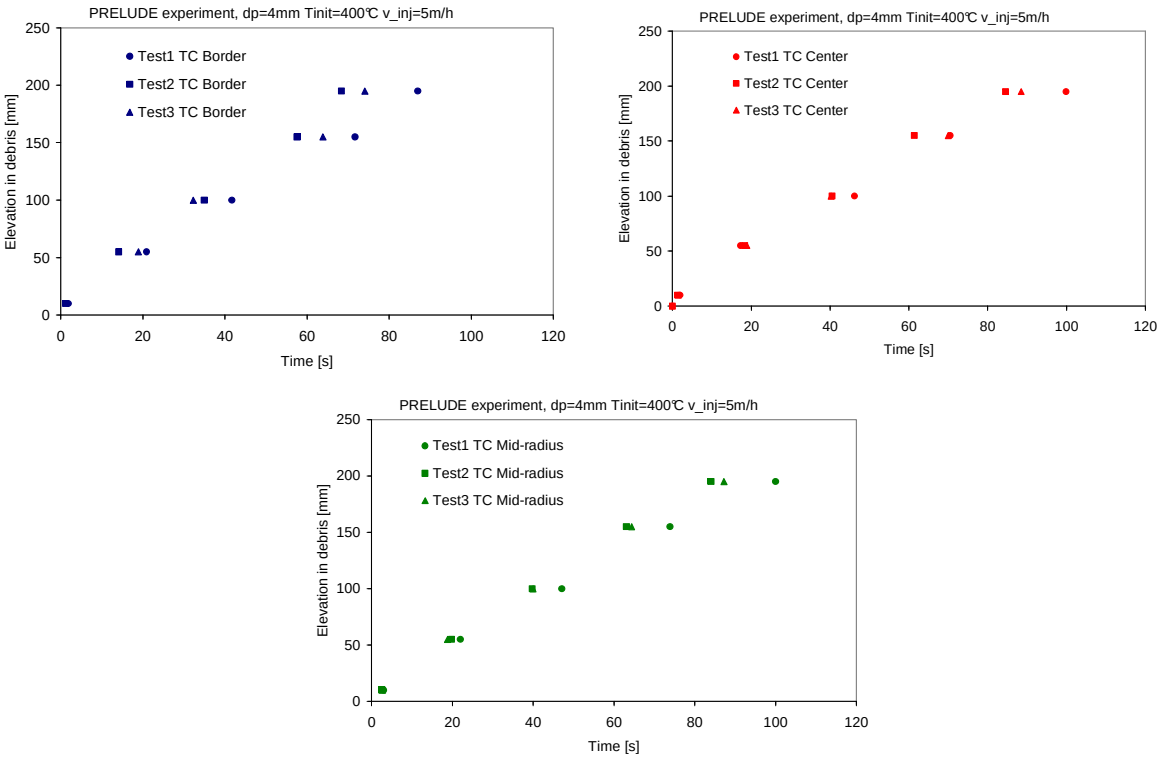

Figure 2.33: Quench front progression for three PRELUDE tests with identical conditions

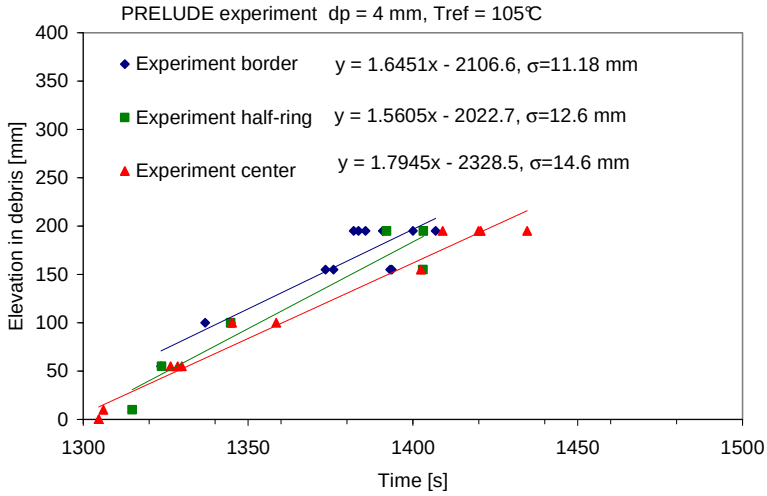

Figure 2.34: Standard deviation between experimental measurements and linear regression

2.6 CONCLUSIONS

The coolability of a severely damaged reactor core is one of the major objectives of severe accident researches. The debris bed configuration and associated complicated heat transfer regimes were studied worldwide in the past 30 years. The bibliographic study of international experimental programs was summarized in this Chapter, taking into account dry-out tests (SILFIDE, STYX, POMECO, DEBRIS and PETIT), top reflood tests (Ginsberg, Dhir, DEBRIS) and bottom reflood tests (Tutu, DEBRIS and PRELUDE). Two sources of information were used for more detailed analyses: PETIT dry-out experiment and PRELUDE experimental program. Currently, the debris bed reflooding is studied at the French Institute of Radioprotection and Nuclear Safety (IRSN), both experimentally and theoretically. The current experimental objectives are to ensure a more representative geometry and volumetric heating of the particles, compared to previous experiments. In addition, the current measuring techniques allow to significantly enhancing the database of experimental results.

Firstly, the analysis of PETIT dry-out experiment focused on identification of elevation where the dry-out occurred. These results will be later used in this thesis used for validation of two-phase flow heat transfer correlations (convective and boiling) in the modeling. Secondly, the PRELUDE experiments focused on bottom reflood of debris bed. The effect of geometry, for instance: test section, particle diameter and the impact of thermohydraulic conditions, for instance: initial temperature, water injection flowrate, were studied. About 40 tests were analyzed and the principal conclusions were drawn on the progression of quench front, steam formation and pressure increase. The first conclusions from these analyses will be later used in this thesis to improve and validate the model for two-phase flow in porous media.

It appears that, for almost all tests, a quasi-steady propagation of the quench front is observed. This is shown by the velocity of the front deduced from temperature measurement but also by the steam flow rate produced and by the pressure difference across the bed. Simple expressions of those quantities have been provided, by fitting experimental results and making a simplified physical analysis of the steady front. An order of magnitude of the maximum heat flux that is extracted from particles was estimated. The interpretation was based on the approximation, supported by some experimental evidence, that the temperature variation inside a steel particle is negligible. This approximation will make modeling easier. For high flow rates or high temperatures, the front is destabilized and two-dimensional effects appear. An experimental criterion for the stability of the quench front seems to be if the pressure gradient created by the steam flow downstream of the quench front is lower than $2.8\rho_l g$.

Finally, the discussion on experimental uncertainty was briefly introduced. It was shown that the interpretation of thermocouple measurements may lead to an uncertainty as high as 50% on the quench front velocity, which is not negligible. Even if the accuracy on the position of thermocouples is good (±3mm), it is also recommended to measure precisely the porosity and

debris bed height. This would reduce some of the uncertainties. The short height of the debris bed (200mm) is also a limitation to an accurate validation: it enhances the impact of transient effects and it leads to a fast recovery of the bed by water, before complete quenching, which disturbs the measurement of outlet steam flow rate. Anyway, the reproducibility tests have been performed and have shown that there are almost no stochastic effects in those experiments. The reproducibility tests confirmed the confidence in experimental results.

Chapter 3

MODELING OF REFLOOD OF DEBRIS BED

3. MODELING OF REFLOOD OF DEBRIS BED

This Chapter is dedicated to the modeling of two-phase flow with phase change in a porous medium, for the particular conditions that were identified in the previous Chapter. In the context of this thesis, one objective is to reduce the relative uncertainties and to evaluate the consequences of the reflooding of a degraded core where a debris bed may have been formed. We recall that the typical particle size in a debris bed is a few millimeters (characteristic length-scale: 1 to 5 mm), i.e., a high permeability porous medium. Moreover, the debris bed formed in a reactor core is considered to be a heterogeneous porous medium i.e. with local variations of porosity, particle size as well as temperature. The experimental interpretation concerning this issue was presented in the previous Chapter. Here, the theoretical developments will be presented.

In this thesis, we have started from earlier developments done in the laboratory. A previous model was proposed initially by [Duval02] and later extended and validated by [Bechaud01]. Recent modifications and applications to reflooding situations were presented in [Fichot06] and [Fichot09]. The general background, from a theoretical point of view, consists in establishing the flow and mass transfer equations in a porous medium by using the volume averaging method. It is assumed that there exists a representative elementary volume (REV) over which the porous medium is considered to be homogeneous. A typical representation of the REV is given in Figure 3.1 where:

- Microscopic scale is the pore scale where the characteristic length l is generally equal to the mean diameter of the pores or of the particles (*mm*);
- Macroscopic scale is represented by length L associated to characteristic length of the observed phenomena that corresponds here to the reactor scale (*m*).

Here, the homogeneity and heterogeneity of medium depend on the size of elementary representative volume where we define the mean properties. The problem is that at pore scale, the flow structure, the topology of liquid-vapor interface result in extremely complex phenomena. This problem cannot be treated by direct numerical simulations at the pore scale for two reasons. First, there is no two-phase flow model sufficiently validated in situations with strong phase change. Methods like VOF (Volume of Fluid), Level Set or Cahn-Hilliard have helped to tackle important issues (like nucleate boiling) but the feedback is not sufficient to be confident to use them in other situations, particularly in porous medium. In this context, the objective is to obtain the macroscopic description of the medium based on the solution of problem at the microscopic scale.

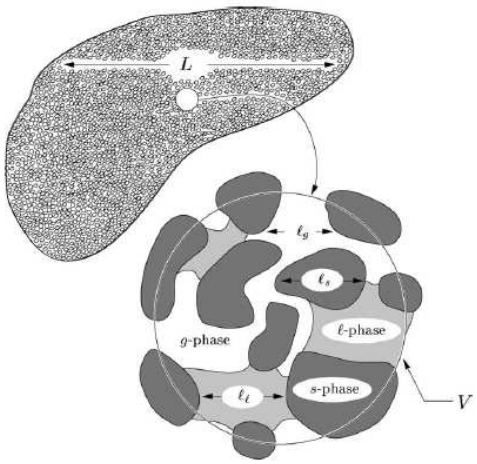

Figure 3.1: Microscopic scale *l* and macroscopic scale *L* of problem

3.1 MACROSCOPIC MODELS OF HEAT TRANSFER

The objective of this paragraph is to present a short review of different macroscopic models existing in the literature and to discuss about their advantages and their limitations.

3.1.1 One temperature models

One-equation models often assume that the fluid and solid are both at the same intrinsic average temperature. Because the heat transfer by convection can be neglected in a gas and liquid phase, the macroscopic model at one-temperature can be written as:

$$\langle\rho\rangle\langle C_p\rangle\left(\frac{\partial\langle T\rangle}{\partial t}+\langle \mathbf{v}\rangle.\nabla\langle T\rangle\right)=\nabla.\left(\mathbf{K}^*.\nabla\langle T\rangle\right)-\dot{m}\Delta h+\langle\varpi_s\rangle \tag{3.1}$$

where $\mathbf{K}^*$ represents the effective thermal dispersion tensor, $\dot{m}$ is the mass flow rate of evaporation, Δh is the latent heat of phase change and ϖ_s is the volumetric heat source generated in the solid phase. In Eq. (3.1) $\langle\rho\rangle\langle C_p\rangle$ is the volumetric heat capacity of the mixture defined as:

$$\langle\rho\rangle\langle C_p\rangle=\varepsilon_g\left(\rho C_p\right)_g+\varepsilon_l\left(\rho C_p\right)_l+\varepsilon_s\left(\rho C_p\right)_s \tag{3.2}$$

where $\varepsilon_g, \varepsilon_l$ and ε_s are the volumetric fractions of the gas, liquid and solid phases respectively. These fractions can be related to porosity ε and the saturation S_l with the relations:

$$\varepsilon_s=1-\varepsilon,\quad \varepsilon_l=\varepsilon S_l,\quad \varepsilon_g=\varepsilon(1-S_l) \tag{3.3}$$

The main difficulty associated to the macroscopic model in Eq. (3.1) is the determination of the effective thermal dispersion tensor K^*.

Intuition certainly motivates the use of a one-equation (single-temperature) model for the study of heat conduction in porous media, provided that the particles or pores are small enough and that the physical properties of each phase are close enough. Truong and Zinsmeister (1978) found that the one-equation model gave good results for transient processes only when the thermal conductivities of the two constituents did not differ widely. On the other hand, Batchelor and O'Brien (1977) were satisfied to employ the one-equation model when the thermal conductivities differed so widely. A one-equation model may be obtained without making the assumption of local equilibrium through a specific definition of the average temperature and deviations. Different authors [Moyne00], [Davit10] have proved that such models are equivalent to the asymptotic behaviour, on a semi-infinite medium, of local non-equilibrium multi-temperature models. Such a model has a different, larger, effective thermal conductivity than the one-equation non-equilibrium model. Each model has to be used within its domain of validity. For instance, [Davarzani10] have shown by using direct numerical simulations over a porous medium made of arrays of cylinders, that the situation evolves in time as follows :

- A short, non-homogenisable situation due to the sharp initial and boundary conditions,
- A stage typical of non-equilibrium, for which a multi-equation models proved to be an acceptable representation,
- A stage corresponding to the asymptotic behaviour (which can also be represented by a one-equation non-equilibrium model),
- A final stage in which the temperature field goes back to a one-equation local equilibrium model because of the influence of the exit boundary conditions.

The situation of local non-equilibrium is particularly interesting in our case, as emphasized by the experimental results. A number of papers have emphasized the existence of non-equilibrium conditions.

However, Nield and Bejan (1992) have pointed out that at sufficiently large Reynolds or Rayleigh numbers, local thermal equilibrium will break down. For instance, this condition of local equilibrium is no longer valid when the particles or pores are not small enough, when the thermal properties differ widely, or when convective transport is important. Moreover, when there is a significant heat generation in any of the phases, the system will become rapidly far from local thermal equilibrium. Finally, it must be noticed too that local thermal equilibrium becomes uncertain for situations involving rapid evaporation–condensation processes.

In the situation of interest for the present work, i.e. the water flooding of an overheated porous bed, several of the conditions are not fulfilled because there is phase change, volumetric heat generation and strong convection with steam. For such extreme conditions, a one temperature description is inadequate to describe correctly both the transients associated with the quench front penetrating the hot dry porous layer and regions where dryout occurs.

3.1.2 Model of thermal non-equilibrium

For the dryout issue and the determination of DHF, thermal equilibrium has traditionally been assumed and all phases are supposed to be at the saturation temperature of water. Therefore, the energy equation is considerably simplified because, not only thermal equilibrium is assumed but also the equilibrium temperature itself is known. This is justified if one considers that the dominant heat transfer is nucleate boiling which is strong enough to quickly transfer the energy dissipated in the particles to the fluid, by evaporation. Obviously, that assumption was verified by thermocouple measurements. However, it is also obvious that such assumption is not valid anymore when the void fraction is close to 1. For 1-dimensional situations, this point is not very important since the detection of dryout corresponds exactly to the identification of a temperature increase in the porous medium (i.e. a departure from equilibrium). For two and three-dimensional flows, the situation is quite different because hydrodynamic effects seem to play a more complex role and lead instabilities in the evolutions of local void fraction and local temperature. Large thermal non-equilibrium has been observed experimentally [Atkhen06] before actual dryout occurred. When the assumption of local thermal equilibrium fails to be valid, one possible solution to model such cases is to develop separate transport equations for each phase. This leads to macroscopic models which are referred to as non-equilibrium models.

For transport through a two-phase material (i.e. a solid matrix and a fluid), non-equilibrium models have been proposed under the form of two-equation models for the fluid phase *f* and the solid phase *s*. Such models have been studied extensively by [Zanotti84] or [Quintard93]. For the diffusive problems under certain approximations, the models can be written in a form:

$$\varepsilon_f \left(\rho C_p\right)_f \frac{\partial \left\langle T_f \right\rangle^f}{\partial t} = \nabla.\left(\mathbf{K_{ff}}.\nabla\left\langle T_f \right\rangle^f + \mathbf{K_{fs}}.\nabla\left\langle T_s \right\rangle^s\right) - h\left(\left\langle T_f \right\rangle^f - \left\langle T_s \right\rangle^s\right) \tag{3.4}$$

$$\varepsilon_s \left(\rho C_p\right)_s \frac{\partial \left\langle T_s \right\rangle^s}{\partial t} = \nabla.\left(\mathbf{K_{sf}}.\nabla\left\langle T_f \right\rangle^f + \mathbf{K_{ss}}.\nabla\left\langle T_s \right\rangle^s\right) + h\left(\left\langle T_f \right\rangle^f - \left\langle T_s \right\rangle^s\right) \tag{3.5}$$

Here, the two phases are represented at the macroscopic scale, where the intrinsic average temperatures $\left\langle T_f \right\rangle^f, \left\langle T_s \right\rangle^s$ are defined as the local temperatures T_f and T_s averaged over the representative elementary volume. At the macroscopic scale, the medium is characterized by the effective properties $\mathbf{K_{ff}}$, $\mathbf{K_{fs}}$, $\mathbf{K_{sf}}$, $\mathbf{K_{ss}}$ and h that is the heat transfer coefficient characterizing the heat exchange between the two phases. The method of volume averaging detailed in Section 3.2.2 was used by [Quintard93]. It uses a steady-state closure of the problem at the microscopic scale. This simplifying assumption may not be relevant because large temperature differences may result in fast and transient heat transfer. Despite of that limitation, the phase exchange term is now simply expressed as the product of a volumetric heat exchange coefficient and the difference between the average temperatures of each phase.
The *quasi-steady* description provides a rather simplistic approximation to the real dynamics of the flux exchange. The space fluctuations of temperatures at a pore-scale are supposed to

evolve in a quasi-steady manner with respect to the mean temperatures. The consequences of the quasi-steady hypothesis on the macroscopic description of the transient processes were studied by [Landereau01], [Quintard93]. Those studies showed that the quasi-steady models gives satisfactory results compared to different direct numeric simulations. One can find also two-equation models without quasi-steady state assumption [Moyne97]. Here, the phase exchange term is expressed in the form of a temporal convolution of the difference between the average temperatures of each phase.

3.2 MACROSCOPIC MODEL OF THERMAL NON-EQUILIBRIUM

Although the two-equation macroscopic models received considerable attention [Landereau, 2001] [Quintard97], the more complex situations involving three phase systems were much less studied [Petit98]. However, Petit et al. model did not take into account the phase change process. That is why, more recently, a three equation non-equilibrium model with phase change was developed by [Duval02], [Duval04]. This model constitutes the starting point for the present work.

One of the outcomes of Duval (2002) studies is the derivation of effective transport coefficients determined on the basis of a comprehensive analysis of the relationship between the pore-scale physics and the macroscopic description. This is an outstanding result because no other previous three-equation approaches allowed their determination. It was emphasized by [Quintard97] that the heuristic approaches do not allow the determination of the effective transport coefficient, such as the heat exchange coefficients that appear in the three-equation models. Postulating the existence of a local pore-scale heat transfer that would lead to a macro-scale heat exchange coefficient, expressed as this coefficient multiplied by the specific area, is misleading since there is no clear boundary layer theory that can be set up in the porous medium context [Quintard97]. One can assume the determination of transport coefficients from experiments, but as was shown in [Grangeot94], [Grosser96] there are several experimental difficulties and the effective properties correlations are very difficult to obtain. In the experiments, different heat transfers should be estimated including the heat losses.

In this Chapter the three-equation macroscopic model of Duval (2002) will be summarized. The limitations of that model with respect to the important physical processes identified in the previous Chapter will be discussed. The two-phase flow in porous medium was studied as a three-phase system as represented in Figure 3.1. The flow of a liquid and its vapor was considered in a rigid porous structure. The solid was identified as the *s*-phase, the liquid as the *l*-phase, and the vapor as the *g*-phase. It was assumed that the physical properties of the fluids do not change strongly with temperature. The drastic assumption that the two-phase flow problem can be decoupled from the heat transfer problem and can be solved independently was adopted. As a consequence, when looking at the heat transfer problem, the velocities of the two phases are assumed to be known. The macroscopic description from up-scaling theory

and detailed analysis of the problem can be found in [Duval02] or [Duval04] and we will not go through the details of that analysis, except when necessary. A quasi-static theory has been proposed, which neglects the effects associated with the possible rapid changes of the two-phase interface as was discussed in a paragraph 3.1.2. In this case, relative permeabilities and capillary pressure relationships can be determined from the pore-scale description. In practice, however, this is only useful if the assumptions made concerning the interface geometry are physically acceptable. Otherwise, the position of the interface must be determined by solving problems that are similar to the original two-phase flow problem, which is an extremely difficult task even in the case of moderately complex porous structures. The above decoupling assumption may be too drastic in many situations, especially in the case of *intense boiling*, and this will be discussed later in this thesis.

3.2.1 Mass and energy pore-scale equations

The pore-scale boundary value problem describes the mass transfer process as:

$$\frac{\partial \rho_g}{\partial t} + \nabla.\left(\rho_g \mathbf{v}_g\right) = 0 \text{, in the g-phase} \tag{3.6}$$

$$\mathbf{v}_g = 0, \text{ at } A_{gs}$$

$$\mathbf{n}_{lg}\rho_g\left(\mathbf{v}_g - \mathbf{w}\right) = \mathbf{n}_{lg}\rho_l\left(\mathbf{v}_l - \mathbf{w}\right), \text{ at } A_{lg}$$

$$\mathbf{v}_l = 0, \text{ at } A_{ls}$$

$$\frac{\partial \rho_l}{\partial t} + \nabla.\left(\rho_l \mathbf{v}_l\right) = 0 \text{, in the l-phase}$$

Here $\mathbf{w}$ is the liquid-vapor interface velocity, $\mathbf{n}_{lg}$ represents the unit normal directed from the *l*-phase towards the *g*-phase and A_{lg} is the *l*-*g* interface. On the other hand, the pore-scale heat transfer problem in the three-phase system is described in terms of the following governing differential equations:

- gas phase

$$\frac{\partial \rho_g h_g}{\partial t} + \nabla.\left(\rho_g h_g \mathbf{v}_g\right) = \nabla.\left(k_g \nabla T_g\right) \tag{3.7}$$

- liquid phase

$$\frac{\partial \rho_l h_l}{\partial t} + \nabla.\left(\rho_l h_l \mathbf{v}_l\right) = \nabla.\left(k_l \nabla T_l\right) \tag{3.8}$$

- solid phase

$$\frac{\partial \rho_s h_s}{\partial t} = \nabla.\left(k_s \nabla T_s\right) + \varpi_s \tag{3.9}$$

where ϖ_s represents a constant homogeneous volumetric thermal source in the solid phase. The compressibility, viscous dissipation and radiation exchange were neglected. The boundary conditions at the liquid-solid and gas-solid interfaces express continuity of both temperatures and heat fluxes:

$$T_g = T_s,\ \mathbf{n}_{gs}.k_g \nabla T_g = \mathbf{n}_{gs}.k_s \nabla T_s \text{ at } A_{gs} \tag{3.10}$$

$$T_l = T_s,\ \mathbf{n}_{ls}.k_l \nabla T_l = \mathbf{n}_{ls}.k_s \nabla T_s \text{ at } A_{ls} \tag{3.11}$$

The boundary conditions at the liquid–vapor interface are more complex because phase change takes place at this interface. It is quite reasonable to assume that the vapor phase is in thermodynamical equilibrium with the liquid phase at the *l–g* interface. This basically means that the interface temperature is fixed at the equilibrium saturation temperature T_{sat}. Under these circumstances, the boundary conditions at the liquid–vapor interface are written as:

$$\begin{aligned} &T_l = T_g = T_{sat} \text{ at } A_{lg} \\ &\mathbf{n}_{lg}.\left(-k_g \nabla T_g + \rho_g h_g (\mathbf{v}_g - \mathbf{w})\right) = \mathbf{n}_{lg}.\left(-k_l \nabla T_l + \rho_l h_l (\mathbf{v}_l - \mathbf{w})\right) \text{ at } A_{lg} \end{aligned} \tag{3.12}$$

3.2.2 Volume averaging

The three-temperature macroscopic model was developed by Duval (2002) using the method of volume averaging. In this method, an averaging volume *V* is associated with every point in space as illustrated in Figure 3.1. Then, the macroscopic transport equations can be obtained by averaging the pore-scale transport equations over this volume. The length scale constraints required in the method of volume averaging are discussed in details elsewhere [Quintard93] and here we note only that the averaging volume must be large compared with the pore-scale characteristic lengths l_g, l_l and l_s but small compared to the macroscopic characteristic length *L*. For some function ψ_β associated with the β-phase, we define two different averages, the phase average $\langle \psi_\beta \rangle$ and the intrinsic phase average $\langle \psi_\beta \rangle^\beta$. These two averages are defined according to:

$$\begin{aligned} \langle \psi_\beta \rangle &= \frac{1}{V} \int_{V_\beta} \psi_\beta dV \\ \langle \psi_\beta \rangle^\beta &= \frac{1}{V_\beta} \int_{V_\beta} \psi_\beta dV \\ \langle \psi_\beta \rangle &= \varepsilon_\beta \langle \psi_\beta \rangle^\beta \end{aligned} \tag{3.13}$$

in which V_β represents the volume of the β-phase contained within the averaging volume and ε_β is the volume fraction of the β-phase ($\varepsilon_g + \varepsilon_l + \varepsilon_s = 1$). The point values ψ_β in the β-phase differ from the intrinsic phase average $\langle \psi_\beta \rangle^\beta$ by a value called the pore scale deviation $\tilde{\psi}_\beta$ according to Gray's spatial decomposition:

$$\psi_\beta = \langle \psi_\beta \rangle + \tilde{\psi}_\beta \tag{3.14}$$

3.2.3 Mass and energy macroscopic balance equations

The major steps leading to the macroscopic forms are detailed in Whitaker (1998). The volume averaging theory, general transport and spatial averaging theorems [Whitaker85]

together with the boundary condition expressed in Eq. (3.6) lead to the following continuity macroscopic equations:

$$\begin{aligned}\frac{\partial \varepsilon_g \rho_g}{\partial t} + \nabla.\left(\rho_g \left\langle \mathbf{v}_g \right\rangle\right) &= \dot{m} \\ \frac{\partial \varepsilon_l \rho_l}{\partial t} + \nabla.\left(\rho_l \left\langle \mathbf{v}_l \right\rangle\right) &= -\dot{m}\end{aligned} \tag{3.15}$$

where $\left\langle v_g \right\rangle$ and $\left\langle v_l \right\rangle$ are the superficial Darcy's velocities and it is assumed that the liquid and vapor phase densities do not vary significantly within the averaging volume and can be identified with the intrinsic phase average densities $\left\langle \rho_g \right\rangle$ and $\left\langle \rho_l \right\rangle$. The mass flow rate of evaporation is defined according to:

$$\dot{m} = -\frac{1}{V}\int_{Agl} \mathbf{n}_{gl} \rho_g \left(\mathbf{v}_g - \mathbf{w}\right) dA \tag{3.16}$$

Again for the pore-scale equations, the volume averaging, general transport and the spatial averaging theorem lead to the macroscopic equations. More detailed development can be found in Carbonell (1984), Gray (1975) and Zanotti (1984). The spatial decompositions and the macroscopic mass transport equations (3.15) result in:

- gas phase

$$\begin{aligned}&\frac{\partial\left(\alpha\varepsilon\left\langle \rho_g \right\rangle^g \left\langle h_g \right\rangle^g\right)}{\partial t} + \nabla.\left(\alpha\varepsilon\left\langle \rho_g \right\rangle^g \left\langle \mathbf{v}_g \right\rangle^g \left\langle h_g \right\rangle^g\right) + \nabla.\left(\left(\rho C_p\right)_g \left\langle \tilde{T}_g \tilde{\mathbf{v}}_g \right\rangle\right) = \dot{m}_g h_g^{sat} \\ &+ \nabla.\left(\varepsilon_g k_g \nabla\left\langle T_g \right\rangle^g + \frac{k_g}{V}\int_{Agl} \mathbf{n}_{gl} \tilde{T}_g dA + \frac{k_g}{V}\int_{Ags} \mathbf{n}_{gs} \tilde{T}_g dA\right) - \nabla\varepsilon_g . k_g \left\langle T_g \right\rangle^g \\ &+ \frac{k_g}{V}\int_{Agl} \mathbf{n}_{gl} . \nabla \tilde{T}_g dA + \frac{k_g}{V}\int_{Ags} \mathbf{n}_{gs} . \nabla \tilde{T}_g dA\end{aligned} \tag{3.17}$$

- liquid phase

$$\begin{aligned}&\frac{\partial\left((1-\alpha)\varepsilon\left\langle \rho_l \right\rangle^l \left\langle h_l \right\rangle^l\right)}{\partial t} + \nabla.\left((1-\alpha)\varepsilon\left\langle \rho_l \right\rangle^l \left\langle \mathbf{v}_l \right\rangle^l \left\langle h_l \right\rangle^l\right) + \nabla.\left(\left(\rho C_p\right)_l \left\langle \tilde{T}_l \tilde{\mathbf{v}}_l \right\rangle\right) = \dot{m}_l h_l^{sat} \\ &+ \nabla.\left(\varepsilon_l k_l \nabla\left\langle T_l \right\rangle^l + \frac{k_l}{V}\int_{A\,lg} \mathbf{n}_{lg} \tilde{T}_l dA + \frac{k_l}{V}\int_{Als} \mathbf{n}_{ls} \tilde{T}_l dA\right) - \nabla\varepsilon_l . k_l \left\langle T_l \right\rangle \\ &+ \frac{k_l}{V}\int_{A\,lg} \mathbf{n}_{lg} . \nabla \tilde{T}_l dA + \frac{k_l}{V}\int_{Als} \mathbf{n}_{ls} . \nabla \tilde{T}_l dA\end{aligned} \tag{3.18}$$

- solid phase

$$\begin{aligned}&\frac{\partial\left((1-\varepsilon)\left\langle \rho_s \right\rangle^s \left\langle h_s \right\rangle^s\right)}{\partial t} = \nabla.\left(\varepsilon_s k_s \nabla\left\langle T_s \right\rangle^s + \frac{k_s}{V}\int_{Asl} \mathbf{n}_{sl} \tilde{T}_s dA + \frac{k_s}{V}\int_{Asg} \mathbf{n}_{sg} \tilde{T}_s dA\right) \\ &- \nabla\varepsilon_s . k_s \left\langle T_s \right\rangle^s + \frac{k_s}{V}\int_{Asl} \mathbf{n}_{sl} . \nabla \tilde{T}_s dA + \frac{k_s}{V}\int_{Asg} \mathbf{n}_{sg} . \nabla \tilde{T}_s dA + \omega_s\end{aligned} \tag{3.19}$$

In these equations, $\langle T_\beta \rangle^\beta$ is the temperature of the β-phase. Areas integral in these equations are closely related to the heat flux exchanged between the phases divided by the averaging volume.

3.2.4 Closed form of the averaged equations

The above summarized macroscopic equations include not only the temperature of the β-phase $\langle T_\beta \rangle^\beta$, but also their fluctuations $\tilde{T}_\beta$. At this stage the macroscopic equations represent a system that is not closed and it is thus necessary to treat the problem applying the local boundary conditions for the deviations $\tilde{T}_\beta$.

The temporal derivatives at the closure level can be discarded by imposing the constraints of quasi-steady treatment of $\tilde{T}_\beta$ fields [Quintard93], [Quintard97]. It is assumed that the interface evolution at the pore level is *quasi-static*. However, the quasi-static approximation may be debatable for liquid-vapor systems especially for local thermal non-equilibrium situations. On the other hand, it is reasonable to assume the spatiotemporal ergodicity for which the spatial average over a given elementary volume containing a lot of interfaces would be implicitly equivalent to a time average of the interfaces movements which, as a result, would evolve as quasi-static. Because of that, from a practical point of view, a quasi-static theory may produce satisfactory results even for situations involving non-quasi-static flows [Duval04].

Under these circumstances, the pore-scale boundary value problem for the deviations can be simplified and the boundary conditions can be decomposed in order to introduce also the phase change temperature [Duval04]. Finally, the spatial deviation temperatures in terms of the macroscopic source terms can be expressed according to the following linear representation:

$$\begin{aligned}\tilde{T}_g = &-s_{li}^g\left(\langle T_l\rangle^l - T_{sat}\right) - s_{gi}^g\left(\langle T_g\rangle^g - T_{sat}\right) - s_{si}^g\left(\langle T_s\rangle^s - T_{sat}\right)\\ &+ \mathbf{b}_{gl}.\nabla\langle T_l\rangle^l + \mathbf{b}_{gg}.\nabla\langle T_g\rangle^g + \mathbf{b}_{gs}.\nabla\langle T_s\rangle^s\end{aligned} \tag{3.20}$$

$$\begin{aligned}\tilde{T}_l = &-s_{li}^l\left(\langle T_l\rangle^l - T_{sat}\right) - s_{gi}^l\left(\langle T_g\rangle^g - T_{sat}\right) - s_{si}^l\left(\langle T_s\rangle^s - T_{sat}\right)\\ &+ \mathbf{b}_{ll}.\nabla\langle T_l\rangle^l + \mathbf{b}_{lg}.\nabla\langle T_g\rangle^g + \mathbf{b}_{ls}.\nabla\langle T_s\rangle^s\end{aligned} \tag{3.21}$$

$$\begin{aligned}\tilde{T}_s = &-s_{li}^s\left(\langle T_l\rangle^l - T_{sat}\right) - s_{gi}^s\left(\langle T_g\rangle^g - T_{sat}\right) - s_{si}^s\left(\langle T_s\rangle^s - T_{sat}\right)\\ &+ \mathbf{b}_{sl}.\nabla\langle T_l\rangle^l + \mathbf{b}_{sg}.\nabla\langle T_g\rangle^g + \mathbf{b}_{ss}.\nabla\langle T_s\rangle^s\end{aligned} \tag{3.22}$$

The variables $s_{li}^s, \mathbf{b}_{sl}$, etc., are the closure variables or the mapping variables that realize an approximate solution of the coupled equations. The nomenclature used for the mapping scalars is such that the superscript always identifies the phase in which the function is defined, while the subscript always indicates which temperature difference is being mapped onto a

spatial deviation. The detailed explanation can be found in Duval (2002), Duval et al. (2004). The closure variables are solution of six pore-scale boundary value problems, the so-called closure problems. When solving the closure problems, either analytically or numerically, it is usually assumed that the porous medium can be represented by a periodic system as shown in Figure 3.2. In this case, the periodic length defines the averaging volume and closure problems have to be solved over representative unit cells of the three-phase system under consideration with periodic boundary conditions. Given the representations in equations (3.20)-(3.22) the macroscopic transport equations (3.17)-(3.19) lead to the following closed form:

- gas phase

$$\begin{aligned}&\frac{\partial\left(\alpha\varepsilon\left\langle\rho_g\right\rangle^g\left\langle h_g\right\rangle^g\right)}{\partial t}+\nabla.\left(\alpha\varepsilon\left\langle\rho_g\right\rangle^g\left\langle \mathbf{v}_g\right\rangle^g\left\langle h_g\right\rangle^g\right)=\nabla.\left(\mathbf{K}_g^*.\nabla\left\langle T_g\right\rangle^g\right)+\dot{m}_g h_g^{sat}\\&-\left(h_{gi}^{gl}+h_{gi}^{gs}\right)\left(\left\langle T_g\right\rangle^g-T_{sat}\right)-\left(h_{si}^{gl}+h_{si}^{gs}\right)\left(\left\langle T_s\right\rangle^s-T_{sat}\right)\end{aligned} \tag{3.23}$$

- liquid phase

$$\begin{aligned}&\frac{\partial\left((1-\alpha)\varepsilon\left\langle\rho_l\right\rangle^l\left\langle h_l\right\rangle^l\right)}{\partial t}+\nabla.\left((1-\alpha)\varepsilon\left\langle\rho_l\right\rangle^l\left\langle \mathbf{v}_l\right\rangle^l\left\langle h_l\right\rangle^l\right)=\nabla.\left(\mathbf{K}_l^*.\nabla\left\langle T_l\right\rangle^l\right)+\dot{m}_l h_l^{sat}\\&-\left(h_{li}^{lg}+h_{li}^{ls}\right)\left(\left\langle T_l\right\rangle^l-T_{sat}\right)-\left(h_{si}^{lg}+h_{si}^{ls}\right)\left(\left\langle T_s\right\rangle^s-T_{sat}\right)\end{aligned} \tag{3.24}$$

- solid phase

$$\begin{aligned}&\frac{\partial\left((1-\varepsilon)\left\langle\rho_s\right\rangle^s\left\langle h_s\right\rangle^s\right)}{\partial t}=\nabla.\left(\mathbf{K}_s^*.\nabla\left\langle T_s\right\rangle^s\right)+\omega_s-h_{li}^{ls}\left(\left\langle T_l\right\rangle^l-T_{sat}\right)\\&-h_{gi}^{gs}\left(\left\langle T_g\right\rangle^g-T_{sat}\right)-\left(h_{si}^{sl}+h_{si}^{gs}\right)\left(\left\langle T_s\right\rangle^s-T_{sat}\right)\end{aligned} \tag{3.25}$$

In these equations, $\left\langle h_\beta\right\rangle^\beta$ and $\left\langle T_\beta\right\rangle^\beta$ are the macroscopic enthalpy and the temperature of the β phase where (β=*g, l, s* for the gas, liquid and solid phase). $\mathbf{K}_\beta^*$ is the effective thermal diffusion tensor and h_{li}^{lg} etc. are the heat transfer coefficients related to the pore-scale physics through the six closure problems detailed in Duval (2002), Duval et al. (2004).

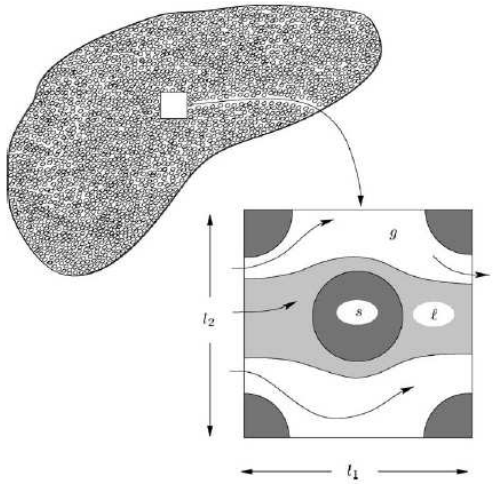

Figure 3.2: Unit cell of a spatially periodic model of a porous medium

One of the attractive features of the proposed three-equation model lies in the derivation of a closed form of the evaporation rate at the closure level without any additional phenomenological relation. The condition necessary to determine the mass rate of evaporation is the approximation that the liquid-vapor interface temperature is fixed at the equilibrium saturation temperature. Using the mass balance equation (3.6) together with the auxiliary condition in equation (3.12) we obtain the following expression for the mass rate of evaporation at the macroscopic level:

$$\dot{m}\Delta h = \frac{1}{V}\int_{Agl} \mathbf{n}_{gl}.\left(k_l.\nabla T_l - k_g.\nabla T_g\right)dA \tag{3.26}$$

where k is the thermal conductivity of the liquid and gas phase respectively. The closed form of the mass rate of evaporation can be obtained using the method of volume averaging. We decompose the point temperatures according to equation (3.14) and we use the representations for the spatial temperatures given by equations (3.20) and (3.21). When the volume fraction gradients and the pseudo-convective contributions are negligible [Duval04] the closed form of the mass rate of evaporation takes the form:

$$\dot{m}\Delta h = \left(h_{li}^{lg} + h_{li}^{gl}\right)\left(\langle T_l\rangle^{l} - T_{sat}\right) + \left(h_{gi}^{lg} + h_{gi}^{gl}\right)\left(\langle T_g\rangle^{g} - T_{sat}\right) + \left(h_{si}^{lg} + h_{si}^{gl}\right)\left(\langle T_s\rangle^{s} - T_{sat}\right) \tag{3.27}$$

Where h_{li}^{lg} etc. are the heat transfer coefficients related to the pore-scale physics through the six closure problems detailed in Duval (2002), Duval et al. (2004) and will be summarized in the next section.

3.2.5 Formulation of heat transfer coefficients- stratified Unit Cells

In the energy equations, it can be easily shown that, under boiling conditions, the heat transfers by diffusion at the macroscopic scale can be neglected because the large gradients occur at the local scale. Therefore, the most important effective properties are the heat transfer coefficients which represent the effects of those large local gradients.

It was mentioned above that the closure variables are solution of six pore-scale boundary value problems that are detailed in Duval (2002), Duval el al. (2004). The proposed closure problems allow determining all the effective transport coefficients for representative Unit Cells. These Unit Cells should be as complex as needed to take into account as much local information as possible concerning the characterization of the system (e.g. matrix structure, liquid–vapor interfaces topology, two-phase flow regime, etc.). However, dealing with very complex Unit Cells represents a very complicated task. Firstly, a study of relatively simple Unit Cells was performed for the stratified cell and Chang's cell [Duval02]. Given the use of periodicity conditions at the closure level, the flow corresponds to a fully developed flow, and, as a consequence, velocity does not play a role (at least for laminar flows) in some of the closure problems, typically for those giving the heat exchange coefficients.

In Duval et al. (2004) two situations were investigated. The first situation is a stable liquid film in contact with the particles: in that case, water and particles must be subcooled for the steady-state to be verified. The second situation is a stable gas film: in that case, steam and particles must be highly superheated for the steady-state to be verified. These two stratified configurations are rather generic, and allowed to derive analytical solutions to the closure problems and obtain explicit relations for the heat transfer coefficients. Those configurations will now be referred to as SLG (solid-liquid-gas) and SGL (solid-gas-liquid) and are respectively shown in Figure 3.3. The model was validated by comparison with analytical solutions of one-dimensional problems involving either slow condensation (SLG configuration) or slow evaporation (SGL configuration) [Duval02].
Obviously, stratified Unit Cells are not highly representative of a real porous medium, but obtaining analytical expression was interesting in terms of theoretical analysis. However, it appears clearly that the two generic configurations that were selected are not likely to exist simultaneously within the same REV because it would require that neighbouring particles may be at very different temperatures (i.e. a temperature interval corresponding the difference between Leidenfrost and saturation temperatures). Two improvements must be sought:

- Expressions taking care of the pore scale complex geometry;
- Expressions taking into account the complex structure created by the intense boiling mechanism.

The last problem will be addressed in the next section of this thesis. However, as for the flow through the porous medium we assume that the flow structure can correspond to a distribution in channels [Tung88]. We assume that for an oriented liquid flow in porous medium we can expect a phase repartition where one phase will be "wetting" and the second phase will eventually flow in the channels in the form of bubbles or slugs. The objective of this simplified study was to provide the first estimates of the effective properties. Moreover, for these simplified geometries the theory was tested versus direct pore-scale simulations [Duval04]. A good agreement was obtained between the theory and the pore-scale calculations. This confirmed the validity and the practical interest of the proposed approach.

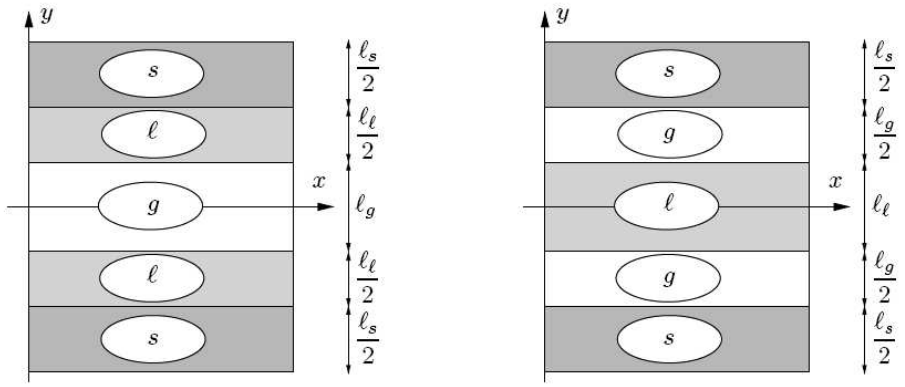

Figure 3.3: Stratified Unit Cell, solid-liquid-gas configuration (left) and solid-gas-liquid configuration (right)

In this section we will summarize the formulations for the heat transfer coefficients obtained for a stratified Unit Cells by Duval (2002).

In the SLG configuration, the coefficients that are not equal to zero are as follows:

- heat transfer coefficient between the gas and interface:

$$h_{gi}^{gl} = \frac{12k_g}{\varepsilon_g H^2} = h_g^0 \tag{3.28}$$

- heat transfer coefficient between the liquid and interface:

$$h_{li}^{lg} = 2g(\varepsilon_l)\frac{12k_l}{\varepsilon_l H^2} = 2g(\varepsilon_l)h_l^0 \tag{3.29}$$

where

$$g(\varepsilon_l) = \frac{(3\varepsilon_l + 2\varepsilon_s\kappa_{ls})}{(3\varepsilon_l + 4\varepsilon_s\kappa_{ls})} \tag{3.30}$$

- the last three coefficients influence the evolution of temperature of liquid and solid:

$$\begin{aligned} h_{li}^{ls} &= 2f(\varepsilon_l)h_l^0 \\ h_{si}^{ls} &= -\frac{2}{3}h_{li}^{ls} = -\frac{4}{3}h_l^0 \\ h_{si}^{lg} &= -\frac{1}{3}h_{li}^{ls} = -\frac{2}{3}f(\varepsilon_l)h_l^0 \end{aligned} \tag{3.31}$$

where the function $f(\varepsilon_l)$ is defined as:

$$f(\varepsilon_l) = (1 + 4\varepsilon_s\kappa_{ls}/3\varepsilon_l)^{-1} \tag{3.32}$$

and κ_{ls} is a fraction of thermal conductivity of liquid phase and solid. We can notice that the three coefficients that govern the temperature evolution of the solid and liquid phases are such that:

$$h_{li}^{ls} + h_{si}^{lg} + h_{si}^{ls} = 0 \tag{3.33}$$

In the SGL configuration, the coefficients that are not equal to zero are as follows:

- heat transfer coefficient between the liquid and interface:

$$h_{li}^{lg} = \frac{12k_l}{\varepsilon_l H^2} = h_l^0 \tag{3.34}$$

- heat transfer coefficient between the gas and interface:

$$h_{gi}^{gl} = 2g(\varepsilon_g)\frac{12k_g}{\varepsilon_g H^2} = 2g(\varepsilon_g)h_g^0 \tag{3.35}$$

where

$$g(\varepsilon_g) = \frac{(3\varepsilon_g + 2\varepsilon_s\kappa_{gs})}{(3\varepsilon_g + 4\varepsilon_s\kappa_{gs})} \tag{3.36}$$

- the last three coefficients influence the evolution of temperature of gas and solid:

$$\begin{aligned} h_{gi}^{gs} &= 2f(\varepsilon_g)h_g^0 \\ h_{si}^{gs} &= -\frac{4}{3}h_{gi}^{gs} = -\frac{4}{3}f(\varepsilon_g)h_g^0 \\ h_{si}^{gl} &= -\frac{2}{3}h_{gi}^{gs} = -\frac{2}{3}f(\varepsilon_g)h_g^0 \end{aligned} \tag{3.37}$$

Where the function $f(\varepsilon_g)$ is defined as:

$$\begin{aligned} f(\varepsilon_g) &= (1 + 4\varepsilon_s\kappa_{gs}/3\varepsilon_g)^{-1} \\ 2g(\varepsilon_g) &= 1 + f(\varepsilon_g) \end{aligned} \tag{3.38}$$

From this point, each transfer coefficient in SGL configuration can be expressed as a function of h_g^0 or h_g^1 as follows:

$$\begin{aligned} h_{gi}^{gl} &= h_g^0(1 + f(\varepsilon_g)) = h_g^0 + h_g^1 \\ h_{gi}^{gs} &= 2h_g^1 \\ h_{si}^{gs} &= -\frac{4}{3}h_g^1 \\ h_{si}^{gl} &= -\frac{2}{3}h_g^1 \end{aligned} \tag{3.39}$$

We can notice that the three coefficients that govern the temperature evolution of the solid and gas phase are such that:

$$h_{gi}^{gs} + h_{si}^{gs} + h_{si}^{gl} = 0 \tag{3.40}$$

These above introduced heat transfer coefficients appear in the closed form of the macroscopic equations (3.23)-(3.25) and (3.27). However, even after a simplification of the expression of those coefficients, it is still difficult to identify the flux really exchanged between two phases because the coupling is made between the three phases, as it can be seen by the relation Eq. (3.40). To make things clearer, a mathematical transformation and redistribution of heat transfer coefficients will be detailed now, for SGL configuration as an example. It is important to note, that a symmetrical formulation is, obviously, obtained for the SLG configuration. The objective of the following operations is to identify the heat transfers applied in each configuration and to allow a physical interpretation of the heat transfer terms.

The equation for the **gas phase** (3.23) has a form:

$$\frac{\partial\left(\alpha\varepsilon\left\langle\rho_g\right\rangle^g\left\langle h_g\right\rangle^g\right)}{\partial t}+\nabla.\left(\alpha\varepsilon\left\langle\rho_g\right\rangle^g\left\langle \mathbf{v}_g\right\rangle^g\left\langle h_g\right\rangle^g\right)=\nabla.\left(\mathbf{K}_g^*.\nabla\left\langle T_g\right\rangle^g\right)+\dot{m}_g h_g^{sat}$$
$$-\left(h_{gi}^{gl}+h_{gi}^{gs}\right)\left(\left\langle T_g\right\rangle^g-T_{sat}\right)-\left(h_{si}^{gl}+h_{si}^{gs}\right)\left(\left\langle T_s\right\rangle^s-T_{sat}\right) \tag{3.41}$$

Applying the relation identified in (3.40) to the equation for the gas phase in SGL configuration, and after some arithmetic transformations, the following terms on the right side reduce to:

$$\begin{aligned}
&-\left(h_{gi}^{gl}+h_{gi}^{gs}\right)\left(\left\langle T_g\right\rangle^g-T_{sat}\right)-\left(h_{si}^{gl}+h_{si}^{gs}\right)\left(\left\langle T_s\right\rangle^s-T_{sat}\right)\\
&=-\left(h_{gi}^{gl}+h_{gi}^{gs}\right)\left(\left\langle T_g\right\rangle^g-T_{sat}\right)-h_{gi}^{gs}\left(\left\langle T_s\right\rangle^s-T_{sat}\right)\\
&=-h_{gi}^{gl}\left(\left\langle T_g\right\rangle^g-T_{sat}\right)+h_{gi}^{gs}\left(\left\langle T_s\right\rangle^s-\left\langle T_g\right\rangle^g\right)=-\left(h_g^0+h_g^1\right)\left(\left\langle T_g\right\rangle^g-T_{sat}\right)+2h_g^1\left(\left\langle T_s\right\rangle^s-\left\langle T_g\right\rangle^g\right)\\
&=-h_g^0\left(\left\langle T_g\right\rangle^g-T_{sat}\right)+h_g^1\left(\left\langle T_s\right\rangle^s-\left\langle T_g\right\rangle^g\right)+h_g^1\left(\left\langle T_s\right\rangle^s+T_{sat}-2\left\langle T_g\right\rangle^g\right)\\
&=-\left(h_g^0-\frac{1}{3}h_g^1\right)\left(\left\langle T_g\right\rangle^g-T_{sat}\right)+\frac{2}{3}h_g^1\left(\left\langle T_s\right\rangle^s-\left\langle T_g\right\rangle^g\right)+\frac{4}{3}h_g^1\left(\left\langle T_s\right\rangle^s+T_{sat}-2\left\langle T_g\right\rangle^g\right)
\end{aligned} \tag{3.42}$$

The equation for the **solid phase** (3.25) has the form:

$$\frac{\partial\left((1-\varepsilon)\left\langle\rho_s\right\rangle^s\left\langle h_s\right\rangle^s\right)}{\partial t}=\nabla.\left(\mathbf{K}_s^*.\nabla\left\langle T_s\right\rangle^s\right)+\omega_s-h_{li}^{ls}\left(\left\langle T_l\right\rangle^l-T_{sat}\right)$$
$$-h_{gi}^{gs}\left(\left\langle T_g\right\rangle^g-T_{sat}\right)-\left(h_{si}^{sl}+h_{si}^{gs}\right)\left(\left\langle T_s\right\rangle^s-T_{sat}\right) \tag{3.43}$$

Applying the relation identified in (3.39)-(3.40) to the equation for the solid phase in a SGL configuration, the following terms on the right side reduce to:

$$\begin{aligned}
&h_{li}^{ls}\left(\left\langle T_l\right\rangle^l-T_{sat}\right)+h_{gi}^{gs}\left(\left\langle T_g\right\rangle^g-T_{sat}\right)+\left(h_{si}^{sl}+h_{si}^{gs}\right)\left(\left\langle T_s\right\rangle^s-T_{sat}\right)\\
&=0+h_{gi}^{gs}\left(\left\langle T_g\right\rangle^g-T_{sat}\right)+h_{si}^{gs}\left(\left\langle T_s\right\rangle^s-T_{sat}\right)\\
&=h_{gi}^{gs}\left(\left\langle T_g\right\rangle^g-T_{sat}\right)-\left(h_{gi}^{gs}+h_{si}^{gl}\right)\left(\left\langle T_s\right\rangle^s-T_{sat}\right)\\
&=h_{gi}^{gs}\left(\left\langle T_g\right\rangle^g-\left\langle T_s\right\rangle^s\right)-h_{si}^{gl}\left(\left\langle T_s\right\rangle^s-T_{sat}\right)\\
&=2h_g^1\left(\left\langle T_g\right\rangle^g-\left\langle T_s\right\rangle^s\right)-\frac{2}{3}h_g^1\left(\left\langle T_s\right\rangle^s-T_{sat}\right)\\
&=\frac{2}{3}h_g^1\left(\left\langle T_g\right\rangle^g-\left\langle T_s\right\rangle^s\right)-\frac{2}{3}h_g^1\left(\left\langle T_s\right\rangle^s+T_{sat}-2\left\langle T_g\right\rangle^g\right)
\end{aligned} \tag{3.44}$$

The equation for the **liquid phase** (3.24) has a form:

$$\frac{\partial\left((1-\alpha)\varepsilon\left\langle\rho_l\right\rangle^l\left\langle h_l\right\rangle^l\right)}{\partial t}+\nabla.\left((1-\alpha)\varepsilon\left\langle\rho_l\right\rangle^l\left\langle \mathbf{v}_l\right\rangle^l\left\langle h_l\right\rangle^l\right)=\nabla.\left(\mathbf{K}_l^*.\nabla\left\langle T_l\right\rangle^l\right)+\dot{m}_l h_l^{sat}$$
$$-\left(h_{li}^{lg}+h_{li}^{ls}\right)\left(\left\langle T_l\right\rangle^l-T_{sat}\right)-\left(h_{si}^{lg}+h_{si}^{ls}\right)\left(\left\langle T_s\right\rangle^s-T_{sat}\right) \tag{3.45}$$

Applying the relation identified in (3.40) to the equation for the liquid phase in a SGL configuration, the following terms on the right side reduce to:

$$\begin{aligned}
&-\left(h_{li}^{lg}+h_{li}^{ls}\right)\left(\left\langle T_l\right\rangle^{l}-T_{sat}\right)-\left(h_{si}^{lg}+h_{si}^{ls}\right)\left(\left\langle T_s\right\rangle^{s}-T_{sat}\right)\\
&=-\left(h_{li}^{lg}+0\right)\left(\left\langle T_l\right\rangle^{l}-T_{sat}\right)-(0+0)\left(\left\langle T_s\right\rangle^{s}-T_{sat}\right)\\
&=-h_{li}^{lg}\left(\left\langle T_l\right\rangle^{l}-T_{sat}\right)\\
&=-h_{l}^{0}\left(\left\langle T_l\right\rangle^{l}-T_{sat}\right)
\end{aligned} \tag{3.46}$$

Finally, applying the relation identified in (3.39)-(3.40) to the **<u>mass rate of evaporation</u>** in equation (3.27) in a SGL configuration, the terms on the right handside reduce to:

$$\begin{aligned}
&\dot{m}\Delta h=\left(h_{li}^{lg}+h_{li}^{gl}\right)\left(\left\langle T_l\right\rangle^{l}-T_{sat}\right)+\left(h_{gi}^{lg}+h_{gi}^{gl}\right)\left(\left\langle T_g\right\rangle^{g}-T_{sat}\right)+\left(h_{si}^{lg}+h_{si}^{gl}\right)\left(\left\langle T_s\right\rangle^{s}-T_{sat}\right)\\
&=h_{li}^{lg}\left(\left\langle T_l\right\rangle^{l}-T_{sat}\right)+h_{gi}^{gl}\left(\left\langle T_g\right\rangle^{g}-T_{sat}\right)+h_{si}^{gl}\left(\left\langle T_s\right\rangle^{s}-T_{sat}\right)\\
&=h_{l}^{0}\left(\left\langle T_l\right\rangle^{l}-T_{sat}\right)+h_{g}^{0}\left(\left\langle T_g\right\rangle^{g}-T_{sat}\right)+h_{g}^{1}\left(\left\langle T_g\right\rangle^{g}-T_{sat}\right)-\frac{2}{3}h_{g}^{1}\left(\left\langle T_s\right\rangle^{s}-T_{sat}\right)\\
&=h_{l}^{0}\left(\left\langle T_l\right\rangle^{l}-T_{sat}\right)+\left(h_{g}^{0}-\frac{1}{3}h_{g}^{1}\right)\left(\left\langle T_g\right\rangle^{g}-T_{sat}\right)+\frac{2}{3}h_{g}^{1}\left(2\left\langle T_g\right\rangle^{g}-\left\langle T_s\right\rangle^{s}-T_{sat}\right)
\end{aligned} \tag{3.47}$$

In summary, the closed form of the macroscopic energy transport equations can be written as follows:

- gas phase

$$\begin{aligned}
&\frac{\partial\left(\alpha\varepsilon\left\langle\rho_g\right\rangle^{g}\left\langle h_g\right\rangle^{g}\right)}{\partial t}+\nabla.\left(\alpha\varepsilon\left\langle\rho_g\right\rangle^{g}\left\langle\mathbf{v}_g\right\rangle^{g}\left\langle h_g\right\rangle^{g}\right)=\nabla.\left(\mathbf{K}_g^{*}.\nabla\left\langle T_g\right\rangle^{g}\right)+\dot{m}_g h_g^{sat}\\
&-\left(h_{g}^{0}-\frac{1}{3}h_{g}^{1}\right)\left(\left\langle T_g\right\rangle^{g}-T_{sat}\right)+\frac{2}{3}h_{g}^{1}\left(\left\langle T_s\right\rangle^{s}-\left\langle T_g\right\rangle^{g}\right)+\frac{4}{3}h_{g}^{1}\left(\left\langle T_s\right\rangle^{s}+T_{sat}-2\left\langle T_g\right\rangle^{g}\right)\\
&=\nabla.\left(\mathbf{K}_g^{*}.\nabla\left\langle T_g\right\rangle^{g}\right)+\dot{m}_g h_g^{sat}-\varphi_{gi}+\varphi_{sg}-\varphi_{gi}^{*}
\end{aligned} \tag{3.48}$$

- liquid phase

$$\begin{aligned}
&\frac{\partial\left((1-\alpha)\varepsilon\left\langle\rho_l\right\rangle^{l}\left\langle h_l\right\rangle^{l}\right)}{\partial t}+\nabla.\left((1-\alpha)\varepsilon\left\langle\rho_l\right\rangle^{l}\left\langle\mathbf{v}_l\right\rangle^{l}\left\langle h_l\right\rangle^{l}\right)=\nabla.\left(\mathbf{K}_l^{*}.\nabla\left\langle T_l\right\rangle^{l}\right)+\dot{m}_l h_l^{sat}\\
&-h_{l}^{0}\left(\left\langle T_l\right\rangle^{l}-T_{sat}\right)=\nabla.\left(\mathbf{K}_l^{*}.\nabla\left\langle T_l\right\rangle^{l}\right)+\dot{m}_l h_l^{sat}-\varphi_{li}
\end{aligned} \tag{3.49}$$

- solid phase

$$\begin{aligned}
&\frac{\partial\left((1-\varepsilon)\left\langle\rho_s\right\rangle^{s}\left\langle h_s\right\rangle^{s}\right)}{\partial t}=\nabla.\left(\mathbf{K}_s^{*}.\nabla\left\langle T_s\right\rangle^{s}\right)+\omega_s\\
&+\frac{2}{3}h_{g}^{1}\left(\left\langle T_g\right\rangle^{g}-\left\langle T_s\right\rangle^{s}\right)-\frac{2}{3}h_{g}^{1}\left(\left\langle T_s\right\rangle^{s}+T_{sat}-2\left\langle T_g\right\rangle^{g}\right)\\
&=\nabla.\left(\mathbf{K}_s^{*}.\nabla\left\langle T_s\right\rangle^{s}\right)+\omega_s-\varphi_{sg}-\varphi_{si}^{*}
\end{aligned} \tag{3.50}$$

- mass rate of evaporation

$$\dot{m}\Delta h = \varphi_{li} + \varphi_{gi} + \varphi_{gi}^{*} + \varphi_{si}^{*} \tag{3.51}$$

The schematic interpretation of the heat transfers is shown in Figure 3.4. In the expressions (3.48)-(3.51), the heat exchanges between gas and solid and between liquid and interface, which are intuitively expected, appear clearly. But, in addition, two "non classical" terms for heat exchange appear that we named φ_{gi}^{*} and φ_{si}^{*}. It appears that in the SGL configuration, the phase change rate is mainly governed by the non equilibrium of the liquid and/or gas phases but the solid temperature has a negligible impact. The closure solutions in Duval et al. (2004) result in zero contribution to the interfacial heat exchange in the case of a steady state, i.e. for steady state gas temperature $\approx 1/2(\langle T_s \rangle^s - T_{sat})$; the "corrective" heat exchanges involving the solid temperature, φ_{gi}^{*} and φ_{si}^{*}, are equal to zero. The heat transfers identified in this Chapter for SGL configuration are summarized in Table 3.1. This is in apparent contradiction with standard correlations for nucleate boiling or even film boiling. In the next section we propose a new formulation of the closure problems derived in Duval et al. (2004) in order to be able to extend the model to more complex situations where the solid temperature must be taken into account more explicitly.

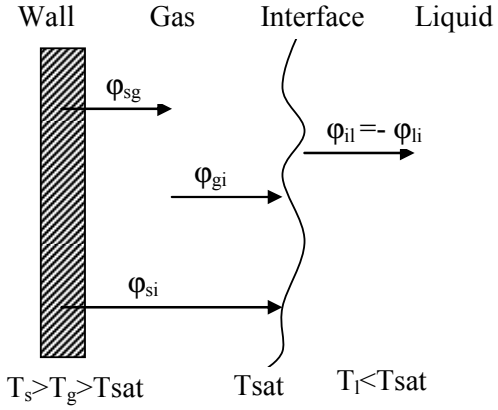

Figure 3.4: Thermal exchanges for SGL configuration

Table 3.1: Formulation of heat transfers in SGL and SLG configurations

SGL configuration	φ_{sl}	φ_{sg}	φ_{si}
	0	$\varphi_{sg} = \frac{2}{3} h_g^1 (T_s - T_g)$	$\varphi_{si}^{*} = \frac{2}{3} h_g^1 (T_s + T_{sat} - 2T_g)$
	φ_{gi}		φ_{li}
	$\varphi_{gi} = \frac{2}{3} h_g^0 f(\varepsilon_g)(T_g - T_{sat})$ $\varphi_{gi}^{*} = \frac{4}{3} h_g^1 (T_s + T_{sat} - 2T_g)$		$\varphi_{li} = h_l^0 (T_l - T_{sat})$
Coefficients	$h_l^0 = \frac{12 k_l}{\varepsilon_l H^2}$		

<table>
<tr><td></td><td colspan="3">$h_g^0 = \frac{12k_g}{\varepsilon_g H^2}$
$h_g^1 = h_g^0 f(\varepsilon_g)$</td></tr>
<tr><td rowspan="4">SLG configuration</td><td>φ_{sl}</td><td>φ_{sg}</td><td>φ_{si}</td></tr>
<tr><td>$\varphi_{sl} = \frac{2}{3} h_l^1 (T_s - T_l)$</td><td>0</td><td>$\varphi_{si}^* = \frac{2}{3} h_l^1 (T_s + T_{sat} - 2T_l)$</td></tr>
<tr><td colspan="2">φ_{gi}</td><td>φ_{li}</td></tr>
<tr><td colspan="2">$\varphi_{gi} = h_g^0 (T_g - T_{sat})$</td><td>$\varphi_{li} = \frac{2}{3} h_l^0 f(\varepsilon_l)(T_l - T_{sat})$
$\varphi_{li}^* = \frac{4}{3} h_l^1 (T_s + T_{sat} - 2T_l)$</td></tr>
<tr><td>Coefficients</td><td colspan="3">$h_l^0 = \frac{12k_l}{\varepsilon_l H^2}$
$h_g^0 = \frac{12k_g}{\varepsilon_g H^2}$
$h_l^1 = h_l^0 f(\varepsilon_l)$</td></tr>
</table>

3.3 IMPROVEMENTS OF MODEL OF THERMAL NON-EQUILIBRIUM

When superheated particles are considered, the modeling must also include boiling processes. The boiling process is characterized by the growth of bubbles at the surface of the particles or even a stable steam film if the temperature is high enough. If the porous medium temperature at the time of water injection is significantly higher than the rewetting temperature, complicated and unsteady flow and heat transfer patterns are generated. In the case of debris reflooding during a severe accident, the very large superheat of the particles would probably induce a film boiling regime, where the particles are surrounded by a stable steam film. As temperature reaches the minimum heat flux temperature (sometimes called Leidenfrost or quench temperature), a transition boiling regime is encountered, where an intermittent wetting of the surface begins and the heat transfer rate increases with decreasing surface temperature. At a surface temperature corresponding to critical heat flux, most of the surface becomes available for wetting and intense nucleate boiling ensues, causing the surface to cool rapidly until the saturation temperature is reached, below which the surface is cooled by single-phase liquid convection.

This “boiling” scenario has been particularly documented for pool boiling over different types of surfaces (flat, wires, …) [Dougall63], [Collier94]. It has also been studied in pipes or arrays of cylinders, such as those found in heat exchangers, these latter situations being closer to a porous medium structure [Bertsch09]. However, such ideas have not been translated into the case of a real porous medium. From crude observations on Petit and Prelude experiments, we believe that similar physical mechanisms take place within pores of highly permeable

media. One of the major proposals of this thesis is to try to implement this boiling curve concept into a macro-scale model.

In this section, a macroscopic model of thermal non-equilibrium is proposed, based on the previously summarized model which is improved in order to take into account intense boiling regimes (in particular nucleate boiling). In the two-phase flows that we consider, one important difference with respect to macrochannel flows is that the liquid flow is laminar. The heat transfer coefficients summarized in the previous section are valid for a laminar flow; they include the dependences on fluid properties and also on pore scale geometry. These heat transfer coefficients are valid for convective regimes and additional effects should be taken into account e.g. turbulences, bubble generation. In Figure 3.5 we have represented schematically the improvements that we have intended to take into account in both SLG and SGL configurations. We introduce additional processes (bubble generation) that may also contribute to phase change. The model that will be presented here involves a few parameters which cannot be evaluated from simple mechanistic models. The complete derivation of these parameters from a multiple-scale analysis is also very difficult because of the rapid transient aspects, moving interfaces, etc. However, those parameters can be bounded, following the analysis of experimental data presented in Chapter 2.

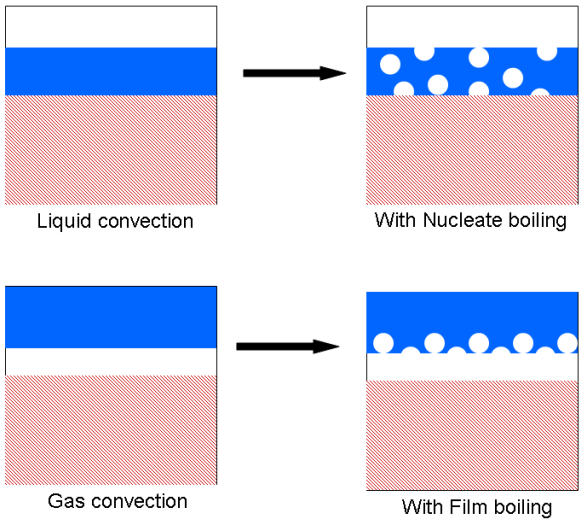

Figure 3.5: Extension of Unit Cells by addition of bubble generation “at the wall”

3.3.1 Regimes with intense phase change

When superheated particles are considered, the modeling must also include other processes which involve a fast motion of the fluid phases and, in particular, nucleation and growth of bubbles along the solid surface, bubble motion and convective transfer with gas at high velocity. To take into account these processes, one of the difficulties of the analysis is that the pore-scale physics cannot be represented correctly using a quasi-steady configuration of the

interface. However, the pore-scale physics may be represented by averaging over an interval of time the unstable and intermittent processes of bubble nucleation and departure or interface fast motion. By using such a method, it is obvious that the fluctuations of temperatures in the fluid phases depend both on time and space. And, practically, the instantaneous volume-averaged quantities used in Duval (2002), Duval et al. (2004) must be time averaged to filter these time fluctuations in the macro-scale equations. Therefore, for the regimes of intense evaporation (i.e., nucleate, transition and film boiling), the time averaging of the volume averaged equations requires the knowledge of quantities that characterize the motion of the gas bubbles and their size, as a replacement of the quasi-steady configurations considered for slow phase change.

But time averaging also induces some simplifications. Because of ergodicity, the volume average of time averaged fluctuations must be equal to zero. Therefore, all terms involving an interfacial average of fluctuations may be set to zero. The remaining terms involve only the gradient of fluctuations. Again, because of ergodicity, the time average of an interfacial exchange term can be estimated by doing a volume average of a steady-state heat transfer resulting from averaging over a sufficient time the transient process followed by a bubble (nucleation, growth and departure). At this stage, it is necessary to introduce a "time averaged" closure relation and a geometrical relation in order to describe the bubble size and frequency of departure.

3.3.1.1 Nucleate boiling regime

The main data that can be obtained from experiments are measurement of the heat flux extracted from the solid phase by the boiling process. For classical boiling problems over simple elementary surfaces, it is commonly expressed as [Collier94], [Griffith60]:

$$\varphi_s^{nb} = C_n (T_s - T_{sat})^i \tag{3.52}$$

where φ_s^{nb} is the nucleate boiling heat flux and the constant C_n and the exponent i depend on the fluid properties and the state and properties of the solid surface. We assume that, for the regime of nucleate boiling, bubbles are generated at the saturation temperature and that the flux φ_s^{nb} only contributes to evaporate water and create the bubbles. Therefore, a negligible amount of heat is transferred to the gas or the liquid in the nucleate boiling regime compared to the phase change process. In this paper, we make the conjecture that a relation similar to equation (3.19) may be used, which allows us to write the following relation:

$$\varphi_s^{nb} = \frac{k_s}{V}\left(\int_{Asl} \mathbf{n}_{sl}.\nabla \widetilde{T}_s dA + \int_{Asg} \mathbf{n}_{sg}.\nabla \widetilde{T}_s dA\right) = C_n (\langle T_s \rangle^s - T_{sat})^i \tag{3.53}$$

So we can naturally introduce a mapping function s_{nb}^s that verifies:

$$\int_{Asl} \mathbf{n}_{sl}.\nabla s_{nb}^s dA + \int_{Asg} \mathbf{n}_{sg} \nabla s_{nb}^s dA = \frac{C_n V}{k_s} \tag{3.54}$$

In order to take into account that nucleate boiling does not necessarily occur everywhere in the control volume because of possible variations of the local temperature of particles, we

introduce a new estimate for the local temperature deviations, for SLG configuration (see also equations (3.20)-(3.22)):

$$\begin{aligned}\widetilde{T}_s &= s_{li}^s\left(\langle T_l\rangle^l - T_{sat}\right)+ s_{si}^s\left(\langle T_s\rangle^s - T_{sat}\right)+ s_{nb}^s\left(\langle T_s\rangle^s - T_{sat}\right)^i\\ \widetilde{T}_l &= s_{li}^l\left(\langle T_l\rangle^l - T_{sat}\right)+ s_{si}^l\left(\langle T_s\rangle^s - T_{sat}\right)\\ \widetilde{T}_g &= 0\end{aligned} \tag{3.55}$$

The direct resolution of closure problems is not possible and we propose an approximate solution by assuming that we may *superimpose* the solutions obtained from two sets of temperature deviations. The first corresponds to the linear deviations used in Duval (2002), Duval et al. (2004), for which we already have either analytical or numerical solutions in simple cases (see equations (3.20)-(3.22)):

$$\begin{aligned}\widetilde{T}_s &= s_{li}^s\left(\langle T_l\rangle^l - T_{sat}\right)+ s_{si}^s\left(\langle T_s\rangle^s - T_{sat}\right)\\ \widetilde{T}_l &= s_{li}^l\left(\langle T_l\rangle^l - T_{sat}\right)+ s_{si}^l\left(\langle T_s\rangle^s - T_{sat}\right)\\ \widetilde{T}_g &= 0\end{aligned} \tag{3.56}$$

The second corresponds to the temperature deviations for which the closure problem is defined by the equation (3.54):

$$\begin{aligned}\widetilde{T}_s &= s_{nb}^s\left(\langle T_s\rangle^s - T_{sat}\right)^i\\ \widetilde{T}_l &= 0\\ \widetilde{T}_g &= 0\end{aligned} \tag{3.57}$$

This non linear closure problem cannot be solved analytically because there is no quasi-steady position of the contact points defining A_{sg} and A_{sl}. However, the useful solution is only the time average of the surface integrals, which is given by the expression for φ_s^{nb} in Eq. (3.52).

3.3.1.2 Film boiling regime

In a similar way, the main data that can be obtained from experiments are measurement of the heat flux extracted from the solid phase by the boiling process. It is commonly expressed for simple elementary cases [Dougall63], [Whalley87]:

$$\varphi_s^{fb} = C_f\left(T_s - T_{sat}\right)^k \tag{3.58}$$

where φ_s^{fb} is the film boiling heat flux, the constant C_f and the exponent k depend on the fluid properties. For our porous medium model, we assume that, for the regime of film boiling, bubbles are periodically released in the liquid part which is at the saturation temperature and that the flux φ_s^{fb} only contributes to evaporate water and create the bubbles. Therefore, no heat is transferred to the gas or the liquid in the film boiling regime besides phase change. Following the strategy previously used, we assume:

$$\varphi_s^{fb} = \frac{k_s}{V}\left(\int_{A_{sl}} \mathbf{n}_{sl}.\nabla\widetilde{T}_s dA + \int_{A_{sg}} \mathbf{n}_{sg}.\nabla\widetilde{T}_s dA\right) = C_f\left(\langle T_s\rangle^s - T_{sat}\right)^k \tag{3.59}$$

We can naturally introduce a mapping function s_{fb}^{s} that verifies:

$$\int_{A_{sl}} \mathbf{n}_{sl}.\nabla s_{fb}^{s} dA + \int_{A_{sg}} \mathbf{n}_{sg}.\nabla s_{fb}^{s} dA = \frac{C_f V}{k_s} \tag{3.60}$$

In order to take into account that film boiling does not necessarily occur everywhere in the control volume because of possible variations of the local void fraction, we introduce different estimates for the temperature deviations in SGL configuration (see also equations (3.20)-(3.22)):

$$\begin{aligned}
\widetilde{T}_s &= s_{gi}^{s}(\langle T_g \rangle^{g} - T_{sat}) + s_{si}^{s}(\langle T_s \rangle^{s} - T_{sat}) + s_{fb}^{s}(\langle T_s \rangle^{s} - T_{sat})^{k} \\
\widetilde{T}_g &= s_{gi}^{g}(\langle T_g \rangle^{g} - T_{sat}) + s_{si}^{g}(\langle T_s \rangle^{s} - T_{sat}) \\
\widetilde{T}_l &= 0
\end{aligned} \tag{3.61}$$

As for the nucleate boiling regime, an approximate solution may be obtained by assuming that it is possible to *superimpose* the solutions obtained from two sets of equations: the linear one, and the non linear one (involving only $\widetilde{T}_s$). The first correspond to the linear deviations used in Duval (2002), Duval et al. (2004), for which we have analytical solutions in simple cases (see equations (3.20)-(3.22)):

$$\begin{aligned}
\widetilde{T}_s &= s_{gi}^{s}\left(\langle T_g \rangle^{g} - T_{sat}\right) + s_{si}^{s}\left(\langle T_s \rangle^{s} - T_{sat}\right) \\
\widetilde{T}_g &= s_{gi}^{g}\left(\langle T_g \rangle^{g} - T_{sat}\right) + s_{si}^{g}\left(\langle T_s \rangle^{s} - T_{sat}\right) \\
\widetilde{T}_l &= 0
\end{aligned} \tag{3.62}$$

The second correspond to the temperature deviations for which the closure problem is defined by the equation (3.60):

$$\begin{aligned}
\widetilde{T}_s &= s_{fb}^{s}(\langle T_s \rangle^{s} - T_{sat})^{k} \\
\widetilde{T}_g &= 0 \\
\widetilde{T}_l &= 0
\end{aligned} \tag{3.63}$$

This non linear closure problem cannot be solved analytically because there is no quasi-steady position of the contact points defining A_{sg} and A_{sl}. However, the useful solution is only the time average of the surface integrals, which is given by the expression for φ_s^{fb} in Eq. (3.58).

3.3.2 Considerations about the phases distribution and flow regimes

When intense boiling occurs, steam accumulates within the pore space and begins to flow under strong buoyancy and viscous forces resulting in various possible phase distribution patterns. For pressure below 50 bars, e. g. nuclear reactor accident conditions, the huge ratio between the liquid and steam densities results in a fast increase of the steam volume fraction. As an example, the bubble size is approximately 2.5mm for steam in water, at atmospheric pressure, and 1.7mm, at 50 bars, if we apply the relation coming from the stability analysis of Kelvin [Lee09]:

$$d_b \approx \left(\frac{\sigma_g}{(\rho_l - \rho_g)g} \right)^{1/2} \tag{3.64}$$

Since we are interested by the flow within a porous medium, it is convenient to compare this free flow characteristic length to the particle characteristic size that we define:

$$D_h = \frac{d_p \varepsilon}{(1-\varepsilon)} = \sqrt{A} \frac{\sqrt{K}}{\sqrt{\varepsilon}} \tag{3.65}$$

where K is the permeability and A is the adjustable constant in Carman-Kozeny approach introduced in Chapter 2. We can define the following non dimensional number:

$$\frac{d_b}{D_h} \approx \sqrt{\frac{1}{A}} \left(\frac{\varepsilon \sigma_g}{(\rho_l - \rho_g)gK} \right)^{1/2} \tag{3.66}$$

When this number is small, the bubbles can easily flow between the particles whereas, when it is large, the "shape" of the bubbles and their motion is strongly affected by the presence of particles. In addition, in a porous medium, the reduced mobility of the gas phase is amplified at low void fractions, as expressed by the coefficient of relative permeability which remains close to zero up to relatively high values of the void fraction (see Darcy generalized equations in Chapter 2). As an example, with a standard formulation of the relative permeability like α^3 [Brooks64], the relative permeability is less than 0.01 for $\alpha = 0.2$. Therefore, it is reasonable to consider that, during the quenching of a superheated porous medium, the combination of intense boiling and large drag force at low void fraction of the steam phase leads to a significant void fraction at the quench front (and also, obviously, downstream of the quench front). This means that the "bubbly flow" regime discussed in [Tung88] has a low probability of occurring, being replaced by a distribution of phase where pockets of steam occupy the pore space. This is consistent with the discussion of Tung and Dhir (1988) who claimed that the bubbly flow regime could not exist if the void fraction is above 0.3 (for particle beds similar to the ones of interest for us). However, it is worth mentioning that it was also assumed by Tung and Dhir that the liquid film could remain around the particles up to a void fraction close to 1. It cannot be the case when intense boiling occurs because bubbles are generated at the surface of particles, with a wetting angle of 90° which does not favour rewetting of the surface by the liquid phase. Therefore, a representation of the distribution of the phases is proposed in Figure 3.5. Moreover, it might be assumed that steam would accumulate at the bottom of particles (for stability reasons, due to density difference) or as pockets surrounding several particles. Vapor slugs are also likely but their conditions of existence are more difficult to evaluate. So they will not be discussed in this paper. Anyway, the general formalism proposed here could be applied to vapor slugs if necessary.

We assume that when the volume of steam pockets increases, it is impossible for water to be in contact with all the surface of particles because the liquid film cannot become infinitely thin due to surface tension. Therefore, the fraction of particle surface in contact with the liquid must decrease when the void fraction increases. This important phenomenon was already observed in small hydraulic diameter channels by several authors [Thome04]. They concluded

that the flows are typically laminar and that the transient evaporation of the thin liquid films surrounding elongated bubbles is the dominant heat transfer mechanism. Without any experimental observations of the flow structure, we assume that an empirical function $g(\alpha)$ gives the fraction of non-wetted surface:

$$A_g/(A_g + A_l) = g(\alpha) \tag{3.67}$$

The introduction of this function is supported also by a bibliographic study, where several authors discussed the particularities of the nucleate boiling regime in a small diameter channels [Mudawar00], [Zhang06]. Many experimental studies have focused on this phenomenon [Thome04], [Bertsch09], [Mukherjee09]. It was concluded that in minichannels, bubbles get confined by the channel walls and hence the channel geometry plays an important role in the bubble growth process. At the same time, since the bubbles may even occupy the entire cross-section of the channels, their area of contact with the walls regulates the liquid flow as well as the wall heat transfer mechanisms [Mukherjee04].

Therefore we make the approximation that the surface integrals in equation (3.19) involving the solid interface may be approximated as:

- SLG configuration

$$\frac{k_s}{V}\int_{A_{sl}} \mathbf{n}_{sl}.\nabla\widetilde{T}_s dA = (1-g(\alpha))\frac{k_s}{V}\int_{A_s} \mathbf{n}_s.\nabla\widetilde{T}_s dA = (1-g(\alpha))\varphi_{sl} \tag{3.68}$$

- SGL configuration

$$\frac{k_s}{V}\int_{A_{sg}} \mathbf{n}_{sg}.\nabla\widetilde{T}_s dA = g(\alpha)\frac{k_s}{V}\int_{A_s} \mathbf{n}_s.\nabla\widetilde{T}_s dA = g(\alpha)\varphi_{sg} \tag{3.69}$$

In addition to the geometrical considerations discussed above, one has to take into account that the shape of the interface between water and steam will depend on temperature conditions at the surface of the particles, and other flow conditions highly determined by the pore-scale structure. The higher the temperature, the more likely is the existence of a stable steam film around the particles. Also, thermal fluctuations of the wall temperature may occur together with instabilities of bubble nucleation. This boiling mechanism is called the transition boiling. It occurs between $Ts\big|_{\varphi_{nb}}$ which is the maximum solid temperature reached in nucleate boiling regime (corresponding to the maximum heat flux) and $Ts\big|_{\varphi_{fb}}$ which is is the minimum solid temperature for which the film boiling regime exists (corresponding to the minimum heat flux). Although continuous research efforts have been devoted to the understanding of this transition process, it still defies a full accounting. Based on steady-state data, an empirical correlation which includes these effects has been devised [Liu93]. It involves a function defined below:

$$f(\theta,\xi) = \theta^{\xi} = \left(\frac{Ts - Ts\big|_{\varphi_{nb}}}{Ts\big|_{\varphi_{fb}} - Ts\big|_{\varphi_{nb}}}\right)^{\xi} \tag{3.70}$$

Then, the approximation is made that the surface integrals in equation (3.54) and (3.60) may be approximated in the transition zone as a linear combination of two terms:

$$\frac{k_s}{V}\left(\int_{A_{sl}} n_{sl}\nabla\widetilde{T}_s dA+\int_{A_{sg}} n_{sg}\nabla\widetilde{T}_s dA\right)=f(\theta,\xi)\varphi_s^{fb} \tag{3.71}$$

$$\frac{k_s}{V}\left(\int_{A_{sl}} n_{sl}\nabla\widetilde{T}_s dA+\int_{A_{sg}} n_{sg}\nabla\widetilde{T}_s dA\right)=(1-f(\theta,\xi))\varphi_s^{nb} \tag{3.72}$$

The linear combination may be interpreted as the change in the intensity of bubble formation, therefore it is not applied to the convective terms φ_{sl} and φ_{sg} which represent heat transfers at locations where bubbles are not generated (following the assumed superposition of independent effects).

3.3.3 Considerations on the momentum equations

This Chapter deals mostly with heat transfer model where the most important development was realized during this thesis. Concerning the momentum balance equations, the theoretical background concerning flow in porous medium was summarized in Chapter 2. In the last paragraph we will shortly introduce only one phenomenon that we studied. It is the effect of the phase repartition on the other transport properties which are the relative permeabilities (Chapter 2, Section 2.1). For the momentum transport equations, it is also expected that the phase repartition and therefore the boiling regime diagram has an important impact on the transport properties. We came from the work of Duval (2002), Duval et al. (2004), where the relative permeabilities were estimated for the stratified cells, in the absence of a real knowledge of the debris bed structure and real phase repartition. We will not detail here the physical development. We recall here, that in the SGL configuration, the relative permeabilities were given by the following relations:

$$K_{rg}^{SGL}=\alpha^2\left[\alpha+\frac{3}{2}(1-\alpha)\right] \tag{3.73}$$

$$K_{rl}^{SGL}=(1-\alpha)\left[(1-\alpha)^2+\frac{3}{2}\frac{\mu_l}{\mu_g}(2\alpha(1-\alpha)+\alpha^2)\right] \tag{3.74}$$

where μ is the dynamic viscosity. The symmetric solution was found for SLG configuration [Duval02]. In this paragraph we propose, following the assumption of intermittent contact between the particles and both fluid phases that the balance of friction forces is:

$$\frac{1}{K_{rl}}=(1-f(\theta,\xi))\frac{1}{K_{rl}^{SLG}}+f(\theta,\xi)\frac{1}{K_{rl}^{SGL}} \tag{3.75}$$

$$\frac{1}{K_{rg}}=(1-f(\theta,\xi))\frac{1}{K_{rg}^{SLG}}+f(\theta,\xi)\frac{1}{K_{rg}^{SGL}} \tag{3.76}$$

The combination represents the change in the wetting phase. The effect of that combination will be illustrated and discussed in Chapter 4 and Appendix.

3.4 CONCLUSIONS

- In this Chapter, we have developed a model starting from the macroscopic model of flow and mass transfer phenomena with phase change in porous media previously developed by Duval (2002).

The model is based on a pore-scale quasi-static assumption for the momentum equation closure i.e., the interfaces do not change rapidly in comparison with viscous dissipation. It was stated that this condition may break down in the case of intense boiling and an alternative approach was developed in Section 3.3. We have also shown that the model did not explicitly include phase change terms involving the solid temperature, as one would intuitively expect.

We have shown that it is formally possible to represent the dynamic processes involved in the nucleate or film boiling, in the case of a porous medium problem, by the addition of a separate set of closure relations which deal essentially with the solid temperature deviation and its gradient at the surface of the particles. The resulting heat transfer terms are obtained by superimposing the solutions coming from the 1^{st} order linear problem and from the non-linear one. Therefore, all the results obtained in the previous model remain valid in the improved one. But the range of application of the new model is greatly extended. In particular, it covers all the range between liquid film condensation and vapour film boiling.

We are now in a position to test the validity and consistency of the proposed model and this is the subject of Chapter 5. To achieve this goal, it is necessary to propose correlation for all the coefficients and parameters introduced in this Chapter. It must also be implemented numerically into a computer code. This will be presented in the next Chapter, before testing the model against some available experimental data.

Chapter 4

NUMERICAL IMPLEMENTATION OF THE MODEL

4. NUMERICAL IMPLEMENTATION OF THE MODEL

The *reflood of a severely damaged reactor* is a phenomenon that is not well modelled in the current computer codes used in nuclear safety studies. However, as it was introduced in Chapter 1, this scenario could, in certain conditions, help to stop the progression of a severe accident. The efficiency of the reflood scenario should be proved, for instance the quantification of benefits and the associated risks of reflood of degraded core. This can only be done by doing calculations where the phenomena are modelled as accurately as possible in order to provide a sufficient level of confidence in the results. The following questions should be answered:

- Is there a chance to stop the progression of the severe accident?
- What is the associated hydrogen production?
- What is the associated pressure increase?

That is the reason why IRSN launched a R&D program where the objective was to reduce the uncertainties related to the evaluation of consequences of core reflood at any stage of its degradation. One of the objectives is to develop detailed and validated models that will be able to evaluate the realistic consequences of reflood. This program is based on actions related to experimental programs as well as the model development. In the frame of this R&D program, the objective of this thesis was to propose and implement a two-phase flow reflood of porous medium model into ICARE-CATHARE V2 code.

It is useful to mention here that a large number of computer codes are used in safety analysis. For the *accident scenarios with core degradation*, the integral severe accident analysis codes are needed to model the progression of an accident sequence from core damage through the containment failure. There exist integral codes e.g. ASTEC, MELCOR, MAAP [IRSN06] which have the following common characteristics:

- Treatment of the complete phenomena;
- Simplified treatment of coupling between phenomena;
- Modularity;
- Fast-running calculations (between 1 and 10 hours per day of accident);
- Application in safety analysis, particularly in evaluation of source term in EPS-2;
- Support for Severe Accident Management Guidelines.

Since integral codes rely on many physical simplifications and numerical approximations, they must be validated with respect to more detailed models. Therefore, IRSN follows a two-lever approach for the development of codes:

- On one hand, a global approach with the system code ASTEC, jointly developed by IRSN and GRS and dedicated to simulation of the whole scope of a severe accident [Pignet03]. It is based on fast-running models;

- On the other hand, a detailed or mechanistic approach with the code ICARE-CATHARE, developed by IRSN and dedicated to simulation of reactor cooling system behavior and core degradation [Guillard01].

4.1 ICARE-CATHARE COMPUTER CODE

The ICARE-CATHARE code results from a coupling between the code of mechanics, chemistry, heat transfers and degradation ICARE2, developed at IRSN and the thermohydraulics code CATHARE2, developed at CEA in collaboration with EDF, AREVA and IRSN. The main objective of the ICARE-CATHARE code is to perform the realistic evaluation of the consequences of severe accidents in terms of fission products release, water, steam and hydrogen release into containment, core and vessel degradation. The objective is also to evaluate the global behaviour of the primary circuit. In order to answer these needs, the code should be able to calculate all the phenomena that may happen during an accident, from the initiating event up to the vessel failure. We can thus distinguish three main phases:

- Beginning of the accident (Blackout or LOCA without availability of high or low pressure injection) followed by the core uncovering without serious damages at this first stage.
- Phase of core degradation with limited damages: oxidation and fusion of first materials, mostly metals.
- Phase of advanced degradation with loss of geometric integrity of the fuel, massive relocalisation of the corium (mixture of molten materials), melt-pool formation and vessel failure.

Currently, the modeling of the last two phases is not well predicted and the development is still ongoing. As for the severe accident approach, additional detailed models are being developed at IRSN for the ICARE-CATHARE code:

- Models of collapse of fuel rods and formation of debris beds;
- Models of oxidation of metal rich relocated mixtures;
- Models of thermal-hydraulic phenomena involved in reflooding of intact fuel rods;
- Models of reflooding of debris bed (which was the motivation for the work done in this thesis).

The objective of this Chapter is to describe the implementation of the model into ICARE-CATHARE. There are several advantages to do so:

- 3D thermohydraulics with resolution of the six-equations model over a finite volume discretization is already implemented into CATHARE2;
- The model used in CATHARE2 was obtained by volume averaging and already deals with thermal non-equilibrium of the three phases, although it was developed in a different context and is not directly applicable to porous media.
- A solver for sets of coupled non linear equations is already implemented (i.e. Newton-Raphson method);

- A first model for two-phase flow in porous medium was already implemented and tested [Bechaud01];
- Physical correlations for reflood of intact fuel rods are implemented and can be tested.
- Applications of the model to reactor scale transients can be done rather easily.

In this Chapter, the numeric implementation of the porous medium reflood model will be presented together with discussions about the physical correlations that have been chosen to deal with heat and momentum transfers.

4.2 PREVIOUS IMPLEMENTATION OF THE MODEL

In the ICARE-CATHARE code, the first model for two-phase flow in porous media was implemented before the beginning of this thesis [Bechaud01]. It was done directly from the results of previous doctoral thesis [Duval02]. The validation of the previous model [Bechaud01] was performed against Ginsberg and Tutu experimental data and was presented by [Fichot06], [Fichot09]. An exhaustive work was performed on model improvement and the testing of different additional physical parameters e.g. friction law, relative permeability and passability terms… However, the calculations showed that the model underestimated the progression of the quench front especially when the liquid velocity was important. Also the first validation against the PRELUDE experimental results was performed by the author of this thesis at the beginning of these studies. It was observed that the model did not provide satisfactory results. Because of lack of proper heat transfer coefficients for regimes of intense boiling, the heat flux transferred from the solid was underestimated which resulted in slow quench front progression (see Appendix A). This motivated the code development presented in this Chapter was performed.

If the debris bed geometry is present at least in a part of the mesh, CATHARE2 will activate the porous medium model. Thus, the specific balance equations have been implemented into CATHARE2 code for this specific geometry. Benefiting from 3D meshing of CATHARE2 code, the porous medium model is able to deal with multi-dimensional flows. The model is based on:

- Two momentum balance equations for the liquid and gas phases;
- Three energy balance equations for the solid, liquid and gas phases.

It is important to note that these equations are independent from the balance equations concerning the intact fuel rod geometry. They are activated only if the debris bed is formed. At the interface between a “porous medium mesh” and a “standard mesh”, one has to be aware that discontinuities of correlations will occur. It must be emphasized also that the development of correct boundary conditions at interfaces between porous media and areas with totally different physics (fluid layers, regions with tube bundles, etc…) is still an open research problem.

For the momentum balance equations, the Darcy generalized law is applied as it was summarized in Chapter 2 (Section 2.1):

-gas phase

$$\begin{aligned}&\alpha\left\langle\rho_g\right\rangle^g\left(\frac{\partial\left\langle\mathbf{v}_g\right\rangle^g}{\partial t}+\left\langle\mathbf{v}_g\right\rangle^g\otimes\nabla\left\langle\mathbf{v}_g\right\rangle^g\right)=-\alpha\nabla\left\langle p_g\right\rangle^g\\&+\alpha\left\langle\rho_g\right\rangle^g g-\varepsilon\alpha^2\left(\frac{\mu_g}{Kk_{rg}}\left\langle\mathbf{v}_g\right\rangle^g+\varepsilon\alpha\frac{\left\langle\rho_g\right\rangle^g}{\eta\eta_{rg}}\left\langle\mathbf{v}_g\right\rangle^g\left|\left\langle\mathbf{v}_g\right\rangle^g\right|\right)\end{aligned}\tag{4.1}$$

- liquid phase

$$\begin{aligned}&(1-\alpha)\left\langle\rho_l\right\rangle^l\left(\frac{\partial\left\langle\mathbf{v}_l\right\rangle^l}{\partial t}+\left\langle\mathbf{v}_l\right\rangle^l\otimes\nabla\left\langle\mathbf{v}_l\right\rangle^l\right)=-(1-\alpha)\nabla\left\langle p_l\right\rangle^l\\&+(1-\alpha)\left\langle\rho_l\right\rangle^l g-\varepsilon(1-\alpha)^2\left(\frac{\mu_l}{Kk_{rl}}\left\langle\mathbf{v}_l\right\rangle^l+\varepsilon(1-\alpha)\frac{\left\langle\rho_l\right\rangle^l}{\eta\eta_{rl}}\left\langle\mathbf{v}_l\right\rangle^l\left|\left\langle\mathbf{v}_l\right\rangle^l\right|\right)\end{aligned}\tag{4.2}$$

where the debris bed is characterized by the permeability and passability terms (K and $\underline{\eta}$). The exponent in the relative permeability and passability terms (K_{rl}, K_{rg} and η_{rl}, η_{rg}) was left as a user-defined parameter (see possible values in Chapter 2).

As for the energy balance equations, the model is based on the three-equation non-equilibrium model that was presented in previous Chapter and we can write:

- gas phase

$$\begin{aligned}&\frac{\partial\left(\alpha\varepsilon\left\langle\rho_g\right\rangle^g\left\langle h_g\right\rangle^g\right)}{\partial t}+\nabla.\left(\alpha\varepsilon\left\langle\rho_g\right\rangle^g\left\langle\mathbf{v}_g\right\rangle^g\left\langle h_g\right\rangle^g\right)=\\&\nabla.\left(K_g^*.\nabla\left\langle T_g\right\rangle^g\right)+\dot{m}_g h_g^{sat}+\varphi_{sg}-\varphi_{gi}^*-\varphi_{gi}\end{aligned}\tag{4.3}$$

- liquid phase

$$\begin{aligned}&\frac{\partial\left((1-\alpha)\varepsilon\left\langle\rho_l\right\rangle^l\left\langle h_l\right\rangle^l\right)}{\partial t}+\nabla.\left((1-\alpha)\varepsilon\left\langle\rho_l\right\rangle^l\left\langle\mathbf{v}_l\right\rangle^l\left\langle h_l\right\rangle^l\right)=\\&\nabla.\left(\mathbf{K}_l^*.\nabla\left\langle T_l\right\rangle^l\right)+\dot{m}_l h_l^{sat}+\varphi_{sl}-\varphi_{li}^*-\varphi_{li}\end{aligned}\tag{4.4}$$

- solid phase

$$\begin{aligned}&\frac{\partial\left((1-\varepsilon)\left\langle\rho_s\right\rangle^s\left\langle h_s\right\rangle^s\right)}{\partial t}=\\&\nabla.\left(\mathbf{K}_s^*.\nabla\left\langle T_s\right\rangle^s\right)-\varphi_{sl}-\varphi_{sg}-\varphi_{si}^*-\varphi_{si}+\omega_s\end{aligned}\tag{4.5}$$

In the previous Chapter we have shown that the "corrective" heat exchanges $\varphi_{\beta i}^*$ involving the solid temperature result in zero contribution to the interfacial heat exchange in the case of a

steady state. These corrective heat exchanges are not more discussed in this thesis. These heat exchanges will be directly added to other terms for convenience of the numerical formulation. The $\langle h_\beta \rangle^\beta$ and $\langle T_\beta \rangle^\beta$, are the macroscopic enthalpy and the temperature of the β-phase respectively ($\beta = g, l, s$ for the gas, liquid and the solid phases). $\mathbf{K}^*_\beta$ is the effective thermal diffusion tensor. The phase change rate is given by the relation:

$$\dot{m}_g = \frac{\varphi_{si} + \varphi_{gi} + \varphi_{li} + \varphi^*_{si} + \varphi^*_{gi} + \varphi^*_{li}}{h_g^{sat} - h_l^{sat}} \tag{4.6}$$

4.3 IMPLEMENTATION OF IMPROVED MODEL

In this section, the details of implementation of the improved two-phase flow porous medium reflood model will be listed. It will include both the choices for correlations and the criteria for transition for one flow regime to another. The improvements of the previously developed two-phase flow non-equilibrium model were summarized in Chapter 3. The basic numerical implementation that will be discussed in this section concerns mainly:

- Energy balance equations: the application of heat transfer coefficients was modified, new heat transfer coefficients were introduced and different flow regimes (see Figure 4.1) were included following the improvements of the model presented in Chapter 3.
- Momentum balance equations: modifications concerning the relative permeability and passability coefficients were introduced and tested.

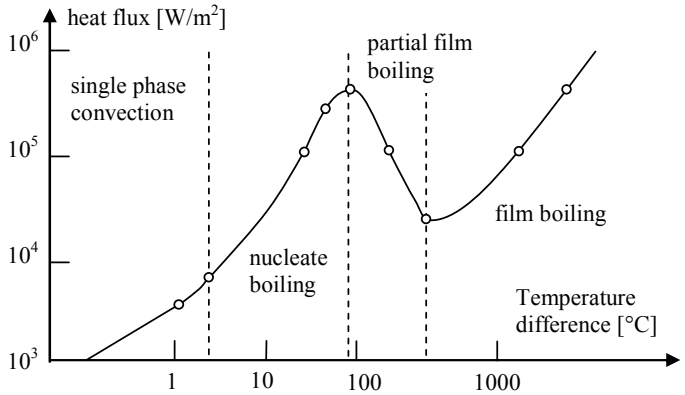

Figure 4.1: Example of flow boiling curve (Nukiyama curve)

The basic improvement of the model consists in the introduction of heat transfers in a case of intense boiling (φ_{si} in Eq. (4.3)-(4.6)) for the regimes of nucleate boiling, film boiling and transition between those two regimes. It was shown in Chapter 3 that it is formally possible to represent the dynamic processes involved in the nucleate, or film boiling, in the case of a porous medium problem, by the addition of a separate set of closure relations which deal essentially with the solid temperature deviation and its gradient at the surface of the particles. The resulting heat transfer terms are obtained by superimposing the solutions coming from the 1st order linear problem and from the non-linear one. For the linear problem, the heat

transfers were expressed with respect to temperature differences between the phases temperatures and the saturation temperature or with respect to more complex expressions as it was introduced in Chapter 3.

For the non linear problem, no analytical solution can be obtained but empirical correlations coming from experimental data, which are explicitly part of the closure problem, are used and, with the assumptions made, it leads to the following heat transfer terms:

$$\begin{aligned} \varphi_{si} &= C_{nb,f}(\langle T_s \rangle^s - T_{sat})^{i,m} \\ \varphi_{s\beta} &= 0 \\ \varphi_{\beta i} &= C_\beta \varphi_{si} = C_\beta C_{nb}(\langle T_s \rangle^s - T_{sat})^{i,m} \end{aligned} \tag{4.7}$$

It is important to note that, rigorously, the non linear problem leads to non zero terms for $\varphi_{\beta i}$ but it is not possible, at this point, to evaluate their importance with respect to the linear ones. However, they should be almost negligible because we have assumed that the main contributor to the phase change rate is as follows:

$$\dot{m}_g \Delta h = \varphi_{si} + \varphi_{li} + \varphi_{gi} \tag{4.8}$$

Therefore, the final proposed expression for the heat exchange terms are the following:

$$\begin{aligned} \varphi_{si} &= C_{nb,f}(\langle T_s \rangle^s - T_{sat})^{i,m} \\ \varphi_{s\beta} &= h_{s\beta}(\langle T_s \rangle^s - \langle T_\beta \rangle^\beta) \\ \varphi_{\beta i} &= h_{\beta i}(\langle T_\beta \rangle^\beta - T_{sat}) + C_\beta C_{nb}(\langle T_s \rangle^s - T_{sat})^{i,m} \end{aligned} \tag{4.9}$$

where the nomenclature for energy transfers (see Figure 4.2) has been chosen to be compatible with the existing ICARE-CATHARE thermohydraulic modeling:

φ_{li} interface to liquid heat flux

φ_{gi} interface to gas heat flux

φ_{sl} wall to liquid heat flux

φ_{sg} wall to gas heat flux

φ_{si} wall to interface heat flux that induces directly vaporization

Here the word “wall” should be understood to be equivalent to the solid phase.

The formulation of energy transfers in ICARE-CATHARE model will be summarized in the next sections.

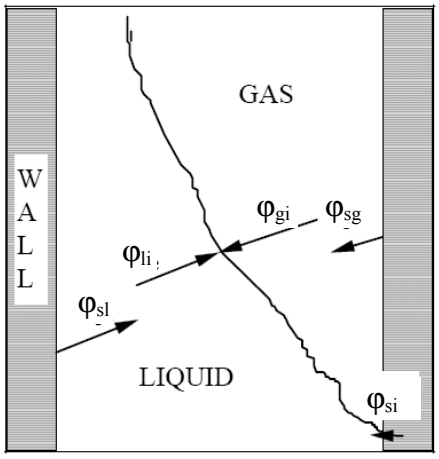

Figure 4.2: Description of energy transfers

4.3.1 Wall to fluid heat transfer

In this paragraph, the ICARE-CATHARE algorithm for the determination of heat transfer modes, especially for wall to fluid heat transfers under different boiling regimes is introduced. The basic assumptions and conditions for each boiling regime have been discussed in the previous Chapter. In the present one, the aim is to provide the logical path that is followed in order to end up with a unique formulation of all the terms appearing in the energy equations, depending on local conditions (void fraction, temperatures, velocities, pressure).
This issue is first addressed by defining a unique boiling curve from which the code selects the appropriate heat transfer regimes (and then the associated coefficients) (see Figure 4.3) for both phases (vapor/liquid) and for the solid. The boiling regimes as well as the transition criteria will be summarized below.

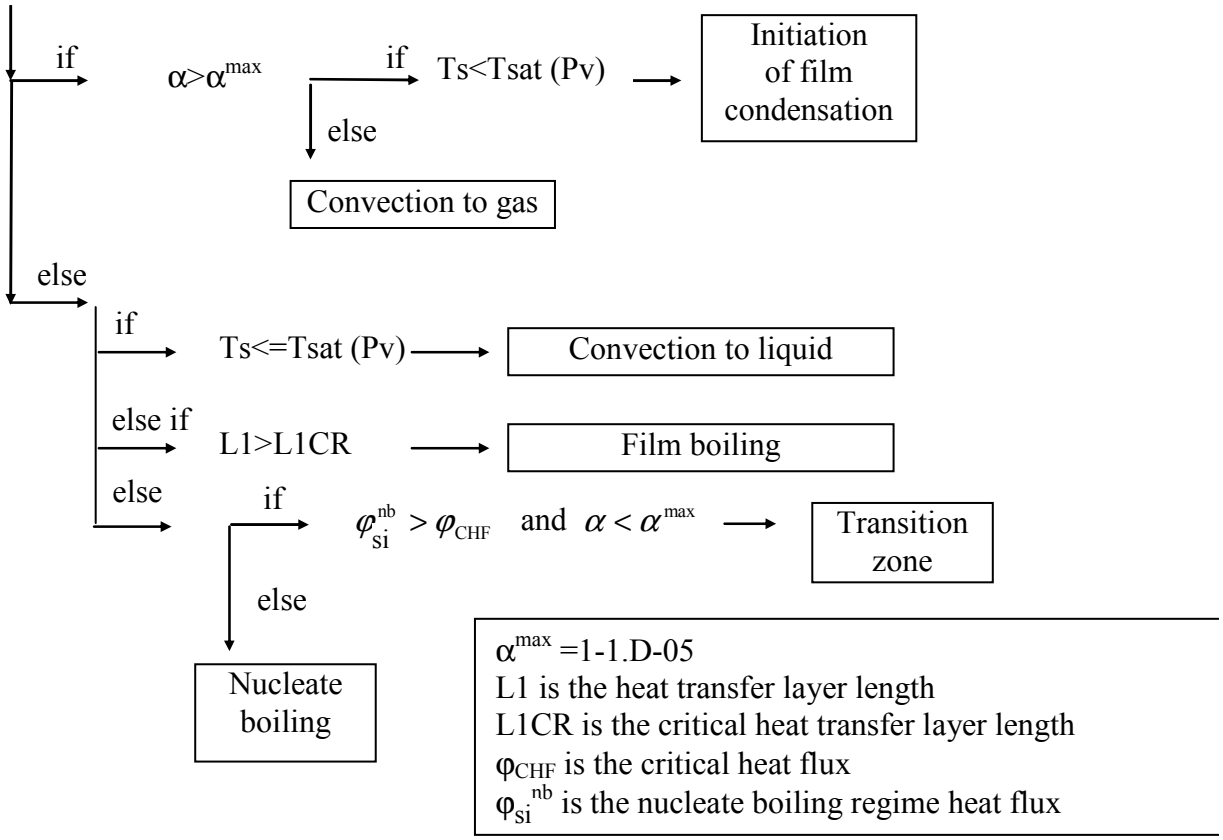

Figure 4.3: Logical map of the heat transfer regimes

4.3.1.1 Heat transfer on wetted solid surface

In this paragraph we will describe two regimes concerning the heat transfer of wetted wall: single phase convection with liquid and nucleate boiling regime.

Single phase convection with liquid

According to the formulation of heat exchange terms in equation (4.9), the heat exchanges applied in regime of *convection with liquid* are as follows:

$$\begin{aligned} \varphi_{sl} &= h_{li}^{ls}\left(T_s - T_l\right) \\ \varphi_{sg} &= 0 \\ \varphi_{si} &= 0 \end{aligned} \tag{4.10}$$

and interfacial heat flux:

$$\begin{aligned} \varphi_{gi} &= h_{gi}^{gl}\left(T_g - T_{sat}\right) \\ \varphi_{li} &= h_{li}^{lg}\left(T_l - T_{sat}\right) \end{aligned} \tag{4.11}$$

where the h_{li}^{ls}, h_{gi}^{gl} and h_{li}^{lg} are the heat transfer coefficients obtained for the SLG stratified Unit Cell configuration summarized in Chapter 3. In this kind of configuration, the heat transfer coefficients do not depend on the phase velocity since this velocity is assumed to be parallel with the infinite-direction. In addition, during reflood of debris bed with safety

injection, the liquid flow is assumed to be laminar because the liquid Reynolds numbers is below 2300. The additional development in equations (4.10) concerned thus the limits for the single-phase flow and the geometry composed of spheres instead of parallel planes (used in the stratified cells calculations).

In equations (4.10), the phase change rate should tend to zero and the model of thermal non-equilibrium for three phases should reduce to the model of thermal non-equilibrium for two phases. Therefore, heat exchange between fluid phase and interface should tend to zero. The heat transfer coefficients used in the $\varphi_{\beta i}$ exchange were thus adapted to follow this trend.

Secondly, the volumetric heat exchange coefficient that comes from the theory is transformed to surface units and applied in φ_{sl} heat exchange. In the absence of the real knowledge of the pore-scale geometry and flow structure, the effective coefficients were built from a combination of simple estimates based on either simple geometrical structures (e.g., the "stratified" unit cell), or extrapolations to porous media of correlations coming from the boiling literature in the case of simple solid surfaces. Precisely, the volumetric heat exchange coefficient obtained analytically for the simple stratified Unit Cell (UC) is divided by its specific area, $1/d_p$, multiplied by the specific area of the real porous medium. For a compact bed of spheres of porosity close to 0.4, the specific area is approximately $10/\mathrm{d_p}$. So this increases the analytical coefficient by a factor 10 if we assume that the whole sphere surface is concerned with heat exchange (which is not entirely exact because of contact areas between spheres). The effect of increasing the convective heat transfer coefficient will be presented in Chapter 5 (Section 5.1.2.1).
At this point, it must be emphasized that the specific area do not really play the role of a scaling factor, since heat diffusion leads to a cut-off in the impact of surface fluctuations. For instance, a grain with a small slit will barely have the same heat transfer characteristics than the grain without the slit while it will have a very different specific area. In the absence of a thorough study of a real debris bed structure, the use of the simple stratified Unit Cell (UC) and the proposed scaling is just a commodity.

Nucleate boiling regime

According to the formulation of heat exchange terms in equation (4.9), the heat exchanges applied in regime of *nucleate boiling* are as follows:

$$\begin{aligned}
\varphi_{\mathrm{sl}} &= \left(1-\mathrm{g}(\alpha)\right)\mathrm{h}_{\mathrm{li}}^{\mathrm{ls}}\left(\mathrm{T_s}-\mathrm{T_l}\right)\\
\varphi_{\mathrm{sg}} &= \mathrm{g}(\alpha)\mathrm{h}_{\mathrm{gi}}^{\mathrm{gs}}\left(\mathrm{T_s}-\mathrm{T_g}\right)\\
\varphi_{\mathrm{si}} &= \left(1-\mathrm{g}(\alpha)\right)\mathrm{C_{nb}}\left(\mathrm{T_s}-\mathrm{T_{sat}}\right)^{\mathrm{i}}
\end{aligned} \tag{4.12}$$

where h_{li}^{ls} is the heat transfer coefficient from SLG configuration (see Chapter 3) and h_{gi}^{gs} is the heat transfer coefficient from SGL configuration (see Chapter 3).
The function $g(\alpha)$ is introduced in equation (4.12) and, as a crude estimation, the fraction of non-wetted surface is assumed equal to the gas volume fraction:

$$g(\alpha) = \alpha \tag{4.13}$$

It is assumed that nucleate boiling is suppressed with an increase in vapor quality which inhibits bubble growth and leads to dry-out. Suppression of the bubbles appears to be largely independent of the channel diameter. The formulation chosen for the present work assumes that pool boiling is not suppressed when $\alpha = 0$ and in the case of saturated steam nucleate boiling is absent if $\alpha = 1$.

The nucleate boiling constants C_{nb} and i are introduced in equation (4.12). In ICARE-CATHARE code for standard applications, Thom's correlation is used and is valid for hydraulic diameters around 8 millimetres. Beside different correlations available in literature [Collier94], [Griffith60], the correlation that is already implemented in ICARE-CATHARE code is [Guillard01]:

$$\begin{aligned} C_{nb} &= 1.97.10^{3} \exp(0.23.10^{-6} P) \\ i &= 2 \end{aligned} \tag{4.14}$$

where P is the pressure in [Pa]. However, in debris bed applications, we assume that for a lower hydraulic diameter the heat transfer coefficient will reach higher values. As an example, this assumption is verified in single phase forced flow in channels, using the standard Dittus-Boelter correlation [Guillard01]:

$$\begin{aligned} Nu &= f\left(Re^{0.8}\right) \\ h &= f\left(\frac{1}{D_h}\right)^{0.2} \end{aligned} \tag{4.15}$$

where the exponent is 0.2. We assume that for a nucleate boiling regime in small hydraulic channels, a similar tendency can be expected. Thus, we introduce into Thom's correlation (4.14) a dependence on the hydraulic diameter. Here, the bibliographic studies are limited and for instance, we propose a boiling correction that comes from Groeneveld boiling studies in channels [Guillard01]. He introduced a function *F1* that is a correction to the boiling constant depending on the hydraulic diameter. As a reference, he studied boiling in channels of 8mm size. He proposed the following corrections that limit the boiling if the hydraulic diameter increases (D_h>16mm) or decreases (D_h<4mm):

$$\begin{aligned} F1 &= \left(\frac{8}{D_h}\right)^{1/3} \quad 4mm < D_h < 16mm \\ F1 &= \left(\frac{8}{16}\right)^{1/3} = 0.79 \quad D_h > 16mm \\ F1 &= \left(\frac{8}{4}\right)^{1/3} = 1.259 \quad D_h < 4mm \end{aligned} \tag{4.16}$$

It may be noted that the hydraulic diameter is lower than 4mm in a debris bed with porosity 0.4 and particle diameter between 1-5mm. Finally, the nucleate boiling constants C_{nb} and i in equation (4.12) are proposed as follows:

$$\begin{aligned} C_{nb} &= F1 * 1.97.10^{3} \exp(0.23.10^{-6} P) \\ i &= 2 \end{aligned} \tag{4.17}$$

Critical heat flux

Most of the correlations for critical heat flux are based on empirical relations and applicability of these relations depends on the experimental conditions and how the geometry and heat flux redistribution corresponds to reactor reflood application conditions. In the conditions of interest for us, the hydraulic diameter (<8mm) and the liquid mass flow rate (<50kg/m^{2}s), the most of the critical heat flux correlations are not valid. It will be shown here. Because of the small hydraulic diameters found typical for porous media flows, a specific critical heat flux correlation should be used.

An extensive database including approximately 2500 saturated critical heat flux data, from 10 different laboratories, for water flowing in small diameter tubes ($0.33 < D_h < 6.22$ mm) have been collected by Zhang et al. (2006). They proposed a new correlation based on the inlet conditions by doing parametric trends analysis of the collected database:

$$\begin{aligned} \frac{\varphi_{CHF}}{G h_{fg}} = 0.0352 &\left[We_D + 0.0119 (L/D_h)^{2.31} (\rho_g / \rho_l)^{0.361} \right]^{-0.295} (L/D_h)^{-0.311} \\ &* \left[2.05 (\rho_g / \rho_l)^{0.17} - x_{eq,in} \right] \end{aligned} \tag{4.18}$$

with

$$We_D = \frac{G^2 D_h}{\sigma \rho_l} \tag{4.19}$$

The Zhang correlation for critical heat flux (Figure 4.4) is based on inlet (upstream) channel conditions. Here, the effect of inlet quality in inlet conditions is expressed in the term $x_{eq,in}$. Thus the quality variations along the channel are taken into account through the dependence on the channel length L. The other variables can be found in the Nomenclature. Consequently, the critical heat flux correlation depends on the parameter (L/D_h).

Secondly, there are the correlations for the critical heat flux that are based on outlet (local) conditions. These correlations are dependent on the outlet enthalpy (or outlet subcooling or quality). Therefore, use of an outlet condition correlation involves indirect estimation of the critical heat flux since outlet quality must first be calculated with the critical heat flux data point using an energy balance over the entire heated length. This is why channel length does not appear in these correlations. A correlation for critical heat flux in small diameter channels based on the outlet conditions was proposed by Mudawar (2000):

$$\frac{\varphi_{CHF}}{G\,h_{fg}} = C_1 We_D^{C_2} \left(\frac{\rho_f}{\rho_g}\right)^{C_3} \left[1 - C_4 \left(\frac{\rho_f}{\rho_g}\right)^{C_5} x_0\right] \tag{4.20}$$

where C1 = 0.0722, C2 = −0.312, C3 = −0.644, C4 = 0.900, C5 = 0.724. The Mudawar correlation for critical heat flux (Figure 4.5) is valid for the hydraulic diameter between 0.25 mm and 15 mm. The validity of the equation is in the range of mass flux 300 < G < 30000 kg/m^{2}s.

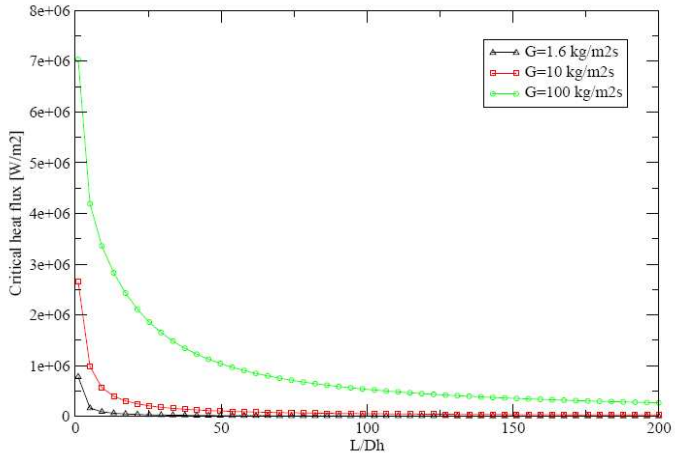

Figure 4.4: Example of critical heat flux predicted by Zhang correlation

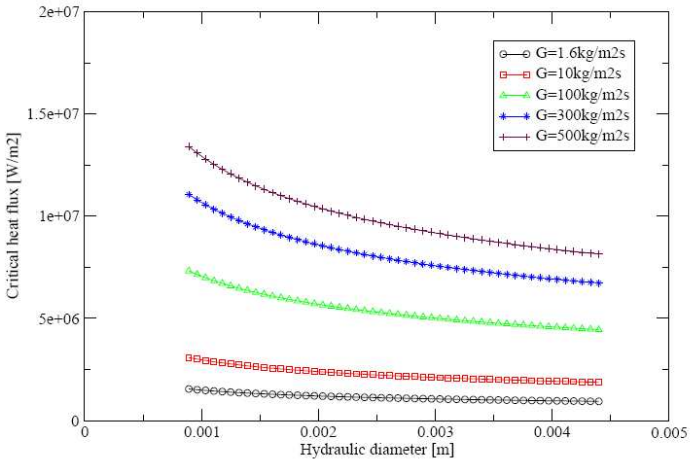

Figure 4.5: Example of critical heat flux predicted by Mudawar correlation

However, the critical heat flux correlations that depend on the characteristic length or outlet conditions are not convenient for reflood of porous media modeling. The characteristic length is difficult to be identified for a given porous medium geometry and outlet conditions are unknown for a bottom liquid injection. That is the reason why we have decided to keep in our modeling the correlation that is already implemented into ICARE-CATHARE and proposed by Groeneveld [Guillard01]. This was validated and verified for many nuclear reactor calculations. This correlation depends on pressure, mass flow and quality:

$$\varphi_{CHF} = F1 * 10^{F(G,P,X)+3} \tag{4.21}$$

where the function *F* is an interpolation function of the Groeneveld table [Guillard01]. We refer the reader to bibliography [Groeneveld96] for details concerning this table. We point out here that the function F1 in the Groeneveld correlation includes a dependence on hydraulic diameter as is expressed in (4.16). However, the Groeneveld correlation for a critical heat flux was not estimated for porous medium and one can assume that it can introduce an error. Because of that, sensitivity calculations on critical heat flux value were performed and the results are presented in Appendix A.

4.3.1.2 Heat transfer on dry solid surface

In this paragraph we will describe two regimes concerning the heat transfer of dry solid surface: single phase convection with gas and film boiling regime.

Single phase convection with gas

According to the formulation for the heat exchange terms in equation (4.9), the heat exchanges applied in regime of *convection with gas* are as follows:

$$\begin{aligned} \varphi_{sl} &= 0 \\ \varphi_{sg} &= h_{gi}^{gs}\left(T_s - T_g\right) \\ \varphi_{si} &= 0 \end{aligned} \tag{4.22}$$

and interfacial heat transfer:

$$\begin{aligned} \varphi_{gi} &= h_{gi}^{gl}\left(T_g - T_{sat}\right) \\ \varphi_{li} &= h_{li}^{lg}\left(T_l - T_{sat}\right) \end{aligned} \tag{4.23}$$

where h_{gi}^{gs}, h_{gi}^{gl} and h_{li}^{lg} are the heat transfer coefficients obtained for the SGL stratified Unit Cell configuration summarized in Chapter 3. As it was previously discussed for the regime of convection with liquid (see paragraph 4.3.1.1), additional development is necessary concerning the limits for the single-phase flow and geometry composed of spheres. For the limits for the single-phase flow and geometry composed of spheres, the same modifications as for the convection to liquid were made.

Here we recall that the heat transfer coefficients that come from the theory applied to stratified unit cells do not depend on the phase velocity [Duval02]. Thus, in a regime of convection with gas that may be laminar or turbulent, a modification depending on the gas phase velocity should be introduced. If the gas velocity increases, different flow regimes according to the Reynolds number can occur:

- If Re<1, Darcy flow regime will be present where the dominant parameter is viscosity.
- If 1<Re<150, the inertial effects will start.
- If 150<Re<300, oscillations phenomena will appear in the pores.

- If 300<Re, the regime of non-steady and turbulent flow will occur.

In reactor reflood application studies, the Reynolds number for the gas flow does not reach high values (<10^3) and thus, it is not necessary to study the heat transfer coefficients valid for high Reynolds number. However, the gas velocity, even if not high, influences the heat exchange density. A particular attention should be paid to the heat transfer coefficient between the solid and gas because it has an impact on the solid temperature downstream of the quench front. Thus, the heat transfer to gas is important and should take into account the gas phase velocity. The following dependence is proposed:

$$\frac{h_{sg} d_p^2}{k_g} = h_{gi}^{gs} f(Nu) \tag{4.24}$$

where k_g is the thermal conductivity of gas, d_p is the particle diameter and h_{gi}^{gs} is the heat transfer coefficient that was introduced in Chapter 3, and h_{sg} is the resulting heat transfer coefficient present in equation (4.22) and *Nu* is a Nusselt number. Different correlations for forced flow convection in channels were found in the literature. The correlations are valid for various ranges of Reynolds number and various geometries. The objective of our study was to find a correlation that is valid for low values of Reynolds number and takes into account the pore-scale geometry.

In (Figure 4.6) we can see a sketch of the transverse flow over tubes. The characteristic length for this geometry is a tube diameter. The correlation is valid for low Reynolds number and for geometrical configuration where S_1 / d_p as well as S_2 / d_p are lower than 1.25, while S_1 and S_2 can be seen on Figure 4.6.

Applying a geometry composed of spheres, the characteristic length is the particle diameter. The S_1 and S_2 (see Figure 4.6) are equal and mean the hydraulic diameter in pores. Consequently, for a hydraulic diameter in pores defined as $\frac{d_p \varepsilon}{(1-\varepsilon)}$, the condition S / d_p reduces to $\varepsilon < 0.555$ which is completely valid for a typical porosity in reactor cores. Thus, the correlation of Isačenko (1981), which was estimated for a transverse flow in tube bundles, is applied in our model:

$$f(Nu) = K.Re^{1/3}.Pr^{1/3}.\left(\frac{Pr}{Pr_s}\right)^{1/4} \tag{4.25}$$

where K is a constant depending on an arrangement of tubes and Pr_s is a Prandtl number estimated using the temperature of solid as the reference temperature. In the Reynolds number, the characteristic length is a diameter of tubes (particle diameter in our case). For a higher porosity and higher Reynolds number, similar correlation can be found in the literature [Isačenko81].

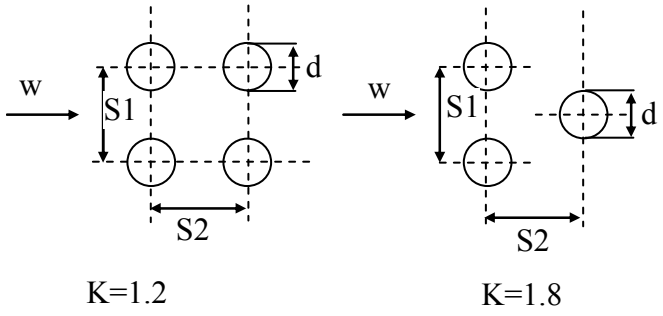

Figure 4.6: Transverse flow over tubes considered in *f(Nu)* correlation

Film boiling regime

According to the formulation of heat exchange terms in equation (4.9), the heat exchanges applied in regime of *film boiling* are as follows:

$$\begin{aligned} \varphi_{sl} &= 0 \\ \varphi_{sg} &= g(\alpha) h_{gi}^{gs} \left(T_s - T_g\right) \\ \varphi_{si} &= \left(1 - g(\alpha)\right) C_{nf} \left(T_s - T_{sat}\right)^m \end{aligned} \tag{4.26}$$

where the h_{gi}^{gs} is the heat transfer coefficient from SGL configuration (see Chapter 3) and the dependence on the gas velocity was introduced as it was presented above. The $g(\alpha)$ is the same function as was discussed in paragraph 4.3.1.1.

The film boiling constants C_{nf} and m are introduced in equation (4.26)(4.12). In ICARE-CATHARE code for standard nuclear applications, Bromley's correlation is used. Beside different correlations available in literature [Dougall63], [Whalley87], the correlation that is already implemented in ICARE-CATHARE code [Guillard01] is as follows:

$$\begin{aligned} C_{nf} &= Br_{mod} \left(34.55.10^{-5} P + 854\right) \\ Br_{mod} &= f(\alpha, Re_l) \\ m &= 0.75 \end{aligned} \tag{4.27}$$

where P is the pressure in [Pa].

For porous medium reflood, one may also consider that the SGL configuration is a sufficient approximation for the film boiling regime e.g. there is no intense boiling present in this regime. That is the reason why in the ICARE-CATHARE code we also propose:

$$\begin{aligned} C_{nf} &= h_{sg} \\ m &= 1 \end{aligned} \tag{4.28}$$

where the h_{sg} is the heat transfer coefficient from SGL configuration (see Chapter 3, h_{gi}^{gs}) and the dependence on the gas velocity was introduced as it was presented above. Bromley's film boiling correlation (4.27) was tested additionally as can be seen in Appendix A.

4.3.1.3 Transition between wetted and dry surface

Between the nucleate and film boiling region, it was explained in the previous Chapter that there is a boiling zone called transition boiling.
The progression of the quench front is strongly influenced by the transition boiling phenomenon. At low pressures, particularly for low flow rate conditions expected during reactor core reflooding, heat transfer coefficients are low. It is very difficult to conduct the steady-state tests which do not result in excessive heater temperatures. Much of the information pertinent to core reflood conditions has therefore been obtained from rod bundle quenching studies and no results are available for porous media. Based on the steady-state data, an empirical correlation has been devised [Liu93]. It involves a function defined below:

$$f(\theta,\xi) = \theta^{\xi} = \left(\frac{Ts - Ts\big|_{\varphi_{nb}}}{Ts\big|_{\varphi_{fb}} - Ts\big|_{\varphi_{nb}}} \right)^{\xi} \tag{4.29}$$

where $Ts\big|_{\varphi_{nb}}$ is the critical heat flux temperature and $Ts\big|_{\varphi_{fb}}$ is the minimum film stable temperature discussed in paragraph 4.3.1.3. In our model, the exponent ξ is fixed to 2 as it is also in the ICARE-CATHARE standard model for rod bundles. However, the impact of the value of ξ on the model behaviour was tested and the results are summarized in Appendix A.
In the transition zone, a linear combination of two terms is proposed:

$$\varphi_{si} = (1 - g(\alpha))(1 - f(\theta,\xi))\varphi_{CHF} + f(\theta,\xi)\varphi_{si}^{fb} \tag{4.30}$$

where the φ_{CHF} is the critical heat flux from Groeneveld correlation in equation (4.21) and φ_{si}^{fb} is the heat flux from the film boiling transfer in equation (4.26). The other energy transfers in the transition boiling regime are as follows:

$$\begin{aligned} \varphi_{sl} &= (1 - g(\alpha))h_{li}^{ls}(T_s - T_l) \\ \varphi_{sg} &= g(\alpha)h_{gi}^{gs}(T_s - T_g) \end{aligned} \tag{4.31}$$

Transition criterion between wetted and dry solid surface

It is necessary to identify properly the minimum temperature for which the liquid cannot be in contact with the surface during reflood (also known as Leindenfrost temperature). Below that temperature, the vapor film collapses onto the surface and the film boiling regime ends. It is replaced by transition boiling where intermittent contact of liquid is assumed. The collapse of the vapor film has traditionally been related to the minimum-heat-flux-point (MHF) of a boiling curve (see Figure 4.1).
There are many correlations available in the literature for the minimum stable film temperature for flow in cylindrical channels. A summary of available correlations can be found in Ohtake et al. (2004). The Berenson correlation estimates the minimum heat flux for the collapse of the vapour film:

- Berenson correlation

$$\varphi_{MHF}^{fb} = 0.09\rho_g h_{fg}\left[\frac{g(\rho_l-\rho_g)}{\rho_l+\rho_g}\right]^{1/2}\left[\frac{\sigma}{g(\rho_l-\rho_g)}\right]^{1/4} \tag{4.32}$$

Here, the minimum film stable temperature corresponds to the temperature, where the minimum heat flux is reached. Other authors propose directly the minimum film stable temperature:

- Nishio at atmospheric pressure

$$T_s\big|_{\varphi fb} = 200°C \tag{4.33}$$

- Dhir and Purohit

$$T_s\big|_{\varphi fb} = 201 + 8\Delta T_{sub}\ [°C] \tag{4.34}$$

where ΔT_{sub} is liquid subcooling. The correlation already introduced in ICARE-CATHARE code [Guillard01] is as follows (for P<9 MPa):

$$\begin{aligned} T_s\big|_{\varphi fb} &= 284.7 + 4.41.10^{-5}P - 3.72.10^{-12}P^2 - \frac{10^4\Delta H_l}{2.82+1.22.10^6 P} \\ \Delta H_l &= \frac{H_l - H_{lsat}}{H_{g\,sat} - H_{lsat}} \end{aligned} \tag{4.35}$$

where H is the enthalpy and P is the pressure in [Pa]. This correlation was tested in debris bed reflood model (see Appendix A). It was concluded that this correlation does not provide satisfactory results because the minimum film stable temperature is too low compared to the experimental observations, in particular PRELUDE experimental results discussed in Chapter 2. Therefore, we have introduced an alternative and more empirical method to define the extent of the region of transition boiling. It is described below.

We propose to identify the transition criterion according to the *position of quench front and the heat transfer layer length*. The notion of heat transfer layer length was introduced in Chapter 2 and the correlation was estimated by analysing the PRELUDE experimental results. We assume that the transition boiling regime length is *L1* and above this region, film boiling regime occurs (see Figure 4.7). In ICARE-CATHARE, the model selects the appropriate local regime in debris bed according to the quench front position and heat transfer layer length. The criterion (illustrated in Figure 4.7) is as follows:

Film boiling regime is applied when:

$$Z_{MESH} - Z_{QF} > L1 \tag{4.36}$$

Transition or nucleate boiling regime is applied when:

$$Z_{MESH} - Z_{QF} < L1 \tag{4.37}$$

where Z_{MESH} is the elevation of mesh and Z_{QF} is the quench front position and L1 is the heat transfer layer length. The correlation to calculate the heat transfer layer length that is used in code was obtained in Chapter 2 and is recalled here:

$$L1 = 0.45 We^{0.32} = f\left(v_{pore}^{0.65}\right)$$
$$We = \frac{\rho_l v_{pore}^2 \left(\frac{d_p \varepsilon}{1-\varepsilon}\right)}{\sigma} \tag{4.38}$$

where v_{pore} is the liquid flow velocity just below the quench front position.

It is interesting to note that a similar modeling based on a heat transfer length was already integrated into ICARE-CATHARE model for intact fuel rods and validated [Chikhi10]. It consists in tracking the quench front location and integrating the small-scale heat flux profile over the heat transfer length in the transition boiling regime. But, contrary to that modeling, the debris bed model uses the local physical correlations in each regime to calculate the heat flux profile (no integration is needed) and the length of heat transfer layer is used only to identify the condition for which the film boiling regime changes to transition boiling.

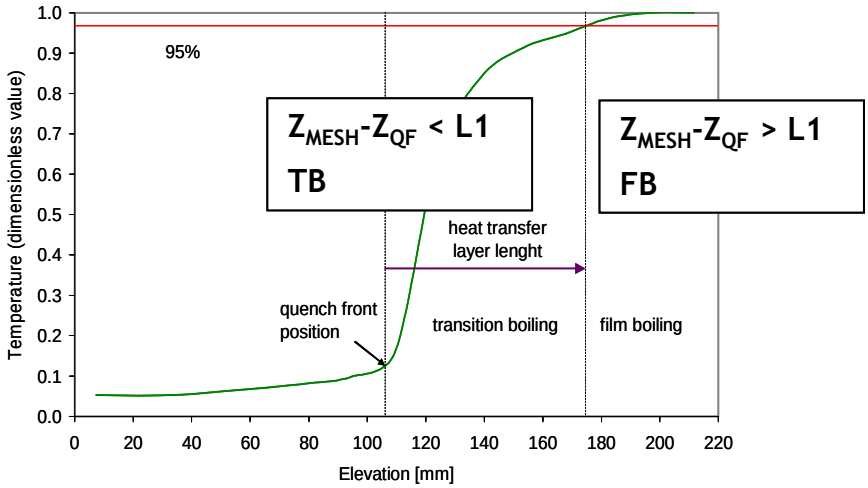

Figure 4.7: Axial temperature profile and boiling regime according to heat transfer layer length; TB- transition boiling, FB- film boiling, Z_{mesh}- elevation in debris bed, Z_{QF}- position of quench front

4.3.2 Discussion on the solid temperature

In this paragraph we will make a point on the solid temperature that is solved from the energy balance equation (4.5). The solid temperature in each elementary volume is averaged, i.e., in the heat transfer relations. In the heat exchanges coded in the ICARE-CATHARE, the T_s is the *mean temperature* of the solid phase instead of *surface temperature* T_p. Consequently, the use of standard correlations using surface temperature may be inaccurate if the gradient of temperature in a solid during a transient process is important e.g. during reflood. Indeed, this is one characteristic of porous media physics that the solid surface temperature is not imposed by an external device but is, instead, a *result* of the process. Hence, classical boundary layer theories, and other approaches based on solid wall controlled temperature are not, in principle, applicable. This may lead to misleading interpretations. Homogenization results and the closure problems do not make such assumptions. However, as already discussed, a complete

upscaling development in the case of boiling is beyond our reach at this time, and we must accept heuristic applications of results developed in a different framework. We tried to develop such an approach in this Chapter.

The gradient of temperature in a spherical particle under quenching was already discussed and summarized in Chapter 2 (Section 2.5.3.3). It was shown that the time needed to quench the *steel particle* is significantly higher than the time needed to make its temperature uniform, , which suggests the use of the average temperature as a replacement for wall temperature in the correlations taken from the literature and presented in this Chapter.

However, we will introduce here the analytical solution for the surface temperature of a spherical particle with inner heat source. It was not implemented because it is not necessary for the particules of interest in our situation. But the final formulation can be directly implemented into a future version of code if further validation and development show that it is necessary.

The heat transfer equation for a steady state case and spherical geometry can be written as:

$$\frac{d^2T}{dr^2}+\frac{2}{r}\frac{dT}{dr}+\frac{q_v}{k}=0 \tag{4.39}$$

where q_v is the volumetric heat flux [W/m3]. This equation can be written also under the form:

$$\frac{1}{r^2}\frac{d}{dr}\left(r^2\frac{dT}{dr}\right)=-\frac{q_v}{k} \tag{4.40}$$

If the right side of equation (4.40) is constant, the solution will be written as:

$$r^2\frac{dT}{dr}=-\frac{q_v}{k}\frac{r^3}{3}+C_1 \tag{4.41}$$

$$T=-\frac{q_v}{3k}\frac{r^2}{2}-\frac{C_1}{r}+C_2 \tag{4.42}$$

However, C1/r does not fit the conditions for which we want to find the solution. Consequently, the constant C1= 0. The integration constant C2 can be found from the boundary condition. We assume that the solid element is surrounded by an environment which temperature is T_f, and that there is a heat transfer between the solid particle surface temperature T_p and this environment. Usually, it is a convective heat transfer that is applied when the solid element is heated or cooled; here h is the heat transfer coefficient. When we apply this boundary condition at r_p we obtain the wall temperature of spherical element with inner heat source q_v and radius r_p from equation (4.41):

$$T_p=T_f+\frac{q_v}{3h}r_p \tag{4.43}$$

Finally, the temperature of solid element at any radius *r* should be found. To find an integral constant C2, we assume that at the radius r_p of solid element, the wall temperature is T_p. Consequently, for $T = T_p$ and $r = r_p$ the equation (4.42) can be written as:

$$T_p = -\frac{q_v}{6k} r_p^2 + C_2 \tag{4.44}$$

Applying the equation (4.43) into equation (4.44) the constant C2 can be calculated:

$$C_2 = T_f + \frac{q_v}{3h} r_p + \frac{q_v}{6k} r_p^2 \tag{4.45}$$

Finally, the temperature of solid spherical element at any radius *r* is as follows:

$$T(r) = T_f + \frac{q_v}{3h} r_p + \frac{q_v}{6k} r_p^2 - \frac{q_v}{6k} r^2 \tag{4.46}$$

The mean temperature through a section of solid element is:

$$\overline{T} - T_p = \frac{q_v}{6k} \frac{4\pi \int_0^{r_p} r\left(r_p^2 - r^2\right) dr}{\frac{4}{3}\pi r_p^2} = \frac{q_v r_p^2}{15k} \tag{4.47}$$

In the applications presented in this thesis, the surface temperature calculation was not implemented into code and the mean solid temperature is used in all heat exchanges with solid.

.

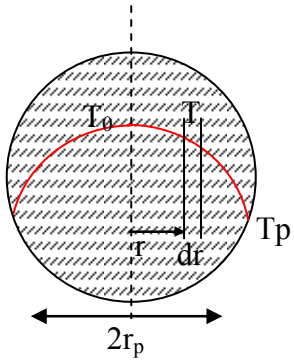

Figure 4.8: Radial temperature profile in a spherical solid element

4.3.3 Momentum balance equations

As it was introduced at the beginning of this Chapter, the momentum balance equations for the two-phase flow in debris bed geometry are based on Darcy - equations (4.1)-(4.2). To be consistent with the assumption of intermittent contact of water or steam, the effect of the phases repartition on the momentum transport properties was also introduced in the improved model. In the work of Duval (2002), Duval et al. (2004), the relative permeabilities were estimated for the stratified cells, in the absence of a real knowledge of the debris bed structure and real phase repartition. Here we propose to combine the relative permeabilities with the same function as for the heat flux between fluid and solid. The relative permeabilities in each configuration are given by the following relations:

- SGL configuration

$$K_{rg}^{SGL} = \alpha^2 \left[\alpha + \frac{3}{2}(1-\alpha) \right] \tag{4.48}$$

$$K_{rl}^{SGL} = (1-\alpha) \left[(1-\alpha)^2 + \frac{3}{2}\frac{\mu_l}{\mu_g}(2\alpha(1-\alpha)+\alpha^2) \right] \tag{4.49}$$

- SLG configuration

$$K_{rl}^{SLG} = (1-\alpha)^2 \left[(1-\alpha) + \frac{3}{2}\alpha \right] \tag{4.50}$$

$$K_{rg}^{SLG} = \alpha \left[\alpha^2 + \frac{3}{2}\frac{\mu_g}{\mu_l}(1-\alpha^2) \right] \tag{4.51}$$

where μ is the dynamic viscosity. The balance of friction forces is:

$$\frac{1}{K_{rl}} = (1 - f(\theta,\xi))\frac{1}{K_{rl}^{SLG}} + f(\theta,\xi)\frac{1}{K_{rl}^{SGL}} \tag{4.52}$$

$$\frac{1}{K_{rg}} = (1 - f(\theta,\xi))\frac{1}{K_{rg}^{SLG}} + f(\theta,\xi)\frac{1}{K_{rg}^{SGL}} \tag{4.53}$$

The combination represents the change in wetting phase. In ICARE-CATHARE code, these formulations for relative permeabilities were tested and compared to standard formulations that do not take into account change in wetting phase ($K_{rl}=(1-\alpha)^3$, $K_{rg}=\alpha^3$). The results are presented in Appendix A.

4.4 CONCLUSIONS

In this Chapter the numerical implementation of the improved macroscopic model for reflood of debris bed geometry was described extensively with respect to the correlations selected and the conditions for identification of boiling regimes. The objective was to completely cover the details of the model.

We found benefits in doing that numerical implementation of the model into an existing code used for severe accident analysis. The code disposes already of numerical solving procedures as well as the many physical correlations used for reflood of intact fuel rods (different geometry compared to debris bed) that could be directly used or tested as alternative choices.

The ICARE-CATHARE V2 reflood of debris bed model is based on two momentum balance equations and three energy balance equations. Because of 3D thermohydraulic meshing in CATHARE2, the modeling of multidimensional effects is possible.

A first implementation of the model developed by Duval (2002) into the ICARE-CATHARE code was done in 2009 before the beginning of this thesis.

During this work, several theoretical and practical improvements have been made. They concern mainly:

- Energy balance equations: the application of heat transfer coefficients was modified, new heat transfer coefficients were introduced and new flow regimes were included following the improvements of the model introduced in Chapter 3.

- Momentum balance equations: modifications concerning the relative permeability and passability coefficients were introduced and tested.

Consequently, the heat transfer relations in ICARE-CATHARE are now described in terms of a unique boiling curve from which the code selects the appropriate heat transfer coefficients for both phases (vapor/liquid). The boiling regimes, heat transfer coefficients as well as the transition criteria are summarized in Table 4.1 and Table 4.2.

The confrontation of calculated results with the experimental results will be presented in next Chapter.

Table 4.1: Formulations of heat transfers in ICARE-CATHARE model for two-phase flow in porous medium

	Regime presence	φ_{sl}	φ_{sg}	φ_{si}	φ_{gi}	φ_{li}
Convection to liquid	$T_s<T_{sat}(P)$	$h_{li}^{ls}(T_s - T_l)$	*0*	*0*	$h_{gi}^{gl}(T_g - T_{sat})$	$h_{li}^{lg}(T_l - T_{sat})$
Convection to gas	$\alpha>\alpha^{max}$	*0*	$h_{gi}^{gs}(T_s - T_g)$	*0*		
Nucleate boiling regime	Z_{mesh}-Z_{qf}<L1 $\varphi_{si}^{nb} < \varphi_{CHF}$	$(1-g(\alpha))h_{li}^{ls}(T_s - T_l)$	$g(\alpha)h_{gi}^{gs}(T_s - T_g)$	$(1-g(\alpha))C_{nb}(T_s - T_{sat})^i$		
Film boiling regime	Z_{mesh}-Z_{qf}>L1	*0*	$g(\alpha)h_{gi}^{gs}(T_s - T_g)$	$(1-g(\alpha))C_{nf}(T_s - T_{sat})^m$		
Transition boiling regime	Z_{mesh}-Z_{qf}<L1 $\varphi_{si}^{nb} > \varphi_{CHF}$	$(1-g(\alpha))h_{li}^{ls}(T_s - T_l)$	$g(\alpha)h_{gi}^{gs}(T_s - T_g)$	$(1-g(\alpha))(1-f(\theta,\xi))\varphi_{CHF} + f(\theta,\xi)\varphi_{pi}^{fb}$		

$h_{\beta i}^{\sigma\gamma}$ effective coefficient of thermal transfer characterizing the exchange $\langle T_\beta \rangle^\beta$ for the phase σ on interface $A_{\sigma\gamma}$ (β,σ,γ =s, l, g), $W.m^{-3}.K^{-1}$

k thermal conductivity $W.m^{-1}.K^{-1}$

P pressure, Pa

Re Reynolds number

α void fraction (volume fraction of gas phase in the free volume)

ε_β V_β/V, volume fraction of β phase (β=s, l, g)

ε $=1-\varepsilon_s$, porosity

C_{nb}, i nucleate boiling constants

C_{nf}, m film boiling constants

H characteristic length of cell $=d_p/(1-\varepsilon)$ for stratified Unit Cell

$\kappa_{\beta s}$ ratio of thermal conductivity of β phase (β=g,l) and solid.

α^{max} maximum void fraction in code, 1-1.D-05

Z_{mesh} axial elevation of mesh

Z_{qf} axial elevation of quench front

L1 heat transfer layer length

g(α) non-wetted surface function g(α)=α

$f(\theta,\xi)$ function of temperature describing the transition zone

Table 4.2: Correlations of heat transfer coefficients in the code

Heat transfer coefficient	*Formulation*
h_{li}^{ls} SLG configuration [Duval02]	$\frac{24k_l}{\varepsilon_l H^2} f(\varepsilon_l)$ $f(\varepsilon_l) = (1 + 4\varepsilon_s \kappa_{ls} / 3\varepsilon_l)^{-1}$
h_{gi}^{gs} SGL configuration [Duval02]	$\frac{24k_g}{\varepsilon_g H^2} f(\varepsilon_g)$ $f(\varepsilon_g) = (1 + 4\varepsilon_s \kappa_{gs} / 3\varepsilon_g)^{-1}$
h_{gi}^{gl} SGL configuration [Duval02]	$\frac{24k_g}{\varepsilon_g H^2} g(\varepsilon_g)$ $g(\varepsilon_g) = \frac{(3\varepsilon_g + 2\varepsilon_s \kappa_{gs})}{(3\varepsilon_g + 4\varepsilon_s \kappa_{gs})}$
h_{li}^{lg} SLG configuration [Duval02]	$\frac{24k_l}{\varepsilon_l H^2} g(\varepsilon_l)$ $g(\varepsilon_l) = \frac{(3\varepsilon_l + 2\varepsilon_s \kappa_{ls})}{(3\varepsilon_l + 4\varepsilon_s \kappa_{ls})}$
C_{nb}, i Thom correlation [Guillard01]	$Fl * 1.97.10^3 \exp(0.23.10^{-6} P)$ $i = 2$
C_{nf}, m Bromley correlation [Guillard01]	$Br_{mod}(34.55.10^{-5} P + 854)$ $Br_{mod} = f(\alpha, Re_l)$ $m = 0.75$
φ_{CHF} Groeneveld correlation [Guillard01] [Groeneveld96]	$\varphi_{CHF} = Fl * 10^{F(G,P,X)+3}$ $Fl = \left(\frac{8}{D_h}\right)^{1/3} \quad 4mm < D_h < 16mm$ $Fl = \left(\frac{8}{16}\right)^{1/3} = 0.79 \quad D_h > 16mm$ $Fl = \left(\frac{8}{4}\right)^{1/3} = 1.259 \quad D_h < 4mm$

Chapter 5

MODEL VALIDATION

5. MODEL VALIDATION

ICARE-CATHARE V2 code introduced in Chapter 4 is a thermal-hydraulic system code. It is a complex tool developed to estimate the transient behavior of light water nuclear power plants during off-normal conditions. The evaluation of safety margins, the optimization of the plant design and related emergency operating procedures are some of the applications of this code. It essentially deals with the resolution of the balance equations for steam-water two-phase mixtures supplemented by constitutive equations, including a 'heat transfer package', i.e., a series of heat transfer coefficient correlations covering the range of parameters expected for the nuclear power plant conditions. Special component models, heat conduction and neutronics equations are also part of this code.

Wide validation programs are necessary to demonstrate the applicability of the code to power plants, considering the stated objectives. Developmental and independent assessment areas can be distinguished, the former being mostly of concern for code developers and the latter of main interest for groups utilizing the code. Generally, these activities have been planned and carried out in national and international contexts [Auria98] at four levels, mainly in the independent assessment area, involving the use of:

- "Fundamental" experiments;
- Separate Effects Test Facilities;
- Integral Test Facilities, including most of the International Standard Problems;
- Real Plant data.

An additional level for code assessment can be identified including the so-called numerical benchmarks, also covering the demonstration of suitability of the adopted numerical solution scheme: this can be considered as belonging to the developmental assessment.

In the frame of validation work of the ICARE-CATHARE code, the first complex validation concerned the code ICARE-CATHARE V1. The implemented models were confronted against certain analytic tests and about 30-40 integral tests. Concerning ICARE-CATHARE V2, the validation of 3D multidimensional flows was necessary. Thus, the previous validations of V1 were not directly applicable into V2. Here, the validation of new models was introduced [Drai11]:

- Models of air oxidation:
  - Validation with the analytic tests (MOZART)
  - Validation with the integral tests (Codex-AIT1, Quench10, Quench11)
- Models of reflood of intact or slowly degraded fuel rods:
  - Validation with the analytic tests (Péricles1D, RBHT)
  - Validation with the degraded geometries (Quench11, Quench03)
- Models of reflood of debris bed:
  - Validation with the tests Ginsberg, Wang/Dhir.

In the frame of R&D at IRSN, the studies concentrated on development of detailed models allowing in particularly to apply the 3D flow module into a debris bed geometry. The objective of this thesis was to propose, implement and validate a debris bed reflood model. The improved macroscopic two-phase flow non-equilibrium model was summarized in Chapter 3. The numerical implementation of the model into ICARE-CATHARE V2 code was described in Chapter 4. Here, the validation of the ICARE-CATHARE V2 code will be extended to two sets of experimental data:

- Petit dry-out experimental results
- PRELUDE reflood experimental results.

Both experiments have been presented and discussed already in Chapter 2.

The criteria of validation will cover also the problems like the influence of "user parameters", discretization, quantification of code accuracy (i.e., estimate of the error in the comparison between measured and calculated results).

5.1 VALIDATION OF MODEL WITH PETIT EXPERIMENTAL DATA

In this paragraph, a validation of ICARE-CATHARE two-phase flow porous media model with respect to Petit experimental results will be presented. These boiling experiments in porous medium were performed during the F. Petit's doctoral thesis in 1998 [Petit98] at ENSAM in Bordeaux, France. The results were summarized in Chapter 2. In the experimental procedure, the debris bed is heated up to the saturation temperature at constant pressure until steady-state boiling condition is reached. Then, the heating power is increased in small steps until the dry-out is reached. An appreciable fast increase in bed temperature above the saturation temperature is defined as dry-out. The objective in validation is to evaluate different phenomena of boiling in a porous medium with internal source, i.e., liquid single-phase flow, two-phase flow and gas-single phase flow. The calculated results will be compared with experimental results.

5.1.1 Modeling of PETIT experiment in ICARE-CATHARE V2.3

In this paragraph, the main characteristics of the ICARE and CATHARE input deck will be summarized. This concerns the geometry, material properties, initial and boundary conditions.

Geometry

In the ICARE input deck, the vessel wall and the porous medium are defined. In the CATHARE input deck, the test section was modelled with three dimensional elements. The geometry of Petit experiment is summarized in Figure 5.1 and Table 5.1.

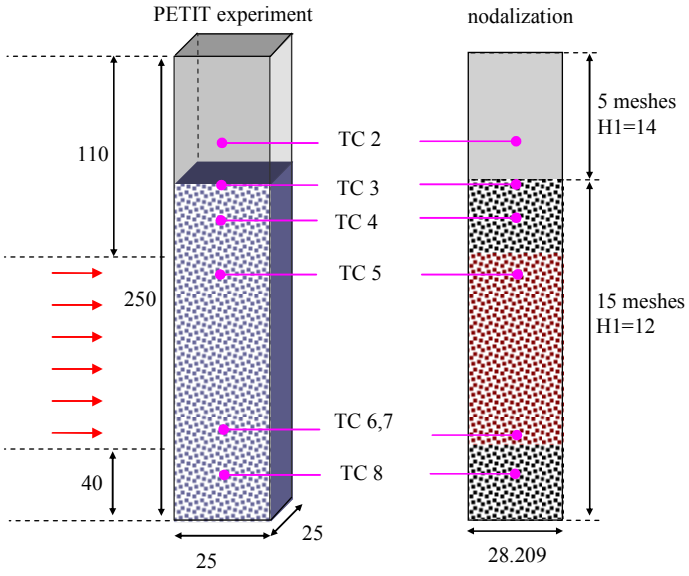

Figure 5.1: Petit experimental facility (left) and ICARE-CATHARE nodalization (right), dimensions in mm

Table 5.1: Geometry characteristics

	PETIT EXPERIMENT	INPUT DECK
Test section	Rectangular 25x25mm	Spherical 28.2mm
Porous medium height	¾ of Height 250mm	Height 187.5 mm
Heated part of Porous medium	Between 40mm-140mm	Between 60-156mm
Lower plenum	No lower plenum	Height 25mm
Upper plenum	¼ of Height 250 mm	Height 62.5 mm
Vessel wall	Thickness not verified	Thickness 3 mm

Material properties

The steel material properties are summarized in Table 5.2. The exact properties of materials in Petit's tests were not actually provided, therefore standard values were assumed. The mass of steel particles was 378g (where 227g were actually heated), with an estimated porosity 0.558 and approximate height of debris bed column 187.5mm.

Table 5.2: Material properties

	PETIT EXPERIMENT	INPUT DECK
Steel particles	Steel (properties not provided) Diameter 6mm	Density 7900 kg/m3 Thermal conductivity 43 W/mK Thermal capacity 500 J/kgK Diameter 6mm
Porosity	0.558	0.558

Induction power

The maximum heating power of the inductor was 3000W. Different heating powers were tested (10-60% of the maximum power). When a first dry-out occurred in the porous medium, the injected power was decreased in order to avoid fast temperature escalation. But, unfortunately, there is no recorded detailed information about this decrease of injected power and it induces some inaccuracy in the determination of the real power when dry-out occurs.

Table 5.3: Induction power

	PETIT EXPERIMENT	**ICARE INPUT DECK**
Heating power	15% of 3000W for most of the tests	Mass power: 0.15*3000/0.227=1982 W/kg
Axial and radial distribution	No information	Homogeneous distribution
Estimated losses	~20-40% depending on power	~20-40% depending on power
Time evolution	Decrease of power No details provided	Decrease of power tested

Water flow

In the experimental procedures, the bed is filled with water and heated up to the saturation temperature at constant pressure until steady-state boiling condition is reached. From the beginning, water is injected at the bottom of the test section. Different liquid flow rates were tested and are summarized below. Temperature of injected water was not measured and was set to 11°C, which is the initial temperature measured by thermocouples.

Table 5.4: Water injection flow rates for different Petit tests

	PETIT EXPERIMENT **Measurement accuracy is unknown**	**CATHARE INPUT DECK**
	Water flow [ml/min]	**Water flow [kg/s]** $\rho_l\left(\frac{flow[ml/\min]}{10^6}\right)\frac{1}{60}$
Increase of temperature up to T_{sat}	Flow 1=15ml/min	$0.249.10^{-3}$
	Flow 0.75=2.175ml/min	$0.036.10^{-3}$
	Flow 0= Natural circulation	1.10^{-7}
Dry-out tests	9.9ml/min	$0.164.10^{-3}$
	15ml/min	$0.249.10^{-3}$
	20.1ml/min	$0.333.10^{-3}$
	27.9ml/min	$0.464.10^{-3}$

Boundary conditions

The boundary conditions are summarized in Table 5.5 below. It may seem surprising that tests were performed in an environment where the temperature was only 11°C. However, the initial temperature measured by thermocouples at the beginning of each test indicated this value, which probably corresponds to the injected water temperature.

Table 5.5: Boundary conditions at Petit tests

	PETIT EXPERIMENT	INPUT DECK
External temperature	Unknown	11°C
Pressure	atmospheric	1 bar

5.1.2 Results of ICARE-CATHARE V2.3 calculations

The ICARE-CATHARE calculations were performed for different tests. The characteristics of the input deck were summarized above. In this section, the calculation results will be presented.

Initial state

We recall here that the test section was initially filled with water. The steel particles were heated by induction from the beginning. The water was injected from the beginning at the bottom of the test section and effect of liquid velocity on temperature evolution within the porous medium was studied. These experimental conditions were simulated in ICARE-CATHARE.

Temperatures evolution

The temperature was measured at different elevations in Petit's experiments (see Figure 5.1). However, there is no detailed information about the position of thermocouples or measurement error. The available information about the position of thermocouples is summarized in Table 5.6. Here we can see that there is a difference between the position of TC7 and TC6 compared to ICARE-CATHARE input deck. Common sense leads us to assume that the information about the position of TC6 and TC7 is not correct. This can be explained by analysing the temperature evolution registered at TC6 and TC7 for one Petit test with injected power 1200W and liquid flow 15ml/min. The results are presented in Figure 5.2. We can see that the TC6 and TC7 are directly influenced by inductor and thus it is very improbable that they are located below the heated zone.

However, on Figure 5.2 we can see that the code prediction does not correspond exactly to measured values. From the experimental results we can see that the temperature stabilized

after its increase. The reason is that the injected power started to be regulated when a dry-out appeared in order to protect the experimental tube against failure. As it was already mentioned, there is no more information about this decrease of injected power. In the first calculations (Figure 5.2) we tried to identify the time of decrease of injected power as well as its value. In the calculations presented in Figure 5.2 the power decreased at 200s down to 840W (70%) and then increased up to 960W (80%). This resulted in a quite good agreement between the calculated and measured temperature evolution at TC4. However, the other results are over or under-estimated. These first analysis leads to conclude that the modification of power was important and it is very difficult to reconstruct the whole scenario without detailed information. Consequently, the analysis concerning the incipience of dry-out should give only an indication about the relevance and good physical behaviour of the model but it is not possible to draw quantitative conclusions because of the lack of instantaneous power records.

Table 5.6: Elevations of thermocouples as indicated and values corrected in input deck after "engineering judgement"

PETIT EXPERIMENT			**INPUT DECK**
Thermocouple	**Position**	**Assumption [mm]**	**Elevation of component (its center) [mm]**
TC7	Same position as TC6	around 40mm	126±6
TC6	At the interface between the no heated and heated zone	around 40mm	114±6
TC5	about 15mm below TC4	around 157.5	138±6
TC4	about 15mm below TC3	around 172.5	150±6
TC3	At the highest elevation of the porous medium	around 187.5	174±6
TC2	Above the porous medium, in a free space	>187.5	201±6

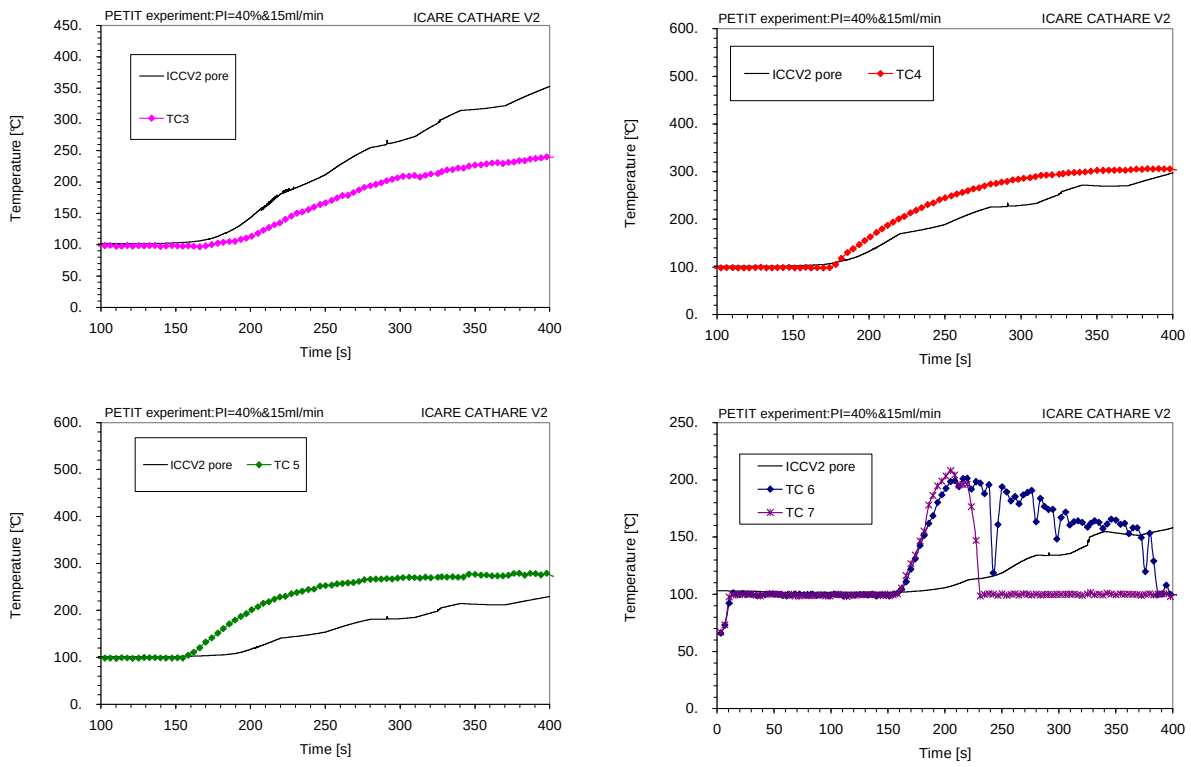

Figure 5.2: Calculated and measured temperature elevation at different positions for one Petit test: P=1200W and liquid flow 15ml/min
Legend: ICCV2 (ICARE-CATHARE code), TC (thermocouple)

5.1.2.1 Increase of temperature up to nucleate boiling regime

The problem concerning the modifications of power level discussed above has no impact on the interpretation of experimental results concerning the *increase of temperature up to nucleate boiling regime* that will be presented here. For these experiments, the power could be kept constant because the temperature increased only up to the saturation temperature. At the initial state, the tube was filled with water at a temperature of 11°C. In these tests, the heating power corresponded to 15% of maximum heating power of the inductor, i.e., 450 W.

The first experiment was performed for the liquid flow 15 ml/min. The temperature evolution at different elevations (TC2, TC3 and TC4) was registered and can be compared with calculation results. In Table 5.6 we can see the elevation of these thermocouples and their correspondence in ICARE-CATHARE nodalization.

The temperature profile at TC2 is shown in Figure 5.3. The later increase of temperature at this position compared to TC3 and TC4 is more visible. From the time equal to 80s, some "instabilities" appear in the flow. This is clearly visible as oscillations of the thermocouple measurement because it is located at the top of the tube, above the porous medium. As for the calculation results, the later increase of temperature is also visible. On the other hand, after

80s, the experimental fluctuations are not predicted by calculations, probably because they are produced by intermittent dry-out and rewetting of the thermocouple, which cannot be modelled with our "averaged" approach.

At this point, we must also mention a limitation of the comparison between experimental and theoretical results. The temperature as measured by the thermocouples is likely to represent a value closer to a point pore-scale value, given the characteristics of the device, while it is not clear what is the size of the control volume, nor which weighting function is associated with the measurement. The true measure is probably some time and space average, with a characteristic time roughly less than 1s and a characteristic "measurement length scale" smaller than the pore radius. On the opposite, theoretical results are obviously volume averaged values, and, in addition, they are time-averaged in the semi-heuristic model proposed to take care of the various pore-scale boiling regimes. Therefore, a direct comparison is not entirely relevant.

The second experiment was performed for a different liquid flow rate. In Figure 5.4 the temperature evolution at TC3 is compared with calculation results. Compared to temperature evolution of TC4, the increase of temperature at TC3 starts later. The reason is that TC3 is located about 15mm above TC4 and there is no direct influence of the inductor, therefore it is heated by convection only, which is a slower process. The high increase of the temperature between 80 and 100s is due to the effect of boiling in the upstream area.

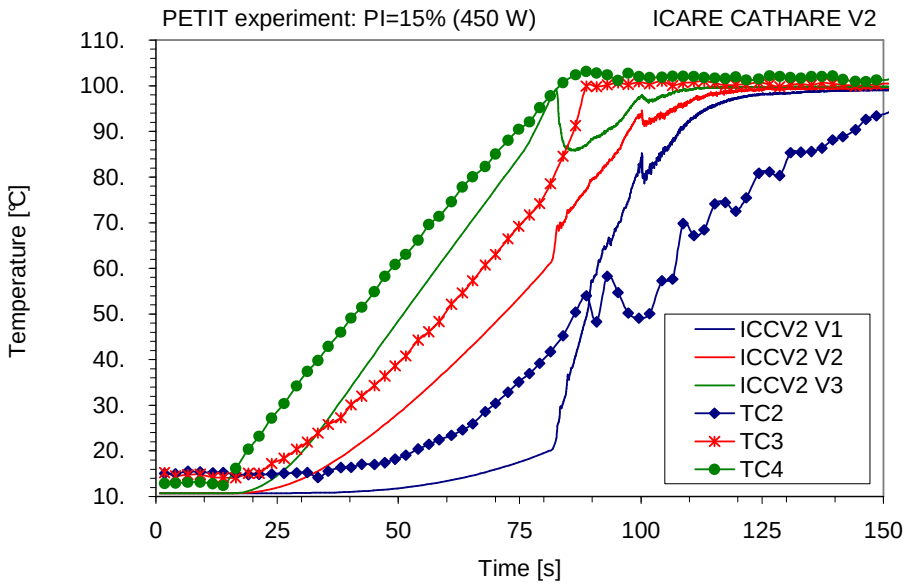

Figure 5.3: Temperature evolutions for a test with liquid flow 15 ml/min
Legend: ICCV2 (ICARE-CATHARE code), TC (thermocouple)

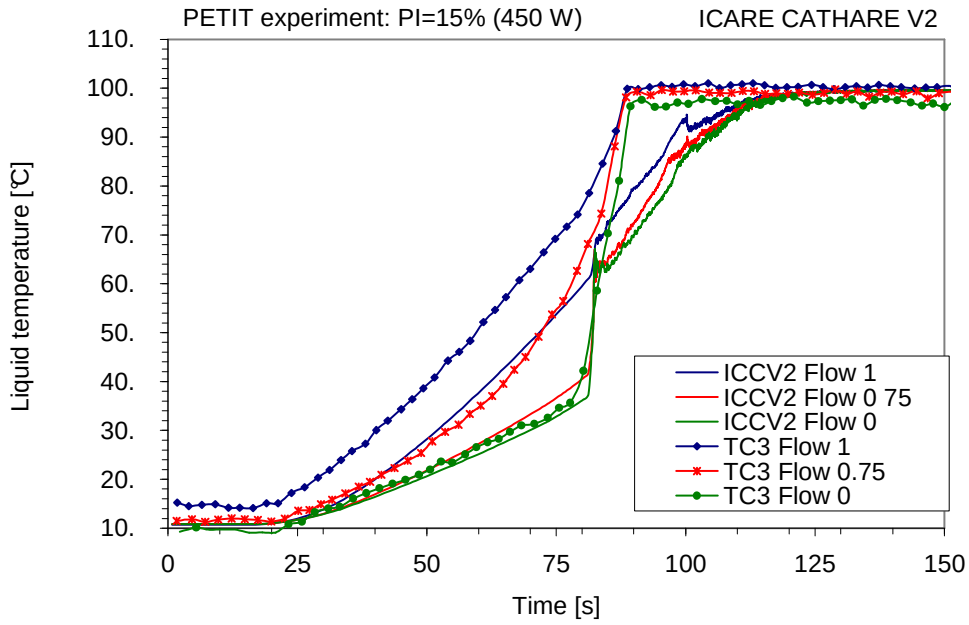

Figure 5.4: Temperature evolution at TC 3. 1: 15 ml/min, Flow 0.75: 2.175 ml/min, Flow 0: natural circulation. Legend: ICCV2 (ICARE-CATHARE code), TC (thermocouple)

The main objective of these calculations is two-fold. Generally speaking, we want to validate the mathematical structure of the proposed non-equilibrium model, in particular, the idea of making dependent the effective transport properties upon the underlying boiling regime diagram. In addition, we need to validate quantitatively the volumetric heat transfer coefficients used in our model. In the absence of the real knowledge of the pore-scale geometry and flow structure, the effective coefficients were built from a combination of simple estimates based on either simple geometrical structures (e.g., the "stratified" Unit Cell), or extrapolations to porous media of correlations coming from the boiling literature in the case of simple solid surfaces (see Chapter 3 and 4).

Precisely, the volumetric heat exchange coefficient obtained analytically for the simple stratified Unit Cell is divided by its specific area, $1/d_p$, multiplied by the specific area of the real porous medium. For a compact bed of spheres of porosity close to 0.4, the specific area is approximately $10/d_p$. So, this increases the analytical coefficient by a factor 10 if we assume that the whole sphere surface is concerned with heat exchange (which is not entirely exact because of contact areas between spheres). Thus, we have performed a sensitivity calculation on the heat exchange coefficient value and we have compared the results with the experimental measurements. In conclusion, the better results are obtained by increasing the heat transfer coefficient and in Figure 5.5 we can see the impact of increasing the heat transfer coefficient by a factor 9. Finally, in the proposed theoretical model, the heat exchange coefficients obtained for the simple stratified Unit Cell are used, multiplied by this factor 9. This somehow heuristic approach could be improved by solving the proposed "closure

problems" on more realistic geometry. It is however interesting to see that simple correlations coming from simplistic geometries do already a good quantitative predictions.

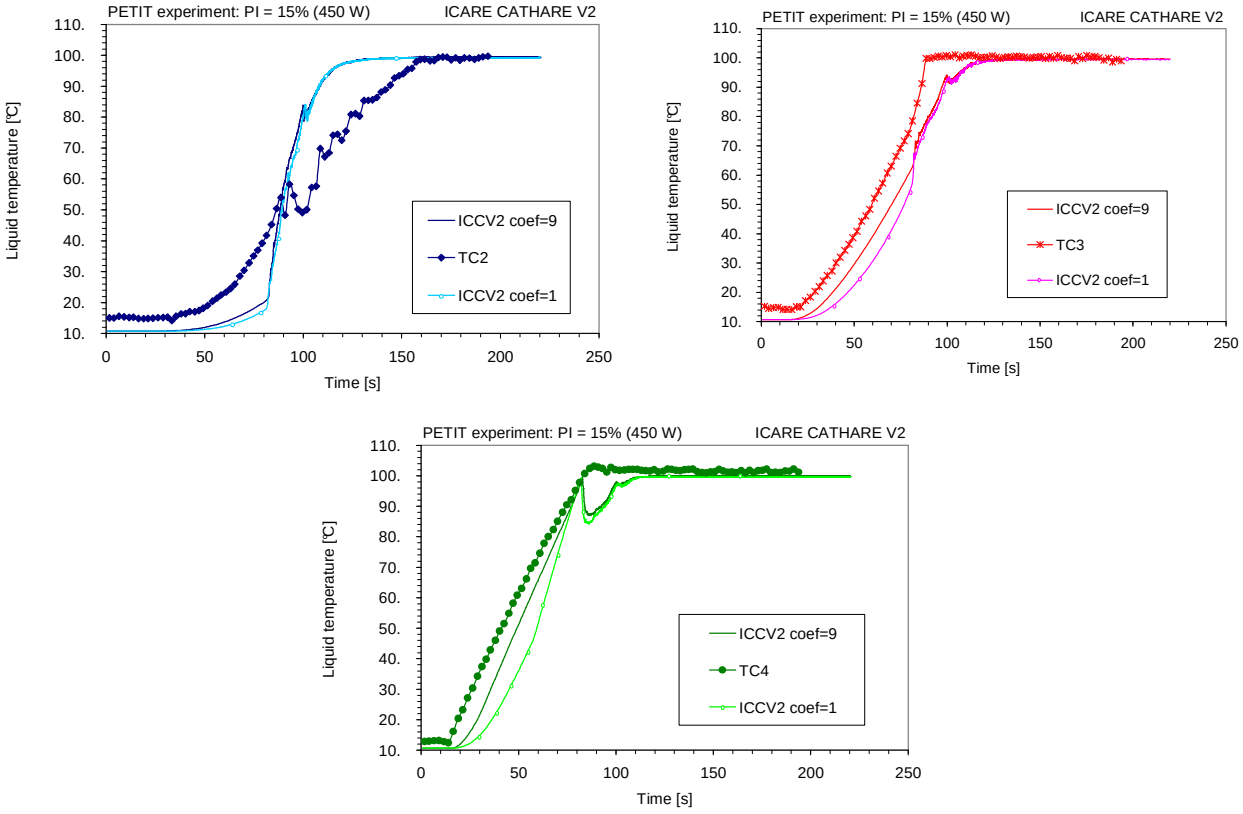

Figure 5.5: Effect of increase of heat transfer coefficient.

Legend: ICCV2 (ICARE-CATHARE code), TC (thermocouple)

5.1.2.2 Incipience of dry-out

The dry-out experimental results are used to validate the nucleate boiling heat flux in our model. If the injected power is sufficiently high, a zone with a single gas phase will appear above a particular elevation in the porous medium (Figure 5.2). The dependence of this elevation on the injected power and liquid flow rate was calculated and compared with experimental results.

In the experiment, the elevation where the dry zone appeared was identified. According to Petit (1998), this elevation was identified from visual observations as well as temperature measurements for the cases where a steady state was reached. When a first dry-out occurred in the porous medium, the injected power was decreased in order to avoid fast temperature escalation. As was discussed above, unfortunately, there is no recorded detailed information about this decrease of injected power.

The calculations were performed for different liquid flow rates and the dry zone elevation was identified for each test. However, the calculations were done with a fixed power set to the initial value, without reducing it after dry-out. In Figure 5.6 the calculation and experimental results are summarized. There are cases for which the dry-out zone is estimated at a lower elevation compared to the experimental observation. This might mean that the boiling heat flux is over estimated, at least in some parts of the particle bed, either because of an imperfect correlation, or simply because the fixed power was maintained during a longer time than it was actually in the experiment. However, the model already predicts in an acceptable manner the trends and quantitative values, as it can be seen on Figure 5.6.

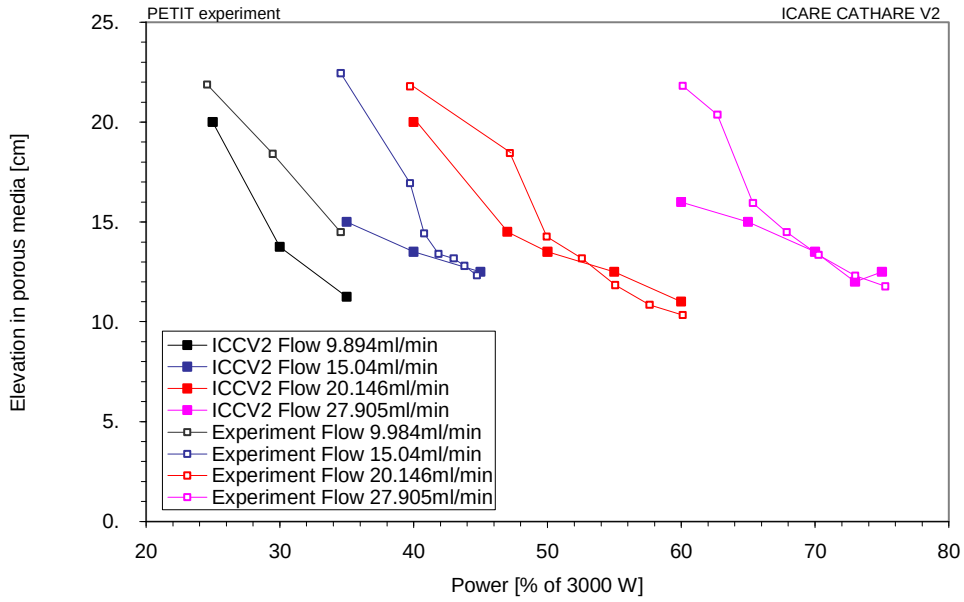

Figure 5.6: Elevation of dry zone. The calculation points are identified from the void fraction axial profile

5.2 VALIDATION OF MODEL WITH PRELUDE EXPERIMENTAL DATA

In this paragraph, the validation of ICARE-CATHARE two-phase flow porous media model with PRELUDE reflood experimental results will be presented. The PRELUDE experimental results were already discussed and presented in Chapter 2. The PRELUDE experiments were performed in 2009-2012.

The reflood experimental procedure differs from dry-out experiments. Here, the debris bed is heated and there is no presence of water initially. The bed is heated up to the desired temperature and quenched with water. The water can be injected from the top or from the bottom.

Different campaigns and analysis of experimental results were presented in Chapter 2. In this paragraph, the calculations of PRELUDE experiments will be presented. In total, 17 PRELUDE tests were calculated, varying the geometry, initial temperature and liquid injection flow rate. The validation matrix can be seen in Table 5.7.

Table 5.7: Validation matrix for reflood of debris bed model

Tests	PRELUDE Geometry	Initial Temperature	Particle diameter	Liquid flow	ICCV2 input deck
9 tests	"1D"	about 400°C	4, 2 and 1mm	2-20m/h	ID1
6 tests	"1D"	about 700°C	4 and 2mm	2-10m/h	ID2
2 tests	"2D"	about 700°C	4mm	5m/h* *top and bottom reflood	ID3

5.2.1 Modeling of PRELUDE experiment in ICARE-CATHARE V2.3

In this section the main parameters for the ICARE and CATHARE input decks will be presented.

Geometry

In the ICARE input deck, the vessel wall and the porous medium were defined. In the CATHARE input deck, the test section was modelled with three dimensional elements. The validation matrix concerned two different test geometries: PRELUDE "1D" and PRELUDE "2D" that was modelled in ICARE-CATHARE, i.e., input decks (ID1, ID2 or ID3). The basic differences in ICARE-CATHARE input decks "ID1, ID2 and ID3" can be seen in Figure 5.8 and Figure 5.9 and can be summarized as follows:

ID1 1 radial mesh, 84 axial meshes, mesh height 7.3mm
ID2 5 radial meshes, 42 axial meshes, mesh height 14.6mm
ID3 5 radial meshes, last mesh "by-pass", 42 axial meshes, mesh height 14.6mm,

The basic differences in PRELUDE "1D" and "2D" geometry can be seen in Figure 5.7. In both cases, the debris bed is formed with *homogeneous steel particles*. The PRELUDE '1D' is, in its conception, 'one dimensional', i.e., the whole bed is homogeneous and there is no designed by-pass. In Chapter 2 we concluded that water progression during the quenching was quasi-steady and the quench front velocity was similar at the centre and mid-radius position. However, a higher quench front velocity was observed at the border. If it occurs, it can result only from an instability in the liquid velocity, and/or the temperature and porosity effects close to the wall.

In PRELUDE "2D", a by-pass is made with quartz particles with diameter 8mm which are placed close to the wall. In the by-pass region, the higher particle diameter generates lower friction and thus the water progression through this region is facilitated. This geometry generates multi-dimensional effects when the water progresses during quenching. Significantly different quench front velocities have been observed in the by-pass compared to the centre or mid-radius region that was formed with steel particles with diameter 4mm or less.

Table 5.8: Geometry characteristics for different tests

	PRELUDE EXPERIMENT		**INPUT DECK**		
	1D	**2D**	**ID1**	**ID2**	**ID3**
Inlet tube	Diameter 15mm Length (not verified)		Diameter 15mm Length 0.1m		
Lower plenum	Height 117 mm (not verified)		Height 117mm		
Test section	Inner diameter 174mm	Inner diameter 290mm	174mm		290mm
Quartz particles	Height 104mm (not verified)		102.2mm		
Steel particles	Height 200mm	Height 250mm	Height 219 mm		Height 248.2mm
By-pass	no by-pass	Quartz Particles, 8mm by-pass thickness about 2.5cm	no by-pass		Quartz particles, 8mm by-pass thickness 2.3mm
Upper plenum	height 190 mm	Height 440 mm	Height 190mm		Height 440mm
Outlet tube	Vertical Diameter 40 mm Length (not verified)		Vertical Diameter 40 mm Length 0.1 m		
Vessel wall thickness	3mm (not verified)	8mm (not verified)	3 mm		8 mm

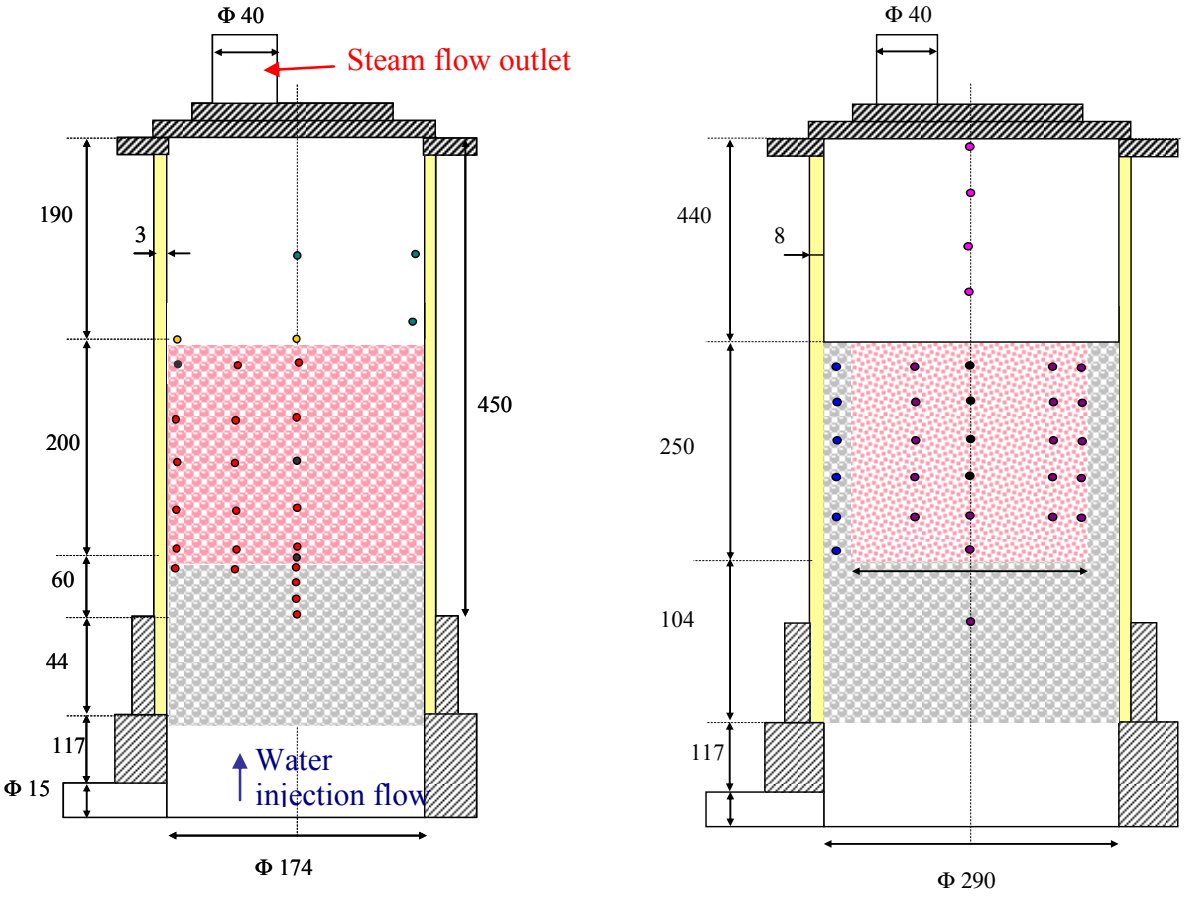

Figure 5.7: PRELUDE "1D" geometry (left) and PRELUDE "2D" geometry (right), dimensions in mm, (points indicate the position of thermocouples)

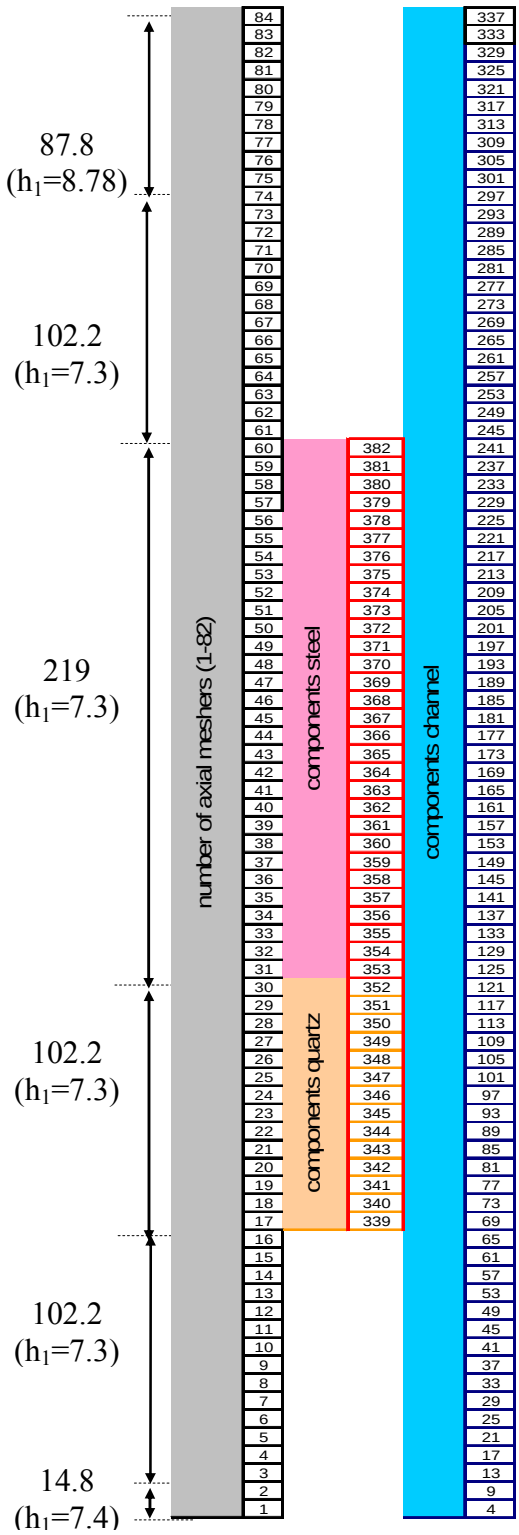

Figure 5.8: ICARE-CATHARE ID1 nodalization (dimensions in mm)

Note: Mesh numbers are interesting only for ICARE-CATHARE user readers

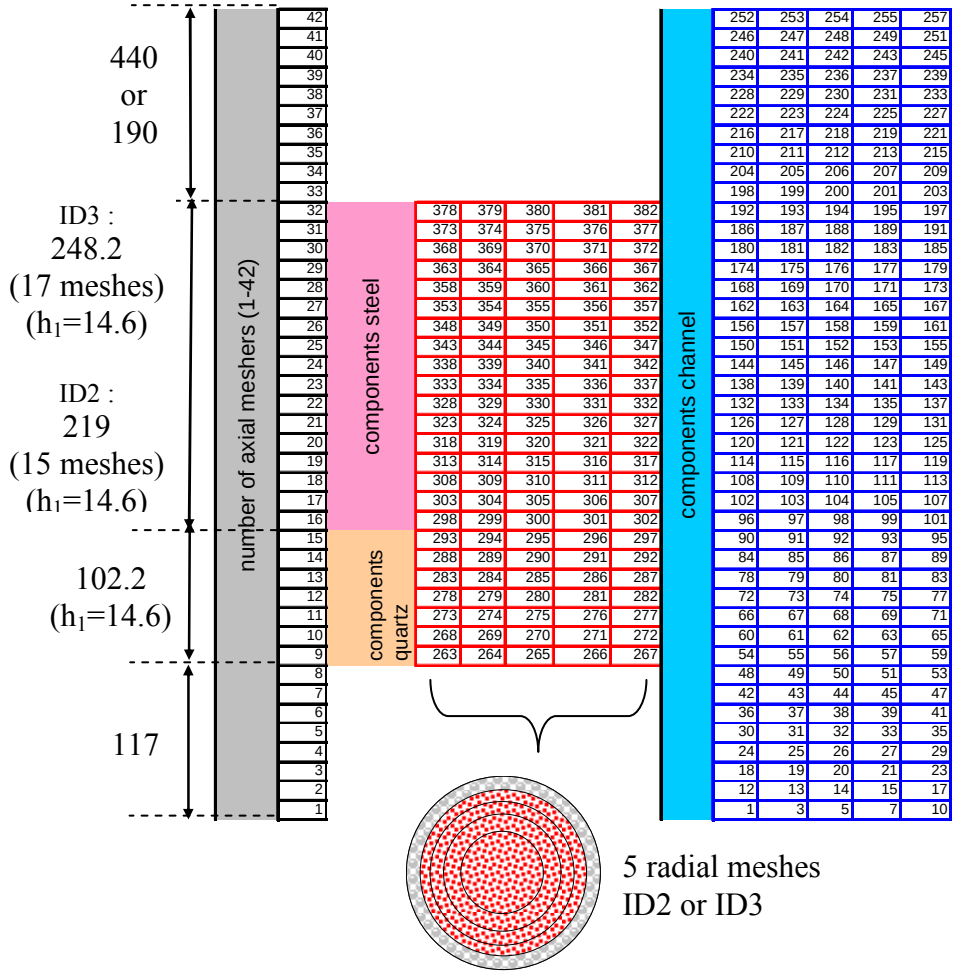

Figure 5.9: ICARE-CATHARE ID2 and ID3 nodalization (dimensions in mm)
Note: Mesh numbers are interesting only for ICARE-CATHARE user readers

Material characteristics

The material properties of steel and quartz used in PRELUDE tests are summarized in Table 5.9. The exact properties of materials actually used in the PRELUDE tests were not provided, therefore standard values were assumed.

In PRELUDE "1D" the mass of steel particles was 24kg, with an estimated porosity 0.4 and approximate height of debris bed column 200 mm. The information about the debris bed height was later corrected by the experimental team to 210mm (see also discussion in Chapter 2, Section 2.5.3.7).

In PRELUDE "2D" the mass of steel particles was 55kg, with an estimated porosity 0.4 and approximate height of debris bed column 250mm. The by-pass thickness was indicated 2.5mm all around the wall. The by-pass was formed with quartz particles with diameter 8mm. In the ICARE-CATHARE input deck, the by-pass thickness was recalculated (2.3mm) in order to conserve the mass of steel particles 55kg.

Table 5.9: Material properties in the input deck

	PRELUDE EXPERIMENT		INPUT DECK
	1D	**2D**	
Steel particles	Inoxydable 316L amagnétique (properties not provided)		Density 7900 kg/m3 Thermal conductivity 43 W/mK Thermal capacity 500 J/kgK Diameter 4, 2 or 1 mm
	Weight 24 kg Diameter 4, 2 or 1mm	Weight 55kg Diameter 4mm	
Quartz (particles, vessel)	Properties not provided		Density 2200 kg/m3 Thermal conductivity 1 W/mK Thermal capacity 800 J/kgK
	No-bypass	By-pass dp=8mm Thickness 2.5mm	
Porosity	0.39 (later specified to 0.4±0.003)		0.4

Induction power

In PRELUDE experiment, the steel particles were heated by induction power. The method used to recalculate the power was presented in Chapter 2. From that, the radial and axial distribution of power is known (see example in Table 5.10). The mass power was prescribed in ICARE input deck, depending on elevation and radial position. The power was maintained during reflood.

In the ICARE-CATHARE input deck ID1, one radial mesh was modelled thus the average of two power values was prescribed, e.g., centre, mid-radius (see example in Table 5.10).

In the ICARE-CATHARE input deck ID2 and ID3, five radial meshes were modelled and thus the power was distributed as it was identified in the experiment, e.g., centre, mid-radius and border.

Table 5.10: Example of interpretation of induction power (W/kg): PRELUDE "1D" test and ICARE-CATHARE input deck ID1, maximum value: 209 W/kg

		PRELUDE EXPERIMENT			ICARE INPUT DECK
Axial elevation [mm]		**Center**	**Mid-radius**	**Border**	**fraction of maximum value**
	0	73			0.35
	10	173	164	174	0.81
	55	179	192	174	0.89
	100	204	200	191	0.97
	155	209	207	198	0.99
	195	200	201	194	0.96

Water flow

In PRELUDE experiment, the debris bed is heated and there is initially no presence of water. The bed is heated up to the desired temperature and quenched with water. The power is maintained during reflood. In PRELUDE "1D" and "2D-bottom reflood" experiments, the water flow at the bottom of the test section was recorded. In ICARE-CATHARE input deck, the instant of water injection at the beginning must be prescribed. In order to identify this instant, the instant of quenching at the lowest elevation (0mm) in the porous medium was taken as reference point. The time of water injection was then recalculated. Temperature of injected water was not measured and was set to 20°C.

Table 5.11: Water injection flow in PRELUDE experiments

Water injection flow [m/h]	**Water injection velocity [mm/s]**	**Water velocity in pores [mm/s], porosity 0.4**
2m/h	0.555mm/s	1.39mm/s
4m/h	1.11mm/s	2.78mm/s
5m/h	1.38mm/s	3.45mm/s
7m/h	1.94mm/s	4.85mm/s
10m/h	2.77mm/s	6.93mm/s
20m/h	5.55mm/s	13.88mm/s

Boundary conditions

The boundary conditions are summarized in a Table 5.12.

Table 5.12: Boundary conditions for PRELUDE tests

	PRELUDE EXPERIMENT	**INPUT DECK**
External temperature	20°C (not verified)	20°C
Pressure	atmospheric	1 bar

5.2.2 Results of ICARE-CATHARE V2.3 calculations

17 reflood tests were calculated. The validation matrix is summarized in Table 5.7. It includes the variation of parameters such as the geometry, particle size, initial temperature and injection flow rate. In this section, the calculation results will be compared with experimental results. The thermocouple positions and the corresponding ICARE-CATHARE elevations in nodalization are summarized in Table 5.13. The sensitivity calculations on nodalization were also performed and the results are presented in Appendix B.

Table 5.13: Axial and radial position of thermocouples and ICCV2 nodalization

PRELUDE		**ICARE-CATHARE INPUT DECK**		
1D	**2D**	**ID1**	**ID2**	**ID3**
Axial elevation [mm] Accuracy: ±3 mm		**Axial elevation of component [mm]**		
0	10	3.65±3.65	7.3±7.3	7.3±7.3
10	40	10.95±3.65		36.5±7.3
55	80	54.75±3.65	51.1±7.3	80.3±7.3
100	120	98.55±3.65	94.9±7.3	124.1±7.3
155	160	156.95±3.65	153.3±7.3	153.3±7.3
195	200	193.45±3.65	197.1±7.3	197.1±7.3
-	240	-	-	240.9±7.3
PRELUDE		**ICARE-CATHARE INPUT DECK**		
1D	**2D**	**ID1**	**ID2**	**ID3**
Radius [mm] Accuracy: ±3 mm		**Radius of component [mm]**		
0	0	0±87	From 0 to 38.9	From 0 to 45
41	60		From 55 to 77.8	From 45 to 75
82	90		From 77.8 to 87	From 75 to 105
-	120	-	-	From 105 to 122
-	By-pass (close to 145)	-	-	From 122 to 145
-		-	-	

PRELUDE '1D' experimental results and ICCV2 'ID1' calculation results

Firstly, the ICARE-CATHARE reflood calculations were performed for PRELUDE "1D" tests with initial debris bed temperature at 400°C. The temperature evolution, quench front velocity, pressure increase and steam formation can be compared with experimental results.

The nodalization and input deck characteristics were summarized above. In the calculations, only one radial mesh was modelled. As for the temperature evolution comparison and the quench front tracking, this may be a limitation since the quench front was observed to progress faster along the tube wall in some experiments (e.g. at 100mm in Figure 5.10). However, in Figure 5.10 we can see that the calculations with one radial mesh are sufficient to predict well the whole temperature evolution, from to the "pre-cooling" up to the fast quenching.

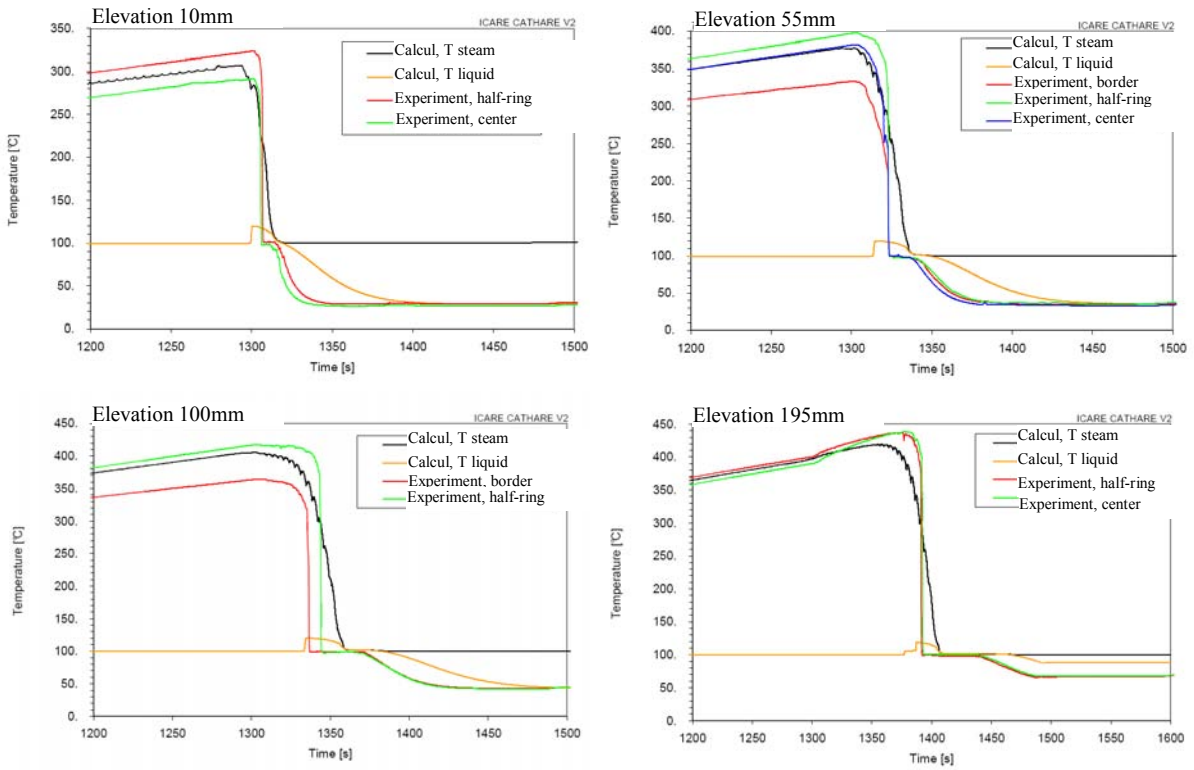

Figure 5.10: Calculated and experimental temperature evolution. Test PRELUDE '1D' with initial temperature 400°C, particle diameter 4mm and water injection flow 5m/h.

Moreover we can see (Figure 5.10) that the temperature measurements in experiments showed a similar trend in temperature and quenching at centre and mid-radius of porous media (see Figure 5.10). Thus, the quench front velocity predicted by the code can be compared with centre and mid-radius quench front velocities observed at experiments. The temperature evolutions were used for tracking the quench front velocity. In Chapter 2 (Section 2.5.3.1) we discussed this method as well as the impact of the reference temperature on the quench front velocities. The quench front velocities identified tracking the reflooding to T_{ref}=105°C may be

interpreted as the velocity of the first quenching of particles. The quench front velocities identified taking T_{ref}=95°C as a reference temperature may be interpreted as the velocity of complete cooling of the bed. Moreover, in experiments the thermocouples are installed in the pores and we assume that if the thermocouple is quenched to 95°C the closest particle temperature may be still around the saturation temperature. In the analysis, it is thus very interesting to analyse both quench front velocities. The difference between those two values corresponds to the uncertainty range in the determination of the quench front velocity. The ideal situation is when the code predicts well both situations, i.e., progression of first quenching to 105°C as well as total quenching to 95°C. The quantitative results for quench front velocity are summarized in Table 5.14. In this table we can see different quench front velocities for T_{ref}=105°C and T_{ref} =95°C.

The results taking T_{ref} =105°C are shown in Figure 5.10-Figure 5.12. Comparisons of temperature evolutions at different elevations show that the model is able to predict quenching velocity for different inlet flow rates and different particle diameters, in the whole range covered by PRELUDE experiments. Obviously, the total time of reflood depends on the initial liquid flow velocity and, as expected, it is lower for higher velocities. Limited discrepancies are observed for tests with particle diameter 1mm (Figure 5.12). However, in these tests the first multi-dimensional effects were observed, i.e., the quench front velocity was significantly higher at the border than at the centre of the bed. The sensitivity calculations on nodalization and radial meshing were performed and are summarized in Appendix B. As it will be shown in the next paragraph (calculations referenced ID2), the prediction of quench front velocity is improved by using five radial meshes in input deck of ICARE-CATHARE.

Table 5.14: Quench front velocities for different tests with initial temperature 400°C. ICCV2-ID1 input deck, PRELUDE '1D' mid-radius and centre quench front velocities.

Particle diameter	Liquid flow –free section at bottom		Quench front velocity for two reference temperatures		% Difference
			Tref = 105°C	Tref = 95°C	Difference
4 mm	v_inj=1.38 mm/s	ICCV2	1.98 mm/s	1.32 mm/s	7.04-9.17%
		Prelude	2.17-2.18 mm/s	1.42-1.43 mm/s	
	v_inj=2.77 mm/s	ICCV2	3.88 mm/s	2.66 mm/s	2.58-19.39%
		Prelude	3.44-3.78 mm/s	2.94-3.3 mm/s	
	v_inj=5.55 mm/s	ICCV2	6.12 mm/s	5.62 mm/s	11.94-29.89%
		Prelude	5.04-6.95 mm/s	3.94-4.24 mm/s	
	v_inj=0.555 mm/s	ICCV2	0.77 mm/s	0.31 mm/s	0.77-31.1%
		Prelude	0.776-0.78 mm/s	0.42-0.45 mm/s	
2 mm	v_inj=1.38 mm/s	ICCV2	2.13 mm/s	1.32 mm/s	0-36.6%
		Prelude	1.35-1.59 mm/s	1.32-1.35 mm/s	
	v_inj=2.77 mm/s	ICCV2	4.75 mm/s	3.02 mm/s	12.25-43.5%
		Prelude	2.68-3.17 mm/s	2.46-2.65 mm/s	
	v_inj=0.555 mm/s	ICCV2	0.79 mm/s	0.38 mm/s	2.47-15.5%
		Prelude	0.81-0.89 mm/s	0.44-0.45 mm/s	
1 mm	v_inj=1.11 mm/s	ICCV2	1.74 mm/s	1.186 mm/s	2.19-43.68%
		Prelude	1.17-0.98 mm/s	1.02-1.16 mm/s	
	v_inj=0.555 mm/s	ICCV2	0.94 mm/s	0.63 mm/s	10-23.4%
		Prelude	0.72-0.81 mm/s	0.7-0.72 mm/s	

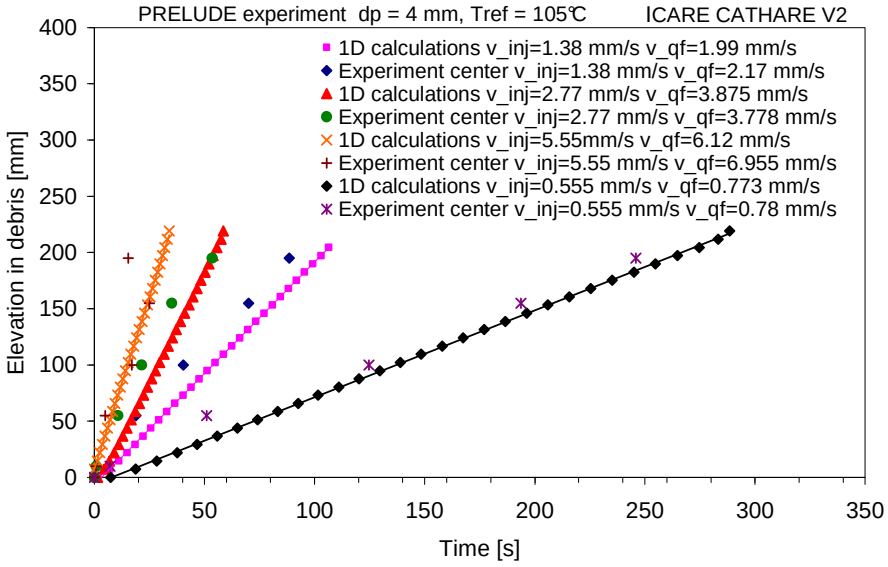

Figure 5.11: Calculated and experimental quench front velocity. Test PRELUDE '1D' with initial temperature 400°C, particle diameter **4**mm and different water injection velocities.

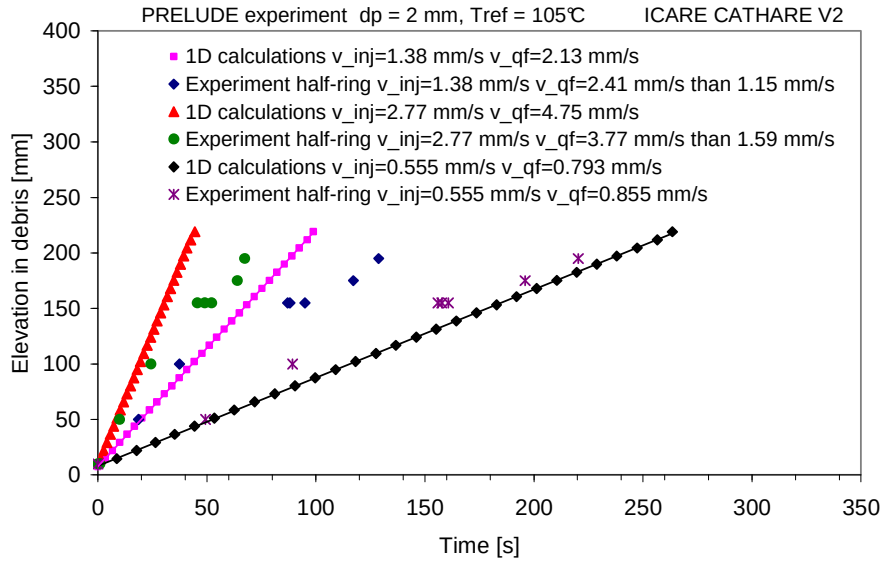

Figure 5.12: Calculated and experimental quench front velocity. Test PRELUDE '1D' with initial temperature 400°C, particle diameter **2**mm and different water injection velocities.

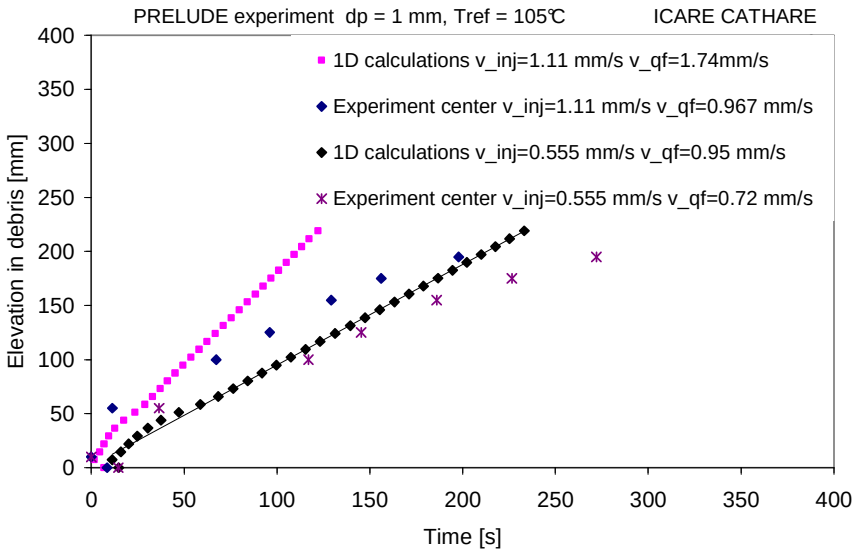

Figure 5.13: Calculated and experimental quench front velocity. Test PRELUDE '1D' with initial temperature 400°C, particle diameter **1**mm and different water injection velocities.

In PRELUDE tests, the steam flow rate was measured at the outlet of the test section (see Figure 5.7). These experimental results can be compared with calculation results (outlet tube is modelled). In Figure 5.14-Figure 5.16, the steam flow rate for different tests is shown. We can see that the time interval in which the steam is produced as well as the maximum value are well predicted. Moreover, a steady-state production of steam is observed in many cases, which confirms the steady-state progression of the quench front. However, for tests with 1mm beads, a steady-state steam production was not reached because the water reached the top of the bed before a steady-state was reached. A fraction of steam produced is re-condensed by contact with water, which quickly covers the top of the bed. Again here we can state that, in these tests, multi-dimensional effects were observed and nodalization with one radial mesh may not be sufficient.

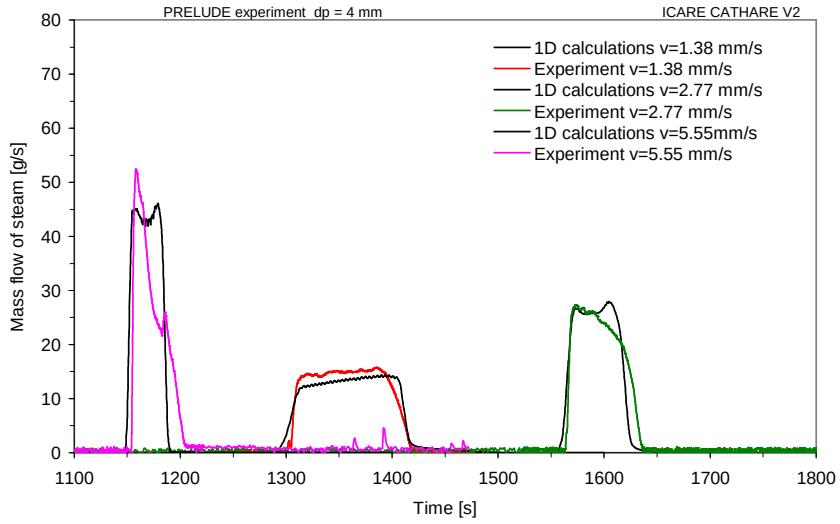

Figure 5.14: Calculated and experimental steam flow. Tests PRELUDE '1D' with initial temperature 400°C, particle diameter 4mm .

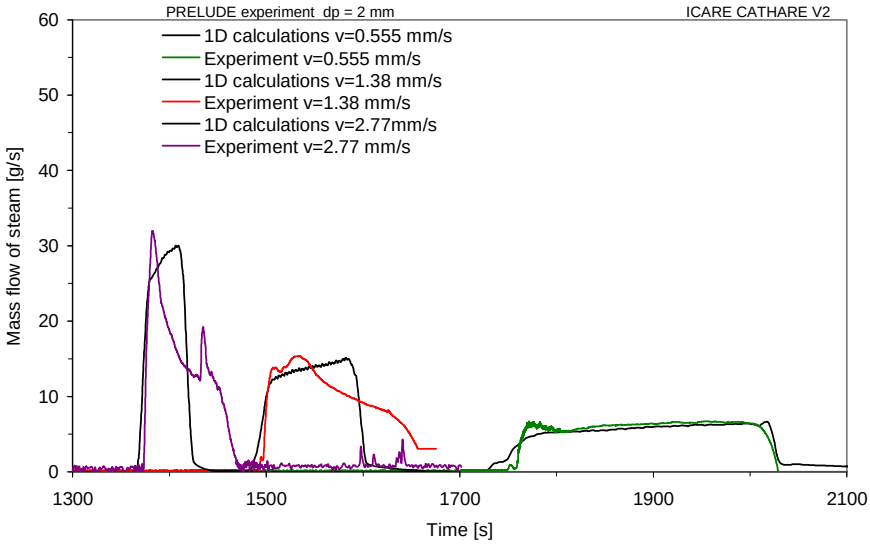

Figure 5.15: Calculated and experimental steam flow. Tests PRELUDE '1D' with initial temperature 400°C, particle diameter 2mm.

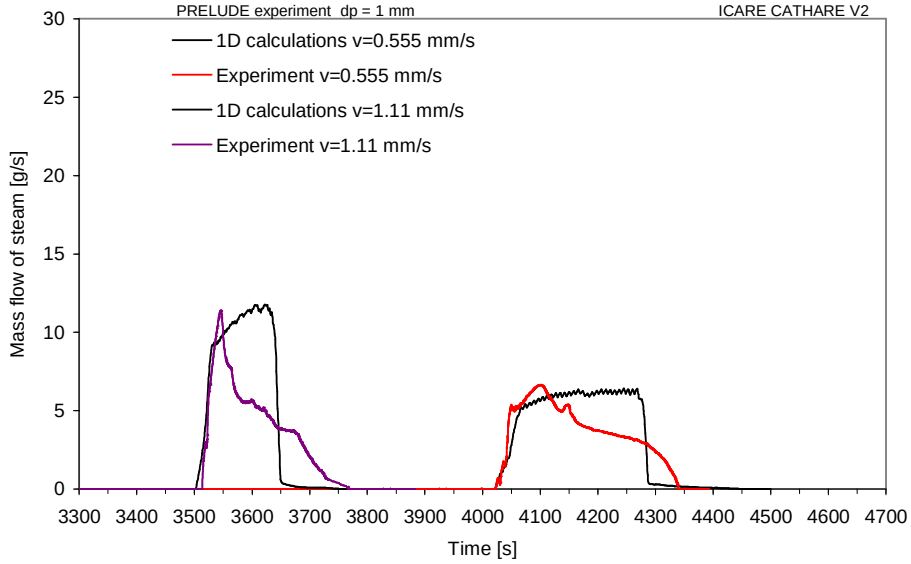

Figure 5.16: Calculated and experimental steam flow. Tests PRELUDE '1D' with initial temperature 400°C, particle diameter 1mm.

The pressure difference between the top and bottom of the bed can also be compared with experimental results. However, the exact position of pressure measurements in the PRELUDE experiment is not known, i.e., it may cover only a debris bed section or the whole experimental tube. This uncertainty does not have important consequences because the main contribution to the total pressure difference comes from the part of the bed located downstream of the quench front (where a fast steam flow is produced). On Figure 5.17-Figure 5.19 the difference of pressure over the test section for different tests is plotted as a function of time. We can see that the pressure difference increases as the liquid flow increases. This happens during the time interval in which the porous medium is quenched and thus the steam is produced. The peak of steam production, if it occurs, is directly related to the peak in steam production. The calculation results are in agreement with experimental results. Again here, different behaviour is observed for 1mm particles. However, the pressure indicates here a steady-state value that was not confirmed by steam flow measurements in Figure 5.16. This tends to confirm that there is a difference between the actual steam flow at the outlet of the debris bed and the steam flow at the location of measurement (condensation occurs between those two points). Moreover, concerning 1mm particles, we concluded that there is also an uncertainty in geometrical characteristics of the debris bed that strongly affects the calculated pressure. Indeed, the debris bed porosity 0.4 identified for debris bed with 4mm particles may be lower for a bed with 1mm particles, i.e., porosity 0.336-0.377 for 1mm non-oxidized or oxidized particles.

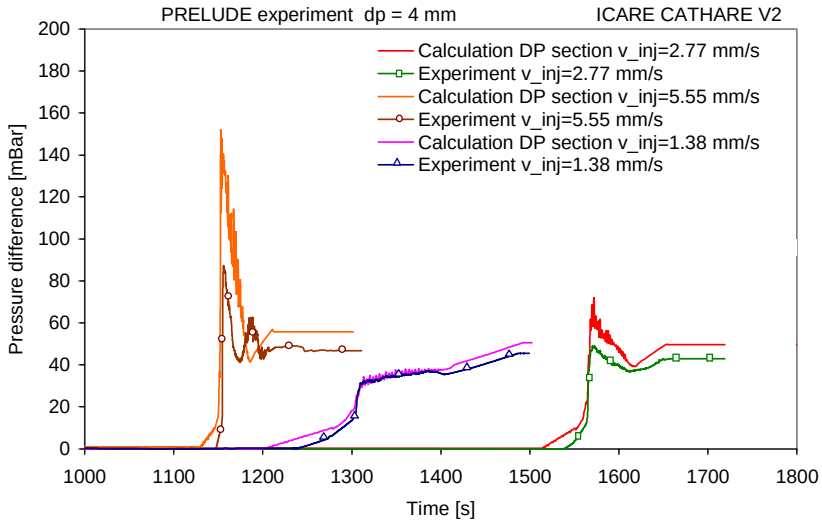

Figure 5.17: Calculated and experimental pressure increase. Tests PRELUDE '1D' with initial temperature 400°C, particle diameter 4mm.

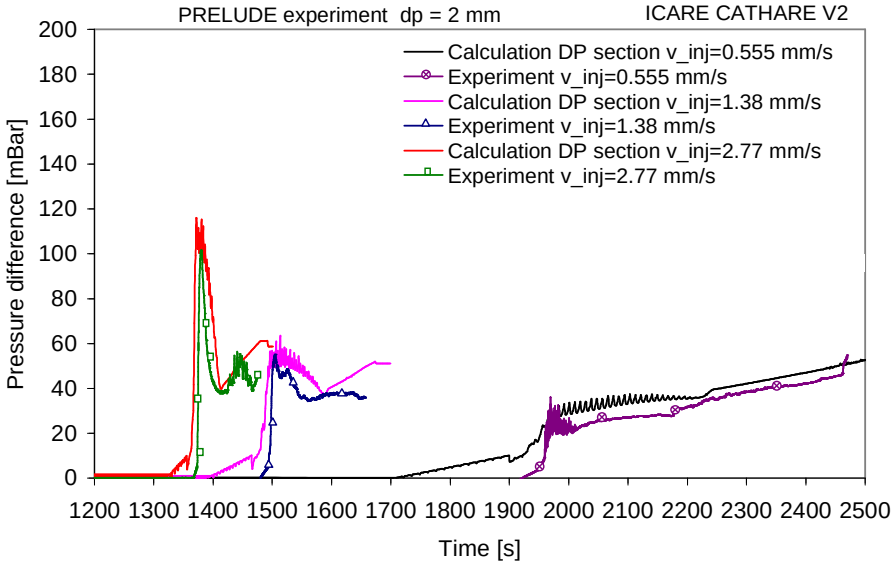

Figure 5.18: Calculated and experimental pressure increase. Tests PRELUDE '1D' with initial temperature 400°C, particle diameter 2mm.

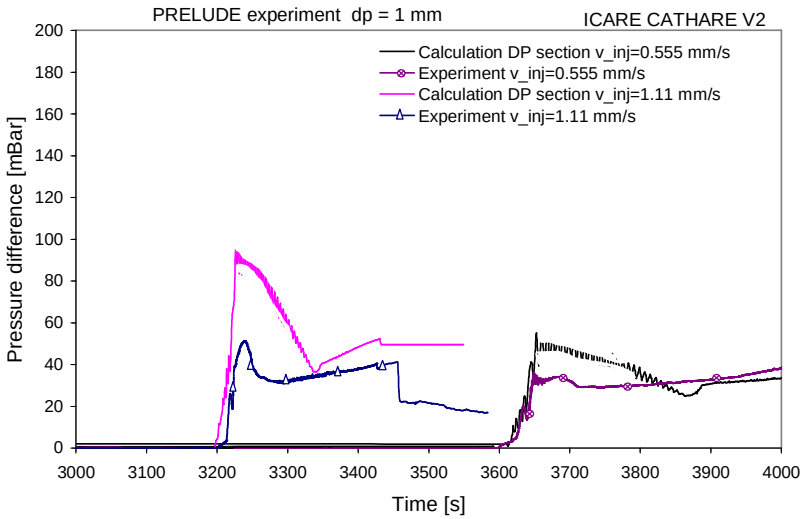

Figure 5.19: Calculated and experimental pressure increase. Tests PRELUDE '1D' with initial temperature 400°C, particle diameter 1mm

The measuring techniques at PRELUDE facility significantly enhanced the database of experimental results. The temperature measurements (particle or in pores), steam flow production and pressure increase were compared with calculation results. However, experimental techniques to measure e. g. local void fractions or velocities are still missing. Here, we will present the local parameters calculated by ICARE-CATHARE code and these results allows to draw supplementary conclusions. In Figure 5.20 we can see an axial evolution of void fraction, heat flux, liquid/gas velocities and pressure at the instant of quenching. According to void fraction calculations, the thickness of the two-phase region was observed to be a few centimetres and appeared to be almost constant during the propagation. The void fraction at the maximum heat flux was observed to reach high values (0.7-0.9). The liquid flow velocity increased before quenching, however the maximum values were small (below 1 cm/s), which indicates that there are no inertial effects on the liquid friction. The calculations of local pressure identified a changing of slope at the quenching position. If this result is confirmed by the future tests with local pressure measurements, this will constitute an additional, and possibly more reliable, criterion to identify the position of the quench front.

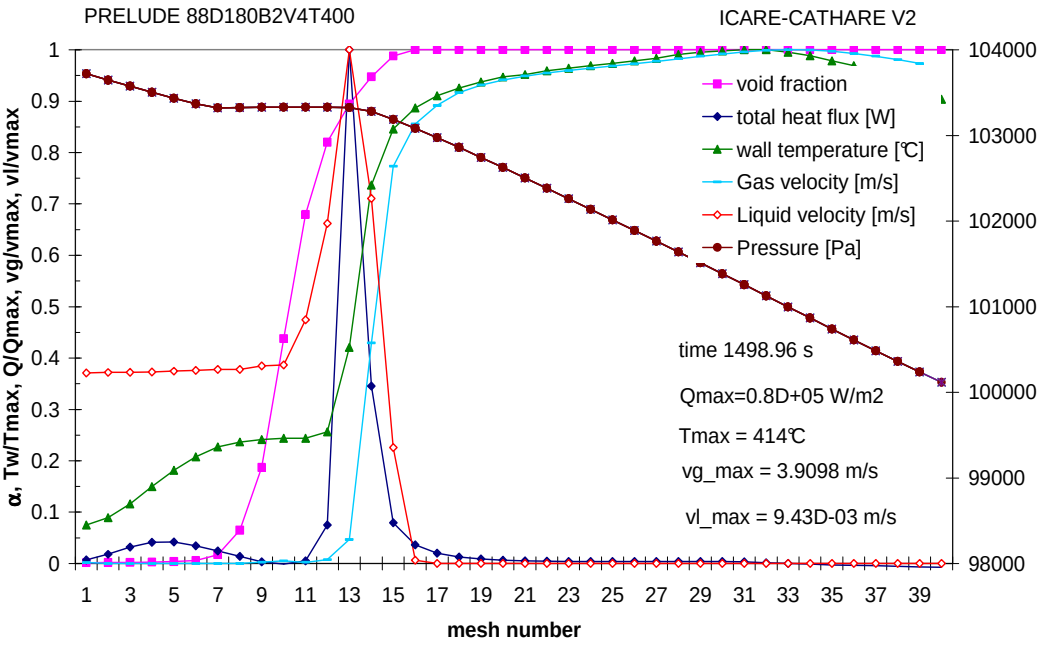

Figure 5.20: Additional calculations for local parameters that were not measured. PRELUDE '1D' test with initial temperature 400°C, particle diameter 2mm and water injection flow 5m/h

PRELUDE '1D' experimental results and ICCV2 'ID2' calculation results

The ICARE-CATHARE reflood calculations were performed for PRELUDE "1D" tests with the initial debris bed temperature at 700°C. The temperature evolution, quench front velocity, pressure increase and steam formation can be compared with experimental results.

The nodalization and input deck characteristics were given in paragraphs above. In these calculations, compared to tests at 400°C, five radial meshes were necessary. The reason is that by increasing the debris bed temperature the quench front instabilities increased, especially for higher liquid flow rates. In order to observe these effects in calculations, five radial meshes were modelled and the quench front velocity was analysed in each radial column (see Figure 5.21).

In these tests, compared to tests with 400°C, the water enters the porous medium initially heated up to higher temperature (see Figure 5.22). Above 400°C, the initial heat transfer and evaporation rate are low because the heat transfer corresponds to film boiling (much less intense). The calculations of these tests allow us to validate the model of film boiling as well as the transition criteria in ICARE-CATHARE (see Figure 5.22). The transition criterion between the "pre-cooling" regime and fast quenching is selected according to quench front position and heat transfer layer length (see Chapter 4). Moreover, the sensitivity calculations on the impact of heat transfer layer length on the calculation results can be found in Appendix A . Assuming an uncertainty about 40% for that length has an impact on the quench front

velocity of about 12% only. The highest difference was observed in the quench front velocity close to the wall.

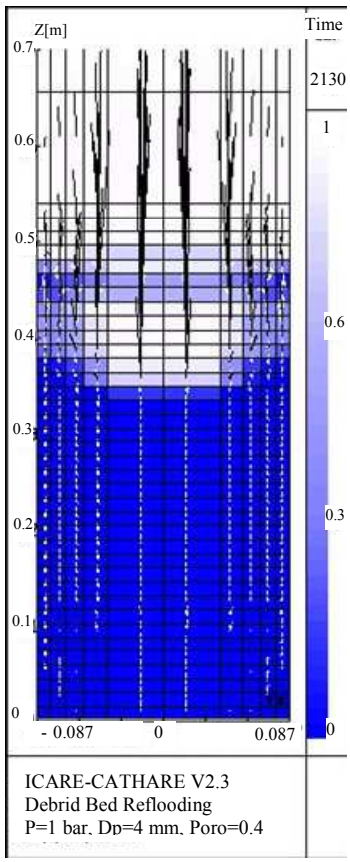

Figure 5.21: Distribution of calculated void fraction showing the faster progression along the side wall

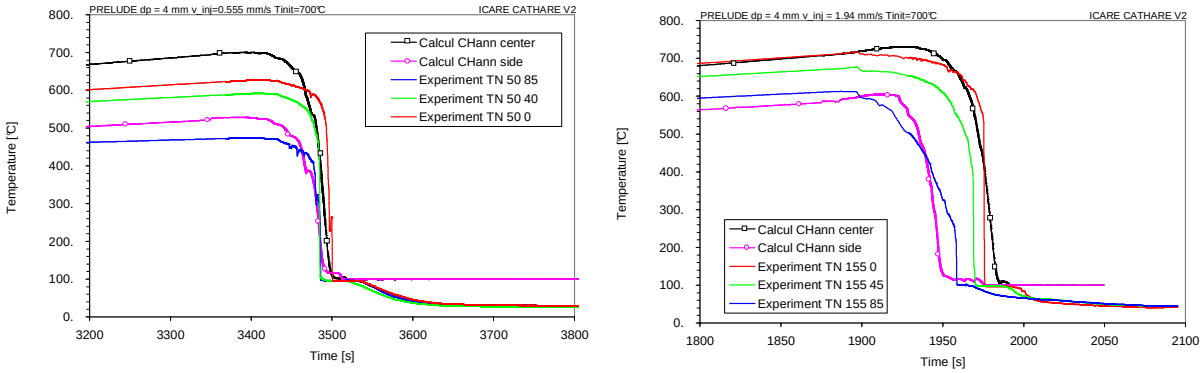

Figure 5.22: Example of temperature evolution at two different PRELUDE tests. PRELUDE '2D' tests with initial temperature 700°C, particle diameter 4mm and water injection velocity 2m/h (left) and 7m/h (right).

The quantitative results of quench front velocities are summarized in Table 5.15. The quench front velocities are summarized for two reference temperatures for quenching: T_{ref}=105°C and T_{ref} =95°C. The importance of these analyses was explained above.
The results taking T_{ref} =105°C are shown in Figure 5.23-Figure 5.26. The calculations show that the two-dimensional effects increase as the liquid injection velocity increases e.g. increasing the liquid injection velocity 5 times, the front was observed to progress almost 2 times faster at the border compared to the centre. It is in agreement with experimental results. The model also predicts correctly the interval of maximum and minimum quench front velocities. The minimum quench front velocity was calculated to be at the centre, for all the tests. However, the experiments with water injection velocity 1.38 and 2.77 mm/s showed that the minimum quench front velocity was at mid-radius. This could not be explained.

Table 5.15: Quench front velocities for different tests with initial temperature 700°C. ICCV2-ID2 input deck, PRELUDE '2D' minimum and maximum quench front velocities

Liquid flow – free section at bottom		Quench front velocity for two reference temperatures		% Difference
		Tref=105℃	Tref=95℃	Difference
v_inj=0.555 mm/s	ICCV2	0.69-0.7 mm/s	0.41-0.43 mm/s	3.16-21.56%
	Prelude	0.71-0.8 mm/s	0.49-0.55 mm/s	
v_inj=1.38 mm/s	ICCV2	1.44-1.9 mm/s	1.18-1.21 mm/s	0-7%
	Prelude	1.39-1.87 mm/s	1.1-1.21 mm/s	
v_inj=1.94 mm/s	ICCV2	1.9-2.82 mm/s	1.8-1.86 mm/s	8.7-18.9%
	Prelude	2.07-2.54 mm/s	1.65-2.3 mm/s	
v_inj=2.77 mm/s	ICCV2	2.02-3.94 mm/s	2.05-2.4 mm/s	0.6-35.7%
	Prelude	2.04-2.9 mm/s	2.11-2.41 mm/s	

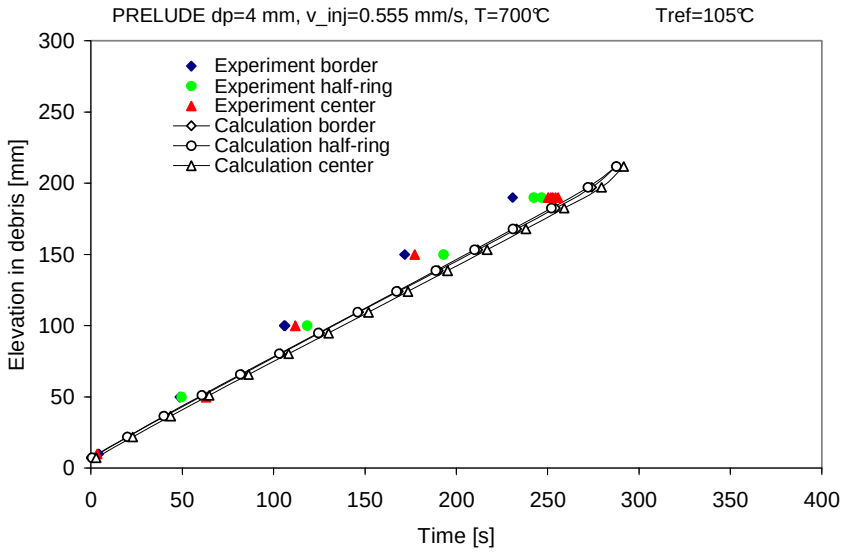

Figure 5.23: Calculated and experimental quench front velocity. Tests PRELUDE '1D' with initial temperature 700°C, particle diameter 4mm and liquid injection flow 2m/h

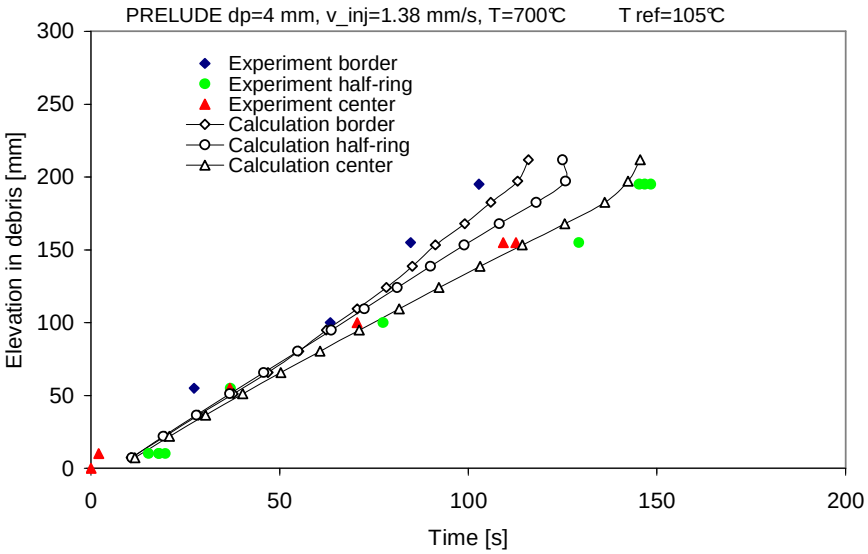

Figure 5.24: Calculated and experimental quench front velocity. Tests PRELUDE '1D' with initial temperature 700°C, particle diameter 4mm and liquid injection flow 5m/h

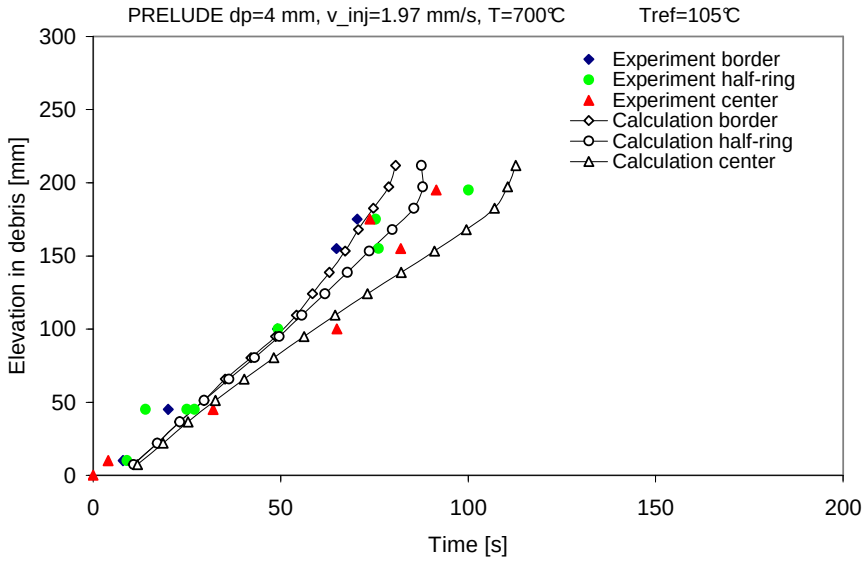

Figure 5.25: Calculated and experimental quench front velocity. Tests PRELUDE '1D' with initial temperature 700°C, particle diameter 4mm and liquid injection flow 7m/h

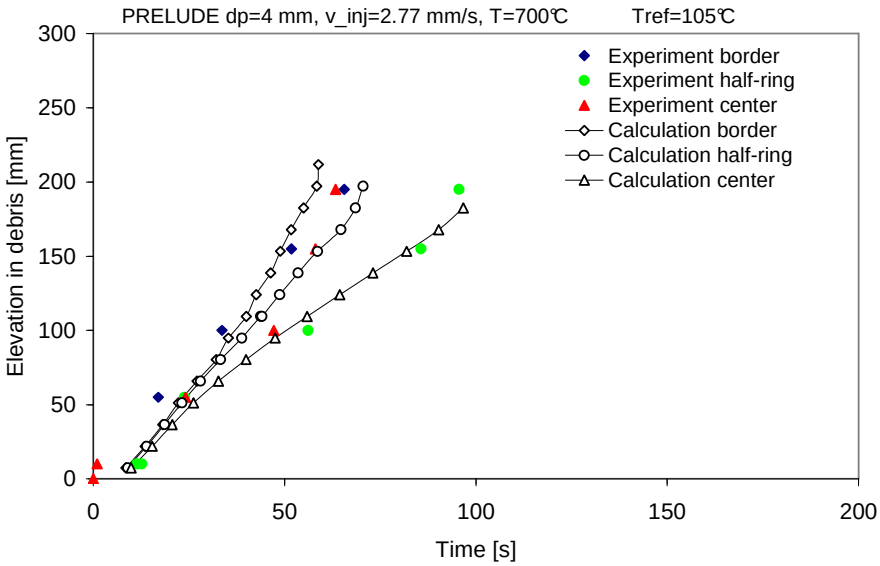

Figure 5.26: Calculated and experimental quench front velocity. Tests PRELUDE '1D' with initial temperature 700°C, particle diameter 4mm and different liquid injection flow 10m/h

In Figure 5.27, the steam flow at the outlet is plotted as a function of time. We can see that the time interval in which steam is produced as well as the mean value are well predicted. However, the value of the very short peak is missed. But if we look at the pressure difference (Figure 5.27 right), the peak appears and is well calculated. Again we may assume that the measured steam flow rate does not correspond exactly to the flow rate generated in the bed.

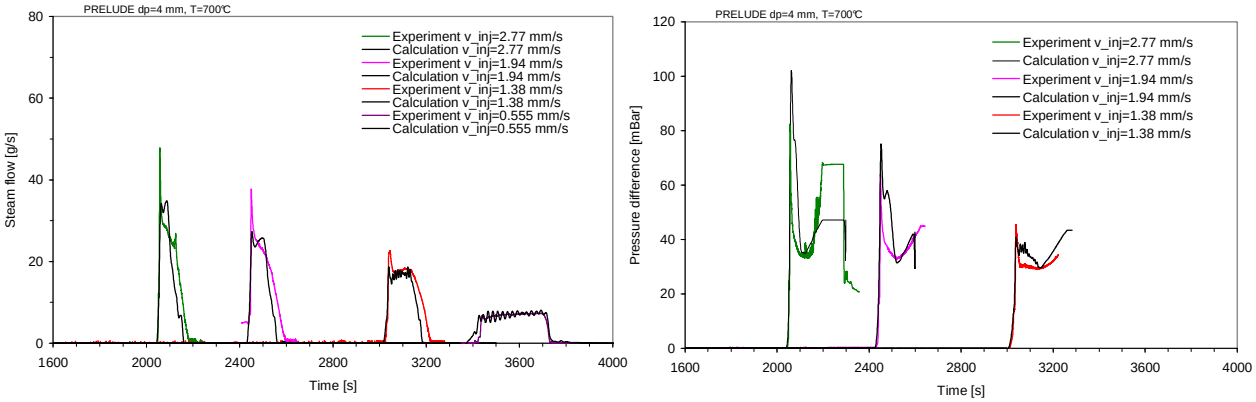

Figure 5.27: Calculated and experimental steam flow (left) and pressure increase (right). Tests PRELUDE '1D' with initial temperature 700°C, particle diameter 4mm and different liquid injection flow.

PRELUDE '2D' experimental results and ICCV2 'ID3' calculation results

The ICARE-CATHARE reflood calculations were performed for PRELUDE "2D" bottom reflood test with initial temperature 700°C and liquid injection flow 5m/h (1.38mm/s), with a lateral "bypass". The temperature evolution, quench front velocity, pressure increase and steam formation can be compared with experimental results.

In the PRELUDE "2D" a by-pass made of quartz particles with diameter 8mm was placed close to the wall. The nodalization and input deck characteristics were given in paragraphs above. In these calculations, five radial meshes were modelled. The quench front velocity was identified in each column. The quench front velocities were analysed with two reference temperatures for quenching: T_{ref}=105°C and T_{ref} =95°C. The calculated and experimental results are shown in Figure 5.28 and Figure 5.29. The quench front velocity at different columns is well predicted. Moreover, we can see that the 2D effects during quenching are present, regarding the first quenching, i.e., reference temperature 105°C. Regarding the reference temperature 95°C (Figure 5.29), the quench front is more 1D. This again emphasizes the importance of analyzing both velocities. As we already mentioned, the code should predict well both situations. However, for the analysis we recommend to take the reference temperature 105°C because more information can be obtained e.g. concerning 2D effects etc.

In Figure 5.30, we can see the experimental and calculated steam flow and pressure increase. The time intervals, as well as the values, are well predicted. It might be interesting to compare here the steam flow from PRELUDE '1D' and PRELUDE '2D' for the same experimental conditions, i.e., initial temperature 700°C, particle diameter 4mm and liquid injection flow 5m/h (Figure 5.27). These two geometries differ in bed section (180mm versus 290mm), debris bed height (200mm versus 250mm) and by-pass region (no by-pass versus by-pass). Because of the larger mass of debris bed (24kg versus 55kg) there is more steam produced at PRELUDE '2D'. However, the peaks in steam production as well as in pressure difference are missing when the by-pass is present (see Figure 5.30). This shows that the by-pass tends to limit the pressure gradient in the debris. Also, there is a fraction of the steam and water flows which go through the by-pass which, in turn, affects the steam production in the bed itself.
The different velocity of water progression in the centre (low permeability) and in the by-pass (high permeability) results from a balance of pressure gradients and the fact that the permeability and passability (pressure drop coefficients) are larger in the centre than in the by-pass. After reflooding and quenching the by-pass, the outlet steam formation reduces. The steam is produced then as a result of quenching of the central zone. The effect of bypass will be discussed in detail in a next Chapter (Section 6.1.2.2) because it is very important concerning the reactor scale applications.

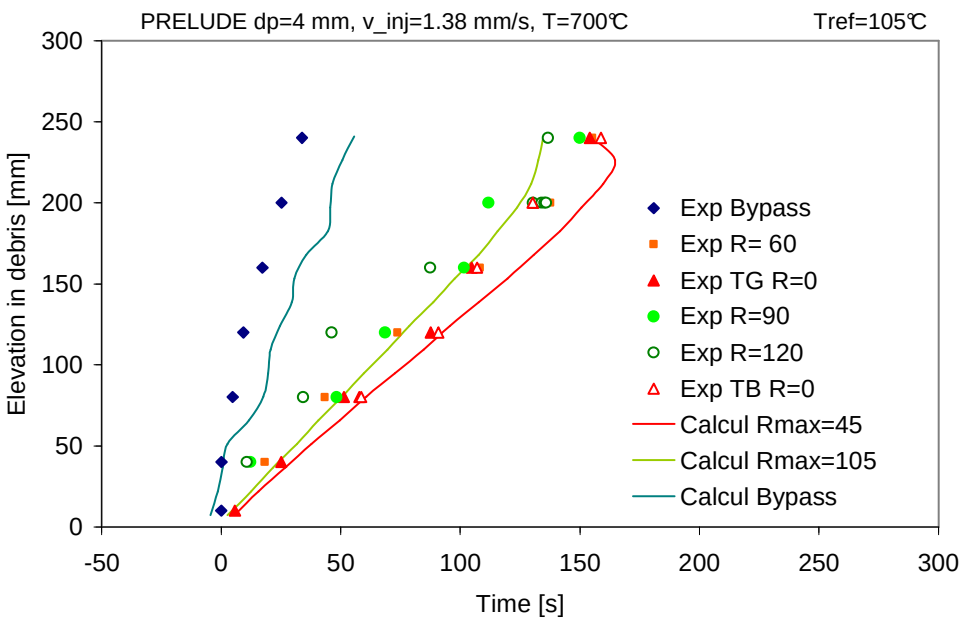

Figure 5.28: Calculated and experimental quench front velocity (T_{ref}=105°C). Test PRELUDE '2D' with initial temperature 700°C, particle diameter 4mm and liquid injection flow 5m/h.

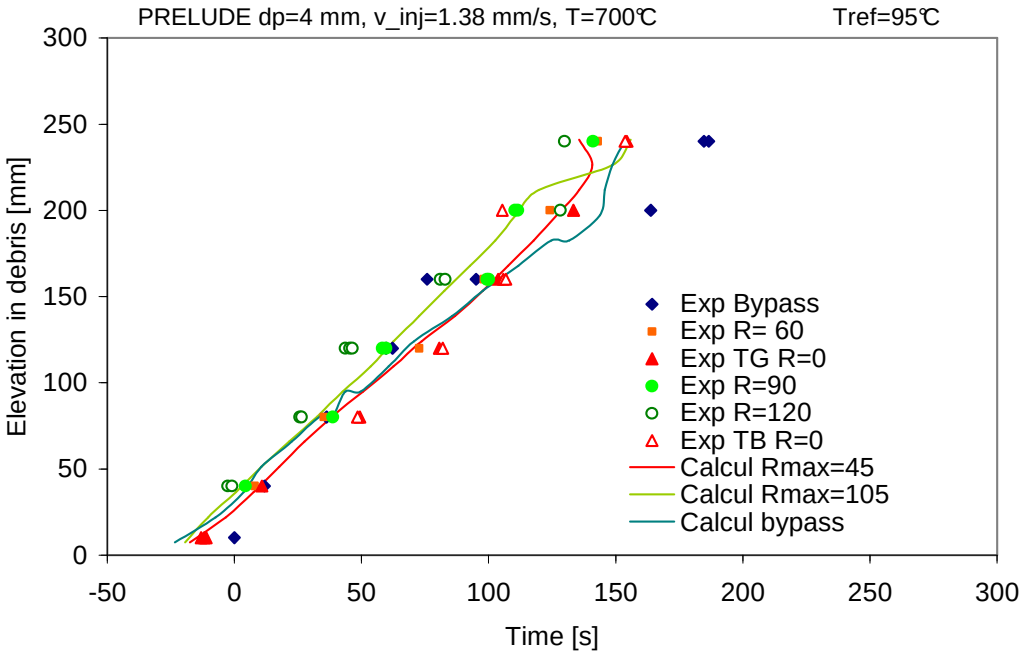

Figure 5.29: Calculated and experimental quench front velocity (T_{ref}=95°C). Test PRELUDE '2D' with initial temperature 700°C, particle diameter 4mm and liquid injection flow 5m/h.

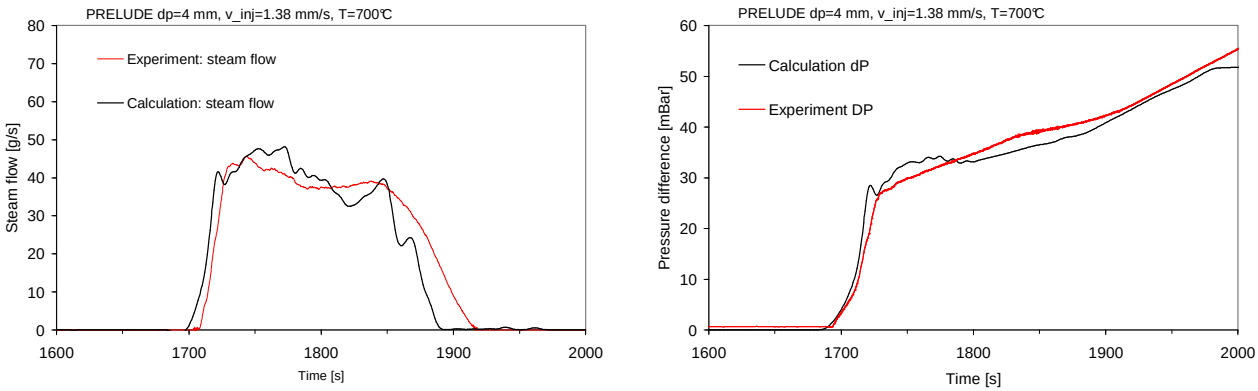

Figure 5.30: Calculated and experimental steam flow (left) and pressure increase (right). Tests PRELUDE'2D' with initial temperature 700°C, dp=4mm and liquid injection flow 5m/h.

5.3 CONCLUSIONS

In this Chapter, the validation of the ICARE-CATHARE V2 code was presented for two sets of experimental data: Petit dry-out experimental results and PRELUDE reflood experimental results.

The objective of PETIT calculations is to validate different phenomena of boiling in a porous medium with internal source, i.e., liquid single-phase flow, two-phase flow and gas-single phase flow. Firstly, calculations concerning the increase of temperature up to nucleate boiling regime were presented. The quantitative validation of volumetric heat transfer coefficients used in our model was performed. In the proposed theoretical model, the heat exchange coefficients obtained for the simple stratified Unit Cell are recommended to be multiplied by factor 9. However, in further studies, this somehow heuristic approach could be improved by solving the proposed "closure problems" on more realistic geometry. Also the calculations were performed for different liquid flow rates and the dry zone elevation was identified for each test. The analysis concerning the incipience of dry-out gave us only an indication about the relevance and good physical behaviour of the model. Because of lack of instantaneous power records, it was not possible to draw quantitative conclusions.

In the second part, the validation of ICARE-CATHARE two-phase flow porous media model with PRELUDE reflood experimental results was presented. In total, 17 PRELUDE tests were calculated, varying the geometry, initial temperature and liquid injection flow rate. Firstly, the ICARE-CATHARE reflood calculations were performed for PRELUDE "1D" tests with initial debris bed temperature at 400°C. Secondly, the calculations were performed for PRELUDE "1D" tests with the initial debris bed temperature at 700°C. In order to observe these effects in these calculations, five radial meshes were modeled. Finally, the calculations were performed for PRELUDE "2D" bottom reflood test with initial temperature 700°C and liquid injection flow 5m/h (1.38mm/s), with a lateral "bypass".

Comparisons of temperature evolutions at different elevations show that the model is able to predict quenching velocity for different inlet flow rates and different particle diameters, in the whole range covered by PRELUDE experiments. The steam flow rate and the pressure difference across the debris bed are also well predicted which indicates that the model behaves consistently. The discrepancies were observed for tests with 1mm particles. It was concluded that the calculations with multi radial meshing gives better results. Here, the difference in quench front velocity between the calculation results and experimental results decreased, e.g. from 43% to 29% and for other tests, it was always below 35%. Moreover, calculations of tests with initial temperature 700°C showed that the transition criterion defined in Chapter 4 predicts well the switch between the "pre-cooling" regime and fast quenching. Finally, the calculations of PRELUDE "2D" test with lateral bypass are presented. The interesting conclusion is that the quench front velocity observed in these calculations is the same as in PRELUDE "1D". This means that the bypass did not influence the front progression in the centre. However, the different velocity of water progression in the center (low permeability) and in the outer ring (high permeability) results from a balance of pressure gradients and the fact that the permeability and passability (pressure drop coefficients) are much larger in the center than at the periphery. This will be discussed in Chapter 6 because the bypass plays an important role in reactor case.

Finally, we will discuss here the model difficulties and the possibilities for further developments. The reader might noticed the problems concerning the "oscillations" of calculated parameters as the pressure and steam flow. The author of this thesis is not specialized in numeric so no detailed numerical analyses were performed. Neither the numerical parameters are shown here e.g. convergence, time steps. This may be an objective of the further studies. However, if the convergence problems during the calculations occurred, the problem was analysed and solved. At the limits of porous medium, at the interface of zone porous and non porous, additional development could be realized.

The calculations with higher initial temperature and lower particle diameter e.g. 700°C and 2mm particles are ongoing. These tests (not showed here) indicate that the temperature profile is well predicted but the end of quenching is sooner compared to the experimental results. Moreover, the top reflooding test results are under analyses and were not summarized here. These tests indicate strong multi dimensional effects and should be precisely modelled.

Chapter 6

REACTOR SCALE APPLICATIONS

6. REACTOR SCALE APPLICATIONS

The confrontation of calculated results with the experimental results in Chapter 5 allows to evaluate the pertinence of the model in the domain of the test conditions. However, there is no guarantee that these conclusions can be extrapolated to the reactor application. Several parameters are likely to play a key role for the reactor application. Obviously, the size of the debris bed is one of those key parameters, but the pressure will also play a role as well as the existence of non homogeneities in the porous bed.

The first question is the applicability of the developed model to an overall analysis of coolability of particulate debris beds that may form in the course of a severe accident in a reactor. Since the model involves essentially correlations for heat transfer or friction that are functions of the local variables (within a mesh), we can consider that, keeping the mesh size constant (i.e. much more meshes for the reactor scale) with respect to the PRELUDE calculations, the correlations will remain valid and, therefore, the model should be reliable, even at a large scale. However, there are at least two difficulties:

1. Mesh size for a reactor calculation is usually 10 times (at least) larger than the finest mesh size used for validation of the model on PRELUDE experiment. Even if the sensitivity shown in Appendix B has shown that we can still obtain acceptable results if the mesh size is 2 to 4 times larger.
2. The "heat transfer length" introduced in the model for transition boiling is a parameter which will obviously produce results that depend on the mesh size. The sensitivity to that parameter has been evaluated in Appendix A.

Therefore, this Chapter will provide a first analysis of application of the model to reactor scale debris bed that should be considered as preliminary. The main objective is to identify the processes which could be different at a large scale. Among the questions they are interesting, we may list the following:

- A quasi-steady progression was observed in PRELUDE and in calculations. Is it still true for a debris bed of a few meters height?
- The large pressure gradient generated by the intense steam flow downstream of the quench front is likely to be the cause of the instability of water progression. Is it likely to observe the same instability at a large scale, with different boundary conditions?
- In PRELUDE, the effect of the volumetric power could be neglected in most cases because the necessary time to reflood the bed was short. In a larger bed, it will have an impact. Is it possible to characterize that effect?

The shape and size of the particles, as well as their arrangement have obviously an impact. In the model, all those parameters are taken into account thanks to only two main parameters: the "average" particle size and the porosity. Here, it must be mentioned that all those issues related to the geometry of the particles and of the bed could not be studied in the present work

which was focused on the thermalhydraulics aspects and the interpretation of experiments made with spheres, with a controlled porosity. However, those issues were studied in parallel in the same laboratory. The main conclusions of that work will be summarized later in this Chapter.

In this Chapter we will introduce mainly the discussion that concerns the effects of large scale and core geometry. Only the scale effects will be discussed and no complex reactor calculations with real core materials are provided here. Firstly, the transposition of PRELUDE (and future PEARL) experimental results to a reactor scale is discussed. Secondly, the reactor scale calculations and sensitivity studies on scenario parameters will be presented in order to draw additional conclusions for reactor safety assessment and accident management.

6.1 REACTOR CASE VERSUS SMALL SCALE PRELUDE

The objective of this Chapter is to draw conclusions about the validity to transpose the PRELUDE (and future PEARL) experimental results to the reactor scale. In this introduction, the main characteristics of PRELUDE that may be irrelevant for the transposition of results up to the reactor scale will be discussed. Secondly, complementary conclusions will be drawn, analysing the large scale calculations using ICARE-CATHARE code.
We briefly recall that the debris bed formed after the collapse of some highly oxidized fuel assemblies may cover a large part of the core (see Figure 6.1). It is likely to be surrounded by intact assemblies at the periphery (as observed after TMI-2 accident) which constitute a by-pass area where water may flow much more easily. Within the porous bed, the porosity and the average particle size are likely to vary because the local burn-up and volumetric power varies between assemblies. The conditions of collapse of assemblies, which are related to the degree of oxidation of the Zircaloy claddings, may also vary, mainly in the axial direction because oxidation strongly depends on the steam flow along the axial direction.

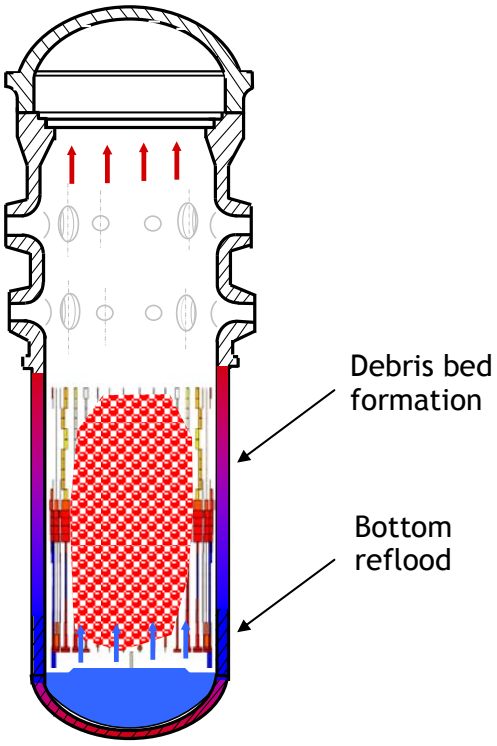

Figure 6.1: Sketch of the debris bed formed after the collapsed of some fuel rod assemblies

- **Scale effect and bypass**

PRELUDE is a small-scale facility (see Table 6.1). The debris bed height is only 200mm. However, it was observed that the effects at the enter may persist up to 50mm of bed height. Moreover, if water reaches the top of the bed, it may affect also few last millimetres of debris bed height. Finally, it remains only about 100mm of debris bed height representative for analysis (see Chapter 2). Moreover, taking into account also the side effects close to the wall, the PRELUDE debris bed geometry may not be sufficient. Consequently, in a future PEARL facility the debris bed height was proposed to be 500mm that may be a better compromise.

The debris bed diameter plays also and important role. However, it may not be so obvious even if there is a presence of "bypass" region close to the side. Generally, the radial propagation follows the axial propagation of the quench front. It is because the pressure gradient is generated due to the difference of height between the water columns in the bypass compared to the centre of the bed. On the other hand, in PRELUDE and later PEARL experiments, the aim is also to observe the 2D effects that will be independent from the conditions at the boundaries of the bed. That is the reason why the debris bed section reaches the criterion: *Diameter(section)>100*Diameter(particle)*. Moreover, in the PRELUDE 2D and later PEARL design, a special attention was paid to the creation of "bypass" region. In the case corresponding to reactor situation, the water has an easier access through the partially degraded fuel rods at the outer ring of active zone. Such bypass corresponds to intact rods which are assumed to be maintained at the periphery of the core. This geometry was observed

after TMI-2 accident [Broughton89] or Paks accident [Hozer10] where the outer ring of fuel rods was much less degraded compared to a completely fragmented center of the active zone. The effect of bypass is discussed in Section 6.1.2.2.

- **Characteristic size and arrangements of particles**

A bibliographic study [Coindeau01] showed that the debris bed may consist of a mixture of particles resulting from two phenomena:

- Natural fragmentation that results in particle size in the range of 2-4mm;
- Spallation caused by growth of fission product bubbles in the fuel. This leads to a range of sizes from grain size (some tens of micrometers) to hundreds of micrometers. However, such debris are only likely to appear in some part (or some assemblies) of the reactor core where high burn-up and particular local conditions of the Zircaloy cladding may exist simultaneously.

The debris bed geometry depends strongly on burn out [Coindeau01]. Consequently, the fragmented reactor core cannot be formed uniquely by small neither the big particles. In addition, the porosity is also likely to vary, from 0.5 down to almost zero in some areas where a large amount of molten material migrated.

In PRELUDE and future PEARL tests, the particles lower than 1mm will not be used due to the risks of fluidization. In order to guarantee the representativeness, the further strategy consists in:

- Study of the mono-disperse beds 1, 2 and 4mm (already done);
- Study of the poly-disperse beds. The first studies are ongoing and concern the one phase flow studies in order to find an "equivalence" with mono-disperse beds;
- Introduction of big particles (8mm) or small particles (<1mm) to form a strong local heterogeneities.

Those aspects were not considered in this thesis but the dependence on particle size and porosity was taken into account in the correlations and model equations. In the next section, the impact of porosity at the reactor scale will be studied.

- **Materials**

For the reactor fragmented core composed of UO2, the initial stored energy for any temperature is the same as in the case of steel particles used in PRELUDE and further PEARL experiment. In Chapter 2 (Section 2.5.3.3) it was shown that the time needed to uniform the temperature of *steel* particle (0.15s) is lower than the time needed to uniform the temperature of *UO2* particle (1.4s). This may impact the reflooding process where the UO2 particles are not totally quenched when the water progresses. However, it is reasonable to assume that the impact on reflooding phenomena will not be so important. Here, the surface temperature is slightly lower than the mean temperature. Moreover, upstream of the quench front, the heat flux is less important and the reflooding is comparable for steel and UO2 particles. It is

important to note that the material effect concern mainly the oxidation and associated energy release.

- **Thermohydraulic conditions**

In PRELUDE and further PEARL experiments the maximum temperature of debris bed reaches 1200°C. However, the reactor core composed of debris bed is expected to reach higher temperatures e.g. above 1500°C (Table 6.1). The studies of debris bed at higher temperature may be interesting for the radiation heat flux analysis [Chahlafi11]. On the other hand, we do not expect a significant impact of higher temperature on thermohydraulic behaviour (the film boiling regime covers all the high temperatures). The reason is that the most important heat transfer occurs at lower temperatures e.g. 100°C or 200°C above the saturation temperature. However, the initial temperature is important concerning the steam formation. At the beginning of reflood, there is a transient behaviour of reflood that may result in a peak of steam production. Anyway, the PRELUDE tests with initial temperature 400-700°C already showed this behaviour. The question of high temperatures is important especially for the cases of *Zr* oxidation that is not studied in PRELUDE and further PEARL experiments.

Concerning the debris bed initial temperature just before the water injection, one can also discuss the effect of residual power. In a reactor core, the decay heat is produced due to the residual power and decreases with time after the reactor scram (see the reference value in Table 6.1). In PRELUDE experiments, the power is maintained during reflooding in order to simulate the effect of residual power. Indeed, in PRELUDE experiment, reflooding is achieved in 3 minutes and the energy added through volumetric heating is small compared to the stored energy. On the contrary, at the reactor scale, reflooding lasts at least half an hour for such small liquid velocity (2.77 mm/s) and the energy produced by volumetric heating cannot be neglected. This will be discussed in detail in Section 6.2.

Table 6.1: Comparison between the experiment and reactor case

	PRELUDE	**PEARL**	**REACTOR CASE***
Core geometry	Diameter 180 or 290mm Height 200mm or 250mm	Diameter 600mm Height 500mm	Diameter 3.28m Height 3.66m
Mass of core	5/24/55 kg	About 500kg	UO2 93.65 ton Zircaloy 23.05 ton
Debris bed	Whole bed in debris Bypass in last tests- quartz particles	Whole bed in debris Bypass – quartz particles	10 or 45 ton of debris, Bypass - (intact fuel rods)
Particle diameter	1/2/4 mm	<1, 2 and 3mm	2mm
Porosity	0.4	0.3 to 0.4	0.4
Core power	About 200W/kg	100, 200 and 300 W/kg	230W/kg ~5h after scram

Debris temperature	400-900°C	~1300	1700°C<T<2200°C
Water flow	2-20m/h	2-20m/h	12m/h
*according to TMI-2 benchmark exercise [Bandini12]			

6.1.1 Modeling of large scale geometry in ICARE-CATHARE V2.3

Preliminary "test" calculations were done with ICARE-CATHARE code for the large scale geometry. Those calculations will be further referred to as "Exercises". The objective of Exercise 1 and 2 (see Table 6.2) was to study only the effect of size and geometry on the thermo-hydraulic behavior during reflooding. Therefore, in order to compare the results with the PRELUDE small scale experimental results, all the characteristic features (except the size) of the larger debris bed are identical to PRELUDE case: debris material is steel and initial temperature corresponds to the test conditions. The Exercises 3 and 4 concern the effect of heterogeneities and pressure on calculation results. This cannot be compared with small scale PRELUDE but the studies are interesting concerning the future reactor applications.

Table 6.2: PRELUDE large scale calculation exercises

Test	Initial Temperature	Particle diameter	Liquid flow
Exercise 1	400°C	2mm	10m/h
Exercise 2	700°C	4mm	5m/h
Exercise 3	700°C	4mm Zone ε=0.2	5m/h
Exercise 4	1400°C	4mm	10m/h
	P=1, 3, 5, 10, 20, 50 and 100 bar		

Geometry

The dimensions of the large scale geometry were chosen to correspond to TMI-2 geometry [Broughton89]. The reactor core debris bed occupies the inner ring with a diameter 2.7m. A special attention was paid to the creation of "bypass" region where water has an easier access through the partially degraded fuel rods at the outer ring of active zone. For simplicity of calculation, the outer ring, which is supposed to be filled with almost intact rods, is formed with steel particles with higher diameter and porosity, 2cm and 0.5 respectively. The vessel outer diameter is 3.29m and its height is 10m. The debris bed height is 3.75m (total height of the core) and the rest of the volume represents lower and upper plenum. The whole geometry was assumed to have cylindrical symmetry. The geometry characteristics can be seen in Figure 6.2 and the nodalization is shown in Figure 6.3.

Material characteristics

As it was already mentioned, the objective of these calculation exercises is to study only the effect of size and geometry. Therefore, the debris bed is formed of steel particles and not UO2 as it is in a realistic reactor accident scenario. The material properties are the same as it was defined in PRELUDE small scale calculations. The total mass of steel in the core corresponds to 144 tons where the mass of "degraded core" (inner ring with diameter 2.7m) corresponds to 62 tons.

Power

In order to be compatible with PRELUDE experiments, the objective of Exercise 1 and 2 is to simulate the tests with the identical initial temperature before reflood. In order to keep that condition of initial temperature all along the whole reflooding, the volumetric power during reflooding is set to zero. Indeed, in PRELUDE experiment, reflooding is achieved in 3 minutes and the energy added through volumetric heating is small compared to the stored energy. On the contrary, at the reactor scale, reflooding lasts at least half an hour for such small liquid velocity (2.77 mm/s) and the energy created by volumetric heating cannot be neglected. That is why it was set to zero, in order to keep it negligible, as in PRELUDE tests. The second series of calculations concern the studies of effect of residual power and are summarized in Section 6.2.

	INPUT DECK
Vessel diameter	3.29m
Lower plenum height	2m
Support structure-quartz	1.25m
Debris bed	Height 3.75m Diameter 2.7m
Bypass	29.5cm each side Steel particles 2cm Porosity 0.5
Upper plenum height	3m
Vessel wall thickness	5.6cm

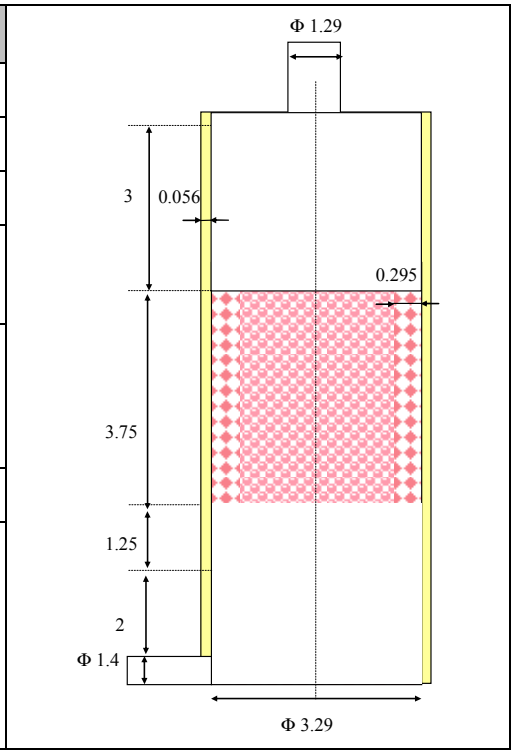

Figure 6.2: Geometry of the "large scale PRELUDE" for the calculation exercise (dimensions in meters)

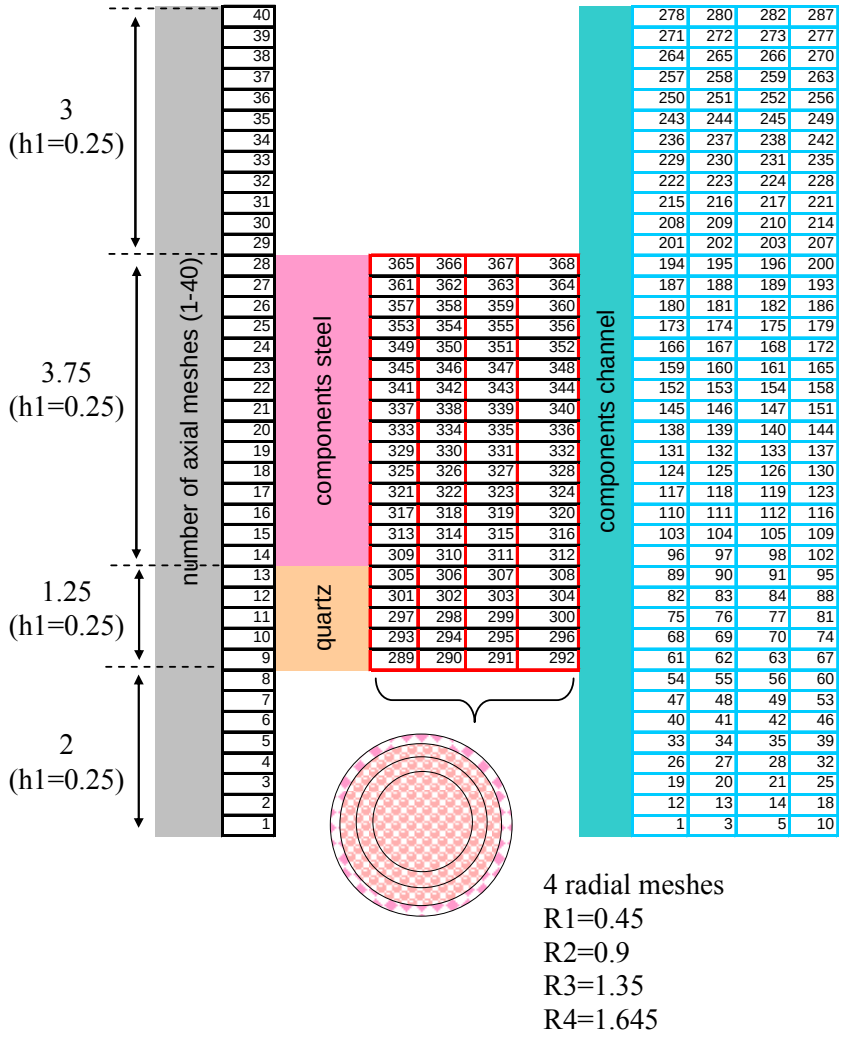

Figure 6.3: ICARE-CATHARE large scale nodalization (dimensions in meters).
Note: Mesh numbers are useful only for ICARE-CATHARE input deck readers

Water flow

In the large scale calculation exercises, the debris bed is heated and there is no presence of water initially. The bed is heated up to the desired temperature and quenched with water. The water flow at the bottom of test section in Exercise 1 and Exercise 2 is identical to PRELUDE experiment. Temperature of injected water was set to 20°C.

Boundary conditions

In order to be compatible with PRELUDE small scale experiments, the boundary conditions in Exercise 1 and Exercise 2 are identical. The outside temperature is set to 20°C, the pressure is atmospheric and heat exchange coefficient is set to 20 W/m^2K. Moreover, the Exercise 4 concerns the effect of pressure on calculation results. The tested pressure is in the range 1-100 bar.

6.1.2 Results of ICARE-CATHARE V2.3 calculations

In this section the large scale calculation results (see Table 6.2) will be presented. The objective of the Exercise 1 and 2 was to show if it is possible to transpose directly the PRELUDE small scale experimental results into a large scale. This will be discussed here. As it was already mentioned, a special attention was paid to the presence of lateral bypass. For simplicity of calculation, the outer ring, which is supposed to be filled with almost intact rods, is formed with *steel particles* with *larger diameter* and *porosity*, 2cm and 0.5 respectively. Finally, the additional Exercises 3 and 4 were made in order to see the effect of local debris bed heterogeneities and pressure on reflood process.

6.1.2.1 Quench front velocity

The quench front velocity was identified from the calculations. The calculation results of Exercise 1 are shown in Figure 6.4 (right) and of Exercise 2 in Figure 6.5 (right). Here, the progression of the quench front is shown, at the center of the debris bed and also in the outer ring. We can see that water progresses with higher velocity through the outer ring where the pressure drop is much lower. The higher quench front velocity through the bypass region appears to affect slightly the liquid flow through the center of debris bed. The calculations without bypass predict the higher quench front velocity in the center compared to calculations with bypass (see Table 6.3). This is due to the fact that in the case without bypass the water passes across the whole section without preference.

It is interesting to compare the quench front velocity measured in PRELUDE (even if without bypass) to the reactor scale prediction. The large scale calculation exercises confirmed that transposing the PRELUDE quench front velocities, the total *time of reflood* will be well predicted (Table 6.3). Moreover, the maximum error in prediction of time of reflood was observed to be only 20%. However, the difference is conservative from the reactor safety point of view. It means that applying the quench front velocity observed in PRELUDE small scale experiments to a reactor debris bed height, we *overestimate* the total time of reflood but only by 20% e.g. overestimation of 12 minutes for an evolution that is predicted to take 1 hour. It is important to note that the initial temperature of the bed is also important. The higher initial temperatures in case of reactor scale will result in the higher time of reflood. But the effect of the initial temperature was not taken into account in this discussion.

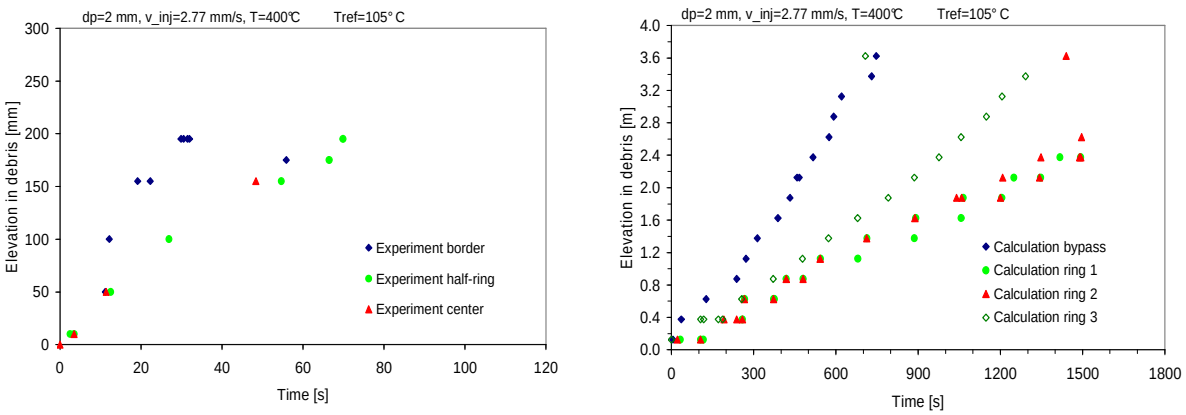

Figure 6.4: PRELUDE small scale experimental results (left) and Large scale calculations with bypass (right); Test with initial temperature 400°C, particle diameter 2mm and liquid injection flow 10m/h

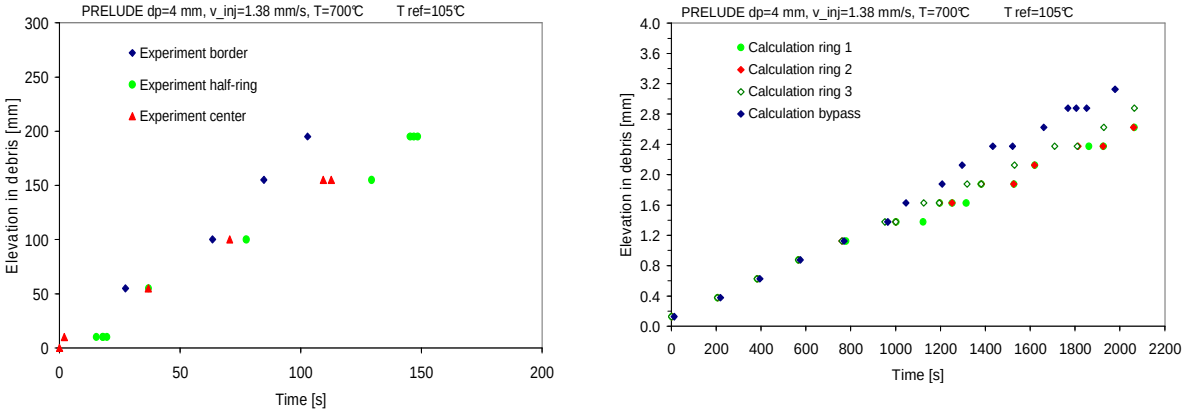

Figure 6.5: PRELUDE small scale experimental results (left) and Large scale calculations with bypass (right); Test with initial temperature 700°C, particle diameter 4mm and liquid injection flow 5m/h

Table 6.3: Comparison of quench front velocities

Dp- particle diameter, v_inj- water injection flow (lower plenum)	Quench front velocity [mm/s]		
	Experimental results	Calculations	
	PRELUDE	**Large scale + bypass**	**Large scale - no bypass**
T=400°C Dp=2mm V_inj=10m/h	2.6-3.71	1.6-4.7	3.1
	PRELUDE	**Large scale + bypass**	**Large scale - no bypass**
T=700°C Dp=4mm V_inj=5m/h	1.39-1.87	1.2-1.6	3.0-3.2

6.1.2.2 Effect of bypass

As it was already mentioned, in the large scale calculations a bypass formed with 2cm particles and porosity 0.5 was simulated. The thickness of the bypass region at each side was 29.5cm. The quench front velocity was observed to be higher in this bypass region. The different velocity of water progression in the center (low permeability) and in the outer ring (high permeability) results from a balance of pressure gradients and the fact that the permeability and passability (pressure drop coefficients) are much larger in the center than at the periphery. On Figure 6.6 we can see that in the calculations with bypass, the resulting pressure gradient through the bed is significantly reduced.

Moreover, the faster progression of water in the outer ring observed in the large-scale calculations affects also the steam production. In the large-scale calculation, after reflooding and quenching of the outer ring, the steam production reduces because of condensation at the top of the bed. The steam is produced then as a result of quenching of the central zone. As a result, the conversion factor (see discussion in Chapter 2, Section 2.5.3.2) between the water injection flow and the produced steam flow cannot be directly transposed from small-scale experiment to large-scale calculations with bypass. After quenching of the bypass region, the conversion factor reaches lower values compared to PRELUDE.

In the large scale calculations we observed that water appears at the top of the debris bed before the bed is fully quenched. The same phenomena were observed in a few PRELUDE experiments. However, in 2D calculations this effect is more obvious. It can happen when the pressure gradient generated by the steam flow during reflooding becomes larger than 3 times the hydrostatic pressure gradient in the water column, which causes liquid to progress faster in the regions of high steam velocity (see Chapter 2).

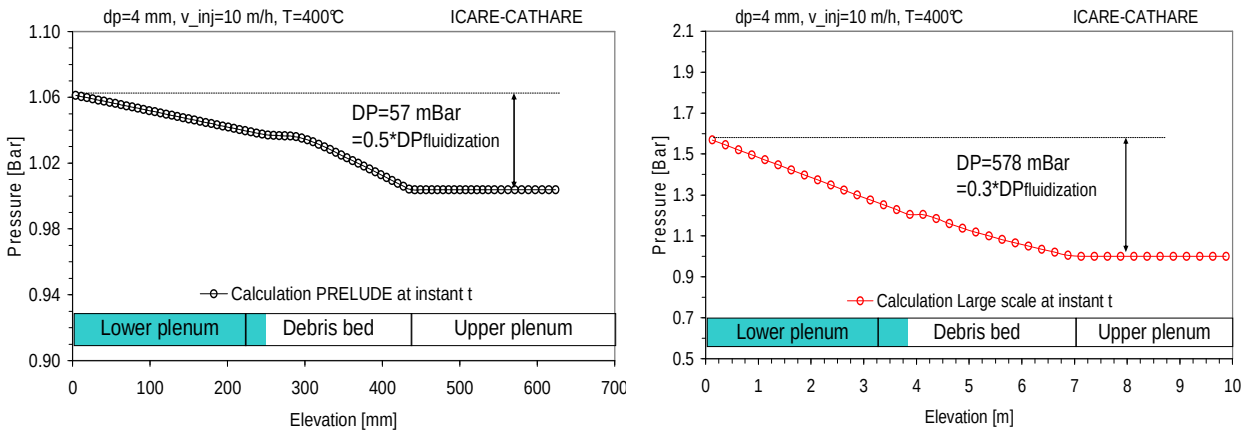

Figure 6.6: Axial pressure profile during reflood. PRELUDE '1D' calculation with initial temperature 400°C, particle diameter **4**mm and liquid injection flow 10m/h (left). Large scale calculations (right)

6.1.2.3 Effect of local heterogeneities

The calculations summarized in this section are complementary. Such geometry was not studied in the PRELUDE small scale experiment. However, in a reactor case, less porous zones might be created in the core during the core degradation. Thus, two calculations were made. The cylindrical zone with porosity 0.2, diameter 0.9m and height 1m was placed in the debris bed core (3.29x3.75m). Firstly, the zone was located in the center, secondly in the upper part of the bed (see Figure 6.7). The quench front velocities and the temperature profiles are shown in Figure 6.7. It can be seen that the presence of the blockage at the center of the bed results in the formation of hot spot that cannot be cooled. However, the second case where the less porous zone is located at the upper part of the bed is coolable. Here, the quenching is made from both sides e.g. from the bottom as water progresses and also from top. The water appears at the top before the bed is fully quenched and improves the coolability. In conclusion, even if there is a presence of local less porous zones in the reactor core, it may be coolable, depending on its position in the core. It is more favorable when the zone is located at the upper part of the core where top flooding can contribute to the reflooding process.

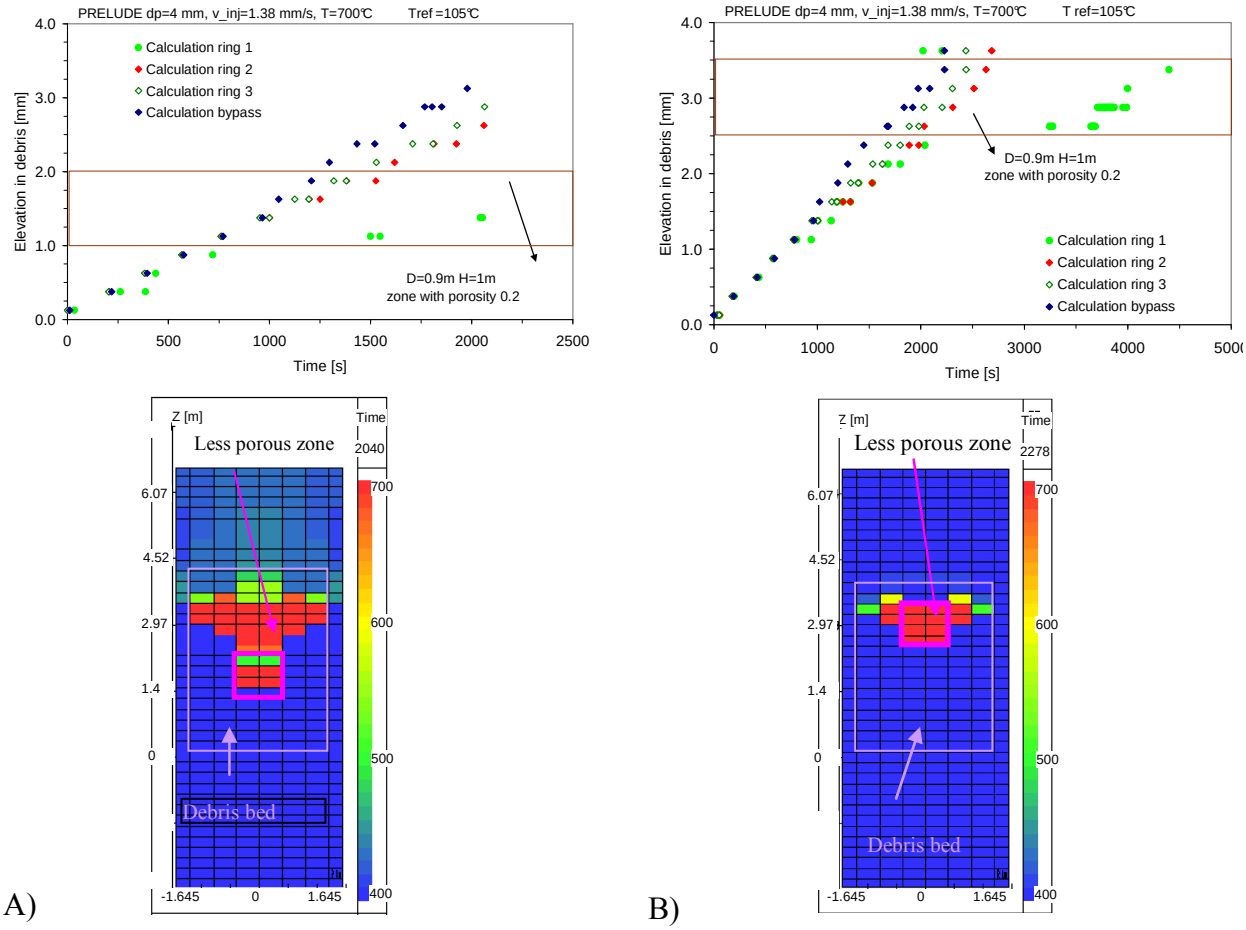

Figure 6.7: Large scale calculations with local less porous zone. Initial temperature 700°C, particle diameter 4mm, water injection flow 10m/h. Quench front progression and temperature profile, not coolable case A) and coolable case B)

6.1.2.4 Effect of pressure

A sensitivity study has been performed with different pressures (from 1 to 100 bars). The progression of the change in debris bed quenching time is plotted in Figure 6.8. Increasing the pressure from 1 to ~50 bars leads to a significant decrease of the reflooding time. These results are consistent with experimental observations [Reed85]. It was actually observed that increasing the pressure from 1 to 50 bars enhances coolability due to the increased density of the steam. The produced steam fills up less volume fraction, leaving more volume for the liquid and therefore more exchange surface between the liquid and the particles. Above 50 bars, the decrease of the latent heat plays a counteracting role and above 70 bars it becomes dominant leading to a reduction of coolability. The previous model [Bechaud01] did not predict these phenomena. In previous calculations [Coindreau09b], the steam production was not significantly affected by the pressure and remained almost the same for the different numerical simulations. In calculations using the new model presented in this thesis, the counteracting effect for high pressures is also obvious (see Figure 6.8).

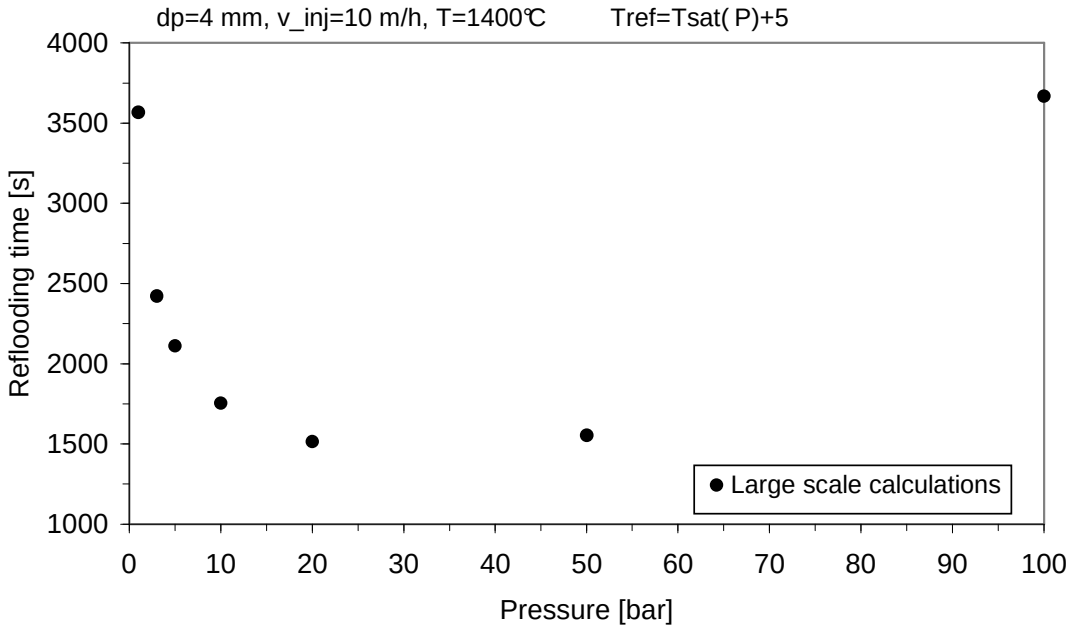

Figure 6.8: Pressure effect on reflooding time. Large scale calculations with initial temperature 1400°C, particle diameter 4mm and water injection flow 10m/h.

6.2 CALCULATIONS WITH RESIDUAL POWER

In the previous section we compared the PRELUDE small scale experimental results with large scale calculation results. It appeared that the scale has a negligible effect on the quench front velocity. It means that the quench front velocity measured in small-scale experiments is relevant also for reactor-scale geometry. These calculations were made for the equivalent initial temperature before reflood, i.e., Large scale versus PRELUDE. In order to reach the same temperatures, it was necessary to set the residual power to zero when the water injection started in large scale calculations. However, in a reactor core, the decay heat impacts the temperature distribution during the whole quenching process. Thus, in this paragraph we will discuss the effect of residual power. In order to study the effect of residual power, different large scale calculations with maintained power during reflood were performed (see Table 6.4). The objective of the Exercise A and B was to study the effect of debris bed redistribution. The mass of debris bed in both exercises was 40 ton, but the diameter and height of debris bed were modified. Finally, the Exercise C was performed with 18 ton of debris bed and different liquid flows. The objective was to show what the coolability limits for this bed are if the power is maintained during reflood.

Table 6.4: Calculation exercises for Large scale geometry with maintained power

Test	Power maintained	Particle diameter	Liquid flow	Mass of debris
Exercise A	yes	4mm	10m/h	40 ton H=3.75m ϕ=1.7m
Exercise B	yes	4mm	10m/h	40 ton H=1.75m ϕ=2.45m
Exercise C	yes	4mm	5, 10, 50, 100 and 200 m/h	18 ton H=3.75m ϕ=1.15m

6.2.1 Effect of debris bed position

The objective was to study the effect of debris bed position on reflooding. In a reactor core, the amount of debris bed and its localisation depends on the accident scenario. In this paragraph, we thus simulated two cases, both with 40 tons of debris bed. The rest of the core was formed with 2cm non heating particles with porosity 0.5. In the first calculations, the debris bed zone with diameter 1.7m and height 3.75m was simulated (Figure 6.9 left). The second case corresponds to a debris bed zone with diameter 2.45m and height 1.75m (Figure 6.9 right). The mass of debris bed in both cases was the same, i.e., 40 tons. In both cases the debris beds was heated up to 1100°C and than the water injection started (see Figure 6.10). Compared to the previous calculations, the power 200W/kg was kept constant after water injection. In the lower plenum, the water progresses with velocity 2.77 mm/s. After the contact with hot debris bed, the water velocity decreases. The typical quench front velocity observed in these calculations was about 0.4-0.5mm/s that represents less than 10% of the initial water velocity (see Figure 6.11).

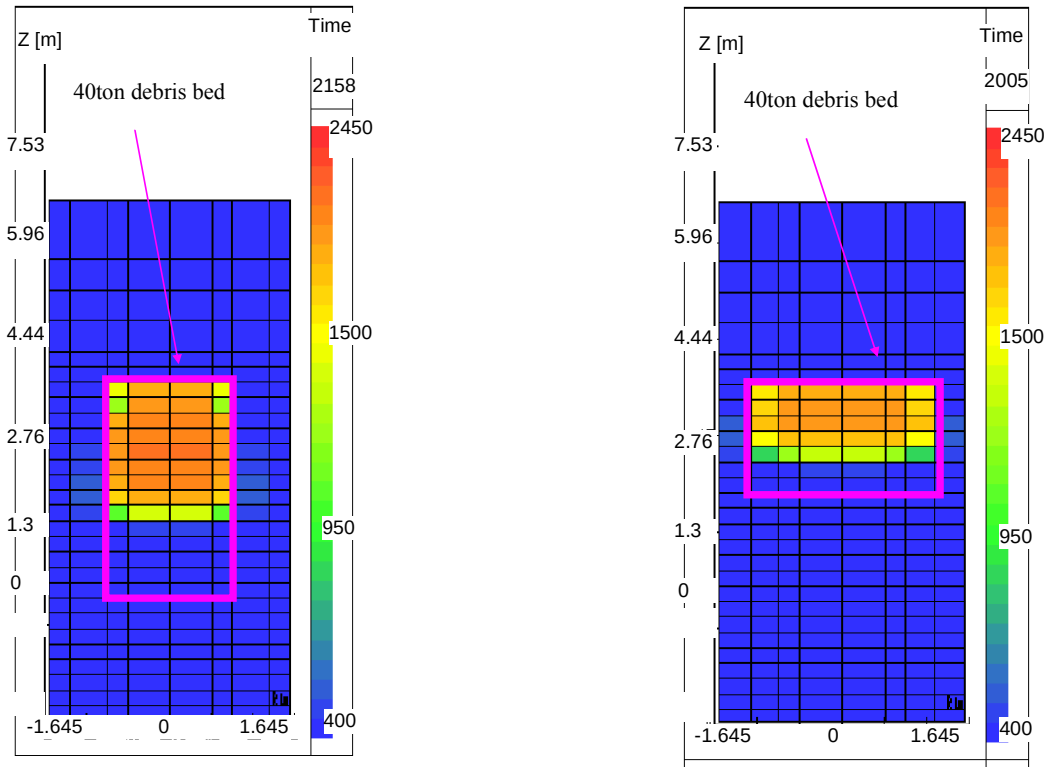

Debris bed: H=3.75m Φ=1.7m Debris bed: H=1.75m Φ=2.45m

Figure 6.9: Position of debris bed in the core. Exercise A (left) and Exercise B (right) with 40 ton of debris bed

In the first case, the debris bed height was 3.75m so it would take about 2 hours in the ideal case to quench this debris bed height. The ideal case means that the initial debris bed temperature is homogeneous over the bed, i.e., about 1100°C. However, due to the effect of residual power, the initial temperature of the bed increases with time downstream of the quench front (Figure 6.10). Consequently, the quench front progression is not quasi-steady but decreases slowly (Figure 6.11 left). It results in 66% of the debris bed height that is quenched, and about 8 tons of debris bed that reach the temperature 2500°C. This corresponds to the fusion temperature in the reactor core so the quenching was not successful in the whole bed. In the second case, the debris bed height was 1.75m situated at the upper part of the core. In order to guarantee the debris bed mass 40ton, the diameter of the debris bed zone increased almost two times. At the beginning, the water reaches the debris bed elevation very quickly, in about 6 minutes resulting from the single phase flow. Then, water progression decreases to 0.4mm/s (Figure 6.11 right). In the ideal case, it will take about 1 hour to quench the debris bed with height 1.75m. In this case, the maximum debris bed reached about 2000°C and the total bed height could be successfully quenched in about one and half hour (Figure 6.11 right).

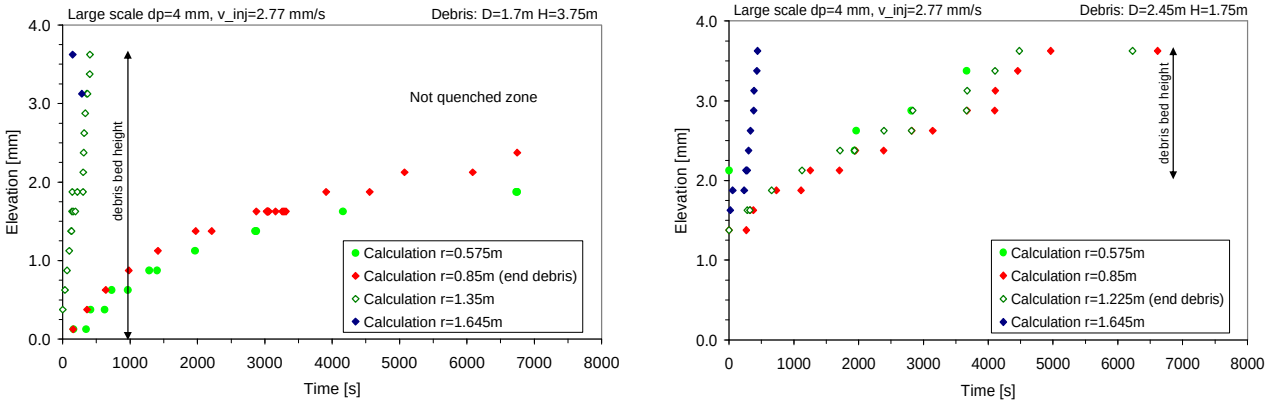

Exercise A Exercise B

Figure 6.10: Quench front velocity. Not coolable case (left) and coolable case (right)

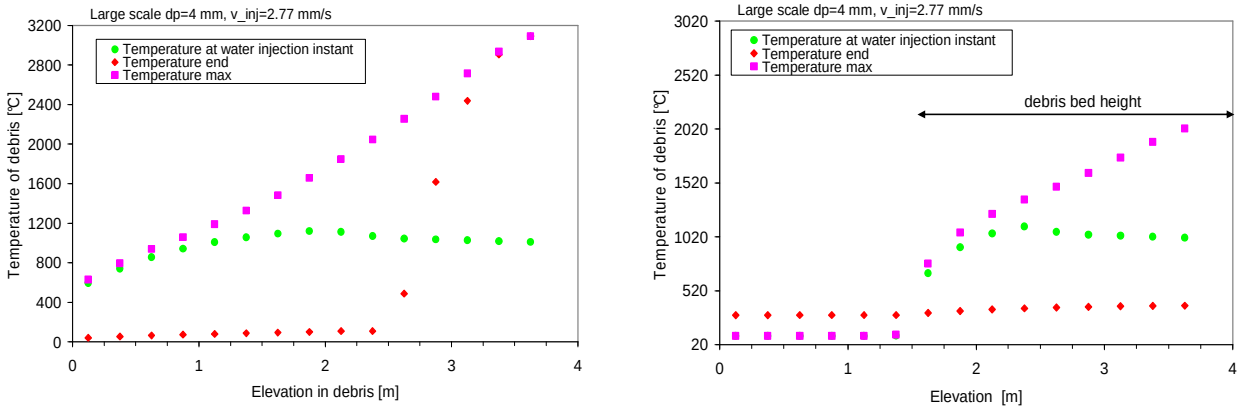

Exercise A Exercise B

Figure 6.11: Axial temperature evolution in the debris bed at the instant of the quenching, during the quenching and at the end.

6.2.2 Effect of water injection velocity

A sensitivity study has been performed with different inlet liquid velocities (from 5 to 200m/h). The objective was to study the effect on reflooding time. Here, we simulated 18 tons of debris bed. The diameter of debris bed zone was 1.7m and height 3.75m. The rest of the core was formed non heated particles with porosity 0.5 and higher permeability. In all cases the debris bed was heated up to ~1000°C and then water injection started. The time needed to fill-up the lower plenum was recalculated for different liquid flows. The instant of water injection was adjusted so water reached the first elevation of heated debris bed at the same instant. The axial temperature distribution in the bed is the same at this instant and can be seen in Figure 6.12 (left).

In these calculations, the power 200W/kg was kept constant after water injection. In the lower plenum, the water progresses with velocity between 5 to 200m/h depending on the simulation exercise. After the contact with hot debris bed, the water progression velocity decreases. The typical quench front velocity observed in these calculations was between 2.61m/h (v_inj=5m/h, v_pore=12.5m/h) to 12.96m/h (v_inj=200m/h, v_pore=500m/h) as is summarized in Figure 6.13. This represents always between 3-20% of the initial water velocity. The debris bed height was 3.75m so it would take between 1.5hour (v_inj=5m/h) to 30minutes (v_inj=200m/h) in the ideal cases to quench this debris bed height. The ideal case means that the initial debris bed temperature is homogeneous over the bed, i.e., about 1000°C. However, due to the effect of residual power, the initial temperature of the bed increases with time downstream of the quench front (see Figure 6.12 right). In the case of lower water injection velocity (5-10m/h), the debris bed temperature reaches 2000°C during quenching due to the effect of residual power. Moreover, in those cases the quench front is not quasi-steady but decreases slowly due to the effect of residual power (Figure 6.13). If the water injection velocity increased (> 50m/h), the effect of residual power on initial temperature seems negligible (Figure 6.12).

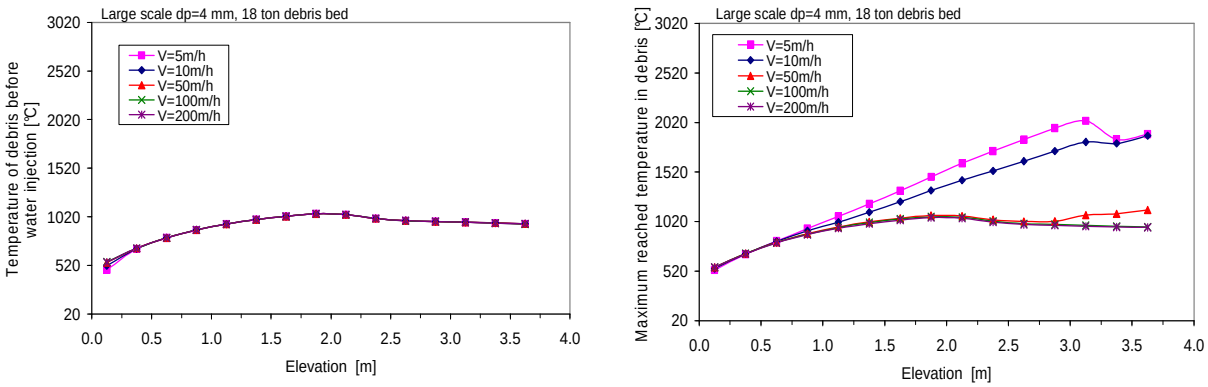

Figure 6.12: Axial temperature profile in the bed. Left- before water injection, Right-maximum reached during quenching

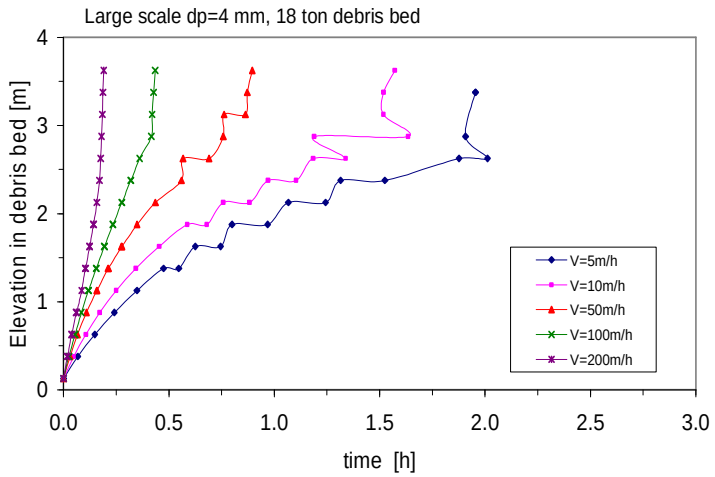

V_inj (lower plenum)	**V_inj** (in pores)	**V_qf** (at the beginning)
5m/h	12.5m/h	2.61m/h
10m/h	25m/h	2.94m/h
50m/h	125m/h	4.57m/h
100m/h	250m/h	6.78m/h
200m/h	500m/h	12.96m/h

Figure 6.13: Quench front velocity for different injection velocities.

We can also plot the reflooding time as a function of water injection velocity. In Figure 6.14 we can see that the time of reflood decreases as the water injection velocity increases. In our simulations we did not observe an asymptotic for this tendency and it seems to go to zero for very large injection velocities. For reactor applications, the limiting safety criterion should also depend on the generated pressure increase. This was not discussed here because the whole primary circuit was not modelled.

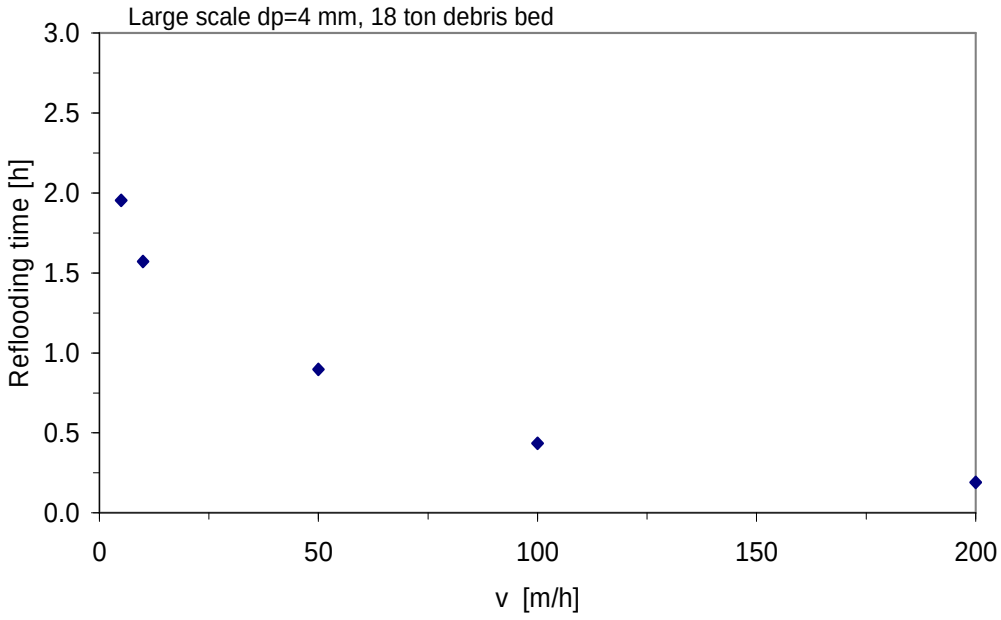

Figure 6.14: Reflooding time as a function of injection velocity.

6.3 CONCLUSIONS

In this Chapter we provided the first analysis of application of the model to reactor scale debris bed. The main objective was to identify the processes which could be different at a large scale. The calculations were realized for a "reactor vessel" with diameter 3.29m and height 10m. The debris bed was situated in the core, the debris bed diameter and height varied depending on the simulation. A special attention was paid to the presence of lateral bypass. For simplicity of calculation, the outer ring, which is supposed to be filled with almost intact rods, is formed with particles with larger diameter and porosity, 2cm and 0.5 respectively.

Firstly, all the characteristic features (except the size) of the larger debris bed were identical to PRELUDE case: debris material steel and initial temperature corresponded to the test conditions. The objective was to compare the results with the PRELUDE small scale experimental results,. In order to keep the condition of initial temperature all along the whole reflooding, the *volumetric power* during reflooding in these calculations was *set to zero*. The important conclusion from these simulations is that the *scale has no effect on quench front velocity if volumetric power can be neglected*. Moreover, the faster water progression through the bypass did not influence strongly the quench front velocity in the debris bed. Thus, the quench front progression was observed to be quasi-steady with the same velocity as in PRELUDE. However, in the calculations with bypass, the resulting pressure gradient through the bed was significantly reduced compared to small scale PRELUDE experiments. Neither the fluidization limits nor the conversion factor between the injected water and produced steam can be transposed from small scale PRELUDE to large scale geometry when the bypass is present.

It is important to note that the previous conclusions on quench front progression did not include the *effect of initial temperature*. Thus, additional calculations were performed also with *maintained power during reflood* which is the realistic situation in reactor case. It was concluded that the maintained power, i.e. 200W/kg representative of reactor case, impacts the initial bed temperature. In case of *low water injection flow (<50m/h)* and reactor core height of a few meters, the initial temperature at the upper part of the bed can significantly increase. Consequently, as the quench front progresses the quench front velocity decreases and is *no more quasi-steady*. In conclusion, the analysis of small scale PRELUDE experimental results based on quasi-steady quench front progression may not be valid at the reactor scale when the effects of residual power are not negligible.

Finally, the interest was to identify the physical parameters that are favorable and increase the efficiency of reflood. The effects of pressure and water injection velocity were studied. The calculations were performed with different pressures (from 1 to 100 bar). It was concluded that increasing the pressure from 1 to ~50 bar leads to a significant *decrease of the reflooding time*. The most of the gain in efficiency is obtained even for 10 bar. On the other hand, *above 50 bar*, the decrease of reflooding time is *less obvious* and above 70 bars it increases. It was

observed, that depressurization of primary circuit has a positive impact in a case of reflood. Although it is a standard accident procedure to decrease the primary pressure, it appears that simple increase up to 10 bar would greatly enhance the efficiency of reflooding. However, the best hydrodynamic conditions are reached for pressures below 50bars. Concerning the *water injection velocity*, no optimum value could not be found. It was shown that any *increase in water injection velocity* (in the range 5-200m/h) leads to *decreasing the time of reflood*. The important conclusion is that the water injection flow has an important *impact on bed maximum temperature, in particular in the upper part*. If the water progression is slow, it results in increased bed temperature due to the residual power. In case of water injection velocity of 5m/h, the debris bed temperature increased two times from its initial temperature, e.g. from 1000°C to 2000°C. It was concluded, that if the *water injection is above 50m/h*, the effect of the *residual power* on the debris bed temperature starts to be *negligible.*

The last point concerns the effect of debris bed geometry and heterogeneities on coolability limits. Different coolable and non coolable situations were simulated. It was concluded that the *debris bed height* is very important. In a case of high debris bed with "small" diameter, high temperatures are reached in the upper part. On the other hand, in case of a low height debris bed with large diameter, the coolability is favored. Concerning the *local heterogeneities* it was concluded that even if local less porous zones are present in the reactor core, they may be coolable, depending on their position in the core. It is more favorable when such zone is located at the upper part of the core where top flooding can also contribute to the reflooding process.

7. GENERAL CONCLUSION AND PERSPECTIVE

This thesis dealt with the reflooding (injection of water) of severely damaged reactor core as a severe accident management scenario. The general issue of severe accidents with core degradation was introduced. The current R&D objectives are to have detailed and validated models that will be able to evaluate the realistic consequences of reflooding at any stage of core degradation i.e. intact or partially degraded fuel rods, debris bed or molten pool. This thesis was dedicated to the reflood of debris beds which correspond to damaged core geometry where the nuclear fuel has collapsed into a bed of small particles, constituting a porous medium.

The coolability of a debris bed is one of the major objectives of severe accident researches. The debris bed configuration and associated complicated heat transfer regimes were studied worldwide in the past 30 years. The bibliographic study of international experimental programs was summarized in the Chapter 2, taking into account dry-out tests (SILFIDE, STYX, POMECO, DEBRIS and PETIT), top reflood tests (Ginsberg, Dhir, DEBRIS) and bottom reflood tests (Tutu, DEBRIS and PRELUDE). Two sources of information were used for more detailed analyses: PETIT dry-out experiment and PRELUDE experimental program. The PRELUDE experiment (made in IRSN) allowed to measure quench front propagation and steam production during water injection from the bottom. A series of experiments performed in 2010-2012 at the PRELUDE facility has provided a large amount of new data that were summarized. On the basis of those experimental results, the thermal hydraulic features of the quench front have been analysed and the intensity of heat transfers was estimated. It was shown that a quasi steady progression of the quench front was established in most of the tests. The velocity of the quench front is proportional to the water injection velocity. The proportionality factor depends on the initial temperature of particles and on the particle diameter. Also multi-dimensional effects during reflood i.e. quench front instabilities were studied and the criterion for a transition between stable/non stable quench front progression were proposed. An experimental criterion for the stability of the quench front seems to be if the pressure gradient created by the steam flow downstream of the quench front is lower than $2.8\rho_l g$. Correlations for other important parameters could be drawn e.g. steam production, pressure increase or heat transfer layer length. The results are presented in Chapter 2.

In Chapter 3, the macroscopic model for two-phase flow with phase change in porous media was presented. It was shown that the current theoretical attempts are to obtain macro-scale models, in particular through the use of a volume averaging theory. The present work started from a generalized three-equation model for the macroscopic description of the two-phase flow heat and mass transfer in porous medium that was introduced in Duval's Doctoral thesis [Duval02]. The model is based on a pore-scale quasi-static assumption for the momentum equation closure i.e., the interfaces do not change rapidly in comparison with viscous dissipation. It was stated that this condition may break down in the case of intense boiling and

an alternative approach was developed. We have shown in Chapter 3 that it is formally possible to represent the dynamic processes involved in the nucleate, or film boiling, in the case of a porous medium problem, by the addition of a separate set of closure relations which deal essentially with the solid temperature deviation and its gradient at the surface of the particles. The resulting heat transfer terms are obtained by superimposing the solutions coming from the 1st order linear problem (Duval's model) and from the non-linear one (additional closure relations). Moreover, we introduced two factors that can limit the intensity of phase change. Firstly the size and number of bubbles that are formed limits the contact surface for water. Secondly, in the regime of film boiling, there is no direct contact of water with particles. The analysis of tests with large liquid flow rate showed that the contact of water with heated surface starts at higher temperatures than the Leindenfrost temperature mentioned in different litterature. Thus, an alternative transition criterion was proposed and is based on heat transfer layer length that was analyzed from experimental results in Chapter 2.

In the Chapter 4 a numerical implementation of the improved macroscopic model for reflood of debris bed geometry was introduced. The objective was to provide a detailed model, that could be validated with experimental results but would be also able to evaluate the realistic consequences of reflooding of a debris bed. The two-phase flow reflood of debris bed model was implemented into ICARE-CATHARE V2 code. The characteristics of this computer code were summarized in the Chapter 4. We found benefits in numerical implementation of the model into an existing code used for severe accident analysis. The code has already numerical solvers adapted to two-phase flow models and it includes some useful and validated correlations that could be used for the developed model. In addition, the meshing is 2D (or even 3D), which was necessary for the prediction of multidimensional effects, as observed in experiments. The first implementation of model of Duval (2002) into ICARE-CATHARE code was performed before the thesis, in 2001. Because of lack of heat transfer coefficients for a regimes of intense boiling in this first model, the heat flux transferred from the solid were underestimated that resulted in slow progression of quench front compared to experimental data. After the work done in this thesis, the heat transfer relations in ICARE-CATHARE are now described in terms of a unique boiling curve from which the code selects the appropriate heat transfer coefficients for both phases (vapor/liquid). The boiling regimes as well as the transition criteria were summarized in the Chapter 4. In addition, alternative formulations for the relative permeabilities and passabilities were implemented and tested.

The confrontation of calculated results with the experimental result was presented in Chapter 5. The criteria of validation include the effect of mesh size and the quantification of code accuracy (i.e. evaluation of the uncertainty range and comparison with experimental uncertainties). Firstly, a validation of the model with PETIT experimental results was presented. These boiling experiments in porous medium were performed during a doctoral thesis of F. Petit in 1998 at ENSAM in Bordeaux, France. The objective of the validation was to evaluate the regimes of convection with water, nucleate boiling and convection with steam in a porous medium with internal source i.e. liquid single-phase flow, two-phase flow and

gas-single phase flow. Firstly, calculations concerning the increase of temperature up to nucleate boiling regime were presented. The quantitative validation of volumetric heat transfer coefficients used in our model was performed. In the proposed theoretical model, the heat exchange coefficients obtained for the simple stratified Unit Cell was recommended to be multiplied by factor 9. However, in further studies, this somehow heuristic approach could be improved by solving the proposed "closure problems" on more realistic geometry. Also the calculations were performed for different liquid flow rates and the dry zone elevation was identified for each test. The analysis concerning the incipience of dry-out gave us only an indication about *the relevance and good physical behaviour* of the model. Because of lack of instantaneous power records, it was not possible to draw quantitative conclusions.

Finally, the ICARE-CATHARE V2.3 calculation results were compared with the first PRELUDE experimental results performed at IRSN in 2009-2012. The analyses concerned 17 tests. Firstly, the ICARE-CATHARE reflood calculations were performed for PRELUDE "1D" tests with initial debris bed temperature at 400°C. Secondly, the calculations were performed for PRELUDE "1D" tests with the initial debris bed temperature at 700°C. In order to observe these effects in these calculations, five radial meshes were modeled. Finally, the calculations were performed for PRELUDE "2D" bottom reflood test with initial temperature 700°C and liquid injection flow 5m/h (1.38mm/s), with a lateral "bypass".

Comparisons of temperature evolutions at different elevations show that the model is able to predict quenching velocity for different inlet flow rates and different particle diameters, in the whole range covered by PRELUDE experiments. The steam flow rate and the pressure difference across the debris bed are also well predicted which indicates that the model behaves consistently. The discrepancies were observed for tests with 1mm particles. It was concluded that the calculations with multi radial meshing gives better results. Here, the difference in quench front velocity between the calculation results and experimental results decreased, e.g. from 43% to 29% and for other tests, it was always below 35%. Moreover, calculations of tests with initial temperature 700°C showed that the transition criterion defined in Chapter 4 predicts well the switch between the "pre-cooling" regime and fast quenching. Finally, the calculations of PRELUDE "2D" test with lateral bypass are presented. The interesting conclusion is that the quench front velocity observed in these calculations is the same as in PRELUDE "1D". This means that the bypass did not influence the front progression in the centre. However, the different velocity of water progression in the center (low permeability) and in the outer ring (high permeability) results from a balance of pressure gradients and the fact that the permeability and passability (pressure drop coefficients) are much larger in the center than at the periphery. This will be discussed in Chapter 6 because the bypass plays an important role in reactor case.

In order to complete the validation, sensitivity studies were also performed to identify the physical parameters which have the strongest influence on the calculation results. The impact of model as well as physical parameters (user-defined) was tested. The results are summarized in Appendix A and B. It was concluded that the most important user-defined parameters are the porosity and initial temperature of the bed before reflood. It is recommended, in validation calculations, to verify precisely the initial bed temperatures and to test the effect of porosity

near the wall on calculation results. In Appendix A we concluded that the model parameters (with the new model), are less important and the proposed correlations predict well the general trends.

In the Chapter 6 we provided the first analysis of application of the model to reactor scale debris bed. The main objective was to identify the processes which could be different at a large scale as well as to identify the parameters that have favorable impact on reflooding in a real reactor case. Firstly, the large scale calculations showed that the scale has no effect on quench front velocity as long as residual power remains negligible (fast reflooding cases). On the other hand, the fluidization limits or the steam conversion factor cannot be transposed especially when a bypass is present. Secondly, the effect of residual power was analysed. In case of *low water injection flow (<50m/h)* and reactor core height of a few meters, the initial temperature at the upper part of the bed can significantly increase. Consequently, as the quench front progresses the quench front velocity decreases and is *no more quasi-steady*. Above 50m/h, the effect is negligible. It was also an interest to identify the physical parameters that are favorable and increase the efficiency of reflood. It was concluded that although it is a standard accident procedure to decrease the primary pressure, it appears that simple increase up to 10 bar would greatly enhance the efficiency of reflooding. Concerning the water injection velocity, no optimum value could be found. It was shown that any *increase in water injection velocity* (in the range 5-200m/h) leads to *decreasing the time of reflood*. The important conclusion is that the water injection flow has an *impact on bed maximum temperature, in particular in the upper part*. If the water progression is slow, it results in increased bed temperature due to the residual power. If the *water injection is above 50m/h*, the effect of the *residual power* on the debris bed temperature is *negligible.*

With respect to model improvements, we can mention three important topics that could be developed in the future. Firstly, the studies of pressure losses for each phase (Darcy equations) in the conditions typical for reflood and debris bed geometry should be studied in order to properly estimate the transport of water. This would help to reduce the uncertainty associated to the "heat transfer length" correlation (which was introduced because of the apparently excessive transport of water downstream of the quench front). Secondly, the issue of unsteady heat conduction may be important in a case of reactor applications where the conductivity of UO2 is low (<5W/mK). The discussion was introduced in this thesis and the non-uniform temperature in a particle was theoretically studied. However, the numeric implementation was not made because the validation concerned steel particles where the temperature was quickly uniform during reflood. Finally, the study of the impact of the repartition of phases on the heat transfer should be validated with relevant experiments where visual observations of the flow can be made at the same time as temperature measurement. We introduced simply a corrective function for the heat flux depending on void fraction. But more experimental studies are necessary. Such tests are ongoing at IMFT and could, eventually lead to relations between the heat flux and the void fraction.

7. CONCLUSION

Ce travail de thèse est motivé par un besoin industriel précis, à savoir l'étude du refroidissement d'un cœur de réacteur fortement dégradé dans le but de stopper la progression d'un accident. Dans ce contexte, l'objectif de l'IRSN est de développer un modèle détaillé dans le logiciel de calcul ICARE-CATHARE, permettant de simuler des écoulements multidimensionnels dans le cas de milieu poreux hétérogènes de type lit de débris.

Le premier volet de notre étude concerne l'étude des résultats des expériences réalisées dans le monde au cours des 30 dernières années. Les analyses approfondies ont concerné les essais d'assèchement (SILFIDE, STYX, POMECO, DEBRIS et PETIT), les essais de renoyage par le haut (Ginsberg, Dhir, DEBRIS) et les essais de renoyage pas le bas (Tutu, DEBRIS et PRELUDE). Deux sources de données ont été analysées en détail : PETIT et PRELUDE. PRELUDE a permis, entre autres, d'obtenir des données (notamment la vitesse de refroidissement des débris, la propagation du front, la production de vapeur et l'augmentation de pression) qui permettent de mieux comprendre la progression du front de trempe et l'intensité du transfert de chaleur. On a ainsi pu évaluer l'intensité maximale du flux de chaleur extrait des particules. On a aussi observé que, sous certaines conditions, le front de trempe n'est pas stable et que l'eau progresse plus rapidement dans certaines parties. Un critère caractérisant cette transition stable/instable a été proposé. Enfin, grâce au grand nombre d'essais réalisés, couvrant une large gamme de vitesse d'injection, de diamètre des particules et de température initiale, il a été possible de quantifier et de corréler certaines grandeurs à ces paramètres, ce qui est utile pour quantifier rapidement l'effet d'un renoyage.

Le deuxième volet de cette thèse concerne l'établissement du modèle macroscopique. Le nouveau modèle comporte plusieurs évolutions par rapport à celui proposé dans la thèse de Duval en 2002. Le changement d'échelle a été effectué dans le cadre d'un découplage, à l'échelle du pore, du problème des transferts de chaleur de celui de l'écoulement diphasique. Ce découplage s'appuie sur une hypothèse négligeant les effets associés aux mouvements rapides des interfaces. Nous avons montré que cette hypothèse est trop contraignante pour les problèmes d'ébullition intense. Ainsi, une amélioration du modèle a été proposée, consistant à ajouter un terme caractérisant la génération rapide de bulles à la surface des particules. De plus, on a introduit deux facteurs pouvant limiter l'intensité du changement de phase : d'une part la taille et le nombre de bulles formées qui limitent la surface de contact disponible pour l'eau et, d'autre part, la température des particules qui, lorsqu'elle dépasse la température de Leindenfrost, empêche le contact direct entre l'eau et les particules. Lorsque le débit de vapeur est très élevé, il semble que la vitesse du liquide dans le milieu poreux soit surestimée par le modèle. On a donc introduit, à partir des données expérimentales, une longueur caractéristique de la zone diphasique, afin de corriger cette lacune du modèle. Ce dernier point nécessitera plus d'études pour être résolu de façon plus rigoureuse et théorique par des modifications des lois de frottements pour chacune des phases.

Dans le Chapitre 5, la validation du modèle a été présentée. On rappelle qu'en 2009, le modèle n'était pas capable de bien calculer un renoyage et la progression du front de trempe.

Le travail de validation a été assez complexe et couvre les résultats d'essais PETIT (assèchement) et 17 essais PRELUDE (renoyage). La validation quantitative sur les données expérimentales est présentée au Chapitre 5 et a montré que le modèle fournit des résultats satisfaisants. Le modèle est capable de prédire la progression du renoyage dans le cœur, la production du vapeur et le pic de pression pour différents diamètres de particules et différents débits d'injection testés. Toutefois, on a pu constater quelques désaccords entre calculs et données expérimentales pour les essais avec des billes de 1mm. Ce point reste à étudier. Pour une température initiale supérieure à la température de Leidenfrost, on a constaté que le transport de la phase liquide est trop rapide dans le calcul mais cela n'affecte pas la vitesse du front de trempe. On peut donc considérer que le modèle proposé reproduit de façon satisfaisante l'historique de refroidissement des particules tout en évaluant bien le taux de changement de phase et le gradient de pression engendré au sein du milieu poreux par l'écoulement de la vapeur à grande vitesse.

Parmi les pistes d'amélioration de la modélisation on peut citer trois thèmes importants. D'une part, l'étude des frottements sur chacune des phases dans les conditions typiques d'un renoyage, à savoir, une très grande vitesse de la vapeur et une vitesse très faible de l'eau qui est quasiment à l'équilibre hydrostatique d'après les calculs actuels. Des études sont prévues à l'IRSN pour étudier ce point.

D'autre part, l'étude des cas où la conduction instationnaire peut jouer un rôle limitant sur le transfert de chaleur entre les particules et l'eau. Cela peut être le cas pour des particules d'UO2 dont la conductivité est faible (inférieure à 5 W/K/m2). Ce point n'a pas été abordé parce que tous les essais ayant servi à la validation faisaient intervenir des billes d'acier pour lesquelles on pouvait supposer la température quasi uniforme dans toute la bille.

Enfin, l'étude de l'impact de la répartition des phases sur les transferts de chaleur. Nous avons introduit une fonction correctrice du flux de chaleur dépendant du taux de vide mais celle-ci repose sur des arguments non justifiés par des observations expérimentales. Une étude expérimentale est actuellement en cours à l'IMFT pour visualiser la distribution des phases dans un milieu poreux modèle 2D dans lequel se produit une ébullition intense. Il devrait alors être possible de relier de manière plus fiable le flux de chaleur moyen au taux de vide moyen.

APPENDIX A

In the Chapters 3 and 4, it was indicated that alternative modeling options could be used for some particular physical processes. We have also presented several available correlations when no obvious choice could be made. In order to demonstrate that the proposed modeling is robust and not too dependent on a very accurate tuning of correlations or model parameters, we will present in this appendix various sensitivity studies. The analysis is made for the same set of experimental results which were used in Chapter 5 for validation.
After identifying the empirical parameters which cannot be evaluated from a theoretical approach, we proposed to limit the range of variation of those parameters, following the correlations from other macroscopic models as well as the analysis of experimental data, including new data obtained from the PRELUDE experimental facility.
The sensitivity calculations on **model parameters** are summarized in Table A. 1.

Table A. 1: Sensitivity studies on model parameters

	Reference	Alternative options
Reflood of debris bed model	New improved model	Previous model '01 [Bechaud01]
Critical heat flux	Groeneveld correlation [Guillard01]	2x, 5x, 10x increased Groeneveld heat flux
Film boiling regime	SGL coefficients [Duval02]	Bromley correlation [Guillard01]
Transition boiling regime	Exponent ξ in temperature function equal to 2. [Guillard01]	Exponent ξ in temperature function equal to 1 or 4.
Transition criterion	Heat transfer layer length	Minimum stable film temperature [Guillard01]
Heat transfer layer length	PRELUDE correlation [Chapter 2]	±40%
Relative permeability	Exponent n=5 [Reed82]	SLG and SGL combination [Duval02]

A.1 Reflood of debris bed model

The macroscopic two-phase flow porous medium model was developed by Duval [Duval02]. The first implementation of this model into ICARE-CATHARE code was realized before this thesis [Bechaud01]. In this model the heat transfer coefficients for SGL and SLG configurations were implemented (resulting from stratified Unit Cells) in the absence of

specific data for real systems. The regimes of intense heat fluxes, e.g., transition boiling and nucleated boiling regime, were dealt before this thesis by a combination of heat transfer coefficients according to void fraction and temperature. As it was already discussed in Chapter 4, the resulting heat flux was underestimated. The results for one PRELUDE test can are compared in Figure A. 1. We can see that the calculation results and also experimental results for one PRELUDE test. We can see that the previous model [Bechaud01] underestimate the progression of quench front. The difference is about 30%. Moreover, the previous model predicts also the water presence at the top of the bed before the bed is quenched. This phenomenon was not observed at this PRELUDE test. The actual model predicts better the quench front velocity. The quench front velocity is underestimated only about 10%, the heat transfers are not underestimated as before. In conclusion the previous model [Bechaud01] underestimated the quench front velocity, especially for tests where the water injection flow was important. Thus, additional development of the model that was realized in the frame of this thesis was important.

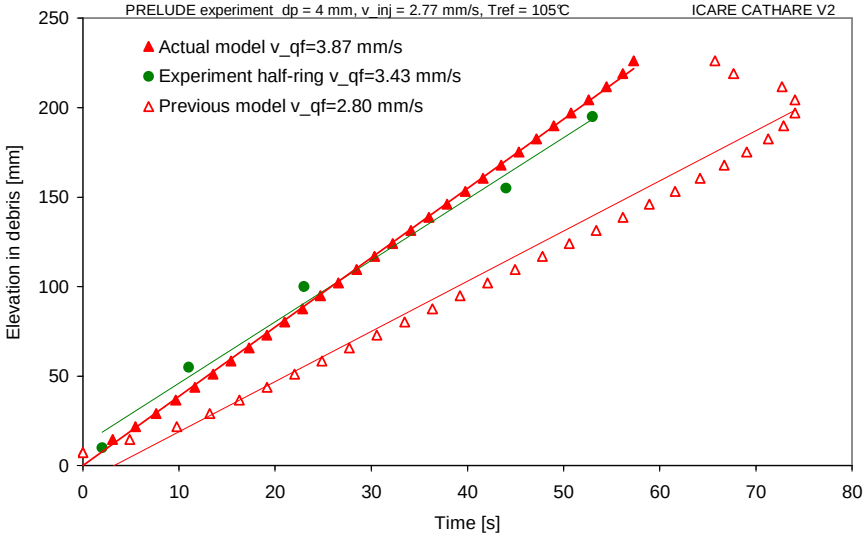

Figure A. 1: Quench front velocity predicted by previous model [Bechaud01] and new improved model presented in this thesis; PRELUDE '1D' with initial temperature 400°C, particle diameter 4mm and liquid injection flow 10m/h

A.2 Critical heat flux value

From the PRELUDE reflood experimental results, it is possible to determine the temperature where the maximum heat flux is reached. The method used to analyze the data was presented in Chapter 2 and identifies an interval of particle temperature where the maximum heat flux is registered. The analysis of experimental results show that the estimated maximum heat flux density transferred from particles to liquid during the nucleate boiling regime is significantly higher than the calculated maximum heat flux density (Figure A. 2).

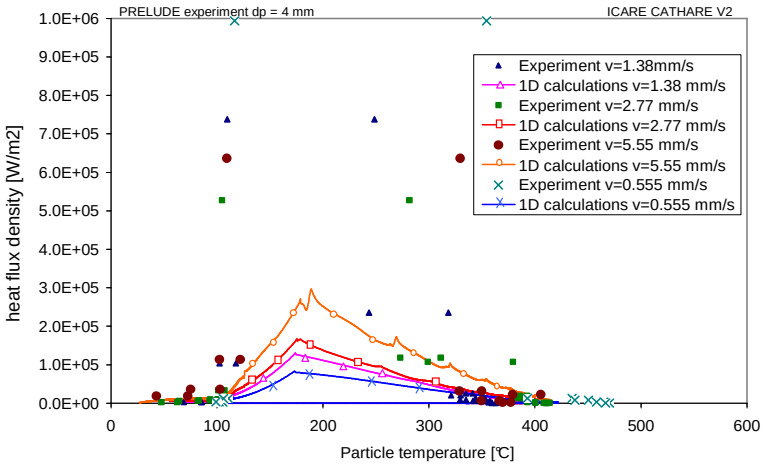

Figure A. 2: Calculated and measured transferred heat flux density during quenching, Tests PRELUDE '1D' with initial temperature 400°C, particle diameter 4mm and different liquid injection flow

This discrepancy may be explained by an underestimation of the model prediction but it must also be noted that the measured heat flux is a very local value corresponding to a single particle (or just a few neighboring particles) whereas the model calculates it over the mesh volume and implicitly assumes that the maximum heat flux does not affect all the particles in the mesh (through the corrective functions $f(\theta,\xi)$ and $g(\alpha)$, see Chapter 4). On Figure A. 3 (left) we can see that the void fraction in the mesh at the instant of critical heat flux, and on the right, we can see the recalculated heat flux density without applying the corrective function $g(\alpha)$.

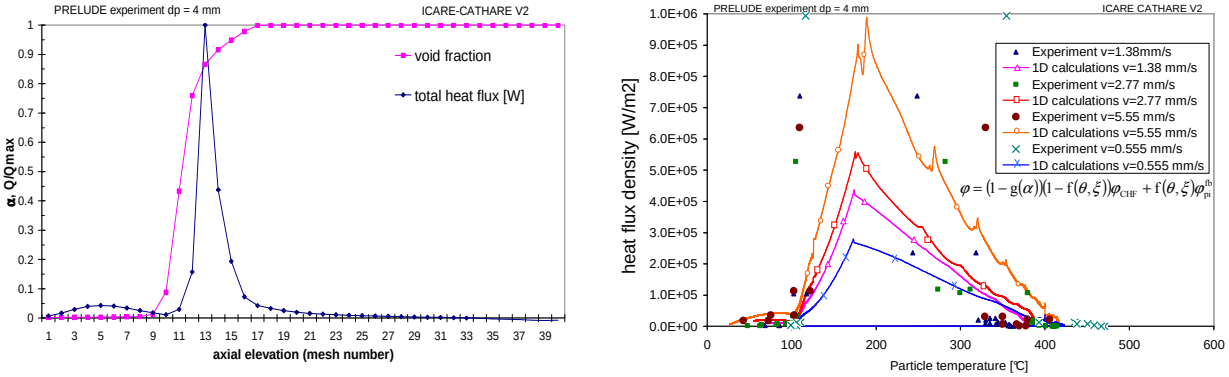

Figure A. 3: Void fraction at instant of critical heat flux (left) and recalculated "maximum local" heat flux density without corrective function g(α) (right)

Consequently, the model will always calculate lower heat flux values, especially if the meshing is not fine enough. However, the maximum heat flux density that is estimated with the present model is high enough (>10^5 W/m^2) to have a good prediction of the quenching time.

In order to check that such an apparent underestimation of local heat flux does not affect the total heat flux integrated over the whole quench front, a sensitivity analysis to the critical heat

flux (CHF) value was made. In Figure A. 4 we can see the effect of increase of CHF on calculation results. We can conclude that the maximum heat flux density that is estimated with the present model is high enough (>10^5 W/m^2) so the quenching time and steam production are well predicted. Increasing it does not change the quench front progression but it is important to mention that it changes the void fraction and temperature profiles across the front (not shown here). The profile becomes steeper with increasing CHF. The systematic analyses for other particle diameters were not performed. However, the general conclusion is that the critical heat flux values are already well estimated and higher heat fluxes do not influence significantly the calculation results.

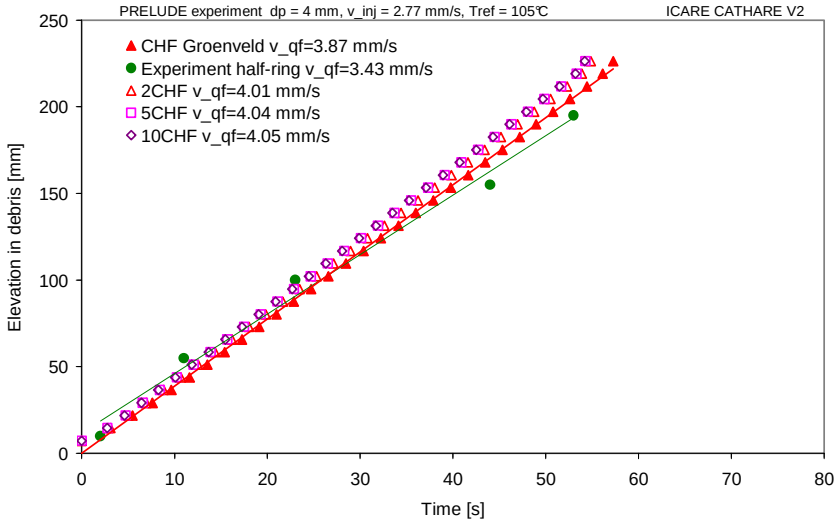

Figure A. 4: Effect of critical heat flux value on quench front velocity; PRELUDE '1D' with initial temperature 400°C, particle diameter 4mm and liquid injection flow 10m/h

A.3 Film boiling regime

The film boiling regime correlations implemented into the ICARE-CATHARE porous medium model were summarized in Chapter 4. In the standard ICARE-CATHARE code, Bromley's correlation is already implemented for describing film boiling regimes in channels. For a porous medium model, this correlation may be tested. On the other hand, we also consider that the SGL configuration [Duval02] is a sufficient approximation for the film boiling regime in porous medium because there is no intense boiling occurring in this regime and SGL heat transfers identified for a stratified Unit Cell are physically relevant. The comparison of these two correlations did not show any significant differences in either the quench front progression nor in the temperature evolution at the beginning of quenching (see Figure A. 5).

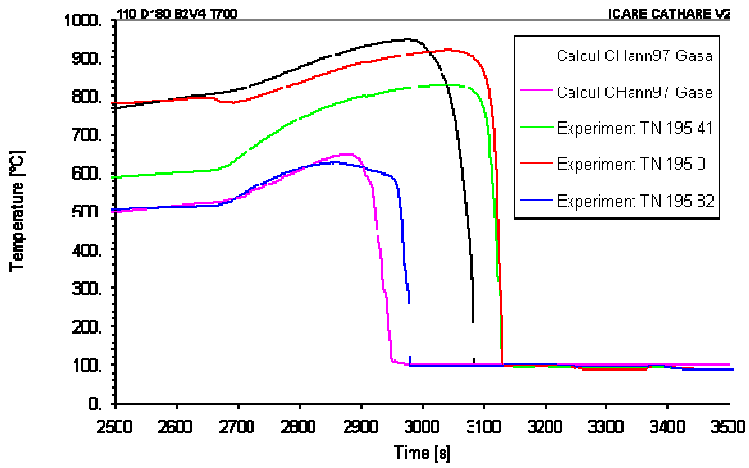

Bromley correlation [Guillard01]

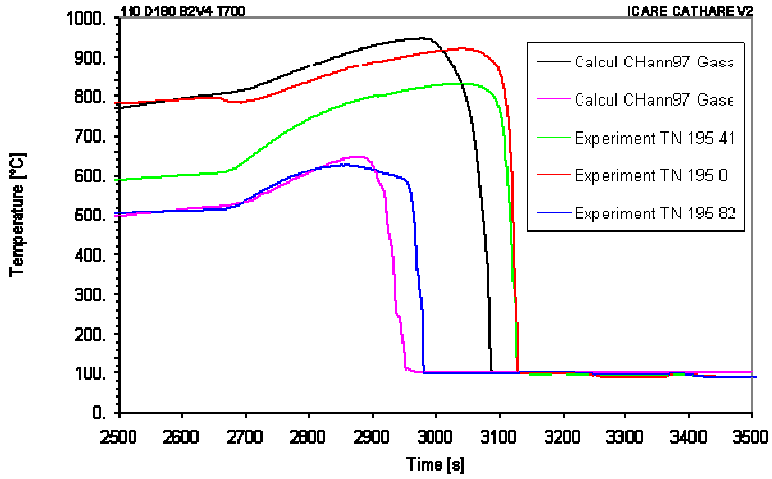

SGL coefficients [Duval02]

Figure A. 5: Comparison of temperature profile for two different correlations in film boiling regime; PRELUDE '1D' with initial temperature 700°C, particle diameter 2mm and liquid injection flow 2m/h

A.4 Transition boiling regime

In the transition boiling regime, the intensity of surface quenching of surface by water should depend also on its temperature. In the model for the transition zone described in Chapter 4, an empirical function $f(\theta,\xi)$ was applied with a temperature exponent ξ equal to 2 (see Figure A. 6), by analogy to correlations obtained for rod bundles. Moreover, we apply also a function of void fraction $g(\alpha)$ that evaluates the fraction of particles surface in contact with water. Consequently, by increasing the coefficient ξ, the heat flux value increases and thus the quench front progresses faster. However, the increased heat flux results in steam formation and more steam is present that reflects in function of void fraction. That is a reason

why in Figure A. 6 we can see that this parameter has only a small impact on quench front progression.

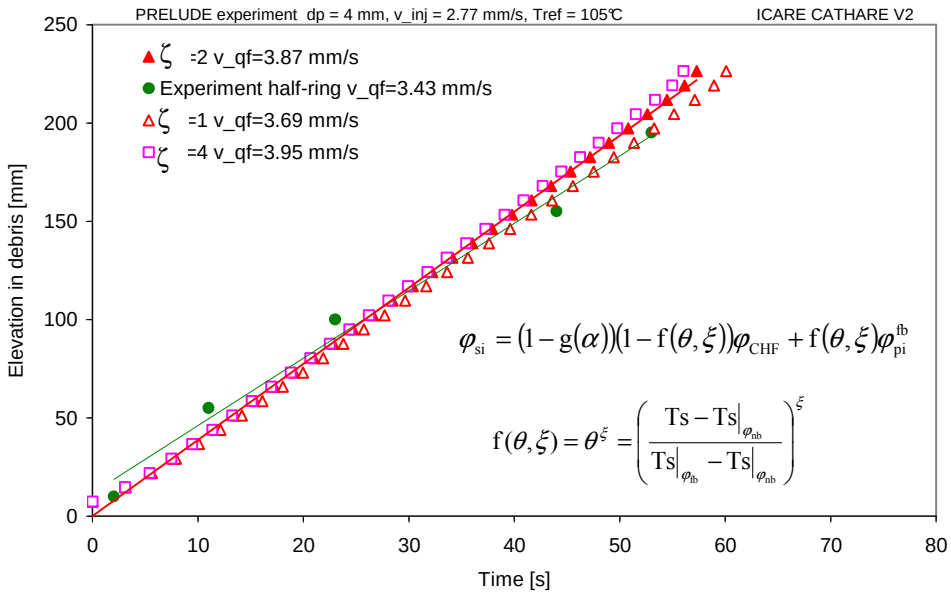

Figure A. 6: Effect of parameter ξ on quench front velocity; PRELUDE '1D' with initial temperature 400°C, particle diameter 4mm and liquid injection flow 10m/h

A.5 Transition temperature

The transition criterion identifies when a significant contact of water with hot solid surface starts i.e. film boiling regime switches to more intense transition boiling regime. In many models commonly used for channel flows, this criterion is associated to a minimum stable film temperature presented in Chapter 4. However, for atmospheric pressure, the minimum stable film temperature is predicted to be about 300°C. The visual analysis of temperature profiles during reflood at PRELUDE facility (see Chapter 2) indicated that the significant decrease and thus intense quenching starts at higher temperatures (see Figure A. 7). The first calculations were performed by setting the minimum stable film temperature equal to 400°C and the resulting temperature evolutions for two different elevations are shown in Figure A. 7. We can see, that the calculated temperature profile does not correspond well to experimental measurements. Firstly, the temperature decrease is linear and, secondly, at 400°C, intense quenching starts.

A significant improvement of the model was made in this area. We proposed a transition criterion depending on quench front position and heat transfer layer length. The method was explained in Chapter 4 and the correlation for heat transfer layer length was proposed by analyzing PRELUDE results (see Chapter 2). Applying this model, the resulting temperature evolutions are shown in Figure A. 7. We can see, that the temperature evolution during "pre-cooling" and the quenching are well predicted.

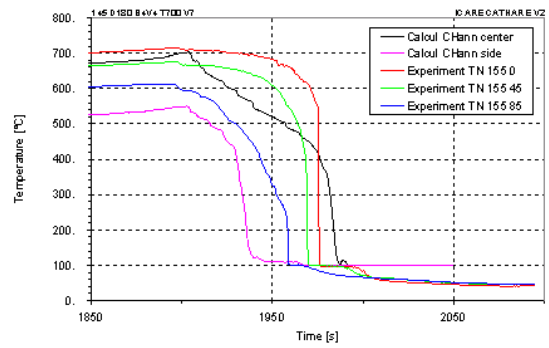

Elevation 155mm, Tmfs=400°C

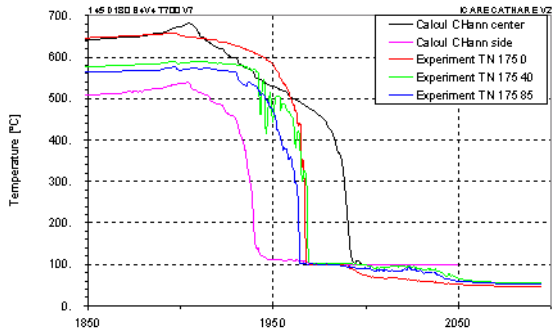

Elevation 175mm, Tmfs=400°C

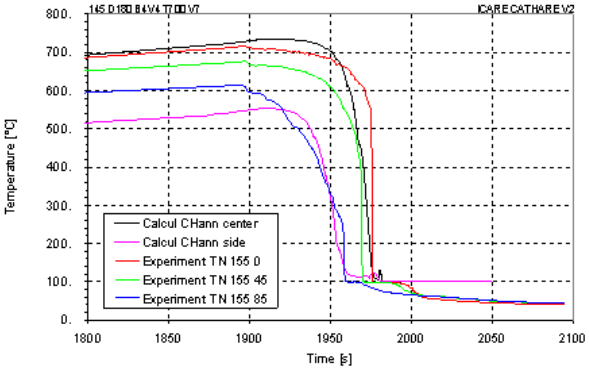

Elevation 155mm, L1 criterion

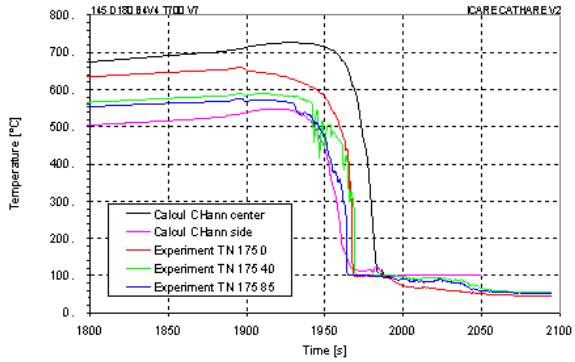

Elevation 175mm, L1 criterion

Figure A. 7: Comparison of temperature profile for two different transition criteria; PRELUDE '1D' with initial temperature 700°C, particle diameter 4mm and liquid injection flow 7m/h

A.6 Sensitivity on heat transfer layer length

The heat transfer layer length was identified by analyzing PRELUDE experimental results. A correlation depending on the Weber number was proposed. Here, the impact of heat transfer layer length value on calculation results is tested. For the PRELUDE '1D' tests with a water flowrate of 10m/h, L1 was estimated around 70mm. In Figure A. 8 the calculations with L1=40mm and L1=100mm are presented, which corresponds to a ±43% difference in L1 was tested. The impact on the quench front velocity is about ±12% (see Figure A. 8). It is interesting to notice that increasing the heat transfer layer length results in an increase of the quench front velocity at border and mid-radius, and the instability (2D effect) in the progression of quench front is more pronounced. Nevertheless, we can conclude that the sensitivity of the model to that heat transfer length is limited and that the proposed correlation can be used with confidence (in the range of parameters studied).

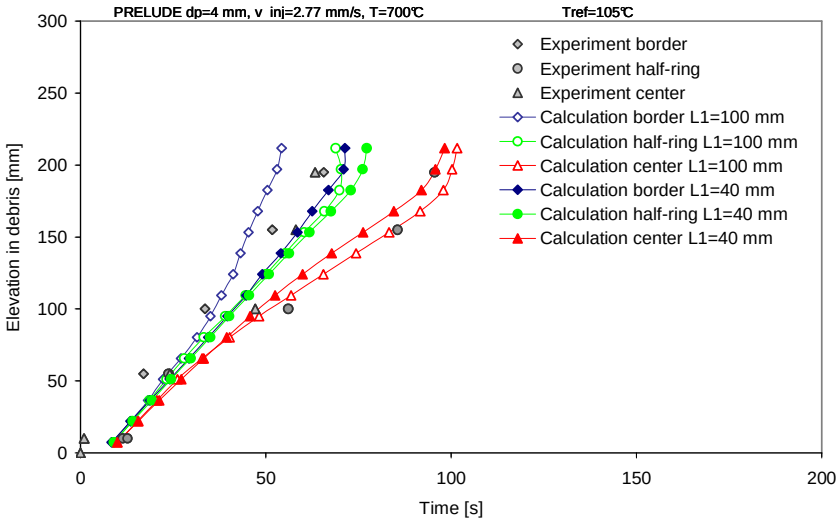

Figure A. 8: Effect of heat transfer layer length on calculation results; PRELUDE '1D' with initial temperature 700°C, particle diameter 4mm and liquid injection flow 10m/h

A.7 Relative permeability

The momentum balance equations in ICARE-CATHARE porous medium model are based on Darcy generalized equations (see Chapter 4). The relative permeabilities have been assumed to depend only on void fraction in order to include the impact of the smaller effective cross section for each phase.

The relative permeability and the relative passability for spherical particles have been chosen from the standard Willey (1962) / Lipinski (1981) correlations (see Figure A. 9 and Figure A. 10). However, for the momentum transport equations, it is also expected that the phase repartition and therefore the boiling regime diagram has an important impact on the transport properties. Thus, we can apply the same splitting function that was used to estimate the heat exchange terms to combine the correlations obtained by Duval (2002) in SGL and SLG configurations (see Figure A. 9 and Figure A. 10). We can see that the correlations differ significantly for the cases where one phase becomes residual, i.e., high void fraction for the case of relative permeability of liquid. Both, Lipinski and Duval correlations were tested in the ICARE-CATHARE code and their impact on pressure increase during reflood is shown in Figure A. 11. We can see that the effect is negligible on the pressure prediction. This just indicates that the most important phenomena occur in areas where the gas phase is not residual and therefore, both correlations are equivalent.

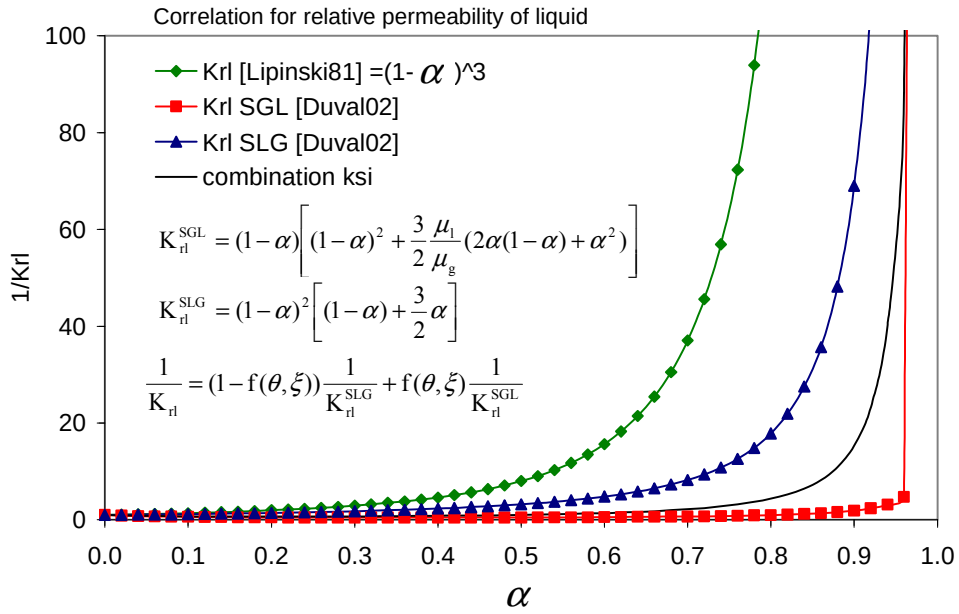

Figure A. 9: Comparison of different correlations for relative permeability of liquid

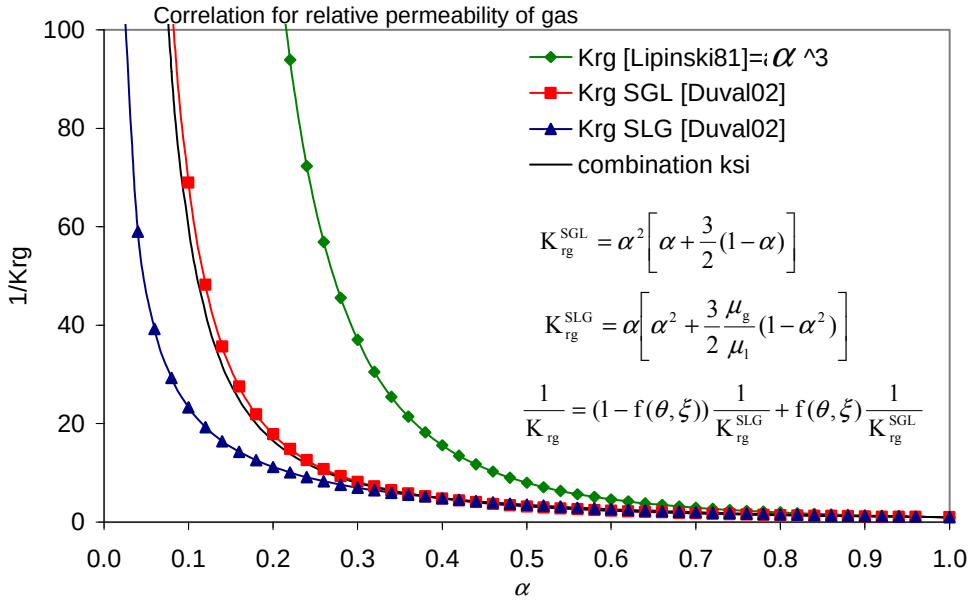

Figure A. 10: Comparison of different correlations for relative permeability of gas

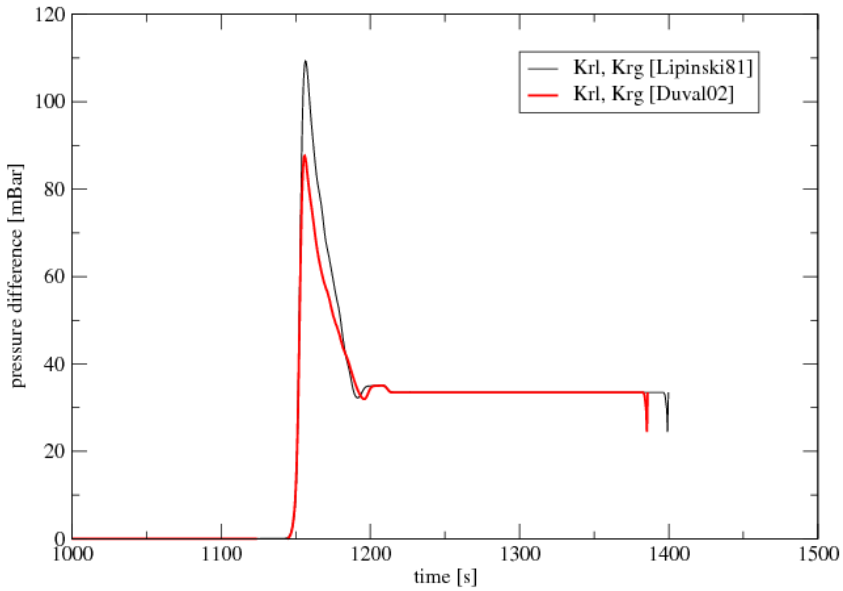

Figure A. 11: Comparison of pressure increase during reflood applying two different correlations for relative permeability of gas and liquid; PRELUDE '1D' experiment with initial temperature 400°C, particle diameter 4mm and liquid injection flow 5m/h

A.8 Conclusions

In this appendix the effect of different physical parameters on calculation results was studied. Firstly it was shown that the first model implemented into the code [Bechaud01] underestimated significantly the heat transfers and thus the quench front progression. Thus, the new model was elaborated during this thesis.

One of the uncertain parameters in a flow thought the porous medium is the critical heat flux. In this appendix we showed that the Groeneveld [Guillard01] correlation predicts well the magnitude of maximum heat flux. The sensibility calculations on this parameter were performed and showed that even if we decrease the critical heat flux 10 times, its impact on calculation results is not significant.

The important improvement of the model was realized for the regimes of film boiling. Also the transition criterion was proposed. It was shown that because of the transition criterion (heat transfer layer length) modeling, the temperature evolution during "pre-cooling" and the quenching are well predicted. Moreover, even if this parameter is very important, the sensitivity of the model to that heat transfer length is limited. We concluded that the proposed correlation can be used with confidence (in the range of parameters studied).

APPENDIX B

In order to demonstrate that the proposed modeling and its numerical implementation are robust, we will present in this appendix various sensitivity studies on user-defined parameters (nodalization, boundary conditions or physical parameters) that influence the calculation results. It is obvious that results of calculations will always depend, to some extent, on the engineering judgment and user experience but it is necessary to have an idea of the dependence on those parameters. In this Appendix, the sensitivity calculations on **user-defined parameters** will be presented (the list of parameters is given in Table B. 1).

Table B. 1: Sensitivity calculations on user-defined parameters

	Reference calculation	**Sensitivity calculations**
Radial nodalization	One radial mesh (1D)	Five radial meshes (2D)
Axial nodalization	15 axial meshes 219mm bed height	6 axial meshes 219mm bed height
Porosity	0.4	N°1: 0.44 at border N°2: Random porosity 0.4±0.03
Initial temperature	400°C	±40°C → 360°C or 445°C
Mass flow rate	62g/s	±4g/s → 58g/s; 66g/s
Temperature of injected water	20°C	±5°C → 15°C; 25°C

B.1 Radial nodalization

The PRELUDE '1D' experiments with initial temperature 400°C were calculated with one radial mesh. The quench front velocity was well predicted for most of the tests comparing with centre/mid-radius quench front velocities from experiments. The highest difference between calculations and experimental results was observed for 1mm particles, where the difference between the calculated and measured quench front velocities was up to 43.7%.
In this Appendix, the calculations of PRELUDE '1D' with initial temperature 400°C, particle diameter 1mm and liquid injection flow 4m/h were performed with 5 radial meshes, as an example. The power was distributed in the two dimensions according to experimental measurements. In these calculations, the porosity at the border was set to 0.45 to simulate the wall effect. In the calculation with 5 radial meshes, the faster progression of water along the wall is well observed (Figure B. 1). In addition, the highest difference between calculated and measured quench front velocity decreases to 29.5%. This clearly shows the necessity to use a 2D meshing in order to catch the progression of water. However, it is striking to notice that the 1D calculations provide a good estimate of the "average" quench front velocity.

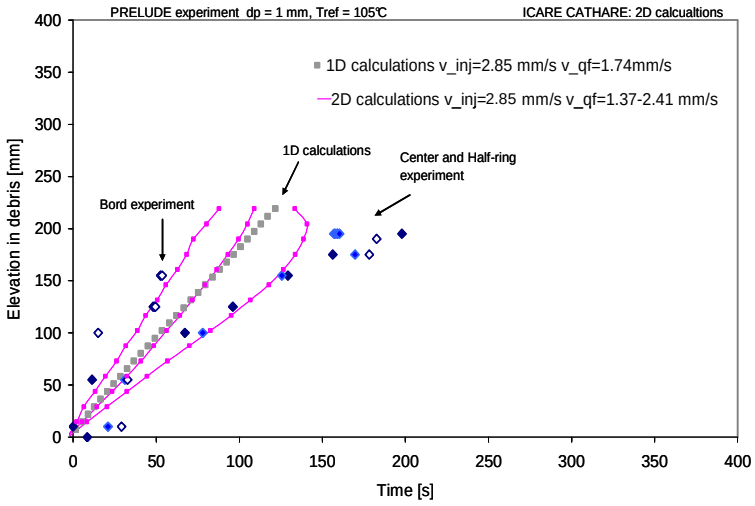

Figure B. 1: Calculated and measured quench front velocities: 1 radial mesh versus 5 radial meshes + porosity modified in one mesh; PRELUDE '1D' with initial temperature 400°C, particle diameter 1mm and injection liquid flow 4m/h

B.2 Axial nodalization

For a reactor transient calculation, the typical mesh size is about 20-25cm. This is expected to be too large with respect to the thickness of the two-phase zone which was observed to be of the order of a few centimetres in reflooding experiments such as PRELUDE. The transition boiling regime zone in channels during reflood was observed to be about 4-8cm. Consequently, for a mesh height 20-25cm, there is a large temperature increase over a short length at the instant of quenching [Chikhi10].

In this section we test the sensibility of the calculated results on the mesh height. The PRELUDE calculations presented in this thesis were performed with mesh heights of 0.73cm or 1.46cm for a total debris bed height about 219mm. Our objective is to increase a debris mesh height. The problem is, that the debris bed height at PRELUDE was limited to 200mm which is a typical mesh size in a reactor transient calculation. However, we do not want to simulate the PRELUDE geometry with only one axial mesh. Thus, we test the following meshing (see Figure B. 2):

- 30 axial meshes (h=0.73cm) that predicted well the quench front velocity for most of the PRELUDE tests that were simulated with one radial mesh.
- 15 axial meshes (h=1.46cm) are the reference calculations that predicted well the quench front velocity and also the 2D effects.
- 6 axial meshes (h=3.65cm) predict well the mean quench front velocity. The 2D effects are not visible.
- 4 axial meshes (h=5.475cm) predict well the mean quench front velocity. The 2D effects are not calculated. The quenching is delayed about 50 seconds.

Calculations with less than 4 meshes were not realized because the reference debris bed height was only 20cm. The performed calculations show, that the quench front is also well

predicted even if the number of meshes decreases. The effect of transition from 30 axial meshes to 15 axial meshes is not us expected. Here, only the quench front velocity at the border changed and is better predicted with 15 axial meshes (compared with experimental points that are not shown here). This was not studied in detail yet. However, the advantage is that the calculation time is shorter and the results correspond to "average" quench front velocity. In order to simulate 2D effects, the calculations with multiple axial meshes are necessary (and, of course, radial meshes as it was already concluded).

A brief point will be done from the numeric point of view. In CATHARE code, the maximum time step can be limited by user, but the minimum time step is regulated in the code, using a CFL condition for convergence. In our calculations, the time step during reflood in the code is between 10^{-3} -10^{-4} s. This is very low compared to the time needed for water to pass across the mesh that is few seconds.

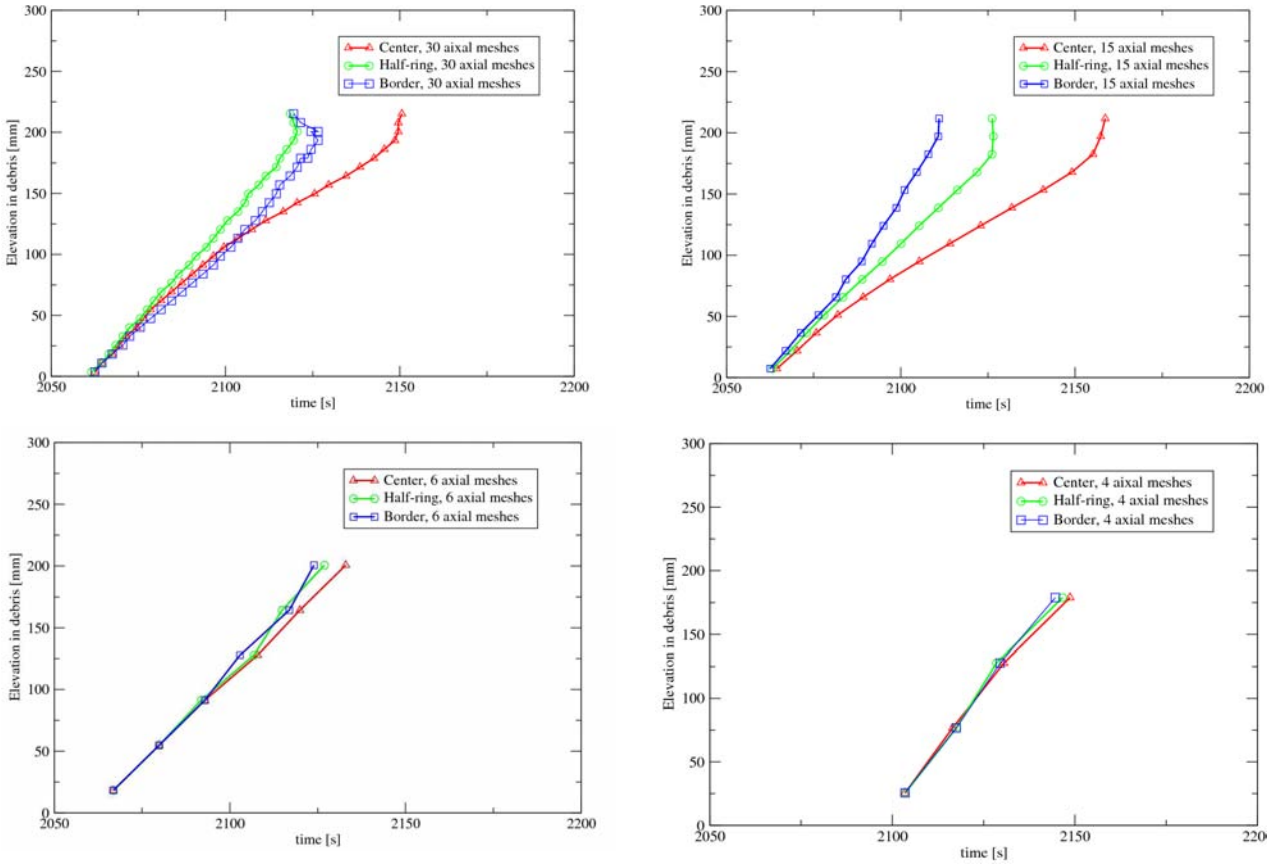

Figure B. 2: Effect of mesh height on calculated quench front progression; PRELUDE '1D' with initial temperature 700°C, particle diameter 4mm and injection liquid flow 10m/h.Legend: 30 meshes (h1=0.73cm), 15 meshes (h1=1.46cm), 6 meshes (h1=3.65cm), 4 meshes (h1=5.475cm)

B.3 Porosity

It is assumed that the porosity near the wall in PRELUDE experiments might be slightly higher because of wall effects on the arrangement of the particles. In Figure B. 3 we can see

the impact of porosity at the border (wall effect). The calculation shows that the porosity at the outer column has a small impact on the quench front progression. As expected, the 2D effects are slightly enhanced by increasing the porosity near the wall. Water progresses with a higher velocity through the outer ring where the pressure drop is lower and, consequently, the quench front velocity at the centre slightly decreases. However, in Figure B. 3 it can be seen that the different porosity in the bed is not the main criterion to trigger 2D effects. On the other hand, it impacts significantly the 2D effects. Because the porosity near the structures, e.g., wall is difficult to be measured or predicted, it stays an important user-defined parameter to be tested in validation calculations.

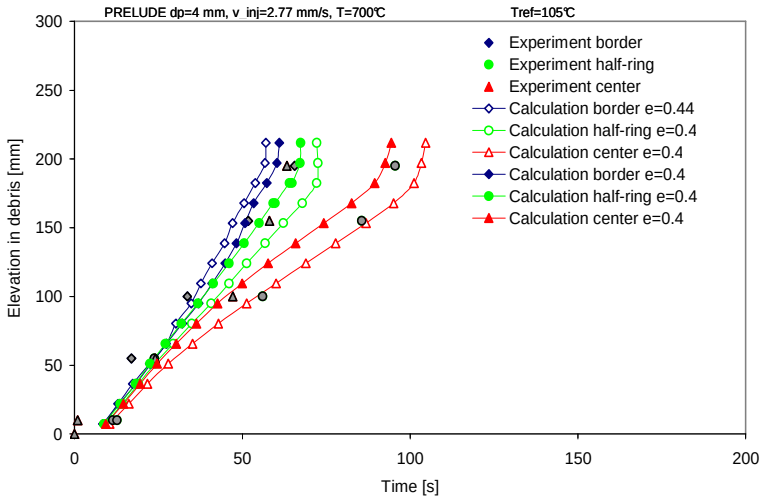

Figure B. 3: Effect of porosity at border on quench front progression; PRELUDE '1D' experiment with initial temperature 700°C, particle diameter 4mm and liquid injection flow 10m/h

Secondly, the sensitivity calculations on the impact of bed porosity were performed. A *random local distribution* of porosity in the *whole bed* was prescribed as 0.4±Random[0-0.03]. The reference calculations Figure B. 4 (right) were performed with the porosity 0.4 in the center of the bed and 0.44 at the border. In Figure B. 4 we can see the calculated quench front velocities for two cases- random and reference case. We can see that the porosity distribution has an impact on the results. The mean quench front velocity is similar for both cases. However, the random porosity does not generate so strong 2D effects as are observed in the reference case. This clearly shows that the generated numerical disturbances do not generate instabilities in the calculations.

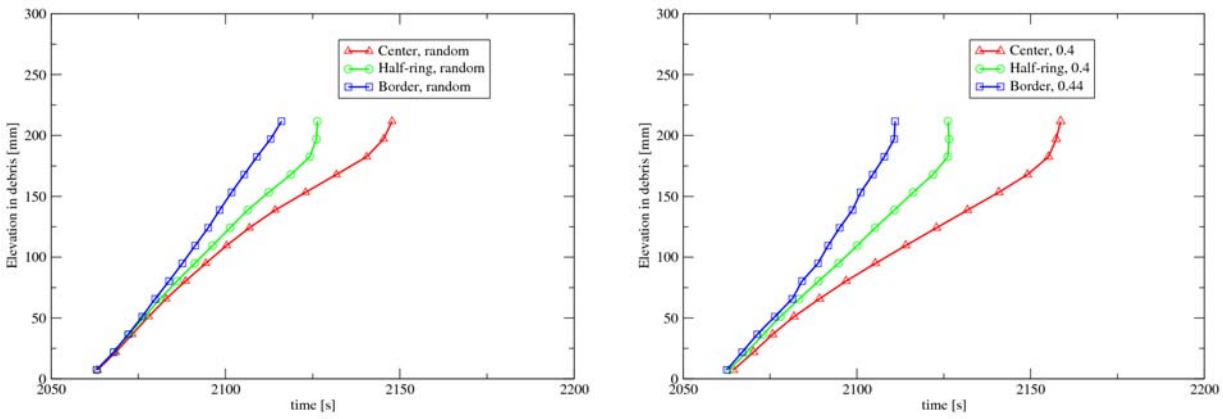

Figure B. 4: Effect of random porosity on quench front progression; PRELUDE '1D' experiment with initial temperature 700°C, particle diameter 4mm and liquid injection flow 10m/h. Mesh height is 1.46cm.

B.4 Initial temperature

In Figure B. 5 we can see the effect of initial temperature on the calculation results. The input power affects the initial porous medium temperature before reflooding. Higher input power results in higher initial temperatures, and, consequently, the quench front velocity is lower.

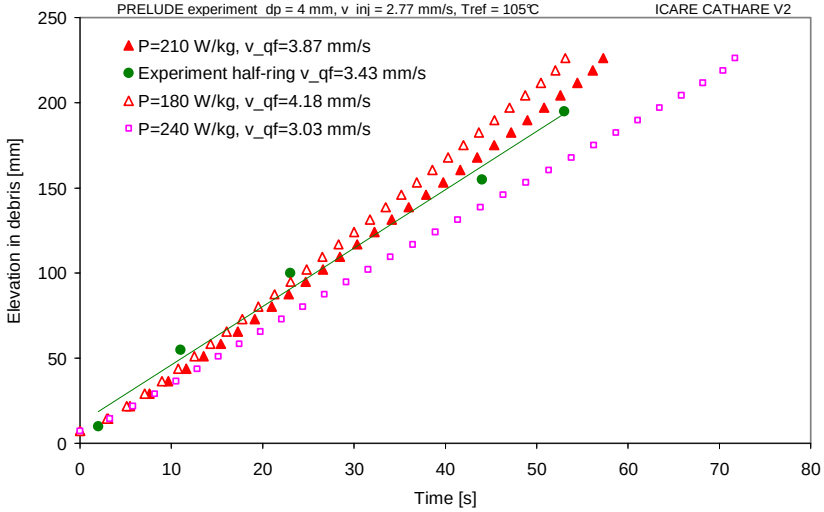

Figure B. 5: Effect of initial temperature on quench front progression (P=210W/kg results in T=400°C, P=180W/kg in T=360°C and P=240W/kg in T=445°C);
PRELUDE '1D' experiment, particle diameter 4mm and liquid injection flow 10m/h

B.5 Totally uniform conditions in the bed

In the paragraph above we have shown that the porosity is not the only criterion to trigger 2D effects. Here, we perform the additional calculations with a homogeneous bed and temperature (no thermal losses). In Figure B. 6 we can see that even if we simulate the homogeneous bed in its porosity and temperature, 2D effects are calculated. Consequently, as we assumed already in Chapter 2, the quench front instabilities result from the liquid injection

velocity and associated steam flow and generated pressure gradient. The bed heterogeneities are not the only criterion. The same conclusion can by found in studies [Fitzgerald98].

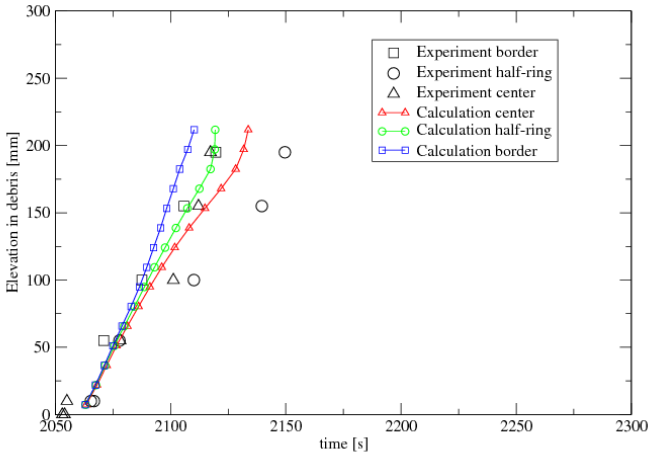

Figure B. 6: Calculations with homogeneous bed (porosity and temperature); PRELUDE '1D' experiment with initial temperature 700°C, particle diameter 4mm and liquid injection flow 10m/h

B.6 Liquid mass flow rate

Figure B. 7 illustrates the effect of liquid mass flow rate on calculation results. We can see that the dependence on inlet velocity on the quench front velocity. We concluded that the variation in liquid injection flow about 6.5% results in an identical variation of quench front velocity.

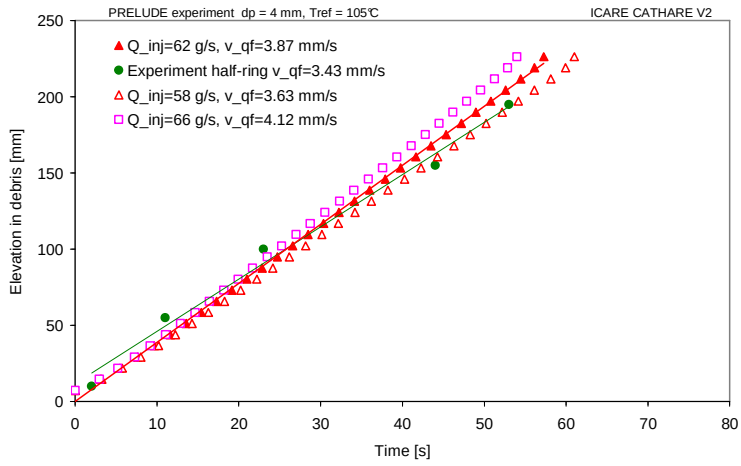

Reference case	
62 g/s	3.87mm/s
Sensitivity calculations	
-6.5% (58 g/s)	-6.2% (3.63 mm/s)
+6.5% (66 g/s)	+6.5% (3.87 mm/s)

Figure B. 7: Effect of liquid mass flow on calculation results, PRELUDE '1D' experiment with initial temperature 400°C, particle diameter 4mm and liquid injection flow 10m/h

B.7 Temperature of injected water

Figure B. 8 illustrates the effect of initial liquid temperature on the calculated results. The initial temperature of liquid was not measured so its effect on quench front velocity and steam

production was studied. We can see that there is no significant effect of liquid temperature on calculation results, in the studied range of liquid temperatures 15-25°C.

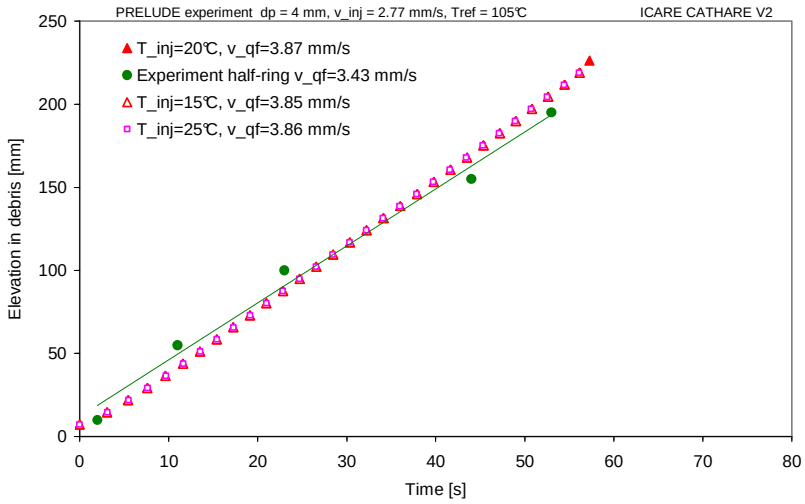

Figure B. 8: Effect of water temperature on quench front velocity; PRELUDE '1D' experiment with initial temperature 400°C, particle diameter 4mm and liquid injection flow 10m/h

B.8 Conclusions

In this appendix we studied the effect of different user-defined parameters on calculation results. We concluded that the axial and radial nodalization have an impact on the certitude of the calculation results. The 2D effects, i.e., instabilities or heterogeneity effects in the quench front progression are better predicted with fine axial as well as radial meshing. However, the calculations with one radial mesh and few axial meshes predict also well the general trends in the quench front progression. As expected, the calculation time decreases with coarse meshes and the user can obtain acceptable predictions in a short time.

Secondly, sensitivity calculations on the debris bed porosity were performed. In the calculations with multiple radial meshes, we had a tendency to increase slightly the porosity of the bed near the vessel wall as an effect of arrangement of particles. In this appendix we can see that there is really a visible impact on the quench front velocity. However, it impacts the quench front velocity which decreases in the center. Higher porosity close to the wall increases the flowrate in this region, and, as consequence, less water passes through the axis. It was concluded that the debris bed porosity is an important parameter. However, it is not always precisely measured or predicted so it stays and important user-defined parameter to be varied. Also the calculations with generated numeric instability, i.e., random porosity in the whole bed 0.4±Random[0,0.03] were realized. In was concluded that the generated numeric instabilities in the case of random porosity do not disturb significantly the calculations.

Moreover, the 2D effects were discussed, i.e., instability in progression of quench front. The whole calculations in this Appendix showed that the instability of quench front depends on

debris bed characteristics. The additional calculations were realized, with homogeneous bed in porosity and temperature, in order to see the impact of hydrodynamic parameters. It was concluded that the water injection velocity 10m/h generates the quench front instabilities (in a bed 700°C). Thus, the debris bed characteristics are not the *only* criteria that generate these effects. The quench front instabilities result from the liquid injection velocity and associated steam flow and generated pressure gradient as was already discussed in Chapter 2 and found independently by different authors [Fitzgerald98].

Finally, the sensitivity calculations on debris bed temperature, water injection flow and water injection temperature were performed. It was concluded that water subcooling does not have a strong impact on the quench front progression, in the studied range ±5%. On the other hand, the initial temperature of the bed before reflood is important. As expected, a higher temperature results in a lower quench front velocity. It is recommended, in validation calculations, to verify precisely the initial bed temperatures. The impact of water injection flowrate was also studied. The interesting conclusion is that the variation in the water injection liquid flow ±6.5% results in the same variation of quench front velocity.

Bibliography

[Amarasooriya91] Amarasooriya W.H., and Theofanous T.G. Premixing of steam explosions: a three-fluid model. Nuclear Engineering and Design, Vol. 126 pp. 23-39, 1991.

[Atkhen06] Atkhen K., Berthoud G. SILFIDE experiment: Coolability in a volumetrically heated debris bed. Nuclear Engineering and Design, Vol. 236, pp. 2126-2134, 2006.

[Auria98] Auria F., and G. M. Galassi. Code validation and uncertainties in system thermalhydraulics. Progress in Nuclear Energy, Vol. 33, No. 1, pp. 175-216, 1998.

[Bachrata10] Bachrata A. In-vessel retention via external reactor cooling. LAP Lambert Academic Publishing, ISBN 978-3-8383-4073-9, 2010.

[Bandini12] Bandini G. Benchmark Exercise on TMI-2 Plant, Specifications for the First Transient Calculation. OECD, 2012.

[Batchelor77] Batchelor G. K., and Obrien R. W. Thermal or electrical conduction through a granular material. Proc. R. Soc. Lond., Vol.355, pp.313-333., 1977.

[Bechaud01] Bechaud, C., Duval, F., Fichot, F., Quintard, M., Parent, M. Debris bed coolability using a 3-D two phase model in a porous medium. In: Proceedings of ICONE-9, Nice, France, 2001.

[Berthoud94] Berthoud G., Valette M. Development of a multidimensional model for the premixing phase of a fuel-coolant interaction. Nuclear Engineering and Design, Vol. 149, pp. 409-418, 1994.

[Bertsch09] Bertsch S. A composite heat transfer correlation for saturated flow boiling in small channels. International Journal of Heat and Mass Transfer, Volume 52, Issues 7–8, Pages 2110-2118, 2009.

[Bevelacqua12] Bevelacqua J. J. Applicability of health physics lessons learned from the Three Mile Island Unit 2 accident to the Fukushima Daiichi accident. Journal of environmental radioactivity, Vol. 105, pp. 6-10, 2012.

[Brooks64] Brooks R., Corey, A. Hydraulic Properties of Porous Media, 1964.

[Broughton89] Broughton J.M., Pui K., Petti D.A., and Tolman E.L. A scenario of the Three Mile Island unit 2 accident. Nuclear Technology, Vol. 87, pp. 34-53, 1989.

[Burger06] Burger M., Berthoud G. Basic laws and coolability of particulate debris: comments on the status and present contributions. Nuclear Engineering and Design, Vol. 236, pp.2049-2059, 2006.

[Carman37] Carman P. C. The determination of the specific surface area of powder. I. J. Soc. Chem. Ind, Vol. 57, pp. 225-234, 1937.

[Chahlafi11] Chahlafi M. Modélisation du rayonnement thermique dans un cœur de réacteur nucléaire dégradé en présence de vapeur et de gouttes d'eau. PhD thesis, Ecole Centrale Paris, 2011.

[Coindreau09] Coindreau O., et al. Characteristics of the geometry of debris beds expected to form during reflooding. OECD-SARNET workshop on in-vessel corium coolability, France, 2009.

[Coindreau09b] Coindreau O., et al. Coolability of an heterogeneous porous medium using a 3-D two phase model. 4th International Conference on Applications of Porous Media, Turkey, 2009.

[Collier94] Collier J.G., Thome J. R. Convective boiling and condensation. Clarendon Press, Oxford, 1994.

[Davarzani10] Davarzani H., Marcoux M., Quintard M. Theoretical predictions of the effective thermodiffusion coefficients in porous media. International Journal of Heat and Mass Transfer, Vol. 53, pp.1514-1528, 2010.

[Davit10] Davit Y., Quintard M., Debenest, G. Equivalence between volume averaging and moments matching techniques for mass transport models in porous media. International Journal of Heat and Mass Transfer, Vol. 53, pp. 4985 – 4993, 2010.

[Decossin00] Décossin E. Ebullition et assèchement dans un lit de particules avec production interne de chaleur: premières experiences et simulations numériques en situation multidimensionnelle. PhD thesis, INP Toulouse, 2000.

[Dhir97] Dhir V. K. Heat transfer from heat-generating pools and particulate beds. Advances in heat transfer, Vol.29, 1997.

[Dorsselaere06] Dorsselaere J. P. et al. Views on R&D needs about in-vessel reflooding issues, with focus on debris coolability. Nuclear Engineering and Design, Vol. 236, pp. 1976-1990, 2006.

[Dougall63] Dougall R. S., Rohsenov W. M. Film boiling on the inside of vertical tubes with upward flow of the fluid at low qualities. Technical Report No. 9079-26, 1963.

[Drai11] Drai P., and Fleurot J. Applications réacteurs avec ICARE/CATHARE V2- Rex et solutions retenues. DPAM-SEMCA-2011-250, 2011.

[Duval02] Duval F. Modélisation du renoyage d'un lit de particules: contribution a l'estimation des propriétés de transport macroscopiques. PhD thesis, INPT, Toulouse, France, 2002.

[Duval04] Duval F., Fichot F. and Quintard M. Local thermal non-equilibrium model for two-phase flows with phase change in porous medium. International Journal of Heat and Mass Transfer, 47(3), 613-639, 2004

[Ergun52] Ergun S. Fluid flow through packed columns. Chem. Eng. Prog., Vol. 48, pp. 89-97, 1952.

[Fichot09] Fichot F., et al. Film boiling in a porous particle bed. In proceedings of ECI International Conference on Boiling Heat Transfers, Brazil, May, 2009.

[Fichot06] Fichot F., et al. The impact of thermal non-equilibrium and large-scale 2D/3D effects on debris bed reflooding and coolability. Nuclear engineering and design, Vol. 236, pp.2144-2163, 2006.

[Fischer04] Fischer M. The severe accident mitigation concept and the design measures for core melt retention of the European pressurized reactor. Nuclear Engineering and Design, Vol. 130, pp.169-180, 2004.

[Fitzgerald98] Fitzgerald D., Woods A. Instabilities during liquid migration into superheated geothermal reservoirs. Water resources research, Vol. 34, No. 9, pp. 2089-2101, 1998.

[Fourar00] Fourar M., Lenormand R. Inertial effects in two-phase flow through fractures. Oil and Gas science and technology, Vol. 55, pp. 259-268, 2000.

[Ginsberg86] Ginsberg, et al. An experimental and analytical investigation of quenching of superheated debris beds under top reflood conditions. Report NUREG/CR-4493, 1986.

[Grangeot94] Grangeot G., Quintard M., Whitaker S. Heat transfer in packed beds: interpretation of experiments in terms of one- and two-equation models. In 10th International Heat Transfer Conference, Brighton, volume 5, pages 291-296, 1994.

[Gray75] Gray W. G. A derivation of the equations for multi-phase transport. Chemical Engineering science, Vol. 30, pp. 229-233, 1975.

[Griffith60] Griffith. The role of surface conditions in nucleate boiling, Chem. Eng. Prog. Symp., Ser. 56, 30, pp.49-63, 1960.

[Groeneveld96] Groeneveld D.C. et al. The 1995 look-up table for critical heat flux in tubes. Nuclear Engineering and design, Vol. 163, 23, 1996.

[Grosser96] Grosser K., Carbonell R.G., Cavero A., Saez A.E. Lateral thermal dispersion in gas-liquid cocurrent downflow through packed beds. AIChE J. 42 (10) 2977-2983, R & D Notes, 1996.

[Guillard01] Guillard, et al. ICARE-CATHARE coupling: three dimensional thermal-hydraulics of severe LWR accidents. Proc. of ICONE-9, Nice, France, 2001.

[Hejzlar04] Hejzlar R. Sdeleni tepla, Vydavatelstvi CVUT, 2004.

[Hewitt84] Hewitt, et al. Multiphase science and technology. Volume 1, ISBN 0-89116-222-4, 1984.

[Hiroyasu04] Hiroyasu O. Study on propagative collapse of a vapor film in film boiling (mechanism of vapor-film collapse at wall temperature above the thermodynamic limit of liquid superheat). International Journal of Heat and Mass Transfer 47, 1965-1977, 2004.

[Hozer10] Hozer Z., et al. Experimental simulation of the Paks-2 cleaning tank incident through separate effect and integral test. Nuclear Engineering and Design, Vol. xxx., 2010.

[Hu91] Hu K., and Theofanous T. On the measurement and mechanism of dryout in volumetrically heated coarse particle beds. Int. J.Multiphase Flow 17, 1991.

[Chikhi10] Chikhi N. and Fichot F. Reflooding model for quasi-intact rod configuration: Quench front tracking and heat transfer closure laws. Nuclear Engineering and Design, Vol. 240, pp. 3387-3396, 2010.

[INSAG99] INSAG 12. Basic Safety Principles for Nuclear Power Plants. IAEA Vienna, 1999.

[IRSN06] IRSN Rapport-2006/73. CEA Rapport-2006/474. R&D relative aux accidents graves dans les réacteurs à eau pressurisée, 2006.

[Isačenko81] Isačenko V.P., Osipova V. Těploperedača,Energoizdat,Moskva,1981.

[Jamialahmadi05] Jamialahmadi M., Muller-Steinhagen H., Izadpanah M. R. Pressure drop, gas hold-up and heat transfer during single and two-phase flow through porous media. International Journal of Heat and Fluid Flow, Vol. 26, pp. 156-172, 2005.

[Kaviany91] Kaviany M . Principles of Heat Transfer in Porous Media. Springer-Verlag, New, 1991.

[Kazachkov02] Kazachkov I. V. Konovalikhin M., Steam flow through the volumetrically heated particle bed. International Journal of Thermal Sciences, Vol. 41, pp. 1077-1087, 2002.

[Landereau01] Landereau et al. Quasi-steady two-equation models for diffusive transport in fractured porous media : large-scale properties for denely fractured systems. Advances in Water Resources, Vol. 24, pp.863-876, 2001.

[Lee09] Lee J., Mudawar I. Critical heat flux for subcooled flow boiling in micro-channel heat sinks. International Journal of Heat and Mass Transfer, Vol. 52, pp. 3341-3352, 2009.

[Leidenfrost56] Leidenfrost J.G. On the fixation of water in diverse fire. A tract about some qualities of common water, 1756.

[Leverett41] Leverett M. C. Capillary Behavior in Porous Solid. Trans. AIME, Vol. 142, pp. 152-169, 1941.

[Li11] Li Liangxing, Ma Weimin. Experimental characterization of the effective particle diameter of a particulate bed packed with multi-diameter spheres. Nuclear Engineering and Design, Vol. 241, pp. 1736-1745, 2011.

[Lindholm06] Lindholm, et al. Dryout heat flux experiments with deep heterogeneous particle bed. Nuclear Engineering and Design, Vol. 236, pp. 2060-2074, 2006.

[Lipinski84] Lipinski R. A coolability model for postaccident nuclear reactor debris. Nucl. Technol. 65, 53-66, 1984.

[Lipinski81] Lipinski R. A one dimensional particle bed dryout model. ANS Trans. 38, 386-387, 1981.

[Lipinski82] Lipinski. A model for boiling and dryout in particle beds. National Technical Information Service,1982.

[Liu93] Liu H. I., et al. Characteristics of transition boiling and thermal oscillation in an upflow convective boiling system. 196-205, 1993.

[Ma10] Ma Weimin, Dinh Truc-Nam. The effects of debris bed's prototypical characteristics on corium coolability in a LWR severe accident. Nuclear Engineering and Design, Vol. 240, pp. 598-608, 2010.

[Moyne97] Moyne C. Two-equation model for a diffusive process in porous media using the volume averaging method with an unsteady-state closure. Advances in Water Resources, Vol. 20, pp. 63-16, 1997.

[Mudawar00] Mudawar I., and Hall D. Critical heat flux CHF for water flow in tubes-II. subcooled CHF correlations. International Journal of Heat and Mass Transfer, Volume 43, Issue 14, Pages 2605-2640, 2000.

[Mukherjee09] Mukherjee A. Contribution of thin-film evaporation during flow boiling inside microchannels. International Journal of Thermal Sciences, Volume 48, Issue 11, Pages 2025-2035, 2009.

[Muskat49] Muskat M. Physical principles of oil production. McGraw-Hill, New York, 1949.

[Nield92] Nield D. A., and Bejan A. Convection in Porous Media. Springer-Verlag, New York., 1992.

[Obot88] Obot N., and Ishii M. Two-phase flow regime transition criteria in post dry-out region based on flow visualization experiments. International Journal of Heat Mass Transfer, Vol. 31, 2559-2570, 1988

[Petit98] Petit F. Ebullition en milieu poreux et renoyage d'un lit de débris de réacteur nucléaire. PhD thesis, Ecole Nationale Supérieur d'Arts et Métiers, Bordeaux, 1998.

[Petit99] Petit F., Fichot F., Quintard M. Ecoulement diphasique en milieux poreux: modele a non-equilibre local. Int. J.Thermal Sci. 38, 239-249, 1999.

[Pignet03] Pignet S., Guillard G. Modeling of severe accidents sequences with the nex modules CESAR and DIVA of the ASTEC system code. In Proceedings of NURETH-10, Seoul, South Korea, 2003.

[Quintard93] Quintard M., and Whitaker S. One- and Two-Equation Models for Transient Diffusion Processes in Two-Phase Systems. Advances in heat transfer, Vol. 23, ISBN 0-12-020023-6, 1993.

[Quintard97] Quintard M., Kaviany M., Whitaker S. Two-medium treatment of heat transfer in porous media: numerical results for effective properties. Advances in Water Resources, Vol. 20, pp. 11-94, 1997.

[Rashid11] Rashid, et al. Experimental results on the coolability of a debris bed with multidimensional cooling effects. Nuclear Engineering and Design, Vol. xxx, pp. xxx-xxx, 2011.

[Reed82] Reed A. The effect of channeling on the dryout of heated particulate beds immersed in a liquid pool. PhD thesis, Massachusetts Institute of Technology, Cambridge, 1982.

[Reed85] Reed A., Boldt K., Gorham-Bergeron E., Lipinski R., and Schmidt T. DCC-1/DCC-2 degraded core coolability analysis. Technical Report NUREG/CR-4390-R3, Sandia National Labs, 1985.

[Repetto11] Repetto G., et al. Experimental program on debris reflooding (PEARL) - Results on PRELUDE facility. Proc. of NURETH 14, Toronto, Canada 2011.

[Repetto12] Repetto G., et al. Investigation of multidimensional effects during debris cooling. ERSMAR, Cologne, Germany, March 21-23, 2012

[Sehgal11] Sehgal B. R. Nuclear safety in light water reactors: severe accident phenomena. ISBN 0123884462, January 2011

[Schmidt07] Schmidt W. Interfacial drag of two phase flow in porous media. International Journal of Multiphase flow, Vol. 33, pp.638-357, 2007.

[Scheidegger60] Scheidegger E. A. The physics of flow through porous media. ISBN 0-8020-1849-1, 1960.

[Schulenberg87] Schulenberg T., and Muller U. An improved model for two-phase flow through beds of coarse particles. Int. J. Multiphase Flow 13 (1), 87-97, 1987.

[Steinke04] Steinke S.G., and M.E Kandlikar. An experimental investigation of flow boiling characteristics of water in parallel microchannels. Trans. ASME J. Heat Transfer Vol. 47, pp. 1925-1935, 2004.

[Stenne09a] Stenne N., et al. Multi-Dimensional Reflooding experiments: the PEARL Program. Joint OECD/NEA - EC/SARNET2 Workshop In-Vessel Coolability , Issy-les-Moulineaux, France, October 12-14, 2009.

[Stenne09b] Senne N., et al. R&D on reflooding of degraded cores in SARNET-Focus on PEARL new IRSN facility. EUROSAFE Forum, Brussels (Belgium), Nov.2-3, 2009.

[Thome94] Thome J.R. Boiling in microchannels: a review of experiment and theory. Int. J. of Heat and Fluid Transfer Conference, Brighton, vol. 5, pp. 291-296, 1994.

[Truong78] Truong H. V., and Zinsmeister G. E. Experimental study of heat transfer in layered. International Journal of Heat and Mass Transfer, Volume 21, Issue 7, Pages 905-909, 1978.

[Tung83] Tung V. X., and Dhir V. K Quenching of a hot particulate bed by bottom quenching. Proc. of ASME-JSME Thermal Engineering Joint Conference, Honolulu, Hawai, 1983.

[Tung88] Tung V. X., and Dhir V. K. A hydrodynamic model for two-phase flow through porous medium. Int. J. Multiphase Flow, Vol. 14, pp. 47-65, 1988.

[Turland83] Turland B.D., and Moore K. Debris bed heat transfer with top and bottom cooling. AIChE Symp. Ser. 79, 256-267, 1983.

[Tutu84] Tutu, et al. Debris bed quenching under bottom flood conditions. Report NUREG/CR-3850, Sandia National Labs, 1984.

[Whalley87] Whalley P. B. Boiling, condensation and gas-liquid flow. Oxford science Publ., 1987.

[Whitaker85] Whitaker S. A simple geometrical derivation of the spatial averaging theorem. Chemical engineering Education 19, pp.18-21, 50-52, 1985.

[Whitaker98] Whitaker S. Coupled transport in multiphase systems : a theory of drying. Advances in Heat Transfer, vol. 31, Academic Press, New-York, pp. 1-102, 1998.

[Whitaker77] Whitaker S. Simultaneous heat, mass and momentum transfer in porous medium: a theory of drying, 119.-203, 1977.

[Yakush11] Yakush S. E., Kudinov P., Lubchenko T. Sensitivity and uncertainty analysis of debris bed coolability. Proc. of NURETH 14, Toronto, Canada 2011.

[Zanotti84] Zanotti F., and Carbonell R. G. Development of transport equations for multiphase systems. Chemical Engineering Science Vol. 39, No. 2, pp. 289-31 I. 1984.

[Zhang06] Zhang W. Correlation of critical heat flux for flow boiling of water in mini-channels. International Journal of Heat and Mass Transfer, Volume 49, Issues 5–6, Pages 1058-1072, 2006

Résumé

Les événements récents au Japon sur les centrales nucléaires de Fukushima ont montré que des accidents conduisant à la fusion du cœur peuvent survenir bine plus souvent qu'on ne l'avait supposé et que leur impact sur l'environnement et la vie publique est considérable. Pour les réacteurs actuels, un des moyens principaux pour stopper la progression de l'accident est de tenter de refroidir le plus rapidement possible les matériaux en utiliser une injection d'eau de secours. Suivant l'instant de déclenchement de l'injection d'eau dans un cœur dégradé (appelée renoyage) les zones du cœur présentent des degrés de dégradation variables. Ceci conduit à des écoulements 3D double phase dans la cuve à cause des hétérogénéités de porosité et de forme des matériaux à refroidir. La modélisation de ces écoulements est primordiale pour les études de sûreté. A l'IRSN, une partie de ces études se fait grâce au code ICARE-CATHARE. Ce code de calcul est utilisé en Europe par des entreprises nucléaires et sert à calculer l'évolution d'un accident dans un réacteur, en se concentrant sur l'état du cœur et du circuit primaire. L'objectif de cette thèse a été de développer un modèle de renoyage 3D (implanté dans ICARE-CATHARE) capable de traiter les configurations du cœur dégradé lors d'un accident grave. Le modèle proposé est caractérisé par un traitement du déséquilibre thermique entre les phases solide, liquide et gazeuse. Il inclut aussi deux équations de quantité de mouvement (une pour chacune des phases fluides). Une des améliorations faites au cours de cette thèse a été de bien distinguer les lois de transfert de chaleur pour différents régimes d'ébullition. On a ainsi proposé un modèle combinant les situations d'ébullition nucléée et d'ébullition en film. Les calculs permettent de mettre en évidence certaines caractéristiques multidimensionnelles de l'écoulement lors du renoyage, en particulier lorsqu'un fort gradient de pression est engendré dans le milieu poreux par l'écoulement de vapeur. En parallèle, l'IRSN a lancé un programme expérimental (essais PRELUDE et PEARL) dont l'objectif est de permettre la validation du modèle sur un dispositif 2D représentatif du renoyage de particules à haute température. L'analyse des résultats expérimentaux a permis de vérifier certains choix faits pour les lois physiques du modèle macroscopique. Néanmoins, la validation reste très globale puisqu'on ne dispose pas de mesures locales. La validation quantitative sur les données expérimentales a montré que le modèle fournit des résultats satisfaisants. Le modèle est capable de prédire la vitesse de progression du renoyage dans le cœur, la production du vapeur (instantanée et cumulée) et le pic de pression pour différents diamètres de particules et différents débits d'injection testés.

Abstract

The TMI-2 accident and recently Fukushima accident demonstrated that the nuclear safety philosophy has to cover accident sequences involving massive core melt in order to develop reliable mitigation strategies for both, existing and advanced reactors. Although severe accidents are low likelihood and might be caused only by multiple failures, accident management is implemented for controlling their course and mitigating their consequences. In case of severe accident, the fuel rods may be severely damaged and oxidized. Finally, they collapse and form a debris bed on core support plate. Removal of decay heat from a damaged core is a challenging issue because of the difficulty for water to penetrate inside a porous medium. The reflooding (injection of water into core) may be applied only if the availability of safety injection is recovered during accident. If the injection becomes available only in the late phase of accident, water will enter a core configuration that will differ from original rod-bundle geometry and will resemble to the severe damaged core observed in TMI-2. The higher temperatures and smaller hydraulic diameters in a porous medium make the coolability more difficult than for intact fuel rods under typical loss of coolant accident conditions. The modeling of this kind of hydraulic and heat transfer is a one of key objectives of this. At IRSN, part of the studies is realized using an European thermo-hydraulic computer code for severe accident analysis ICARE-CATHARE. The objective of this thesis is to develop a 3D reflood model (implemented into ICARE-CATHARE) that is able to treat different configurations of degraded core in a case of severe accident. The proposed model is characterized by treating of non-equilibrium thermal between the solid, liquid and gas phase. It includes also two momentum balance equations. The model is based on a previously developed model but is improved in order to take into account intense boiling regimes (in particular nucleate boiling). Moreover, the criteria characterizing the transition between different flow regimes were completed. Currently, the French IRSN sets up two experimental facilities, PEARL and PRELUDE. The aim is to predict the consequences of the reflooding of a severely damaged reactor core where a large part of the core has collapsed and formed a debris bed e.g. particles with characteristic length-scale: 1 to 5mm. This means the prediction of debris coolability, front propagation and steam production during the quenching after the water injection. A series of experiments performed in 2010-2012 at the PRELUDE facility has provided a large amount of new data that are summarized. On the basis of those experimental results, the thermal hydraulic features of the quench front have been analyzed and the intensity of heat transfer regimes is estimated. A three-equation model for the two-phase flow in a heat-generating porous medium was validated. The quantitative validation of model with experimental results was realized and showed that the model provides satisfactory results. The model is able to predict the quench front velocity in the core, steam production (instantaneous and cumulated) as well as the pressure increase during reflood for different particle diameters and different injection liquid flows.